Modelling the Starch, TAGs and Functional Biomass Kinetics of Green Algae as a Function of Nitrogen Concentration and Light Flux

A thesis submitted for

the degree of

DOCTOR OF PHILOSOPHY

by

Fahim Murshed Shamsuddin

B Engineering (Chemical) / BSc Chemistry

Discipline of Chemical Engineering

THE UNIVERSITY OF NEWCASTLE, AUSTRALIA

This research was supported by an Australian Government Research Training Program (RTP) Scholarship

July 2019

STATEMENT OF ORIGINALITY

I hereby certify that the work embodied in the thesis is my own work, conducted under normal supervision. The thesis contains no material which has been accepted, or is being examined, for the award of any other degree or diploma in any university or other tertiary institution and, to the best of my knowledge and belief, contains no material previously published or written by another person, except where due reference has been made. I give consent to the final version of my thesis being made available worldwide when deposited in the University's Digital Repository, subject to the provisions of the Copyright Act 1968 and any approved embargo.

Fahim Shamsuddin

Acknowledgements

A PhD is a journey. A journey of challenges, of ups and downs that took me to the other side of the world and back. I would like to thank my supervisors Professor Geoffrey Evens and Dr. Roberto Moreno-Atanasio for giving me the opportunity to work on this novel project. Not many PhD candidates get the opportunity to work on a project of their own innovation and with the freedom that was allowed to me, which I am grateful for. I completed an internship at the Wageningen University and Research Centre to learn how to measure the composition of algae. I would like to thank Dr. Douwe Van der Veen, Ilse and Mitsue for teaching me how to measure algal composition. After my experimental training, I collaborated with the Port Stephens Fisheries Institute to conduct my experiments. I am grateful to the technical staff and scientists Lynn, Steve and Dr. Wayne O'Connor for allowing me to use their facilities as well as training me in cell counting and algal culturing. Working on my PhD would not have been the same without my fellow students who kept me company, so I would like to thank Pavel, Deside, Sagar, Simi, Dilruba, Arif, Raju, Ai, Linhan, Subhashish, Ahamad, Hamed, Wahid, Mehdi, Layla and Tuyen. Meeting and working with all of you has been a pleasure and I wish all of you the best of luck in your future when you complete your PhDs. Finally, I would like to thank my mother, father and younger brother for supporting me during my PhD. It is always those closest to you who experience in the fullest the best and worst of what you go through your journey, but we came out stronger together on the other side and that is what truly matters.

Abstract

Algae as a potentially sustainable source of fuel, feed and nutraceuticals has led to interest in the algae biorefinery concept for production of sustainable products. The cultivation of algae has several advantages as algae can grow in non-potable water and in non-arable land and can sequester CO_2 from flue gas. In addition, different components of the algae produce different value-added products such as biodiesel, which is obtained from TAGs, bioethanol from starch and animal feed from functional biomass. However, there is a lack of commercial viability for photosynthetic algae due to limitations in biomass productivity and the capacity to optimise the chemical composition of the algae, both of which are caused by suboptimal nutrient loading and low light conditions. Therefore, this thesis aims to understand how to optimise the production of the individual biochemical algae components, namely, starch, TAGs and functional biomass by modelling batch photosynthetic cultures. Special attention was given to the influence of external nitrogen and light conditions on composition kinetics. The primary species studied in this thesis is *Chlorella vulgaris* for varying nitrogen load and *Scenedesmus obliquus* for varying light flux. Biochemical measurements on *S. Obliquus* for different light conditions were reported and compared with the simulation model. Finally, trial experiments on the effect of glucose relative to a photosynthetic control on algal growth were also performed on *Nannochloropsis oculata* and *Tetraselmis Chuii.*

A review of algal composition modelling was carried out to assess the current gap in modelling functional biomass, starch and TAGs/lipids as a function of light and extracellular nitrogen. It was found that batch and fed batch studies simulated the algae as being composed of only two fractions, lipids and functional biomass. However, the

starch fraction was omitted in most published work, although it is a major component of algae and possesses different kinetic behaviour from lipids and functional biomass. Nevertheless, there were some studies of continuous cultures on starch, TAGs and functional biomass, but to date there are no batch mode studies on photosynthetic cultures that model starch, TAGs and functional biomass simultaneously.

A mathematical model of starch, TAGs and functional biomass kinetics of *C. vulgaris* was developed to elucidate the primary mechanisms of photosynthetic kinetics. This was achieved by explicitly modelling starch, TAGs and functional biomass fractions for a batch photosynthetic reactor. In addition, TAGs production due to starch glycolysis was also considered in the model. This biochemical pathway has not been previously modelled in the literature. The model was composed of six coupled ordinary differential equations and 11 secondary equations and was coded and solved in Matlab. The parameters were tuned by minimising an objective function, which was the overall relative error of the model. There were 15-17 biological fitting parameters in the model depending on the limiting conditions affecting starch glycolysis. Four sets of limiting conditions were identified for modelling starch glycolysis and TAGs synthesis from photosynthesis.

The first study carried out was the analysis of the influence of extracellular nitrogen on composition kinetics. The nitrogen quota and light dependant photosynthetic activity were found to be primary regulators for starch-TAG kinetics in *C. Vulgaris*. In contrast metabolite saturation, C-N uptake ratio and starch concentration did not have a significant impact on composition kinetics.

Once the influence of nitrogen concentration was investigated, the following step was to test if starch glycolysis was dictating composition kinetics under the influence of

moderate to high light intensities. In order to model the influence of carbon uptake for different light fluxes, an exponential decay function, in contrast to the Poisson's single hit model used in the previous chapter for *C. vulgaris,* was utilised. The species that was modelled was *S. obliquus* and the light intensities tested were 200 µmols/m^2.s and 1000 µmols/m^2.s. The selection of these conditions was due to the existence of experimental literature values that allowed the validation of the model. The model predicted the experimental data with an average percentage error of 10 % for 200 µmols/m^2.s and 17 % for 1000 µmols/m^2.s. The only discrepancy between the model and experiment was for starch concentration for 1000 µmols/m^2.s light intensity. The origin of this discrepancy was attributed to not accounting for metabolite catabolism of TAGs. This occurred at high light intensities because the culture may have reached a point in its growth phase, where substrate catabolism began.

Experimental work was carried out to investigate the composition of *S. obliquus* for different nitrogen concentration and light conditions. The starch, TAGs, protein and chlorophyll contents were in good agreement with literature values and batch culture model predictions. This agreement between modelling and experiments was arguably attributed to the fact that nitrogen quota, which dictates starch, TAGs and protein kinetics, is independent of reactor running mode, i.e., batch or continuous. Preliminary experiments for mixotrophic algae were conducted at The Port Stephens Fisheries Institute (PSFI) to assess whether mixotrophic cultivation of green algae could improve yields relative to a photosynthetic control. The species that were investigated included *N. oculata* and *T. Chuii*. During the first 7 days of growth, cell densities for mixotrophic and phototrophic algae were similar. After this initial period, cell densities of mixotrophic algae were half the density of the photosynthetic culture. Bacterial contamination was the primary reason for a lack of improvement in cell density.

It was hypothesised in this thesis that starch glycolysis linked starch degradation to TAGs accumulation during nitrogen depletion. This hypothesis was tested for two different species, *C. vulgaris* and *S. obliquus* for different nitrogen and light levels. It was found that starch glycolysis could explain the kinetic behaviour of algae during nitrogen depletion and light intensities in the light limited and saturated region for batch photosynthetic studies. Currently, this has not been reported in literature models. Future studies may attempt to validate this model for species other than green algae or for different growth modes such as heterotrophy or mixotrophy using acetate as a carbon source due to its ability to inhibit bacterial growth.

Table of contents

1 Introduction 1

2 Review of the Emerging Field of Algal Composition Modelling 7

2.1 Introduction 7

2.2 Algal Growth Mode: Phototrophic, Heterotrophic and Mixotrophic Nutrition 8

2.2.1 Biomass Growth on Photosynthetic Algae 9

2.2.2 Mixotrophic Algae: Interactions between Phototrophy and Heterotrophy15

2.3 Composition Kinetics of Algae 22

2.3.1 Effect of Nitrogen on Composition Kinetics 22

2.3.2 Effect of Light on Composition Kinetics 27

2.3.3 Effect of Temperature on Composition Kinetics 30

2.4 Composition Kinetic Models 35

2.4.1 Model Mechanisms 35

2.4.2 Mathematical Models 48

2.4.3 Model Implementation 56

2.4.3.1 Error Minimisation 57

2.4.3.2 Biological Parameter Constraints 60

2.5 Conclusion and Recommendations 78

3 Model Development 79

3.1 Introduction 79

3.2 State Variable Equations 81

3.3 Equations for Secondary Variables 83

3.4 Model Implementation & Validation 87

3.5 Conclusion 91

4 Modelling Starch, TAGs and Functional Biomass Kinetics as a Function of Nitrogen Concentration 93

4.1 Introduction 94

4.2 Model Development 95

4.2.1 Proposed Mechanism and Model Assumptions 95

4.2.2 Modelling the Limiting Factors Affecting TAGs Production from Photosynthesis and Starch Glycolysis 98

4.2.3 Elemental Mass Balance Validation 101

4.2.4 Model Selection 101

4.2.5 Input Parameters 102

4.3 Results and Discussion 104

4.3.1 Nitrogen Concentration, Nitrogen Quota, Chlorophyll Content, and Functional Biomass Concentration Results 109

4.3.2 Prediction of Starch-TAGs Kinetics Based on the AIC Criterion 110

4.3.3 Comparison with Literature 113

4.3.4 Testing Model Limitations 115

4.4 Conclusion and Future Recommendations 119

5 Modelling the Effect of Light Intensity on the Composition Kinetics of *Scenedesmus Obliquus* 121

5.1 Introduction 121

5.2 Model Implementation 122

5.3 Results and Discussion 125

5.3.1 Nitrogen and Chlorophyll kinetics 129

5.3.2 Functional Biomass Kinetics 131

5.3.3 Starch and TAGs Kinetics 132

5.3.4 Intracellular Carbon Flux Analysis 136

5.3.5 Comparing the Effect of Light Intensity on Composition Kinetics 140

5.4 Conclusion and Recommendations 143

6 Trial Experiments on Photosynthetic and Mixotrophic Algae 145

6.1 Introduction 145

6.2 Materials and Methods for Experimental Design 146

6.2.1 Materials 146

6.2.1.1 Stock Solutions for Starch Analysis 148

6.2.1.2 Cell Lysis Buffer Solution for Protein Analysis 149

6.2.1.3 Stock Solutions for TAGs Measurement 150

6.2.2 Experimental Setup 150

6.2.3 Culturing Procedure 152

6.2.3.1 Sterilisation of the Reactor Vessel 152

6.2.3.2 Inoculation of Experimental Reactors 152

6.2.3.3 Experimental Reactor Operation: CO_2 and Light 153

6.2.3.4 Cell Counting 154

6.2.4 Biochemical and Nutrient Measurement Experimental Design 154

6.2.4.1 Total Biomass Analysis 154

6.2.4.2 Glucose 155

6.2.4.3 Nitrates Analysis 157

6.2.4.4 Total Chlorophyll 157

6.2.4.5 Protein Analysis 158

6.2.4.6 Starch Analysis 159

6.2.4.7 TAGs Analysis 162

6.3 Preliminary Experiment Results and Discussion 164

6.3.1 Biochemical Analysis 165

6.3.2 Batch Model Predictions for 500 µmols/m^2.s and 0 g N/m^3 170

6.3.3 Bioreactor Mass Transfer Optimisation 172

6.3.4 pH Measurement of the Cultures 173

6.3.5 Phototrophic and Mixotrophic Culture Trials 174

6.3.6 Comparison between Experimental and Model Prediction for Biomass Yield…….....178

6.4 Conclusion and Recommendations 179

7 Conclusion and Recommendations 181

8 References 188

9 Appendices 214

9.1 Elemental Mass balances 214

9.1.1 Case Study on Literature Model 214

9.1.2 Carbon Balance 217

9.1.3 Nitrogen Balance 219

9.1.4 Oxygen Balance 220

9.1.5 Hydrogen 221

9.2 Additional Experimental work 224

9.2.1 Further Preliminary Results on Photosynthetic and Mixotrophic Cultivation 225

List of figures

Figure 1.1 Algae bio-refinery concept showing the growth modes of algae, reactor types available for growth, processing methods and products that can be produced from internal metabolites such as starch, TAGs and functional biomass/proteins 2

Figure 2.1 Growth response of *C. vulgaris* to light intensity. It follows the typical response curve including a linear light limited region, saturated region and .. photo-inhibited region (Yeh et al., 2010). 10

Figure 2.2 Functional biomass-lipid mechanism used by literature models. The dotted lines indicate processes or compounds that differ between the papers 36

Figure 2.3 Mechanism separating the primary fractions as the functional biomass and storage molecules, which contains the carbohydrates and lipids. The dotted lines indicate processes or compounds that differ between the papers (Adesanya et al., 2014; Kunikane & Kaneko, 1984) 39

Figure 2.4 A mechanistic model for a non-steady state continuous system where carbon is assumed to first produce sugars/carbohydrates before being converted to functional biomass and lipid (Mairet et al., 2011) 42

Figure 2.5 three fraction mechanism depicting carbon partitioning into starch, TAGs and functional biomass (Klok et al., 2013; Zhang et al., 2014) 44

Figure 3.1 Plot of the final relative error between the experimental and simulated state variables as a function of the magnitude of the parameter multiplier. 90

Figure 4.1 Proposed biological mechanism for composition kinetics within an algal cell. Modelled processes based on literature equations are represented by solid black arrows and the contribution of this study by dashed arrows. 96

Figure 4.2 A comparison of the prediction of extracellular nitrogen uptake (A), functional biomass concentration (B), chlorophyll content (C), TAGs concentration (D),

starch concentration (E), total biomass concentration (F) and nitrogen quota (G) for LCs 1-4 under an initial nitrogen (as nitrates) concentration of 25 g N/m^3 based on literature experimental data (Adesanya et al., 2014). 106

Figure 4.3 Comparison of the prediction of extracellular nitrogen uptake (A), functional biomass concentration (B), chlorophyll content (C), TAGs concentration (D), starch concentration (E), total biomass concentration (F) and nitrogen quota (G) for LCs 1-4 under an initial nitrogen concentration (as nitrates) of 125 g N/m^3 based on literature experimental data (Adesanya et al., 2014). 107

Figure 4.4 Comparison of experimental data of TAGs and model prediction based on fitting parameters of 25 g N/m^3 for microalgal growth (Breuer, Lamers, Martens, Draaisma, & Wijffels, 2012). 114

Figure 4.5 Simulated concentration of functional biomass (A), TAGs (B), starch (C) and total biomass (D) over 150 days for LCs 4, tested at initial nitrogen concentrations of 25 g N/m^3 (dashed lines) and 125 g N/m^3 (solid lines). 116

Figure 4.6 Effect of minimum and maximum starch and TAGs content on functional biomass (A), TAGs (B), starch (C) and total biomass (D) concentration up to 150 days for LCs 4, tested at initial nitrogen concentrations of 25 g N/m^3 (solid lines) and 125 g N/m^3 (dashed lines). 118

Figure 5.1 Plots of model and experimental data at an initial nitrogen concentration of 0 g N/m^3 and incident light flux of 200 µmols/m^2.s for *S. Obliquus*. The data was collected from Breuer et al., (2015). 128

Figure 5.2 Plots of model and experimental data at an initial nitrogen concentration of 0 g N/m^3 and incident light flux of 1000 µmols/m^2.s for *S. Obliquus*. The data was collected from Breuer et al., (2015). 129

Figure 5.3 Plot of the starch to TAGs fraction against time for *S. Obliquus* at an initial nitrogen concentration of 0 g N/m^3 and light fluxes of 200 and 1000 µmols/m^2.s respectively (Data from Breuer et al., 2015) 136

Figure 5.4 Model predicted carbon fluxes of *S. Obliquus* at 200 µmols/m^2.s and 1000 µmols/m^2.s where *p* is the photosynthetic rate (g C/m^3.d), S_g is the starch glycolysis rate (g C/m^3.d), T_P is the TAGs synthesis rate from photosynthetic fixed carbon (g C/m^3.d), S_P is the starch synthesis rate from photosynthesis (g C/m^3.d) and F_P is the rate of functional biomass synthesis (g C/m^3.d) 138

Figure 5.5 Plots of the composition and total biomass of *S. obliquus* as a function of time and light intensity. Light intensities plotted were 40 µmols/m^2.s (solid line), 200 µmols/m^2.s (triangles) and 1000 µmols/m^2.s (squares). The light data for light fluxes of 1000 µmols/m^2.s and 200 µmols/m^2.s were measured data whilst . 40 µmols/m^2.s is a model prediction 141

Figure 6.1 Bioreactor setup for culturing algae during the trial experiments at PSFI .. 151

Figure 6.2 Algal stock cultures shown for *N. oculata* 153

Figure 6.3 Plot of the chlorophyll content as a percentage of total biomass for a number of samples of *S. Obliquus*. The results show a tight fit for chlorophyll measurements for all samples. 166

Figure 6.4 Protein content of biomass for a number of samples. The varying protein content amongst sample number is most likely due to different nitrogen loads on the continuous cultures of *S. obliquus*. 167

Figure 6.5 Plot of the starch content as a percentage of total biomass for a number of different samples of experimental runs of *S. obliquus*. 168

Figure 6.6 Plot of the TAGs and polar lipids of *S. obliquus*. Run number 1-3 was for 0.1384 g N/l.d nitrogen load, runs 4-6 for 0.1038 g N/l.d nitrogen load and runs 7-9 for 0.0519 g N/l.d nitrogen load. 169

Figure 6.7 starch, TAGs, proteins and chlorophyll content as a percentage of total biomass for a light flux of 500 µmols/m^2.s and initial nitrogen concentration of 0 g N/m^3. The results correspond to *S. Obliquus*. 170

Figure 6.8 Comparison of the effect of gas flow rate on algal growth *N. oculata*. Approximately 2 % CO_2 (v/v) enriched air was passed through the cultures. The total flow rate was 0.6 LPM for reactors 1-3 and 0.4 LPM for reactors 4-6. 173

Figure 6.9 The pH of the photosynthetic cultures of *N. oculata* operating at 0.4 and 0.6 LMP did not change significantly. 174

Figure 6.10 Growth of *N. Oculata* on 2 g/l glucose added from day 0 for three of the reactors. The culture where glucose was added had half the cell number yield after 7 days. 174

Figure 6.11 Comparison of photosynthetic and mixotrophic *T. Chuii* under the effect of 0 and 3 g/l of glucose in triplicate. There was no significant difference in algal growth as a function of glucose load. 176

Figure 6.12 Comparison of the photosynthetic yield of *N. oculata* (triangles), *T. chuii* (circles) experiments with modelling for *C. vulgaris* at 25 g N/m^3 (solid line) and *C. vulgaris* at 125 g N/m^3 (dotted line). 178

Figure 9.1 The composition of the algal biomass is divided into functional biomass (F) and storage molecules (St) for a literature system (Adesanya et al., 2014). The carbon flow diagram shows inputs as photosynthetic fixation and heterotrophic carbon uptake. Functional biomass accumulation is regulated by a linear nitrogen quota term whilst

carbon loss from the system is from the sum of storage molecule, respiration and carbon quota (non-storage carbon) generation rate.....214
Figure 9.2 Diagram depicting the carbon flux and balance in algal cells. 217
Figure 9.3 Mass balance of the nitrogen in the system. 219
Figure 9.4 Example of elemental mass balance for 25 mg N-NO_3^-/l for batch culture for LCs 4. The closed circles show accumulation rate of the elemental species whilst the open circles show the difference between the generation and consumption rate of the species. For the model to be consistent in terms of conservation of mass, the accumulation rate must equal the difference between generation and consumption. ...222
Figure 9.5 Example of elemental mass balance for 125 mg N-NO_3^-/l for batch culture for LCs 4. The closed circles show accumulation rate of the elemental species whilst the open circles show the difference between the generation and consumption rate of the species. For the model to be consistent in terms of conservation of mass, the accumulation rate must equal the difference between generation and consumption. ...223
Figure 9.6 Cell number of *C. Muelleri* are within error regardless of whether it is under photosynthetic or mixotrophic growth. 0, 2 g/l of glucose was added to the cultures to determine whether addition of glucose had any effect. 225
Figure 9.7 *P. lutheri* was grown in 500 ml reactors for 8 days under photosynthetic and mixotrophic (3 g/l glucose) conditions. 226
Figure 9.8 *P. lutheri* growth in 1 L reactors. Addition of 2 g/l of glucose did not improve yield compared with photosynthetic algae.....226
Figure 9.9 plot of aerated photosynthetic algae and non-aerated mixotrophic *T. Chuii*. Mixotrophic cultures did not grow as fast as photosynthetic algae. 227

Figure 9.10 Comparison of *Isochrysis* sp. growth as a function of glucose load (0, 2, 4 g/l). Addition of glucose reduced algal growth possibly due to metabolite excretion or inhibition by bacterial proliferation. 227

Figure 9.11 growth of *P. lutheri* as a function of glucose load (0, 2 g/l of glucose) in 1 L reactors with a 500 ml working volume.....228

List of tables

Table 2.1 Report of the optimum temperature for growth of different species of algae. 15

Table 2.2 Comparison of photosynthetic, heterotrophic and mixotrophic biomass yield and comparison of apparent mixotrophic yield with expected yield if mixotrophy operates via independent additive phototrophy and heterotrophy. In the table, enriched aeration means the system is not CO_2 or O_2 limited. If there is, no enriched aeration the system may likely become oxygen or carbon limited depending on growth mode 20

Table 2.3 Kinetic expressions for modelling composition of the functional biomass-lipids mechanistic model approach 49

Table 2.4 kinetic equations describing functional biomass-storage molecule behaviour 50

Table 2.5 Kinetic expressions defining functional biomass, carbohydrates and lipids behaviour 51

Table 2.6 Reported literature values of common model parameters with proposed constraints 62

Table 2.7 Literature values of the chlorophyll specific absorptivity. All values are model fitted unless stated otherwise in the operating details 63

Table 2.8 Model fitted maximum and minimum nitrogen quota values used in composition and nutrient-kinetics models 66

Table 2.9 Model fitted values of the maximum specific nitrogen uptake rate. 68

Table 2.10 Estimates of the half saturation coefficients. Values are fitted unless stated otherwise 70

Table 2.11 Fitted values of the maximum chlorophyll to nitrogen ratio 71

Table 2.12 Model fitted values of the average quantum yield 72

Table 2.13 Literature values of the saturation light intensity of photosynthetic algal cultures 75

Table 3.1 Parameter sets and relative error for the simulation for the initial un-optimised parameter guess, the optimised parameter set for the initial guess and the parameter set of the minimum final error from 11 different initial guesses. 91

Table 4.1 Sets of equations for synthesis of TAGs from photosynthetic fixed carbon and starch glycolysis. 98

Table 4.2 Reported state variables and their initial values. The initial value of the nitrogen quota was determined by estimation, because no measured data were found. 103

Table 4.3 The initial parameter estimates to be optimized by the MATLAB code. 103

Table 4.4 Best-fit parameter sets for 25 g N/m^3 and 125 g N/m^3 for all Starch-TAG kinetic sets of equations. Parameter values as reported in the literature are also shown. 108

Table 4.5 Comparison of four different kinetic sets of equations for Starch-TAG composition under two initial nitrogen concentrations (25 g N/m^3 and 125 g N/m^3)... 111

Table 5.1 The initial conditions of state variables for the modelling of algae cultivation 123

Table 5.2 The input parameters tuned by the minimisation of the objective function and manual input. These parameters were the input for both experimental light intensities of 200 and 1000 µmol.m^{2}s. 124

Table 5.3 Parameter estimates from the fitting the model to the two experimental data sets for light intensities of 200 and 1000 µmol.m^{2}s. The parameters estimate for analysing the prediction of the 40 µmol.m^{2}s case 126

Table 6.1 Concentration of the different compounds in 1 l of culture media composed of estuarine water and f/2 nutrient media. 147

Table 6.2 Volumes of BSA and lysis buffer required to make the standard curves for protein analysis..... 158

Table 6.3 Experimental operating conditions for biomass samples used for starch measurement. 160

Table 6.4 Volumes of standard and RO water required to obtain the required glucose concentration. 161

Table 6.5 Relative nitrogen loads used for cultivation of continuous mode *S. obliquus* for TAGs analysis. 162

Table 9.1 Variables affecting trial experiments on green algae..... 224

Nomenclature

Symbol	Parameter	Units
a	Exponent modifying specific photosynthetic rate	none
$A_{1,b}$	Absorbance of the blank at 340 nm at before addition of hexokinase	none
$A_{1,s}$	Absorbance of the solution before addition of hexokinase at 340 nm	none
$A_{2,b}$	Absorbance of the blank at 340 nm with hexokinase added	none
$A_{2,s}$	Absorbance at 340 nm of sample containing glucose-6-phosphate	none
$A_{652.4}$	Absorbance of chlorophyll at 652.4 nm	none
$A_{665.2}$	Absorbance of chlorophyll at 665.2 nm	none
b	Maintenance respiration rate of algae	g C/g F.d
B	Chlorophyll content	g Chl/g F
c	Exponent modifying phosphorus to nitrogen quota	none
C	Carbon concentration	g C/m^3
C_c	Carbon consumption rate	g C/m^3.d

C_g	Carbon generation rate	g C/m^3.d
$C_{glucose}$	Glucose concentration	g Glucose/m^3
Chl_a	Chlorophyll a content	g Chl/m^3
Chl_b	Chlorophyll b content	g Chl/m^3
Chl_{tot}	Total chlorophyll content	g Chl/m^3
C_i	Consumption rate of elemental species *i*	g i/m^3.d
C_n	Nitrogen content	g N/g X
C_p	Phosphorous content	g P/g X
C_O	Organic carbon concentration	g C/m^3
d	Path length for light absorption	m
D	Dilution rate	/d
D_F	Chlorophyll dilution factor	g/m^3
DW	Dry weight	g/m^3
E_k	Saturation light intensity	µmols/m^2.s
$f_{s,min}$	Minimum starch content of biomass	g S/g X
$f_{T,max}$	Maximum TAGs content of biomass	g T/g X
F	Functional biomass concentration	g F/m^3
$\dot{G}_C$	Glucose consumption rate	g Glucose/m^3.d

$\dot{G}_G$	Glucose generation rate	g Glucose/m^3.d
G_i	Generation rate of elemental species *i*	g n/m^3.d
h	Light path	m
i	Iteration number	none
I	Average culture light intensity	µmols/m^2.s
I_o	Incident light intensity	µmol/m^2 .s
k_d	Functional biomass specific decay rate	g C/g F.d
$k_{multiplier}$	Parameter multiplier	none
K	Correlating constant for lipids	g L/m^3
K_g	Half saturation constant of photosynthetic activity	g C/m^3.d
K_{gCN}	Half saturation constant for carbon fixed into TAGs from starch glycolysis	g C/g N
K_I	Half saturation constant of light	µmols /m^2.s
$K_{i,s1}$	Inhibition constant of glycine	g Glycine/m^3
$K_{i,s2}$	Inhibition constant of glucose	g Glucose/m^3
K_L	Half saturation constant for lipid production	g L/m^3
K_n	Half saturation constant of Nitrogen	g N/m^3

K_{pCN}	Half saturation ratio of C/N uptake ratio for carbon fixed into TAGs from photosynthesis	g C/g N
K_q	Half saturation of nitrogen quota content	g N/g F
$K_{S/X}$	Half saturation constant of starch glycolysis	g S/g X
K_{s_2}	Half saturation coefficient of glucose uptake	g Glucose/m^3
L	Lipid concentration	g L/m^3
L_{min}	Minimum lipid concentration for growth	g L/m^3
$\dot{L}_C$	Lipid consumption rate	g L/m^3.d
$\dot{L}_G$	Lipid generation rate	g L/m^3.d
m	number of measured state variables	none
M_g	Glucose molar mass	g/mol
MS	Multiplier step	none
n	number of experimental data points	none
N	Nitrogen concentration	g N/m^3
N_{in}	Rate of nitrogen into the algae	g N/m^3.d
p	Gross rate of photosynthesis	g C/g F.d
P_H	Prey concentration	g C/m^3
P_{max}	Maximum chlorophyll specific photosynthesis rate	g C /g Chl.d

p_n	Net rate of photosynthesis	g C/g m^3.d
p_o	Nitrogen quota mediated photosynthesis rate	g C/g Chl.d
Q_c	Carbon quota	g C/g F
$Q_{c,min}$	Minimum carbon quota	g C/g F
$Q_{H,N}$	heterotrophic nitrogen quota or status	g N/g C
$Q_{n,max}$	Maximum nitrogen quota	g N/g F
$Q_{n,min}$	Minimum nitrogen quota	g N/g F
Q_n	Nitrogen quota	g N/g F
$Q_{n/x}$	Total biomass specific nitrogen quota	g N/g X
$Q_{n/x,max}$	Maximum specific nitrogen quota per unit of total biomass	g N/g F.g X
$Q_{o,n}$	Initial nitrogen quota	g N/g F
$Q_{p/n,max}$	Maximum nitrogen to phosphorus quota	g P/g N
$Q_{p/n,min}$	Minimum nitrogen to phosphorous quota	g P/g N
$Q_{P,N}$	Photosynthetic nitrogen quota status	g N/g C
$Q_{T,N}$	Total nitrogen quota of the marine mixotrophic biomass	g N/g C
r_M	Mixotrophic growth rate	g X/m^3.d

r_{Ph}	Rate of volumetric photon absorption	mol photon/m^3.d
R	Respiration of carbon from maintenance and synthesis	/d
R_M	Respiration rate	g C/m^3.d
$RSSE$	Relative sum squared error	varies
R^2_{RSSE}	Coefficient of determination for relative sum squared error	none
S	Starch concentration	g S/m^3
s_1	Glycine concentration	g Glycine/m^3
s_2	Glucose concentration	g Glucose/m^3
S_g	Concentration of starch consumed through glycolysis	g S/m^3
S_p	Concentration of starch generated from photosynthesis	g S/m^3
S_t	Storage molecule concertation	g S_t/m^3
S_u	Sugar concentration	g S_u/m^3
t	Time	d
T	TAGs concentration	g T/m^3
T_g	concentration of TAGs from glycolysis	g T/g m^3

T_p	TAGs concentration from photosynthetic fixed carbon	g T/m^3
v	Sample volume	ml
V	Final volume of diluted sample	ml
V_H	Rate of voidage of excess matter	d
$V_{max,LC}$	Maximum lipid consumption rate	g L/m^3.d
$V_{max,LG}$	Maximum lipid generation rate	g L/m^3.d
$V_{n,max}$	Maximum uptake rate of Nitrogen	g N/g F.d
$V_{S,max}$	Maximum starch glycolytic rate	g S /g F.d
w_f	Final weight of filter plus tray plus algae	g
w_i	Initial weight of filter plus tray	g
W_{ij}	Error weight	varies
$WSSE$	weighted sum error	none
x	Sample volume	ml
X	Biomass concentration	g X/m^3
X_{max}	Maximum biomass concentration	g X/m^3
X_o	Initial biomass concentration	g X/m^3
y_{ij}	Experimental measurement of a state variable	varies

y_{ij_r}	Experimental measurement of the reference variable	varies
$\hat{y}_{ij}$	Predicted value	varies
$\bar{y}_{ij}$	Average value of the state variable	varies
$\bar{y}_{ij_r}$	Average value of the reference variable	varies
$Y_{F/C}$	Carbon to functional biomass yield	g F/g C
$Y_{F/e}$	Yield of functional biomass from electrons	g F/mol electron
$Y_{F/G,n}$	Nitrogen specific yield of functional biomass from sugars	g F/g G.g N
$Y_{F/L,n}$	Nitrogen specific yield of functional biomass from lipids	g F/g L.g N
$Y_{F/S}$	Storage molecule to functional biomass yield	g F/g St[3]
$Y_{S/e}$	Electron to starch yield	g S/mol electron
$Y_{T/e}$	Electron to TAGs yield	g T/mol electrons
$Y_{L/C}$	Carbon to TAGs yield	g L/g C
$Y_{L/G,n}$	Nitrogen specific yield of lipids from sugars	g L/g G.g N
$Y_{L/X}$	Lipid yield from biomass	g L/g X

$Y_{Ph,e}$	Minimum quantum requirement of electron release from water	mol photons/mol electron
$Y_{S/C}$	Carbon to starch yield	g S/g C
$Y_{St/C}$	Carbon to storage molecule yield	g
$Y_{T/C}$	Carbon to TAGs yield coefficient	g T/g C
$Y_{T/S}$	Starch to TAGs yield coefficient	g T/g S

Greek symbols

α	Optical cross section of algae	m^2/g Chl
Δ_{blank}	Absorbance difference for blank	none
$\Delta_{glucose}$	Absorbance difference for glucose	none
Δ_{sample}	Absorbance difference for sample	none
ε	A coefficient dependent on the nitrogen quota and photosynthetic rate	g Chl/m^3.g F
ε_a	Extinction coefficient	L /mol.cm
θ_{max}	Maximum nitrogen specific chlorophyll concentration	g Chl/g N

κ	Coefficient dependent on the nitrogen quota and photosynthetic rate	g Chl/g N
λ_j	Scaling factor	varies
μ	Specific growth rate	/d
μ_{max}	Maximum specific growth rate	/d
$\mu_{c,max}$	Maximum gross specific carbon fixation rate	g C/g F.d
μ_f	Specific functional biomass synthesis rate	g F/g F.d
$\mu_{f,max}$	Maximum functional biomass synthesis rate	g F/g F.d
ρ_{gf}	Functional biomass specific uptake rate of glucose	g C /g F.m^3.d
ρ_n	Nitrogen uptake rate	g N/m^3.d
$\rho_{n,f}$	Functional biomass specific nitrogen uptake rate	g N /g F.d
$\rho_{n,r}$	Reference nitrogen uptake rate	g N /m^3.d
$\rho_{n,x}$	Biomass specific nitrogen uptake rate	g N /g X.m^3.d
ρ_s	Uptake rate of starch	g S/m^3.d
ρ_{s2}	Uptake rate of glucose	g Glucose/m^3.d
ρ_T	Rate of TAGs generation	g T/m^3.d
σ_j	Standard deviation of measured variable	none

σ_N	Slope of electron yield from nitrogen	mol electron/g N
σ_S	Slope of starch	mol starch/m^3
φ	Quantum yield	g C/μmol photon

Subscripts

max	Maximum
min	Minimum

1 Introduction

Microalgae are eukaryotic organisms that grow primarily via photosynthesis. This process involves utilising light as the energy source, which splits water through photolysis to produce electrons, protons and oxygen gas. The protons and electrons are used to reduce CO_2 into sugar intermediates that can be utilised for energy or synthesis of new biomass (Subramanian et al., 2013). Algae may also grow via heterotrophy and mixotrophy (Katarzyna & Facundo-Joaquin, 2004). Heterotrophy uses oxygen and organic carbon as an energy source. Cellular energy is produced via aerobic respiration and CO_2 is expelled as a waste product. Mixotrophy is a combination of both photosynthesis and heterotrophy. It involves using both light and sugars as an energy source whilst CO_2 and sugars are utilised as the carbon source. Oxygen and CO_2 are cycled within the cells as they are both waste products and substrates for the respective photosynthetic and heterotrophic pathways (Yanming Wang, Rischer, Eriksen, & Wiebe, 2013).

Recently, increasing CO_2 emissions from the burning of fossil fuel derived commodities has contributed to an enhancement of the greenhouse effect causing global climate change. Land clearing for biofuels has also resulted in habitat destruction and competition with food crops. Additionally, finite quantities and increasing demand of commodities such as animal food and petroleum-derived products have resulted in scarcity and price increases. Algae cultivation has been suggested as an alternative platform for the production of products shown below in Fig. 1.1 by processing internal metabolites such as triacylglycerides (TAGs), starch and proteins. TAGs can be utilised for biodiesel production, lubricants and cooking oil, starch can be used for the production of bioplastics and bioethanol whilst proteins (functional biomass) can be converted into animal feed, emulsifiers and food additives (Foley, Beach, & Zimmerman, 2011).

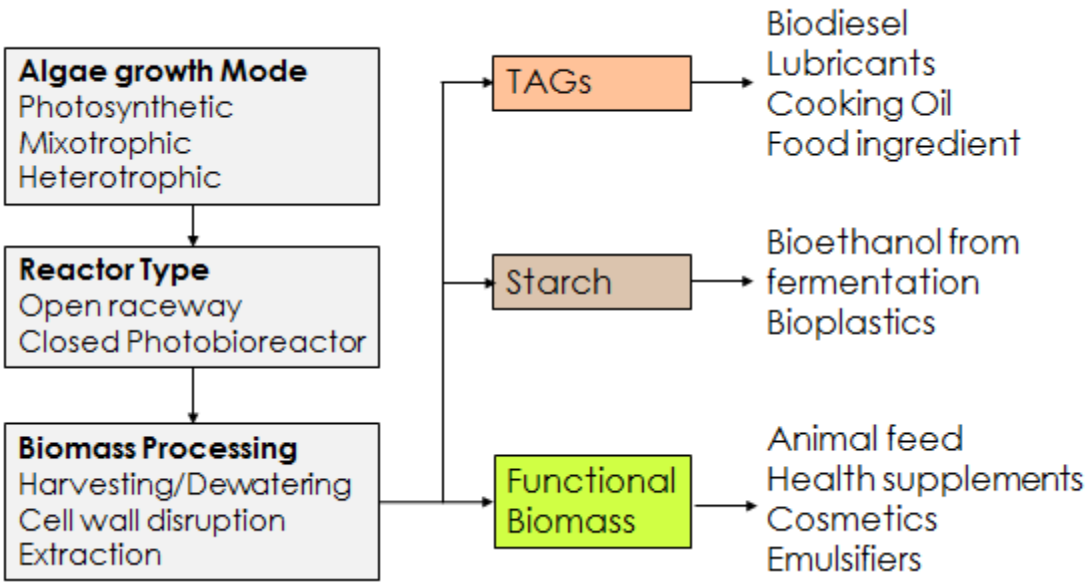

Figure 1.1 Algae bio-refinery concept showing the growth modes of algae, reactor types available for growth, processing methods and products that can be produced from internal metabolites such as starch, TAGs and functional biomass/proteins

Currently, on a commercial scale, photosynthetic algae are predominately grown in raceway ponds for nutraceutical production as health supplements and antioxidants (Saha & Murray, 2018). There has also been interest in using algae to treat wastewater and produce biodiesel at a pilot plant scale. Typical biomass concentration in ponds ranges from 0.1-1 g/l with areal productivity ranging from 10-30 g/m^2.d (Lee, Jo, Shin, & Lee, 2014; B. K. Park, 2013; J. Park, Craggs, & Shilton, 2011). These pond reactors have limitations on biomass yield due to contamination by bacteria, poor light and nutrient optimisation, and, fluctuating light and temperature. Raceway ponds are shallow, only 0.3 m in depth. Therefore, an increase in biomass concentration will limit the penetration depth of light, thus, limiting biomass growth. For instance, a biomass concentration of only 0.3 g/l will limit light penetration to only 15 cm. Thus, the ponds require mixing to ensure that cells can be transported to the light active layers while preventing settling (J. Park et al., 2011). However, this would still meant that half of the pond volume is dark and unproductive.

In the literature (J. Park et al., 2011) maximum theoretical photosynthetic conversion of sunlight to biomass for an open raceway pond under climatic conditions for a study in New Zealand was estimated to be only 2.5 % corresponding to 27 $g/m^2.d$. However, algal cultures in Hawaii reached up to 40 $g/m^2.d$ with an average of 30 $g/m^2.d$ due to more conducive climatic conditions (Edward A Laws, Taguchi, Hirata, & Pang, 1988). This is much lower than the theoretical conversion of light to biomass for a completely optimised system at about 11-12 % (B. K. Park, 2013).

Low efficiency has limited production to high value products such as health supplements rather than the production of low value animal feeds, plastics and fuels. This limitation of high value products is due to low biomass yield and poor optimisation of growth conditions to specific biomolecules.

A low biomass yield is usually due to suboptimal light conditions and poor nutrients. As the biomass grows, light penetration decreases, reducing the growth rate of algae towards the bottom of the ponds. To solve this issue, tubular photobioreactors in which the light path is smaller than in open raceway ponds have been designed.

Closed tubular photobioreactors growing outdoors have improved productivity to 47 $g/m^2.d$ with respect to ~27-30 g/m^2d usually encountered in raceway ponds. This is due to an increase by a factor of 1.5 in the photosynthetic conversion efficiency. In addition, pilot studies using closed tubular photobioreactors have produced an order of magnitude higher biomass density than open ponds at 2-8 g/l (Ozkan, Kinney, Katz, & Berberoglu, 2012). However, the operating costs of these types of photobioreactors are at least twice as high as open raceway ponds due to greater energy demand and capital costs (Jonker & Faaij, 2013).

In addition, light is only available for a limited time of day and its flux ranges from light limited to photo-inhibitory. This cyclical variation in light affects not only biomass

production but also composition kinetics and thus, and the possibility of producing specific value-added products.

The effect of CO2 on algae composition has been extensively studied (Salih, 2011; S. P. Singh & Singh, 2014). A culture of *Euglena gracilis* grew fastest at 5 % CO_2 (v/v), but stopped growing at CO_2 volume percentages above 45 %. This demonstrates that some species of algae can tolerate high CO_2 concentrations. However, it is not known if this inhibition above 45 % (v/v) was due to pH inhibition of CO_2 substrate inhibition (Y. Nakano & Takenaka, 1996). Another downside to increasing CO_2 volume percentage is that the efficiency of CO_2 sequestration reduces. For instance, a study on *C. vulgaris* found that when the CO_2 concentration was at 0.12 % (mol/mol) 26 % of the incoming CO_2 was sequestered into biomass. It was also found that mass transfer was optimised at this concentration with no further increases in biomass growth above this concentration. This resulted in a reduction in the CO_2 sequestration efficiency when the mol percent of CO_2 increased to 0.325 and 1.45 % to 9.7% and 2.1% (Langley, Harrison, & Van Hille, 2012).

Generating more biomass requires additional micronutrients with the most important being nitrogen. Nitrogen concentration in the system has a significant impact on biomass as well as composition kinetics, with all known composition models incorporating the effect of this variable on kinetics (Adesanya, Davey, Scott, & Smith, 2014; Packer et al., 2011; Yoo, Kim, & Lee, 2014). Nitrates are a common nitrogen source that increases the pH upon consumption. This can be controlled by CO_2 addition, which acts as a buffer. Although nitrogen can be controlled better than light, it has a significant influence on the yield of proteins, starch or TAGs.

Thus, to maximise productivity of algal metabolites two variables will be investigated on composition kinetics or biomass kinetics in this thesis: nitrogen load and light flux. As

modelling of starch, TAGs and functional biomass is novel for batch photosynthetic cultures new biological processes and mechanisms must be considered. The primary biological process, hence the primary contribution of this thesis, is the development and validation of starch glycolysis to TAGs. The modelling of separate starch and TAGs fractions also involves other relevant starch-TAG kinetic expressions such as separate expressions for the conversion of photosynthetically fixed carbon into starch or TAGs, respectively. Different species of algae respond differently, in terms of composition kinetics, to variations in light intensity and nitrogen load. Therefore, this thesis will validate the proposed mechanism for starch-TAGs kinetics for two different species of algae *C. vulgaris* and *S. obliquus*.

The aim of this work will be to simulate the starch, TAGs and functional biomass as a function of nitrogen concentration and light intensity on algal biomass productivity relative to photosynthetic cultures. This was achieved in the following thesis chapters:

1. This chapter contains the introduction to the thesis.
2. Literature review on photosynthetic, heterotrophic and mixotrophic composition models to gain insight into current progress and limitations in light and nitrogen regulated composition kinetics.
3. Chapter 3 contains the general model development for batch photosynthetic cultures
4. Chapter 4 presents the analysis of the influence of nitrogen concentration on photosynthetic algae. To achieve this objective, four sets of equations to model starch glycolysis were considered. The experimental data for *C. Vulgaris* from Adesanya et al. (2014) was utilised to validate the model. In addition, the model parameters were further utilised to validate experimental results for *S. Obliquus.*
5. This chapter presents the analysis of the influence of light intensity on algae composition. The model was tested against experimental results for *S. obliquus*.

6. Trial experiments on mixotrophic algae to compare yields with photosynthetic controls for *N. oculata* and *T. chuii*. This is to initially determine whether mixotrophic growth mode can increase algal yields before proper experiments begin and data is collected for modelling. The chapter will also include results of biochemical analysis trials for *S. obliquus*.
7. Chapter 7 presents the conclusions and suggestions of future work.

2 Review of the Emerging Field of Algal Composition Modelling

2.1 Introduction

Algae are eukaryotic organisms that may grow via phototrophy, heterotrophy or mixotrophy (Katarzyna & Facundo-Joaquin, 2004). Phototrophy utilises light as the energy source and CO_2 as the carbon source and heterotrophy oxidises organic carbon as an energy and carbon source. Cellular energy, in heterotrophy, is produced via aerobic respiration and CO_2 is expelled as a waste product. Mixotrophy is a combination of both photosynthesis and heterotrophy. Mixotrophy involves using both light and sugars as an energy source whilst CO_2 and sugars are the carbon source. Oxygen and CO_2 are cycled within the cells as they are both waste products and substrates for the respective photosynthetic and heterotrophic pathways (Y. Wang et al., 2013).

These three modes of growth involve different biochemical processes, which result in different biomass production (Baroukh, Turon, & Bernard, 2017; Wen et al., 2019). To understand biomass production, numerous models for the different growth modes exist in the literature (Adesanya et al., 2014; De la Hoz Siegler Jr, 2011; Ketheesan & Nirmalakhandan, 2013; Packer et al., 2011; Yoo et al., 2014). Most of the models do not consider the composition of the algae, such that biomass is directly related to environmental conditions without considering the production of biomolecules such as protein (functional biomass), lipids and starch. Some other models consider the production of storage molecules such as functional biomass and lipids (De la Hoz Siegler, Ben-Zvi, Burrell, & McCaffrey, 2011; Packer et al., 2011). The importance of these models arises from the fact that lipids such as TAGs can be converted into biofuels, carbohydrates such as starch into bioethanol and functional biomass into animal feed. Nevertheless, there are limited steady state models that independently simulate functional biomass, lipids and carbohydrates (Klok et al., 2013). In

addition, there is no comparison between the predictions of the different models. Such predictions would be of practical significance as composition models attempt to model the different components of algae that are converted into value added products.

This chapter reviews the extant literature on algal composition modelling, which facilitates an assessment of recent progress made in the simulation of functional biomass/proteins, starch and lipids/TAGs as a function of light and nitrogen. The review covers both batch and continuous mode models. The review begins with a review of the effect of different parameters, such as nitrogen light and temperature on photosynthetic biomass growth. This is then compared with mixotrophic algae growth, which has the potential to improve yields relative to photosynthetic cultures. An analysis of the effect of nitrogen, light and temperature on the algal composition kinetics is then carried out. The review then analyses the different aspects of mathematical composition modelling such as different mechanistic models of starch, TAGs and functional biomass. This is followed by comparison of kinetic expressions for algal composition, which is based on the mechanistic models. The next step in the modelling process to be reviewed is the objective function minimisation techniques, parameter validation by comparing with constraints and literature parameter values and finally mass balance validation.

2.2 Algal Growth Mode: Phototrophic, Heterotrophic and Mixotrophic Nutrition

The most common way to cultivate algae is via photosynthetic means with almost 36 000 papers on photosynthetic algae in Elsevier journals. On the other hand, heterotrophic algae have 14 000 search results and mixotrophic algae have just over 2500 search results. Mixotrophy is of note as it can significantly increase photosynthetic biomass yields to be at least 50 % greater (Adesanya et al., 2014). Increased biomass yields correspond to increased

yield of value-added products from algae, hence economic viability of algal biorefinery plants. Heterotrophic nutrition is another growth mode that is pursued for algae cultivation (Surisetty, Hoz Siegler, McCaffrey, & Ben-Zvi, 2010). It can produce yields of greater than 100 g/l, which is about two orders of magnitude greater than photosynthetic cultures (De la Hoz Siegler, 2012). Yields of heterotrophic algae were shown to be 20-50 % less than mixotrophic yields for a variety of agricultural residues (Mitra, van Leeuwen, & Lamsal, 2012). Furthermore, heterotrophic cultures being completely reliant on biomass derived organic carbon indirectly compete with food crops and the growth of the biomass feedstock results in habitat destruction. This factor has not been considered by some life cycle analysis calculating the environmental impact of heterotrophic cultures in comparison to phototrophic cultures (Smetana, Sandmann, Rohn, Pleissner, & Heinz, 2017). Phototrophs on the other hand can be grown on flue gas CO_2 and sunlight making them more environmentally friendly. However, the yield of phototrophs is comparatively lower than heterotrophs as demonstrated (De la Hoz Siegler et al., 2011; Takeshita et al., 2014). Mixotrophy, on the other hand, has greater yields than phototrophy and heterotrophy and represents a compromise in environmental sustainability as its ability to grow on light reduces organic carbon demand. Therefore, it is more environmentally friendly than heterotrophic growth mode, but less sustainable than phototrophic growth mode.

Given the advantages of photosynthetic growth as well as the importance of photosynthesis on mixotrophic growth, the following two sections will review biomass production on photosynthetic and mixotrophic algae.

2.2.1 Biomass Growth on Photosynthetic Algae

There are four main parameters that modulate photosynthetic algal biomass growth in outdoor cultures: light, nitrogen, CO_2 and temperature. A typical example of a growth

response, applicable to all species of algae, to light intensity is shown below for *C. vulgaris* (Yeh, Chang, & Chen, 2010) in Fig. 2.1.

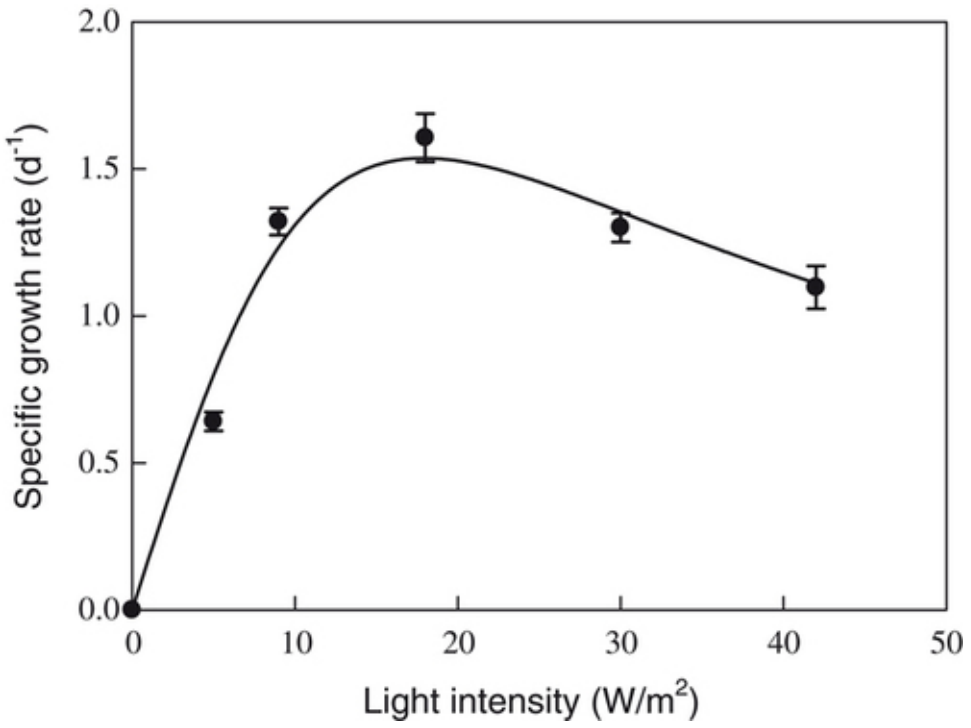

Figure 2.1 Growth response of *C. vulgaris* to light intensity. It follows the typical response curve including a linear light limited region, saturated region and photo-inhibited region (Yeh et al., 2010).

The growth of algae at low light intensities shows a linear relationship between specific growth and light intensity. This is because at low light intensity, carbon fixation is limited by light absorption (Sforza, Simionato, Giacometti, Bertucco, & Morosinotto, 2012). In the light limited region, the rate of electron transport for water photolysis is equal to that of CO_2 reduction. The slope of this region is normally denoted as α, which has units specific to either chlorophyll or biomass (Johan U. Grobbelaar, 2008). In this thesis α is known as the specific absorptivity of chlorophyll. Physically, this represents the specific absorption property of chlorophyll.

When light intensity increases further, the rate of electron transport and proton formation becomes uncoupled from CO_2 fixation. In this region, the rate of absorption exceeds electron production in photosystem II. This transition from light limited to light saturation can be abrupt or gradual (Leverenz, 1987). In the light saturated region, any further increase in light intensity results in no further increase in photosynthetic rate. Thus, photosynthesis reaches a maximum rate, p_{max}. In fact, after reaching this maximum value, biomass production decreases because the algae is not able to acclimate to these high light intensity values.

There are numerous ways in which photosynthetic organisms have adapted to higher light intensities to balance the kinetics of the light and dark reactions (CO_2 fixation reactions). Regulation of kinetics mainly involves controlling the light reactions where light harvesting capacity is altered by reduction of chlorophyll pigment concentration (Neidhardt, Benemann, Zhang, & Melis, 1998). Reducing pigment concentration reduces light absorption hence photosynthetic rate and harmful by-products of photosynthesis. This adaptive mechanism allows algae to grow under many different light intensities. Non-photochemical quenching is also employed to reduce the harmful effects of high light intensity. This process involves activated chlorophyll centres relaxing by releasing absorbed photon energy as heat (Müller, Li, & Niyogi, 2001). Fluorescence is another adaptive mechanism of algae. It involves excited chlorophyll centres emitting excess absorbed energy in the form of lower wavelength photon energy (Schubert, Schiewer, & Tschirner, 1989).

In the photo-inhibited region (high light intensities) microalgal specific growth rate decreases as shown in Fig. 2.1. This is due to the production of free radical oxygen species, which damage the photosynthetic apparatus. In addition, high light intensities deactivate photosystem II centres. The elevated oxygen concentrations in the cells also reduce the specificity of the rubisco enzyme to CO_2. Normally CO_2 is the favoured reactant for fixation by rubisco due to the concentration of CO_2 in the carboxyzomes, intracellular compartments

where carbonic anhydrase converts dissolved bicarbonate ions into CO_2. However, at elevated O_2 levels rubisco fixes O_2 in a process known as photorespiration, which competes with CO_2 fixation in the Calvin cycle (Spalding, 1989).

Another factor influencing photosynthetic biomass growth is short-term light-dark cycles. These cycles may be influenced by turbulence in the ponds where algal cells mix vertically in layers of water, which have decreasing light intensity as a function of greater depth. The light-to-dark ratio is dependent on the volume of reactor that is illuminated and in the dark. A higher volume of dark regions will reduce the light-to-dark ratio. The fluctuation in light intensity experienced by algae creates a flashing light effect, which is known to increase algal growth rates relative to continuous light (Kok, 1953). A study (Johan U Grobbelaar, Nedbal, & Tichý, 1996) on light-dark frequency found that when the frequency is less than 1 Hz algal photosynthetic growth rate increase exponentially with increasing frequency of light-dark cycles. A longer dark period than light period increased photosynthetic growth as well. At long light-dark frequencies, the algae became low light acclimated and at shorter light-dark frequencies algae became high light acclimated.

Nitrogen is one of the key limiting micronutrients of algal growth. The ability of algae to grow in nitrogen-limited conditions is dependent, mathematically, on the half saturation constant of nitrogen uptake. As this value decreases, the uptake of nitrogen at lower concentrations increases (J. Grobbelaar, 2004). Nitrogen limitation may be modelled by Monod or Droop kinetic expressions. Monod kinetic expressions depict algal growth as being a function of the enzyme substrate kinetics. Monod kinetics can be derived theoretically. However, not all organisms show a direct relationship between extracellular nitrogen concentration and growth rate. This is especially pertinent for algae during nitrogen-depleted conditions. In such a situation, cellular growth becomes uncoupled from nitrogen concentration. This phenomenon is better explained by the Droop model of kinetics, which

states that cell growth is dependent on intracellular nitrogen quota rather than extracellular nitrogen. The relationship between nitrogen quota and cell division is described by a linear relationship rather than a non-linear relationship as evidenced for Monod kinetics (M. Droop, 1974). Whilst the Monod expression can be derived theoretically, the Droop expression was initially derived empirically. However, it was later shown that the Droop nutrient kinetic model could be derived theoretically (Lemesle & Mailleret, 2007).

CO_2 is the key macronutrient affecting algal growth in photobioreactors. It is not only a macronutrient but also a buffering agent to maintain the pH at a relatively constant level. The half saturation constant for CO_2 is higher than for nitrogen at 0.49 µM for *Thalassiosi oceanica* (C. Y. Chen & Durbin, 1994). Whilst low and moderate CO_2 concentrations have a stimulating effect on the algal growth, excessively higher concentrations can actually inhibit algal growth. This can be due to acidification of the culture from elevated CO_2 concentrations.

A culture of *C. vulgaris* ARC1 was grown in ambient concentrations of CO_2, 6 % (v/v) and 20 % (v/v) CO_2. CO_2 uptake of 18.3 mg CO_2/d was fixed by the culture under the influence of ambient CO_2 concentrations. The culture under 6 % CO_2 fixed a greater quantity of CO_2 at 38.4 mg CO_2/d, whilst the culture under 20 % CO_2 stopped growing. The growth of algae as a function of CO_2 volume % does not follow a linear response. This may indicate that the algae saturated at a lower concentration of CO_2 than 6 %. Overall the yield of algae on enriched CO_2 was 20 times higher under a concentration of 6 % compared with ambient concentrations (Chinnasamy, Ramakrishnan, Bhatnagar, & Das, 2009). In contrast, a different study on *Chlorella* KR-1 found that the algae grew well at CO_2 concentrations up to 50 % (v/v). However, the algae stopped growing at 70 % (v/v). A reason for better growth at higher CO_2 levels may be due to the pH tolerance of this strain (Sung, Lee, Shin, & Park, 1999). For *S. obliquus* the maximum dry weight concentration of 2.3 g/l was obtained at a CO_2

concentration of 15 % (Kaewkannetra, Enmak, & Chiu, 2012). CO_2 enriched cultures of *Zygnema* yielded 1.9-38 times more biomass than cultures grown under ambient conditions.

Biomass growth can also be affected by the interaction between CO_2, oxygen and pH. Studies investigating the correlation between these factors have been carried out in the literature (Celia Y. Chen & Durbin, 1994). The primary trends observed in photobioreactors are an increase in oxygen concentration due to water photolysis from photosynthesis, which inhibits biomass. The pH also increases as more CO_2 and nitrates are consumed which reduces CO_2 losses from the medium since a higher pH favours the equilibrium to shift towards more dissolved rather than gaseous CO_2. Continuously supplying CO_2 can mitigate pH fluctuations an oxygen concentration by buffering the culture and stripping the supersaturated media of oxygen (Grima, Fernández, Camacho, & Chisti, 1999).

Temperature also has a strong effect on the growth of algae. Algal growth initially increases with rising temperature until an optimum is reached and then, decreases with increasing temperature. The decrease with rising temperature may be due to an increase in photorespiration rates in algae, where the rubisco enzyme favours the fixation of O_2 over CO_2 (Coleman & Colman, 1980). For example, a culture of *Chlorella minutissima* had a specific growth rate of 0.12 /d at 10 ºC and maximised at 0.66 /d at 30 ºC. At temperatures above 30 ºC, the growth rate of *C. minutissima* decreased. The temperature in outdoor photobioreactors varies widely due to weather patterns and absorption of solar radiation. Therefore, it is difficult to maintain optimal algal productivity, unlike heterotrophic fermentation vessels, which have temperature control. In general, the optimum temperature of algae varies from 15-30 ºC (S. P. Singh & Singh, 2015b). Table 2.1 below summarises the optimum temperature for various species of algae.

Table 2.1 Report of the optimum temperature for growth of different species of algae

Study	Species	Optimum Temperature (°C)
F. Han et al., 2013	*Chlorella pyrenoidosa*	30
D. P. Maxwell, S. Falk, C. G. Trick, & N. P. Huner, 1994	*C. vulgaris*	27
Ruangsomboon, 2012	*Botryococcus braunii*	25-30
Ruangsomboon, 2012	*B. braunii* KMITL2	32
Xin, Hong-ying, & Yu-ping, 2011	*Scenedesmus* sp. LX1	20
Evans, Niedz, & Kirkpatrick, 2008	*Haematococcus pluvialis* UTEX	27

2.2.2 Mixotrophic Algae: Interactions between Phototrophy and Heterotrophy

The metabolism and thus, biomass production, in mixotrophic algae is more complex than phototrophic systems. While light makes use of CO_2 and produce O_2, sugars consume oxygen and produce CO_2. However, there are nutrients that can be synergistically utilised by both processes, i.e. photosynthesis and heterotrophy, making the biomass yield higher than is found in photosynthetic or heterotrophic cultures. To quantify this synergistic effect, the ratio between the biomass produced from mixotrophic processes and the sum of photosynthetic and heterotrophic biomass is employed. A ratio large than one suggests synergistic effects, while a ratio smaller than one indicates inhibitory processes.

Increasing nitrogen concentration from 25 g $N\text{-}NO_3^-/m^3$ to 125 g $N\text{-}NO_3^{--}/m^3$ appears to strengthen synergistic growth for *C. vulgaris* from 5 % to 19 % greater than the additive sum of phototrophic and heterotrophic growth modes (Adesanya et al., 2014). This result has some support from steady state continuous carbon balances on *Chlorella protothecoides* showed that adding more nitrogen into the system improves the carbon to biomass yield percentage for mixotrophic cultures from 53.7 to 62.6 %. The remainder carbon was expelled as CO_2 varying from 37.8 to 32.7 % respectively. This was for a system where 95 % of carbon entered in the form of glucose and 5% was in the form of CO_2. (Y. Wang et al., 2013).

It would be expected that under extended batch studies, in general, the biomass yield be limited by the nitrogen content if there is adequate temperature, light or sugar for biomass growth. This may explain why some studies have found that mixotrophy does not yield greater than heterotrophy or may have a lower yield under similar nitrogen and glucose loads (Chojnacka & Noworyta, 2004; De la Hoz Siegler Jr, 2011). These experiments mask the greater productivity of mixotrophic biomass in the exponential phase (first few days of growth) relative to heterotrophy. In these cases, before the mixotrophic stationary phase the biomass yield is greater than heterotrophic biomass yield. However, after the mixotrophic stationary phase, heterotrophic yield approaches or even exceeds mixotrophic yield whilst the mixotrophic yield is constant or decreases due to respiration. It has also been observed, that an initial large concentration of nitrogen favours CO2 fixation through photosynthesis, whilst (C. Yang, Hua, & Shimizu, 2000) whilst heterotrophy became more dominant in the later phases, i.e., linear and stationary phases (Woodworth, Mead, Nichols, & Kolling, 2015). In contrast, low nitrogen concentration favours heterotrophy in all stages of biomass growth.

CO_2 and O_2 supplied by mixotrophic reactions can result in very high synergistic growth (Kobayashi, Kakizono, Yamaguchi, Nishio, & Nagai, 1992; Lalibertè & de la Noüie, 1993; Ogawa & Aiba, 1981; Smith, Bangert, Wilkinson, & Gilmour). The literature have shown

that in the presence of acetate and glucose and in the absence of CO_2 enriched air, the biomass yield was 1.14-7.2 greater than the additive sum of phototrophy and heterotrophy (Kobayashi et al., 1992; Lalibertè & de la Noüie, 1993; Ogawa & Aiba, 1981; Smith et al.). This is because mixotrophic algae can produce their own CO_2 and O_2 for carbon fixation via phototrophy and aerobic respiration via heterotrophy. The result is greater dissolved CO_2 and O_2 in mixotrophic cultures than in phototrophic or heterotrophic cultures. Therefore, it is possible to conclude that factors such as light, organic carbon load and nitrogen are more important than CO_2 and O_2, as they are the primary factors determining the rate of CO_2 and oxygen evolution and consumption in mixotrophic algae.

When CO_2 and O_2 are in excess simultaneously, there is less synergistic growth of mixotrophic biomass than under ambient air conditions. Therefore, the ratio between the mixotrophic and the addition of photosynthetic and heterotrophic biomass production is found to be between 0.8 and 1.5, indicating small inhibitory or synergistic effects (Chojnacka & Noworyta, 2004; Kucharoenphaibul, Limtong, & Yongmanitchai, 2014). In contrast, adding more CO_2 could inhibit mixotrophic growth due to culture acidification (Sforza, Cipriani, Morosinotto, Bertucco, & Giacometti, 2012). This inhibition has been observed for strict photosynthetic cultures when the CO_2 volume percentage is greater than 20 % for species such as *Scenedesmus* sp. (Salih, 2011). However, the inhibition threshold is lower for mixotrophic cultures, showing inhibition if the CO_2 concentration was only 5 % (v/v) due to production of additional CO_2 from consumption of organic carbon (Sforza, Cipriani, et al., 2012).

Glucose can inhibit photosynthetic carbon fixation as it reduces chlorophyll synthesis rates and chlorophyll content in mixotrophic cells (Xiong, Gao, Yan, Wu, & Wu, 2010). The chlorophyll content of mixotrophs is reported to be 20-90 % lower than phototrophs but greater than chlorophyll content of heterotrophs. Therefore, the chlorophyll content of

phototrophs was more than 90 % lower than phototrophs and could also approach undetectable levels (Bhatnagar, Chinnasamy, Singh, & Das, 2011; Cheirsilp & Torpee, 2012).

Mixotrophic algae, with its lower chlorophyll content, may be resistant to photoinhibition. This is supported by some limited work (Chojnacka & Noworyta, 2004) showing that mixotrophic growth mode was more resistant to photoinhibition at high light intensities as well as having a greater half saturation coefficient. It has also been suggested that glucose plays a protective role against light inhibition (Chojnacka & Noworyta, 2004). The protective role may be due to less absorption of light by cells since chlorophyll production is inhibited. Other reasons could be that the consumption of glucose also reduces the intracellular oxygen concentration therefore reducing the rate of competitive photorespiration, which would otherwise inhibit CO_2 fixation. This can also reduce the concentration of radical oxygen species which can be produced at higher light intensities (Chojnaka & Marquez, 2004). The result could possibly mean synergistic mixotrophic biomass yield when light intensities are above saturation.

Temperature affects the two carbon uptake pathways of mixotrophy, phototrophy and heterotrophy differently. Most photosynthetic algae achieve an optimum temperature between 20-30 ºC (S. P. Singh & Singh, 2015a). Reduction in growth rates above the optimum have been attributed to increased photorespiration rates as the carbon fixing enzyme Rubisco becomes more specific towards oxygen fixation (Bernacchi, Singsaas, Pimentel, Portis Jr, & Long, 2001). Comparative studies have indicated that mixotrophs and heterotrophs have a higher optimum temperature for growth (T. Li, Zheng, Yu, & Chen, 2014; Wilken, Huisman, Naus-Wiezer, & Donk, 2013) greater than 30 °C. Furthermore, mixotrophic algae became more heterotrophic as the temperature increases with reduced chlorophyll content in cells (T. Li et al., 2014).

At elevated temperatures, the preference for glucose will also increase the intracellular CO_2 concentration whilst decreasing O_2. This would change the ratio of CO_2-O_2 to be more favourable towards CO_2 fixation rather than photorespiration improving photosynthetic carbon fixation relative to a strict photosynthetic process. Eventually further increases in temperature will negate this benefit due to increasing specificity towards photorespiration.

Finally, the interaction effect between phototrophy and heterotrophy in mixotrophic biomass can be characterised by the ratio between the mixotrophic yield and the sum of the photosynthetic and heterotrophic yields $\left(\frac{X_M}{X_P+X_H}\right)$. The interaction effect of mixotrophy is shown below in Table 2.2

Table 2.2 Comparison of photosynthetic, heterotrophic and mixotrophic biomass yield and comparison of apparent mixotrophic yield with expected yield if mixotrophy operates via independent additive phototrophy and heterotrophy. In the table, enriched aeration means the system is not CO_2 or O_2 limited. If there is, no enriched aeration the system may likely become oxygen or carbon limited depending on growth mode

Study	**Operating Conditions**	X_P (g/l)	X_H (g/l)	X_M (g/l)	$\frac{X_M}{X_P + X_H}$
Spirulina platensis (Marquez, Sasaki, Kakizono, Nishio, & Nagai, 1993)	20 µmols/m^2.s, 2 g/l glucose, enriched aeration	1.770	0.827	2.521	0.97
C. Vulgaris (Adesanya et al., 2014)	80 µmols/m^2.s, 0.5 g/l glucose, continuous light, 125 mg N-NO_3^-, enriched aeration	2.7	0.25	3.5	1.19
	Same as above but with 25 mg N-NO_3^-/l, enriched aeration	1.8	0.1	2	1.05
Chlorella sorokiniana (Kucharoenphaibul et al., 2014)	62.5 µmols/m^2.s, 10 g/l glucose, 50 mg N-NO_3^-/l, enriched aeration	2	3	7.5	1.5

Spirulina sp. (Chojnacka & Noworyta, 2004),	49.0 W/m^2, 2.5 g/l glucose, enriched aeration	0.247	0.368	0.497	0.808
Chlamydomonas humicola (Lalibertè & de la Noüie, 1993)	70 µmols/m^2.s, 0.82 g/l acetate, no enriched aeration	0.0268	0.0724	0.247	2.50
Micractinium inermum (Smith et al., 2015)	91 µmols/m^2.s, 1.2 g/l acetate, no enriched aeration	0.025	0.15	0.7	4
	91 µmols/m^2.s, 1.2 g/l glucose, no enriched aeration	0.025	0.1	0.9	7.2
C. Vulgaris (Martínez & Orús, 1991)	70, µmols/m^2.s, 5 g/l glucose, enriched aeration	1.95	1.2	3.16	1
	70, µmols/m^2.s, 5 g/l glucose, no enriched aeration	0.85	1.08	2.48	1.28
C. Vulgaris (Ogawa & Aiba, 1981)	70.2 µmols/m^2.s, 5 g/l acetate, enriched aeration	2.64	2.35	4.75	0.95
H. pluvialis (Kobayashi et al., 1992)	20 µmols/m^2.s, 0.6 g/l acetate, no enriched aeration	0.32	0.18	0.57	1.14

2.3 Composition Kinetics of Algae

2.3.1 Effect of Nitrogen on Composition Kinetics

Nitrogen is a key ingredient in the manufacture of proteins, nucleic acids and enzymes. In contrast to proteins, nitrogen concentration and lipid accumulation depict an inverse relationship. When the nitrogen concentration is less than 3 % of total biomass the system is generally considered nitrogen starved. Under replete conditions, the nitrogen concentration depicts carbon uptake to be 7-10 times greater than nitrogen assimilation (Sajjadi, Chen, Raman, & Ibrahim, 2018). When compared to the nitrogen content of algal proteins, which can vary from 6-12 %, (Becker, 2007) the rates seem to be appropriate in balancing the nitrogen to carbon ratios of the algae. Some species were reported to regulate nitrogen supply whilst other regulated energy supply to nitrogen assimilation. The synthesis of storage compounds such as TAGs and starch is an example of energy storage in algae (Sajjadi et al., 2018).

When nitrogen depletion was initiated, the cellular protein content decreased as cells continued to divide but protein synthesis was reduced or halted. Carbon is then channelled towards the production of starch and TAGs the primary components of carbohydrates and lipids respectively, especially under nitrogen depletion. Overall, nitrogen limitation imposes the following changes in algae: a decline in the thylakoid membrane content, responsible for light reactions within the chloroplast; upregulates acyl COA hydrolase, which is responsible for fatty acid synthesis in the mitochondria; and activates phospholipid (polar lipid) hydrolysis. This may increase the cellular concentrations of the fatty acid acyl-CoA. Nitrogen limitation may also upregulate the conversion of acyl-CoA into TAGs thus, providing the link between nitrogen depletion and TAGs synthesis (Takagi, Watanabe, Yamaberi, & Yoshida, 2000).

Nitrogen limitation in general depicts a decline in protein or functional biomass content, with a subsequent increase in starch and TAGs. Photosynthetic efficiency and growth rate that are coupled to functional biomass growth rate also decline with nitrogen depletion. However, discrepancies from the generally described trends can occur. *Prorocentrum donghaiense* depicted no reduction in protein content in response to nitrogen depletion (Liang, Zhang, Gu, & Cong, 2013). Lipid content could increase by 2-3 times in 4-9 days under nitrogen starvation for green algae, whilst mixed results of increasing and decreasing TAGs was observed for diatoms, which was species dependent (Liang et al., 2013). In another study it was shown that lipid accumulation began hours not days after nitrogen starvation (Sajjadi et al., 2018). In general, lipid contents increase to 30-70 % of total biomass under nitrogen starvation. The highest reported lipid content was by *Monallantus salina* at 72 % whilst *B. braunii*, *C. vulgaris* and *Nannochloropsis* sp. reached 61.4 %, 57.9 % and 55 % respectively (Sajjadi et al., 2018).

However, lipid productivity declines due to reduced algal growth rates, which are negatively impacted by nitrogen depletion. This is why one study found that the content for optimal lipid productivity was only 20 % (De la Hoz Siegler Jr, 2011), as there us a trade-off between content and productivity. Thus, maximising TAGs productivity for biofuels, a major area of interest for algae, may be better suited to faster growing algae.

A study on six different species of algae for lipid productivity found that they continued to simultaneously grow and accumulate lipids in conjunction, depicting little trade-off between lipid content and productivity. It was found that *C. Vulgaris* and *Chlorella oleofaciens* were relatively unaffected by nitrogen starvation in contrast to *C. sorokiniana, Neochloris oleoabundans, Scenedesmus dimorphus* and *S. naegleii* (Adams, Godfrey, Wahlen, Seefeldt, & Bugbee, 2013).

Nitrogen can also have interaction effects with other variables. One study on *Ankistrodesmus falcatus* found that nitrogen and phosphorus depletion coupled with low iron concentration (3 mg/l) inhibited lipid synthesis, whilst an increasing iron concentration to 6 mg/l resulted in greater lipid productivity under nitrogen depletion (P. Singh, Guldhe, Kumari, Rawat, & Bux, 2015). Another study on interaction effects, found that TAGs content was independent of light flux, but nitrogen deficient cultures had TAG content vary from 18-40 % based on temperature and pH. Maximum TAG content was reached at a temperature of 27.5 °C and pH of 7 (Breuer, Lamers, Martens, Draaisma, & Wijffels, 2013).

An experiment on nitrogen limitation for *A. falcatus* (Kilham, Kreeger, Goulden, & Lynn, 1997) favoured a higher lipid content compared with nitrogen replete cultures where lipid content increased from 48 % to 60 %. However, the concentration of lipids was the same for both instances, therefore the reappropriation of carbon towards lipids synthesis did not yield more lipids. Carbohydrates content increased when nitrogen was depleted from 11 % in replete cultures to 20 %. The overall final concentration of carbohydrates improved from 0.35-0.5 g/l; a 42 % increase. Protein content however decreased from 39 % to 20 % with protein concentration declining from 1.2-0.5 g/l, a decrease of more than 50 %. Therefore, most of the decline in carbon going into proteins was channelled into producing more carbohydrates and lipids. It also makes reasonable sense that protein content is proportional to nitrogen concentration since nitrogen forms an essential nutrient to produce proteins.

Another study investigating the effect of reducing nitrogen concentrations in continuous cultures of *C. sorokiniana* found that lipid content remained unchanged when the nitrogen content in the cells decreased from 10-4 %. On the other hand, carbohydrates increased as a fraction of biomass, whilst protein content decreased as expected (Richardson, Orcutt, Schwertner, Martinez, & Wickline, 1969).

For a culture of *Parachlorella, kessleri* the starch content was higher under normal nitrogen conditions, at 20 %, compared with nitrogen, which was, diluted fivefold (10 %) and 10-fold (10 %). Lipid content however improved significantly from 10 % to 47 % in the fivefold diluted culture, and up to 55 % for the 10-fold nitrogen diluted culture after four days. This did come at the expense of growth with yield reduced from 8 g/l to 3.8 g/l under a fivefold dilution of nitrogen and 1 g/l under the 10-fold diluted medium. The penalty of reduced growth overcompensates for the increase in lipid productivity from nitrogen depletion. Interestingly, starch decreased a little, which was found to be divergent behaviour to what normally happens when a culture is nitrogen starved: an increase in starch concentration. Protein content as usual was directly related to nitrogen concentration in the media dropping to its lowest content in the 10 fold diluted medium (X. Li et al., 2013).

Starch accumulation in batch studies varied significantly as a function of species from 7-45 % where the minimum content was detected for *Scenedesmus acuminatus* and maximum content for *Chlamydomonas reinhardtii* UTEX2247 (Dragone, Fernandes, Abreu, Vicente, & Teixeira, 2011) . Different strains in the same study exhibited varying levels of starch accumulation after 20 days of growth. For example, *Scenedesmus* sp. TISTR 8982 had a starch content of 13 % whilst *Scenedesmus* sp. TISTR 8579 had a starch content of 20 %. Other strains showed little difference in starch content with time. For instance *S. obliquus* TISTR 8522 had a starch content of 24 % and *S. obliquus* TISTR 8546 had a starch content of 23 % after 20 days (Rodjaroen, Juntawong, Mahakhant, & Miyamoto, 2007).

Starch could be maximised by using the following growth strategy: cultivating the algae under nitrogen replete conditions and then transferring and cultivating the algae under nitrogen-depleted cultures. This strategy was employed for *C. vulgaris* achieving a maximum content of 41 % suggesting the suitability of this species for starch accumulation (Dragone et al., 2011). Another study found that it was difficult to simultaneously maximise starch

productivity and concentration of biomass. However maximum productivity of starch at 0.49 ± 0.06 g/l.d, did correlate with maximum starch content at 54.0 ± 4.1 %, suggesting *Tetraselmis subcordiformis* was a superior species of algae for starch accumulation (Yao, Ai, Cao, Xue, & Zhang, 2012). More importantly, this was achieved using a single stage of cultivation thus, reducing the complexity of cultivation to achieve high starch yields.

Functional biomass is mostly composed of proteins. As such, it is closely correlated with nitrogen concentration. The cellular protein concentration was 1.2 ng/cell, which decreased to 0.5 ng/cell when the nitrogen concentration was diluted to 1/20 of the control (Vanucci, Guerrini, Milandri, & Pistocchi, 2010). This correlation between the organic nitrogen pool and extracellular nitrogen concentration was also evidenced by a study on *Skeletonema costatum*. In this paper the amino acid pool decreased by 90 % within 24 hours of nitrates becoming depleted (Espen Granum, Ståle Kirkvold, & Myklestad, 2002). A culture of *C. minutissima* showed a linear relationship between nitrogen concentration and protein concentration where nitrogen concentration increased from 7-35 mg N/l the protein content subsequently increased from 21-52 % after four days of culture. The reason for such correlation between nitrogen and protein concentration is that the algal protein requires nitrogen as a nutrient for synthesis. Depletion of nitrogen results in denial of this essential nutrient for protein synthesis (Ördög, Stirk, Bálint, van Staden, & Lovász, 2012). However, not all species of algae show this trend for protein content. For instance, *Chlorella emersonii* protein content varied from 32-28 %, *C. protothecoides* from 38-36 % and *C. sorokiniana* from 45-42 % under nitrogen replete (~173 mg N/l) and low nitrogen (~43 mg N/l) (Illman, Scragg, & Shales, 2000) conditions. Perhaps this was due to not all the nitrogen becoming depleted in the system thus, not initiating a reduction in protein content.

2.3.2 Effect of Light on Composition Kinetics

Each year the Earth receives 3.9×10^6 MJ of energy as light every year from the sun. A small fraction of this is harvested by photosynthetic organisms such as algae to supply the energy for fixing CO_2. However, algae are only capable of utilising 43 % of incident solar radiation at ground level (between 400-700 nm). Therefore, light intensity and wavelength become important factors in determining composition kinetics. Photosynthesis can be divided into light dependant and light independent dark reactions. Light dependant reactions involve the absorption of light and harvesting this light to split water, producing oxygen and protons for CO_2 reduction in the dark reactions. The electrons produced in the light reactions are transferred to the proteins, photosystem I and photosystem II to produce ATP and NADPH (Choi et al., 2015).

The dark reactions, also known as the Calvin-Benson cycle, occur without the presence of light; but occur at the same time light is being absorbed and processed in the light reactions. The primary phases of the Calvin cycles involve the fixation of CO_2, reduction and regeneration of the enzymes, involving 13 different enzymes. The first step of CO_2 fixation involving the enzyme rubisco generally accepted as the rate-limiting step of photosynthesis. Excess light can result in photo-oxidation as a result of oxygen free radical build up in the cells, damaging photosystem II, reducing microalgal productivity (Quaas et al., 2015).

The light-dark cycle of incident light is another factor affecting algal composition. Altering the light-dark cycle changes the composition of the algae; it can also change the photosynthetic efficiency of the algae (Krzemińska, Pawlik-Skowrońska, Trzcińska, & Tys, 2014). For instance, a study on *Nannochloropsis* sp. found that lipid productivity was optimised at 18:6 h rather than a 12:12 cycle. This was because at a longer duration of light cultures could grow well at higher light intensities of 200 μmols/m^2.s whilst the shorter light

duration cultures grew well at lower light intensities, 100 µmols/m^2.s. Although cultures grown at lower light intensities grew better at shorter light duration, the algal growth for this regime was lower than for higher light intensity cultures. This could be due to a combined effect of shorter light duration and lower incident light intensity.

Algae absorb red and blue light strongly; therefore, photosynthetic efficiency can be improved under these wavelengths. Lipid productivity is optimal at blue wavelengths whilst carotenoids productivity is optimal at red wavelengths. Improving algal productivity means optimising wavelength, intensity and light-dark cycles to get a balance between photoprotection and photosynthesis. Providing protection from photoinhibition from excessively high light intensities is an important consideration, especially for outdoor cultures where incident light fluxes can reach 2000 µmols/m^2.s in summer. This is well above the 500 µmols/m^2.s light flux considered to be the saturation light intensity for algae (Sun et al., 2014).

A study on *N. oleoabundans* investigated the effect of a two stage cultivation process, divided into a growth stage in the first six days and an accumulation stage in the second stage for lipid and carbohydrates (Sun et al., 2014). In the second stage nitrogen nitrates was depleted from the system after two days and light flux was varied from 50-300 µmols/m^2.s. It was found that protein and residual biomass production (ash) that make up most of the functional biomass was maximised at a light flux of 50 µmols/m^2.s, whilst carbohydrates was maximised at a light flux of 100 µmols/m^2.s. TAGs productivity was maximised at 200 µmols/m^2.s which also coincided with maximum lipid productivity since more than two thirds of lipid was TAGs for this species. Overall low light intensities favoured functional biomass (mainly proteins) formation, medium light favoured carbohydrates production and higher light intensities favoured lipids and TAGs production.

Another study using a similar two stage process was performed on *S. obliquus* CNW-N (Ho, Chen, & Chang, 2012). Under nitrogen-depleted conditions, the light flux was varied between 180-540 µmols/m^2.s. Biomass productivity rose as a function of light flux from 250 mg/l.d at 180 µmols/m^2.s to 800 mg/l.d at a flux of 420 µmols/m^2.s, but dipped down to 500 mg/l.d at 540 µmols/m^2.s. Lipid content for this strain of *S. obliquus* maximised at the lowest light flux at 12 %, but since this also corresponded with the lowest biomass productivity it did not translate into maximum lipid productivity. Instead, lipid productivity was maximised at 95 mg/l.d at the maximum light intensity of 540 µmols/m^2.s when lipid content was at 11 %. Carbohydrates meanwhile, reached maximum content of 37 % and productivity of 330 mg/l.d at 420 µmols/m^2.s. Proteinaceous functional biomass was also maximised at the greatest biomass productivity at a rate of 405 mg/l.d. This shows that when light was the independent variable, for nitrogen-depleted cultures, biomass productivity was the most important factor dictating composition kinetics rather than fraction content.

When studying the effect of light regime on cultures (Takeshita et al., 2014), it was found that continuous light favoured starch and lipids production in comparison to a light-dark cycle when tested for eight strains of six species of *Chlorella*. Starch concentration improved by 10-80 % whilst lipids improved by 25-125 %. These rises in lipids and starch concentration were at the expense of proteins, which declined as a fraction of total biomass. Another study in contrast found that *C. vulgaris* did not have a significant difference between starch content between continuous light cultures and one with a 12:12 light: dark cycle (Mizuno et al., 2013). In this work, the same trend was found for *Chlorella Iobophora*, but *P. kessleri* showed that under a light: dark cycle the starch content was higher by 50 %. Lipid content was higher under light dark cycles for *C. vulgaris* and *P. kessleri* at 25% and 27 % respectively compared with 10% and 15 % for continuous light cultures. In contrast, cultures of *C. sorokiniana* and *C. Iobophora* showed a higher lipid content for cultures under

continuous light maximising at 40 % and 50 % respectively; the light/dark-cycle cultures, meanwhile, had lipid contents of 25 % (*C. sorokiniana*) and 30 % (*C. Iobophora*). Protein content for *C. vulgaris* was greater for continuous light cultures than light/dark-cycle cultures at a content of 70 % compared with 60 % for light: dark cycle cultures. *C. sorokiniana* and *C. Iobophora* showed a preference for functional biomass for cultures with a light: dark cycle rather than continuous light. Overall, these results show that there is no consensus or clear trends between species of algae when it comes to determining the effect of light mode on composition kinetics (Mizuno et al., 2013).

A study on testing the effect of light on different growth modes of *Chlorella zofingiensis* found that starch synthesis was upregulated for photosynthetic culture relative to heterotrophic cultures. Starch content for heterotrophic cultures reached 30 % after 10 days whilst for photosynthetic cultures it reached 50 %. Lipid content on the other hand reached 50 % for heterotrophic cultures whilst reaching 32.5 % for photosynthetic cultures after 10 days. Protein content, meanwhile, remained relatively constant at 20 % for heterotrophy and 17.5 % for photosynthetic cultures after 10 days (T. Chen et al., 2015). Addition of glucose for a culture of *C. pyrenoidosa* increased starch content in the stationary phase to 30 % whilst the photosynthetic culture had a content of 25 %. The protein content in the photosynthetic culture was 55 % whilst it was 50 % for the mixotrophic culture. Lipids were 20 % in both photosynthetic and mixotrophic cultures (C. Yang et al., 2000).

2.3.3 Effect of Temperature on Composition Kinetics

Temperature is an important factor dictating composition kinetics as it fluctuates in outdoor environments, varying between 10-45° C depending on the region, leading to changes in algal productivity and composition. Since biological processes as a rule of thumb double for every ten degree rise in temperature it can be reasoned that fraction production would increase

concurrently with temperature. This is a somewhat erroneous belief as temperature stress at elevated levels may decrease cellular growth rates, hence fractional productivity. For example at a temperature of 38 °C,.*C. vulgaris* biomass died after they stopped growing with cells turning from green to brown (Converti, Casazza, Ortiz, Perego, & Del Borghi, 2009). According to the Arrhenius equation the enzymatic activity would also decrease with temperature, therefore, a bell-shaped curve would be evident for growth rate as a function of incident temperature. The temperature for zero productivity is known as the lethal temperature, which for mesophilic algal species is 30-35 °C.

Microalgae are capable of growing in a wide range of temperatures (between 15-30° C), but grow optimally in a narrow range particular to each species; for instance being 32 °C for *Dunaliella* sp., 25-30 °C for *C. vulgaris* (Converti et al., 2009) and 15-20° C for *C. minutissima* (Cao, Yuan, Li, & Yang, 2014). The optimal temperature for biomass growth was found to vary significantly for the *Chlorella* genus. Literature has shown that *Chlorella* species of algae can grow at optimal levels between temperatures of 26-32° C for *C. protothecoides, C. Vulgaris, P. Kessleri* and *Chaperina. Fusca*. Biological systems are divided into three categories depending on what their optimal growth temperature; 17 °C for psychrophilic strains; 20-25 °C for mesophilic species; and 40 °C for thermophilic species. Studies on microalgal growth above optimal temperature are scarce for mesophilic and psychrophilic species. Factors such as medium composition may also change the optimal temperature with literature reports of sodium chloride concentrations changing from 0.125-1.5 M increasing optimal temperature by 6 °C for *Dunaliella tertiolecta*.

For algae to grow there must be a balance between the energy entering the cells from light absorption and internal energy consumption and fluxes to synthesise new biomass or used in respiration. Energy supply and demand imbalances caused by environmental stress can induce changes in the photosynthetic apparatus such as rubisco activity. Other responses to

stress involve cell shrinkage to cope with differences between anabolic and catabolic processes because of temperature rises. Thus, shrinkage is a result of algae reducing metabolic costs and increasing their nutrient uptake rates (Atkinson, Ciotti, & Montagnes, 2003). This phenomenon has been observed in *Scenedesmus acutus* and *Dunaliella* sp. along with decreases in photosynthetic rates and respiration rates (Staehr & Birkeland, 2006) (García, Freile-Pelegrín, & Robledo, 2007). Despite some negative short-term effects on microalgae kinetics long adaptation to elevated temperature was observed for *S. acutus*after it adapted to 30 °C after 15 generations, 35 °C after 30 generations and 40 °C after 135 generations.

For a culture of *N. oculata*, increasing the temperature from 20-25 °C doubled lipid content from 7.9-14.9 % (Converti et al., 2009), but at the cost of lower cellular growth rate. In another study on *Isochrysis galbana*, high temperatures resulted in lower lipid and carbohydrate contents and higher protein content. The specific growth rate was found to reduce neutral lipid content whilst increasing glycol and phospholipid content (C. J. Zhu, Lee, & Chao, 1997). For most species, it was observed that low temperatures improved lipid content, had minimal effect on carbohydrates content and reduced protein content. The reduction in protein content may be due to amino acid synthesis being inhibited by lower temperatures. In contrast glycolysis intermediates increase in concentration upregulating acetyl-CoA, hence fatty acid synthesis and lipid production (Yuancong Wang, He, Sun, & Chen, 2016).

For *Scenedesmus* sp. decreasing the temperature from 25-20 °C only decreased growth rate by 8 % whilst improving lipid content by 150 % (Xin et al., 2011). A similar result was found for *C. Vulgaris* when temperature was reduced from 30-25 °C, without compromising growth rates, the lipid content increased by 2.5 times (Converti et al., 2009). However, reducing the temperature from 26-18 °C for *C. sorokiniana* reduced growth rate significantly so that

overall lipid productivity was 25 % lower (Yuancong Wang et al., 2016). Adding Glycine betaine could enhance lipid and biomass productivity at both temperatures without changing composition, thus improving lipid productivity. In addition to increasing lipid content, lower temperatures also reduce carboxylase activity so that there are imbalances in energy supply and demand, reducing the light saturation intensity. Algae normally adapt to these conditions by reducing chlorophyll content such as in the case of *C. vulgaris* and *Dunaleila salina* (D. P. Maxwell, S. Falk, C. G. Trick, & N. Huner, 1994) (Kró, Maxwell, & Huner, 1997), but *S. costatum* increased chlorophyll content as temperature was lowered.

A study found that the combined effect of nitrogen starvation and temperature stress improved lipid productivity over a short period of time then treating with nitrogen depletion alone (Fakhry, 2015). Other studies found similar results for *eustigmatophyte*, *Nannochlorospsis salina* (Boussiba, Vonshak, Cohen, Avissar, & Richmond, 1987), *Nannochloropsis* sp. (Fakhry, Massoud, & Ahmed, 2015) and *Chrysophytan ochromonas Danica* (Aaronson, 1973). However, another study on *C. sorokiniana* found that there was no significant increase in lipid productivity (Patterson, 1970).

Temperature can also have an impact on the lipid composition of algae. Increased temperature normally decrease the ratio of unsaturated to saturated fatty acids (Renaud, Thinh, Lambrinidis, & Parry, 2002). When culture temperature was increased beyond the optimal level monounsaturated fatty acids increased whilst polyunsaturated fatty acids reduced in concentration. In contrast, the saturated fatty acid content increased with a rise in temperature. This was not found for all species of algae: *Nannochloropsis* sp. and *C. vulgaris* reduced their saturated fatty acid content with higher suboptimal temperatures (Converti et al., 2009). Lower temperature was thought to improve the total lipid content and the polyunsaturated fatty acid content in the lipid fraction. This was seen as a means to improve membrane fluidity at low temperatures (Suga et al., 2002).

A study on *B. braunii* found that lipids content decreased as the temperature increased from 25 ºC to 32 ºC reducing by 5 – 25 %. The carbohydrates fraction meanwhile rose compensating for the lower lipids content (Kalacheva, Zhila, Volova, & Gladyshev, 2002). This trend for carbohydrates was not found for all cases. One instance measuring the carbohydrate, starch, found that its content decreased as temperatures rose. This degradation was thought to be due to the enzymes α-amylase and α-glucan phosphorylase activity. Carbohydrate composition changes as temperature increases in some instances. For example, for *C. vulgaris*, the starch content reduced to 17 % whilst sucrose rose to 57 % of carbohydrates when the temperature was increased to 38 °C for only 10 minutes after the algae was exposed to 20 °C for 30 minutes (Nakamura & Miyachi, 1982b). However, another study on *C. vulgaris* at 38 °C found lower rates of degradation of starch (Nakamura & Miyachi, 1982a). This may be due to the first study cultivating algae at a lower temperature before increasing the temperature suddenly whilst the second study had the temperature fixed at 38 ºC. Nakamura et al. (1982b) also found that starch changed forms from high molecular weight amylopectin-like molecule fraction at lower temperatures to low molecular weight amylose-like molecule fraction.

Protein synthesis decreased as temperatures rose due to declined growth rate. The literature reported that *Phaeodactylum tricornutum* had greater protein synthesis rates at night time when it was cooler. This may be due to temperature dependence, but was also cited as being a result of night-time conditions favouring protein synthesis (Morris, Glover, & Yentsch, 1974). Another study on *Scenedesmus* sp. found that protein concentration increased with temperature (Rhee & Gotham, 1981). Similarly, a culture of *Ulva pertusa* showed higher free cell amino acid concentrations increasing from 840 to 1810 mg/100 g dry weight. These greater concentrations are consistent with lower fixed protein content (Kakinuma et al., 2006).

2.4 Composition Kinetic Models

2.4.1 Model Mechanisms

The objective of a mechanistic model is to accurately describe a simplified version of true intracellular composition kinetics. The validity of the corresponding mathematical model is then dependant on how well the biological system is described in the mechanistic model based on the assumptions and depiction of biological processes and factors regulating composition kinetics. For this reason, validating mechanistic models, the underlying theoretical principles of biological behaviour, is just as important as validating the mathematical model. One of the primary assumptions common to all conceptual models reviewed is that physicochemical variables based on dissolved CO_2, O_2 and pH either optimised or assumed to have a negligible effect on kinetics. Temperature and micronutrients apart from nitrogen are also optimised.

As such, the scope of this review, on composition kinetics of photosynthetic cultures, is to investigate the effect of nitrogen and light on algal monoculture composition kinetics. There are two objectives that a metabolic mechanism is expected to satisfy before mathematical model development:

1. Explaining composition behaviour for a wide range of nitrogen conditions including exhaustion in media as well as light intensities above and below light saturation
2. The number of fractions should be enough to model possible interaction between the different fractions and be enough to be applied to algal biorefinery applications

This section will review mechanistic models based on their ability to predict behaviour under wide nitrogen and light conditions as well as ability to simulate the behaviour of the different fractions.

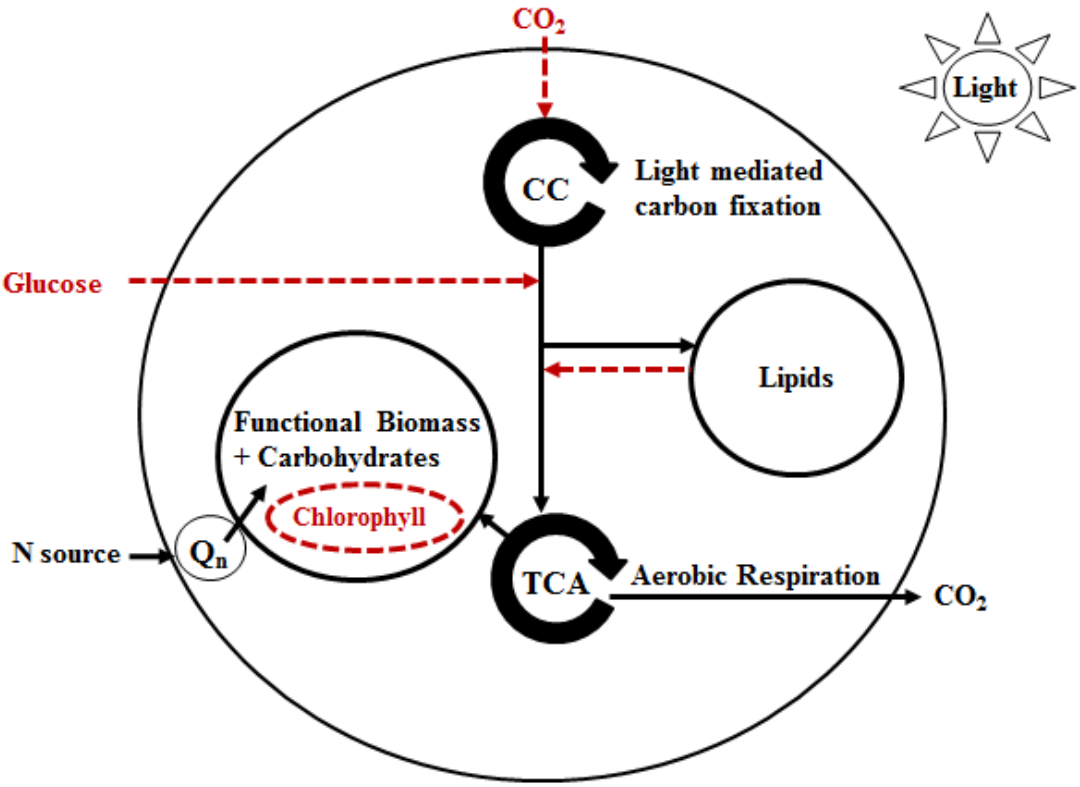

Figure 2.2 Functional biomass-lipid mechanism used by literature models. The dotted lines indicate processes or compounds that differ between the papers

Many composition model papers use the approach in Fig. 2.2 to separate the fractions (De la Hoz Siegler et al., 2011; Packer et al., 2011; Quinn, de Winter, & Bradely, 2011; Surisetty et al., 2010; Tevatia, Demirel, & Blum, 2012; J. Yang et al., 2011; Yoo et al., 2014). However, there is a large degree of variability between conceptual models indicated by the dotted lines in Fig. 2.2 primarily due to the growth mode of the algae.

Not all light dependant models depict photosynthesis as being a function of chlorophyll kinetics (J. Yang et al., 2011; Yoo et al., 2014). They assume that the chlorophyll content remains roughly constant as nitrogen is depleted and culture light intensity changes. However, it has been shown by other studies that chlorophyll content can more than half under nitrogen depleted conditions (Adesanya et al., 2014). It is assumed that carbon uptake is primarily regulated by light intensity and nitrogen instead. Homogenous biomass models,

ones that don't distinguish between the different fractions of algae, that don't include chlorophyll have still been able to achieve reasonably accurate model fits to within 15 % of experimental data (Ketheesan & Nirmalakhandan, 2013) under batch conditions.

The use of nitrogen quota as a regulatory factor is common to almost all models regardless of operating environment or reactor configuration. It was first introduced as an empirical regulator affecting cell growth (M.R. Droop, 1975). Later it was found that there was a theoretical basis to the nitrogen quota kinetic expression (Lemesle & Mailleret, 2007). However when applied as a regulator at nutrient replete conditions of 240 g N/l for a batch culture it was not found to be an accurate regulator of composition kinetics (Packer et al., 2011). Other factors such as light may be more important than internal nitrogen status during nitrogen repletion in the exponential growth phase.

Some conceptual models contained a lipid consumption term (Packer et al., 2011) which, became kinetically important after nitrogen had been exhausted from the media after 7 days. In the study, there was no biological reasoning applied to how and why lipids were catabolised other than to fit the experimental data. Possible causes of lipid consumption may be due to external carbon uptake being reduced below the cell respiration rate. Since algal lipids are an energy dense compound they can be utilised as an energy source for the production of ATP via aerobic respiration in the mitochondria (Subramanian, Barry, Pieris, & Sayre, 2013). Therefore, the incorporation of a lipid catabolic term is important when the external carbon uptake is less than the cell maintenance requirement. A reason for this term not being used in most models is that it would only be expected to be important in the late stationary phase, when nutrients and carbon uptake are negligible, whilst many experiments cease in the early to mid-stationary phase.

One of the main assumptions made in some of these types of conceptual models is that the algae are composed of mainly lipids and proteinaceous functional biomass, which represents the metabolically active component of the algae. Carbohydrates although metabolically inactive, thus not technically functional biomass, are assumed to be present in low concentrations and have small dynamic fluctuations. Therefore, it is incorporated as a minor component of functional biomass. This contradicts other mechanistic models which assumed that carbohydrates not lipids are the primary storage compound (Kunikane & Kaneko, 1984).

Furthermore, experimental studies indicate that both lipids and carbohydrates concentrations can fluctuate between 20-50 % of total biomass (Adesanya et al., 2014; R. Singh, Balagurumurthy, & Bhaskar, 2015; Valenzuela-Espinozaa, Millán-Núñezb, & Núñez-Cebrero, 2002). The kinetics of the three fractions: functional biomass, lipids and carbohydrates do not follow the same trend (Takeshita et al., 2014; Zhang et al., 2014). Functional biomass content is strongly dependent on nitrogen content, lipids have an inverse relationship with nitrogen and carbohydrates increase at intermediate nitrogen levels. This suggests carbohydrates have growth related (Klok et al., 2013) and non-growth related accumulation behaviour (Takeshita et al., 2014). Therefore, since carbohydrates accumulation is not always coupled to protein up to 50 % of the 'functional biomass' (Adesanya et al., 2014) is in fact metabolically inactive carbohydrates meaning that in some cases the assumption of carbohydrates having a negligible impact on kinetics is invalid.

The algal species likely plays an important role in determining which fractions would be present in substantial quantities. The mechanistic model of Quinn et al., (2011) supported the idea that constant low concentrations of carbohydrates to be valid for *Nannochloropsis* sp. However, this trend is not exhibited for *Chlorella* sp. (Takeshita et al., 2014) limiting the applicability of such a conceptual model as a general model of biological behaviour. Other composition studies on *Nannochloropsis* sp. indicate that whilst carbohydrates do not vary as

much as lipids it is still significant ranging from 20-40 % of biomass (Wan, Bai, & Zhao, 2013; Xia et al., 2013) as a function of nitrogen status. Thus, it is apparent that for most species of algae carbohydrates cannot be assumed a minor fraction of the functional biomass.

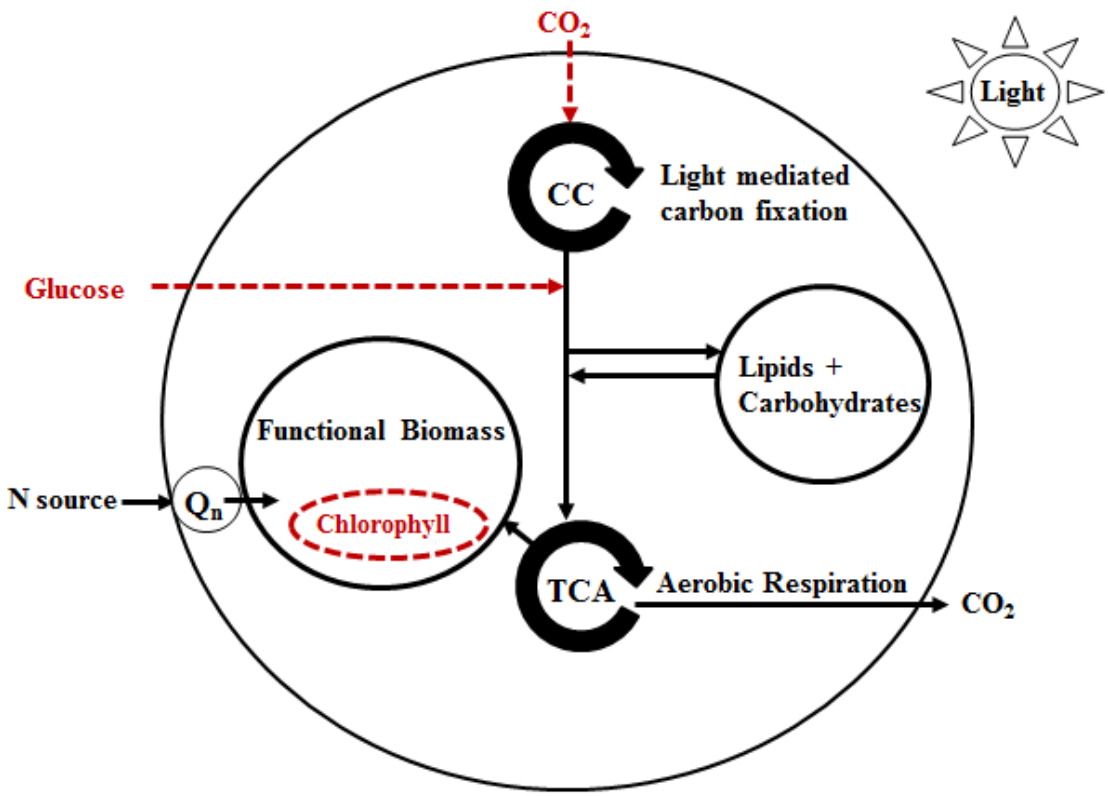

Figure 2.3 Mechanism separating the primary fractions as the functional biomass and storage molecules, which contains the carbohydrates and lipids. The dotted lines indicate processes or compounds that differ between the papers (Adesanya et al., 2014; Kunikane & Kaneko, 1984)

An alternate two fraction conceptual model (Adesanya et al., 2014; Kunikane & Kaneko, 1984) in Fig. 2.3 which, depicts functional biomass as an independent fraction with a storage component being composed of carbohydrates and lipids. The concept involves a growth and nitrogen related functional biomass fraction with excess carbon being channelled towards storage molecule production, which is deficient of nitrogen. Therefore the C:N ratio of uptake appears important in dictating composition kinetics (Adesanya et al., 2014). Storage molecule

generated is coupled to photosynthetic carbon fixation and consumed for functional biomass synthesis (Perez-Garcia, Escalante, de-Basahn, & Bashan, 2011).

It was assumed by one of the models (Kunikane & Kaneko, 1984) that for *S. Dimorphus* the storage component was almost completely composed of carbohydrates although other experiments indicate that this is only valid under higher nitrogen conditions. When nitrogen becomes lower, the lipid fraction can account for 40 % of the storage molecule (L. Wang, Lia, Sommerfeld, & Hua 2013). This model also did not use chlorophyll to regulate photosynthetic carbon uptake kinetics but obtained a good fit. The fit was obtained despite reported chlorophyll content in literature varies between 0.05-3 % (Ajayan, Selvaraju, & Thirugnanamoorthy, 2012; Grima et al., 1994; Riemann, Simonsen, & Stensgaard, 1989). Chlorophyll is regulated by nitrogen to ensure that energy entering from light dependant reactions is balanced by energy requirement in carbon fixation in dark reactions. Nitrogen depletion also results in degradation of the rubisco enzyme (John A Berges & Mulholland, 2008), the rate limiting enzyme for CO_2 fixation. This enzyme can be degraded to provide an additional nitrogen pool in times of nutrient stress (Recuenco-Muñoz et al., 2015). Therefore, reduction in chlorophyll content due to nitrogen depletion also coincides with reduction of CO_2 fixation in the dark reactions, which are the rate-limiting step. Thus, it is possible to equate the dark reactions, commonly depicted as the rate limiting step (Subramanian et al., 2013), to nitrogen status directly rather than using nitrogen mediated chlorophyll synthesis.

The implementation of this type of mechanistic model in Fig. 2.3 to optimisation and life cycle analysis may be limited, since they do not distinguish lipids and carbohydrates, which are processed into different end products. Carbohydrates have use as biobutanol and bioethanol (Maity, 2015) whilst lipids can be converted into biodiesel (Foley et al., 2011), lubricants and surfactants (McGinnis, Dempster, & Sommerfeld, 1997). Due to the different nature of utilisation for lipid and carbohydrate metabolites, a two-fraction model separated

either as functional biomass-lipids or functional biomass-storage molecules is not practical. On a more fundamental level, the three fractions also show different kinetics in response to nitrogen and light limitation.

A better approach to separating the fractions is by defining functional biomass, carbohydrates and lipids as different fractions which appears to have been done for some continuous phase rectors (Klok et al., 2013; Mairet, Bernard, Masci, Lacour, & Sciandra, 2011; Zhang et al., 2014). The increased complexity of modelling a three component system has meant that operating conditions have been simplified for example by blocking the effect of light, thus only accounting for nitrogen effects (Mairet et al., 2011) operating under steady state conditions (Klok et al., 2013), or using a semi-empirical model to simulate composition kinetics (Zhang et al., 2014). These simplifications limit the practical utility of composition models in reactor design, process optimisation and life cycle analysis, which require robust, predictive and dynamical models capable of simulating behaviour under a wide variety of nitrogen and light. Nevertheless, they provide a foundation to combine the effects of fraction interaction, between lipids, functional biomass and carbohydrates, and nitrogen and light regulation.

A non-steady continuous system with variable dilution and nutrient loading was investigated by Mairet et al. (2011). The concentration of biomass was maintained below 60 mg/l so that most of the light was not absorbed by the culture. The mechanistic model below in Fig. 2.4 assumed that carbon was first converted into a sugar pool before being converted into lipids and functional biomass. Some of the lipids could be converted into functional biomass as polar membrane lipids. This conceptual model is a simplification of another model proposed by Mairet et al. (2013) where intermediate Free Fatty Acids (FFA) were produced and converted into either polar membrane lipids or neutral lipids, which are mostly composed of TAGs. Since FFA concentration was relatively low, it was assumed not to be rate limiting

and subsequently removed. This simplified mechanism is illustrated below in Fig. 2.4 and would be more apparent in times of nitrogen recovery from a previously depleted state (Fernandes et al., 2013; Mairet et al., 2011).

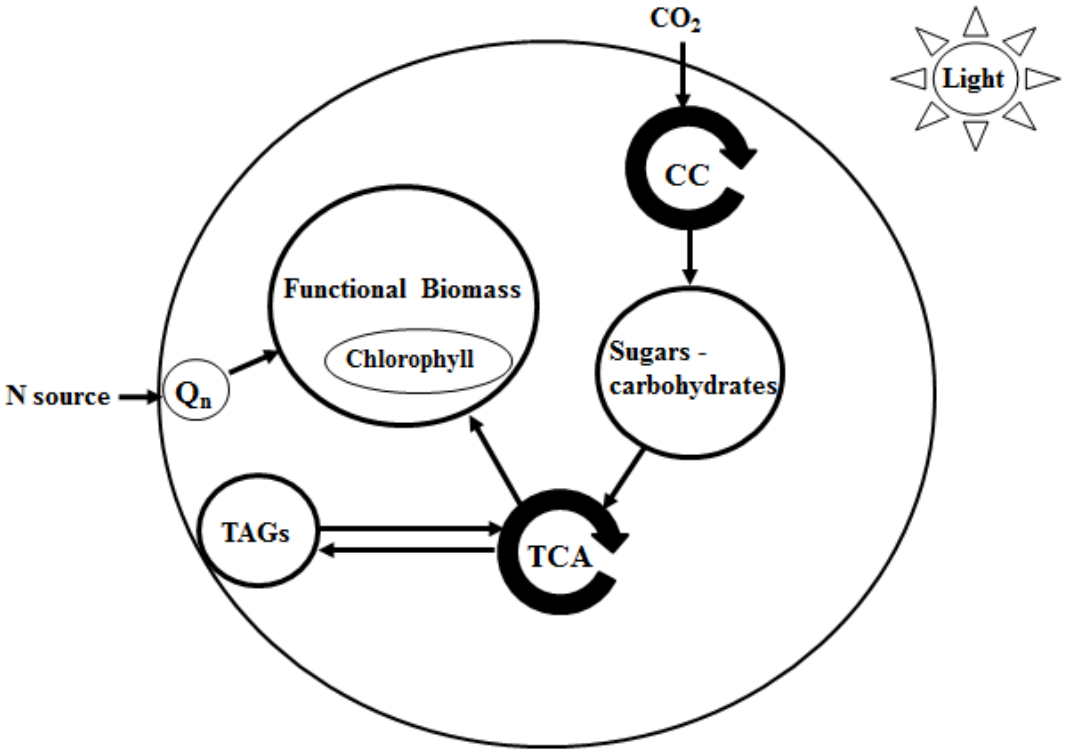

Figure 2.4 A mechanistic model for a non-steady state continuous system where carbon is assumed to first produce sugars/carbohydrates before being converted to functional biomass and lipid (Mairet et al., 2011)

Nitrogen quota dependant lipid concentration was demonstrated to decrease due to catabolism for maintenance respiration when nitrogen and carbon were exhausted (Yoo et al., 2014). The nitrogen quota had reached a value of 0.04 g N/g C which was less than the model predicted minimum quota of 0.05 g N/g C. This violates the minimum nitrogen quota constraint, which represents the subsistence level of nitrogen, meaning that lipids may be over predicted during simulation since generation rate is inversely proportional to the nitrogen quota. Additionally, if the rate of carbon uptake is less than the rate of aerobic

respiration of sugars then lipids are likely to be catabolised to meet energy requirements. This may explain why using the mechanistic model of Packer et al. (2011) in Fig. 2.2 for the lipids resulted in over prediction in stationary phase by 10 % of the experimental data, accounting for measurement error, when catabolism was not included. Thus, lipids may be overpredicted if parameter constraints are not met which will be discussed in more detail later or if lipid catabolism is not included, especially for late stationary cultures where all external carbon and nitrogen has been consumed.

Packer et al. (2011) also stated that the model mechanism did not apply for lipid & functional biomass behaviour under nitrogen replete or high biomass growth conditions. The mechanistic model of Mairet et al. (2011) accounts for this by relating lipid generation growth, carbon uptake and consumption for synthesis of functional biomass to nitrogen uptake. This consumption may provide the carbon skeletons for biomass synthesis (Perez-Garcia et al., 2011). Conceptually this would mean that lipids would accumulate fastest during nitrogen limiting conditions whilst also being able to accumulate due to cell division-based biomass growth. Thus, there is both a growth and non-growth component proposed for lipid kinetics.

An assumption by Mairet et al., (2011) made on cellular biological processes is that carbon is fixed into sugars such as glucose-6-phosphate before being converted into functional biomass and lipids (Mairet et al., 2011). Metabolic reaction diagrams indicate that CO_2 can be reduced to glyceraldehyde-3-phosphate or 3-phosphoglycerate prior to glucose-6-phospahte formation and undergo glycolysis to form functional biomass and lipids (J. Li et al., 2014; Perez-Garcia et al., 2011; Subramanian et al., 2013). A carbon flux analysis in the exponential phase confirmed that for photosynthetic and mixotrophic *C. pyrenoidosa* more than 90 % of fixed carbon is channelled into Glyceraldehyde-3-phosphate where it can undergo glycolysis to produce functional biomass, lipids and aerobic phosphorylation or undergo gluconeogenesis

via glucose-6-phosphate (C. Yang et al., 2000) to produce starch. Therefore, the assumption that carbon is primarily converted to sugars before functional biomass and lipid synthesis per se is incorrect. However, it was also observed by Mairet et al., (2011) that intermediate compounds such FFA were not rate limiting hence did not affect composition kinetics. Thus, carbon conversion into intermediates such as glucose-6-phosphate or glyceraldehyde-3-phosphate is moot, rather it is limiting factors that regulate the production of end products such lipids, sugars and functional biomass. Based on this premise it is proposed that after carbon is utilised for maintenance energy the three fractions compete for remaining free carbon dictated by composition regulators, which will be discussed later.

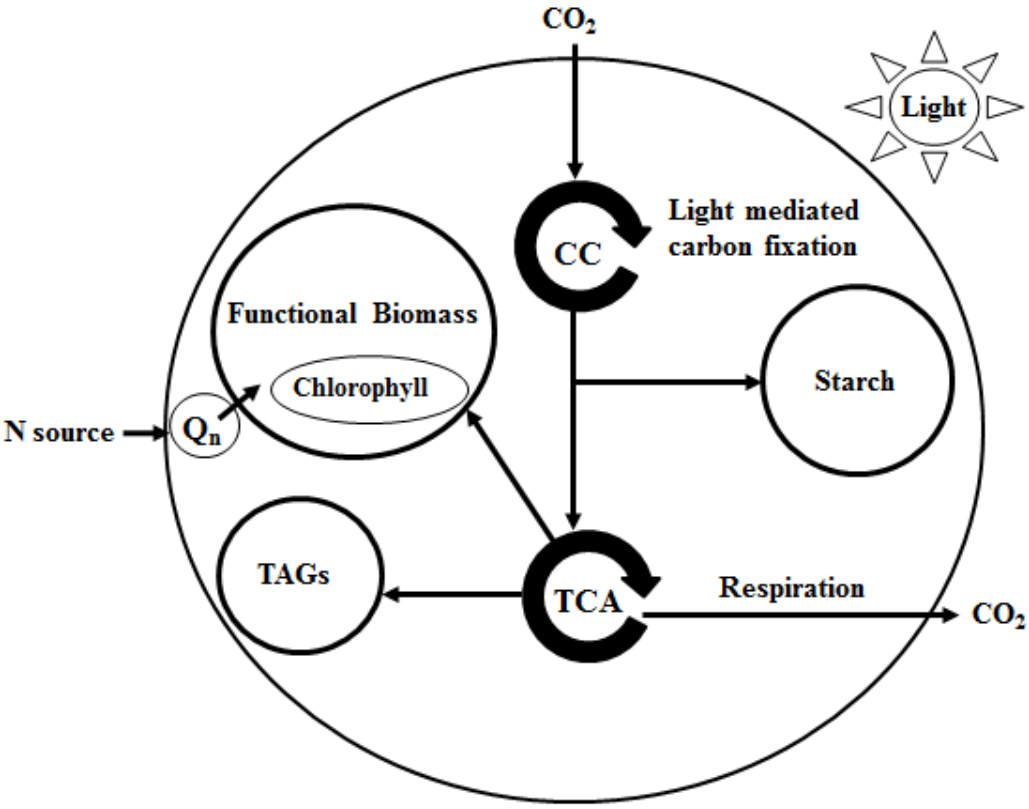

Figure 2.5 three fraction mechanism depicting carbon partitioning into starch, TAGs and functional biomass (Klok et al., 2013; Zhang et al., 2014)

Another mechanistic model (shown in Fig. 2.5) forming the basis of a three-fraction model (Klok et al., 2013; Zhang et al., 2014) incorporates aerobic respiration and energy dissipation both of which were not included by the 3-fraction model of Mairet et al. (2011).

Interestingly, although the two authors model the same compounds, the basis of the models differs from conventional carbon equivalent-based composition models. Klok et al., (2013) used an electron balance to describe metabolite synthesis whilst Zhang et al., (2014) used the photosynthetic quotient.

For the Klok et al., (2013) model light entering the cells splits water to form electrons and protons. Electrons produced in this manner will then be converted into NADPH, be dissipated, catabolised or fixed into biomass to maintain a balance between electron flow in the light dependant reactions and downstream reactions. There are in fact two metabolic/kinetic electron balances being described here. The first electron balance is between light and dark photosynthetic reactions, which has been incorporated somewhat in chlorophyll synthesis by others (Adesanya et al., 2014; R. J. Geider, MacIntyre, & Kana, 1998). Electrons may be used for CO_2 fixation in the dark reactions or be dissipated in two ways via non-photochemical quenching where excited chlorophyll release absorbed light as heat (Szabó, Bergantino, & Giacometti, 2005) or as fluorescence where excited chlorophyll return to ground state by emitting light of a lower wavelength (Maxwell & Johnson, 2000). Dissipation is important in light saturated systems depicting imbalance between light and dark reactions but is not normally incorporated in most composition models since they generally operate in light limited conditions. The second reason is the partitioning of reduced CO_2 from the dark reactions into biomass generation or consumption for ATP as energy for maintenance and biomass synthesis. Since dissipation, maintenance and biomass synthesis cost cannot be easily distinguished they were lumped into one parameter term. However, some mechanistic models which incorporate photosynthetic dissipation explicitly and include

photoinhibition and repair have been developed (F. García-Camacho, A. Sánchez-Mirón, E. Molina-Grima, F. Camacho-Rubio, & J. C. Merchuck, 2012).

It was proposed by Klok et al. (2013) that starch and functional biomass are preferred in a nutrient replete environment, whilst TAGs are preferred when there is an excess of electrons entering cells relative to carbon fixation during high light intensity or nutrient depletion. Thus, starch is the preferred source of carbon storage during growth whilst TAGs are favoured during suboptimal growth conditions. The concept of using an electron balance, in the context of algal composition modelling, is novel having strengths in relating the energy balance between photosynthetic light and dark reactions with catabolic and dissipation losses and metabolite anabolism.

The interaction between the different composition components in the study of Klok et al. (2013), such as for lipids, is not as advanced as other mechanistic models (Adesanya et al., 2014; Kunikane & Kaneko, 1984; Mairet et al., 2011; Yoo et al., 2014) due to the simplicity of the operating system as a steady state continuous reactor. Models applied to larger scale pilot plants (Grima et al., 1999; James & Boriah, 2010; Ketheesan & Nirmalakhandan, 2013) normally involve dynamic batch or plug flow systems limiting the practical application of this composition mechanism. It may be useful in future to work to include processes for lipids catabolism for energy or functional biomass synthesis.

Zhang et al., (2014) uses the photosynthetic quotient as the basis of their mechanistic model for composition kinetics. The quotient is the molar ratio of oxygen released by algae over the net molar uptake of CO_2 (Edward A. Laws, 1991). Production of carbon skeletons for metabolite synthesis, NADPH formation and energy production in the form of ATP represent the three carbon sinks within algal cells. The starch, TAGs and functional biomass fraction specific quotients, molar masses and yield coefficients can be calculated form the

stoichiometry of their respective reactions. The overall photosynthetic quotient was measured using CO_2 and oxygen mass balances. The apparent photosynthetic quotient is the weighted sum of the photosynthetic quotients of each fraction with the weights being the mass fraction of each component of total biomass. The change in the mass fraction describes the dynamic nature of composition kinetics.

Since the mass fraction can be any arbitrary value between zero and one and there is no model to predict fraction kinetics. The model is empirical in nature rather than predictive unlike previous composition models described. Therefore, there is no explanation as to what is regulating the composition of algae as it is found simply from model fitted mass fractions and empirically measured stoichiometry and quotients. However, the Klok et al., (2013) model does show the fraction of carbon which is dedicated towards energy requirement cost as well as determining that portion of energy goes towards production of reducing agents, NADH, $FADH_2$. It was assumed that the production of ATP from photophosphorylation (conversion of ADP to ATP) was negligible meaning that aerobic respiration was the primary source of energetic molecule formation. This has important practical consequences since it shows how carbon to biomass yield and energy yield can vary with time and nutrient status affecting process economics. However, the empirical nature of the model means that the connection between carbon to biomass & energy yields with environmental conditions is not established meaning that the framework in its current form cannot be applied to predictive modelling for process optimisation.

However, the use of fraction stoichiometry and its incorporation into photosynthetic quotient is an important development in algal composition modelling as it opens the possibility of integration with physicochemical models. The primary assumption made in all conceptual frameworks is that CO_2 kinetics is negligible. However, the dynamic nature of outdoor ponds and close photo bioreactors receiving a cyclical light flux results in fluctuations in the H^+,

CO_2 and O_2 concentrations (Craggs, Sutherland, & Campbell, 2012; Jiménez et al., 2003). Experiments have also shown that CO_2 enrichment can affect composition by increasing the fatty acid content of algae (Gordillo, Goutx, Figueroa, & Niell, 1998; Tsuzuki, Ohnuma, Sato, Takaku, & Kawaguchi, 1990) and polyunsaturated fatty acid productivity (Chrismadha & Borowitzka, 1994). This may be related to a higher carbon to nitrogen uptake rate favouring lipid accumulation to balance the excess carbon flux fixed into biomass. The consumption of CO_2, production of O_2 and H^+ uptake can be determined from stoichiometric reactions as they are a function of the photosynthetic quotient (Zhang et al., 2014). Integration with physicochemical models (Grima et al., 1999; Ketheesan & Nirmalakhandan, 2013) will then be possible presenting further research potential into determining how physico-chemistry dictates algal composition kinetics in outdoor reactors.

2.4.2 Mathematical Models

The simplified mechanism forms the basis of the mathematical model in terms of mass balances and kinetics expressions. This section will evaluate the use of kinetic regulators in mathematical models for describing algal composition kinetics. Tables 2.3 to 2.5 below show the mathematical models of starch and/or carbohydrates, TAGs and/or lipids and functional biomass derived from the mechanistic models of Figs 2.2 to 2.5. The symbols for parameters and variables are explained in the nomenclature. The uptake of carbon from photosynthesis, heterotrophy or mixotrophy as a function of light, nitrogen and glucose are not shown as they are either already well developed (Kevin J Flynn & Mitra, 2009; F. García-Camacho et al., 2012; R. J. Geider et al., 1998) and not within the scope of this study which focuses on composition kinetic modelling not growth mode modelling.

Table 2.3 Kinetic expressions for modelling composition of the functional biomass-lipids mechanistic model approach

Reference	Species and growth mode	Functional Biomass (g F/m^3.d)	Lipids (g L/m^3.d)
Surisetty et al., 2010	Heterotrophic *C. protothecoides*	$\frac{dF}{dt} = (\mu - D)F$ $\mu = \mu_{max}\left(\frac{Q_{n,max} - Q_n}{K_q + Q_n}\right)\left(\frac{s_2}{K_{s_2} + s_2}\right)$	$\frac{dL}{dt} = \mu F \dot{L}_G - DL$ $\dot{L}_G = V_{max,LG}\left(\frac{s_2}{K_L + s_2}\right)\left(1 - \frac{L}{X}\right)$
Packer et al., 2011	Photosynthetic, *Pseudoclorococum* sp.,	$\frac{dF}{dt} = \mu F$ $\mu = min\left\{\mu_{max}\left(1 - \frac{Q_{n,min}}{Q_n}\right), \frac{p}{Q_{c,min}}\right\}$	$\frac{dL}{dt} = pF - Q_{c,min}\frac{dF}{dt}$
J. Yang et al., 2011	Photoheterotrophic *C. minutissima*	$F = \frac{X_o X_{max} e^{\mu_{max} t}}{X_{max} - X_o + X_o e^{\mu_{max} t}} - L$	$L = Y_{L/X} X + K$
De la Hoz Siegler et al., 2011	Heterotrophic *C. protothecoides*	$\frac{dF}{dt} = (\mu - D)F$ $\mu = \mu_{max}\frac{s_2}{K_{s_2} + s_2 + \frac{s_2^2}{K_{i,s2}}}\frac{Q_n}{K_q + Q_n} exp\left(-\frac{Q_{o,n} + \int_0^t Q_n dt}{K_{i,s1} t}\right)$	$\frac{dL}{dt} = V_{max,LG}\left(\frac{s_1}{K_{s_2} + s_2}\right)\left(1 - \frac{Q_n}{Q_{n,max}}\right)$
Yoo et al., 2014	Mixotrophic, *C. prototheccoides*	$\frac{dF}{dt} = (\mu - D)F$ $\mu = \mu_{max}\left(1 - \frac{Q_{n,min}}{Q_n}\right)\left(1 - \frac{L_{min}}{L}\right)\left(\frac{s_2}{K_{s_2} + s_2}\right)\left(\frac{I_o}{K_I + I_o}\right)$	$\frac{dL}{dt} = \dot{L}_G - \dot{L}_C$ $\dot{L}_G = \left(\frac{s_2}{K_L + s_2}\right)\left(1 - \frac{Q_n}{X}\right)\left(1 - \frac{L}{X}\right)$ $\dot{L}_C = V_{max,LC}\left(\frac{K_{i,s2}}{s_2 + K_{i,s2}}\right)\left(1 - \frac{L_{min}}{L}\right)$

Table 2.4 kinetic equations describing functional biomass-storage molecule behaviour

Reference	Operating Details	Functional Biomass (g F/m^3.d)	Storage Molecule (g St/m^3.d)
Adesanya et al., 2014	Photosynthetic & mixotrophic, *C. Vulgaris*	$\frac{dF}{dt} = \mu F$ $\mu = \frac{p + \rho_{s2}}{Q_{c,min}}\left(1 - \frac{Q_{n,min}}{Q_n}\right)$	$\frac{dS_t}{dt} = \left(p + \rho_{s2}\right)F - Q_{c,min}\frac{dF}{dt}$
Kunikane & Kaneko, 1984	Photosynthetic, *S. Dimorphus*	$\frac{dF}{dt} = \mu_f F$ $\mu_f = \mu_{f,max} f\left(\frac{C_p}{C_n}\right)^c \frac{N}{K_n + N}$ $f\left(\frac{C_p}{C_n}\right) = \frac{C_p/C_n - Q_{p/n,min}}{Q_{p/n,max} - Q_{p/n,min}}$	$\frac{dS_t}{dt} = \left(\mu_p - \frac{1}{Y_{F/S}}\mu_f - k_d\right)F\frac{Q_{n/x}}{Q_{n/x,max}}$ $\mu_p = \mu_{c,max} f\left(\frac{C_p}{C_n}\right)^a$

Table 2.5 Kinetic expressions defining functional biomass, carbohydrates and lipids behaviour

Reference	Operating Details	Functional Biomass (g F/m^3.d)	Starch/Sugars (g S/m^3.d) or (g Sugars/m^3.d)	Lipids/TAGs (g L/m^3.d) or (g T/m^3.d)
Mairet et al., 2011	Photosynthesis, *I. galbana*	$\frac{dF}{dt} = \left(Y_{F/G,n} + Y_{F/L,n}\right)\rho_{n,x}\mathrm{X} - \mathrm{DF}$ $\frac{dX}{dt} = \mu_{max}\left(1 - \frac{Q_{n,min}}{Q_n}\right)\mathrm{X} - \mathrm{DX}$	$\frac{dS_u}{dt} = \dot{G}_G - \dot{G}_C$ $\dot{G}_G = \mu_{max}\left(1 - Y_{L/G,n}Q_n\right)\left(1 - \frac{Q_{n,min}}{Q_n}\right)X$ $\dot{G}_C = Y_{F/G,n}\rho_{n,x}X + DS_u$	$\frac{dL}{dt} = \dot{L}_G - \dot{L}_C$ $\dot{L}_G = \mu Y_{L/G,n}Q_nX$ $\dot{L}_C = Y_{F/L,n}\rho_{n,x}X + DL$
Klok et al., 2013	Photosynthesis, *N. oleoabundans*	$0 = \rho_F - DF$ $\rho_F = Y_{F/e}\sigma_N\rho_n$	$0 = \rho_s - DS$ $\rho_s = Y_{S/e}\left(\sigma_N\rho_n + \frac{r_{Ph}}{Y_{Ph,e}}\right)$	$0 = \rho_T - DT$ $\rho_T = Y_{T/e}\sigma_N(1 + \sigma_S)\left(\rho_{n,r} - \rho_n\right)$

The functional biomass kinetic expressions are primarily regulated by external nitrogen, internal nitrogen quota and the quantity of carbon entering the cells for molecule synthesis. For heterotrophic cultures the carbon source is organic following Monod kinetics (Surisetty et al., 2010) with some models including substrate inhibition terms (De la Hoz Siegler et al., 2011) occurring at excessive concentrations. Photosynthetic cultures are regulated by photosynthetic carbon fixation rate under light limited conditions. Thus, mixotrophic and photoheterotrophic functional biomass kinetic expressions would be regulated by both photosynthetic carbon fixation and heterotrophic organic carbon uptake as shown in the literature (Adesanya et al., 2014; Yoo et al., 2014).

When CO_2 was, saturated external nitrogen uptake was assumed to be regulating functional biomass synthesis for continuous cultures (Klok et al., 2013; Mairet et al., 2011). Lipids were also identified as being a source of functional biomass carbon being proportional to nitrogen uptake (Mairet et al., 2011). In contrast batch models of functional biomass use nitrogen quota as the primary regulator for synthesis when nitrogen has become depleted (Adesanya et al., 2014; Packer et al., 2011). This could suggest that nitrogen quota is not an important regulator of functional biomass kinetics at nutrient replete conditions, rather bulk nitrogen concentration may be important as suggested by other expressions (Klok et al., 2013; Mairet et al., 2011). However, external nitrogen uptake rate is not only a function of external nitrogen concentration but coupled to nitrogen quota (Lehman, Botkin, & Likens, 1975). Therefore functional biomass synthesis kinetics can be regulated by both intracellular and extracellular nitrogen, with nitrogen quota becoming important when nitrogen is depleted or at very low concentrations whilst bulk nitrogen is an important regulator during nitrogen replete conditions (Lehman et al., 1975).

The regulators of lipid kinetics can be divided into component saturation, intracellular and extracellular substrate limitations and nitrogen, which can be either internal nitrogen quota or external nitrogen concentration. Component saturation occurs because cells can only occupy a finite volume putting a limit on the fraction of cell volume or mass dedicated towards storing lipids. This normally involves a linear expression being asymptotic to a limiting mass fraction which is a fitted parameter (De la Hoz Siegler, 2012) or being limited to the total biomass (Surisetty et al., 2010; Yoo et al., 2014). As the lipid concentration approaches the total biomass or estimated lipid parameter limit the rate of generation decreases.

Carbon uptake due to photosynthesis, organic uptake or both is another regulator, which promotes lipid accumulation. Lipid accumulation is depicted as proportional to organic carbon uptake and modelled by Monod kinetics (Adesanya et al., 2014; Surisetty et al., 2010; Yoo et al., 2014). In contrast, light dependant lipid generation is regulated by photosynthetic carbon uptake using Poisson single hit models or modified Monod kinetics expressions (Adesanya et al., 2014; Packer et al., 2011; Yoo et al., 2014).

The nitrogen quota is another important regulator of lipid kinetics having an inverse relationship with lipids. This contrasts with functional biomass, which has a positive correlation with external and internal nitrogen. A reason for the inverse relationship may be because enzymes responsible for glycolysis become upregulated during nitrogen depletion increasing carbon flux towards fatty acid synthesis (J. Li et al., 2014). This relationship is normally expressed using an inverse linear relationship similar to ones used for functional biomass kinetic expressions (De la Hoz Siegler et al., 2011; Yoo et al., 2014).

According to the carbon and nitrogen related kinetic expressions high carbon uptake coupled with a low nitrogen concentration would increase lipid generation rate. This is due to high carbon to nitrogen uptake ratio favouring the formation of carbon rich compounds. In response, functional biomass productivity would decrease eventually to zero once the minimum subsistence quota is reached. The generation of lipids would only be limited by component saturation and the energy requirement for cell maintenance and metabolite synthesis.

When modelling from an electron balance perspective, Klok et al., (2013) simulated TAGs accumulation being proportional to the excess quantity of electrons not already fixed in functional biomass and starch. This essentially gives preferences to carbon channelling towards starch and TAGs before being utilised for TAGs synthesis. Similarly, conventional carbon equivalent-based models prioritise carbon fixation into functional biomass (Adesanya et al., 2014; Mairet et al., 2011; Packer et al., 2011) but do not show any relation to starch kinetics. It was found through linear regression analysis that only 8.6 % of excess electrons were channelled towards TAGs with the remaining being dissipated through maintenance, catabolism and dissipation of excess light. This suggests that TAGs are not a priority for the channelling of excess electrons. Logically the biomass is channelling electrons towards maintenance energy and biomass synthesis before fixing into TAGs. Excess light is also dissipated to ensure that electron transfer rate between light and dark photosynthetic reactions are equal.

Restoring nitrogen in the system would result in channelling the carbon fixed in lipids towards functional biomass once again as shown in experiments and in composition modelling (Fernandes et al., 2013; Mairet et al., 2011). Therefore, consumption terms are generally a function of the functional biomass growth rate or concentration indicating growth related consumption (Mairet et al., 2011; Packer et al., 2011). This suggests why lipids do not

accumulate to a high percentage of cell constituents during nitrogen replete conditions. Yoo et al. (2014) related lipid consumption to cell energy requirement. This process was promoted when the external carbon concentration approached zero meaning that when the rate of carbon entering the cells becomes less than the basal energy requirement the lipids fraction is broken down for energy. The other regulator was lipid saturation with higher cell lipid content increasing kinetics towards consumption.

Storage molecule formation follows similar kinetics to lipid metabolism since lipids form a significant proportion of storage molecules. The other major component is carbohydrates. Generation is a function of photosynthetic or organic carbon fixation and consumption is a function of either functional biomass concentration (Kunikane & Kaneko, 1984) or functional biomass productivity (Adesanya et al., 2014).

Explicit kinetic models of starch or carbohydrates are scarce (Klok et al., 2013; Mairet et al., 2011) despite carbohydrates having importance as a feedstock for animal feed (Luque, 2010) and chemicals (Bozell & Petersen, 2010). The synthesis of carbohydrates was related growth and nitrogen uptake (Klok et al., 2013; Mairet et al., 2011) but appeared to be limited by an increasing nitrogen quota which is also a growth related regulator (Mairet et al., 2011). This suggests carbohydrates may accumulate fastest at moderate nitrogen concentrations or mild nitrogen depletion in the early stationary phase shown by some experimental studies (Chia, Lombardi, da Graça Gama Melão, & Parrish, 2015; Fernandes et al., 2013; Takeshita et al., 2014). This may be why carbohydrates is the dominant storage form under more growth promoting conditions and lipids accumulate under more severe nutrient depletion uncoupled from growth, which has been noted by other authors (T. Li et al., 2015; S. Zhu et al., 2014).

One limitation is that models show limited if any relationship between starch and other fractions of algae. In contrast, lipids can be utilised for functional biomass synthesis or are formed from excess electrons being channelled to a sink. Mairet et al. (2011) showed some interaction by developing a model, which prioritised carbon into functional biomass, followed by lipids and then carbohydrates. Thus, the kinetics of carbohydrates was dictated by the synthesis of lipids and functional biomass. Sugar could also be converted into lipids with the remainder forming the carbohydrate fraction of algae. Both sugar catabolic terms towards functional biomass and TAGs were proportional to either extracellular nitrogen concentration or intracellular nitrogen quota. This does not account for behaviour under nitrogen depletion where studies show for some green algae, starch and TAGs generation become inversely related to nitrogen (Adesanya et al., 2014; Fernandes et al., 2013). The starch concentration eventually decreases in extended depletion whilst TAGs is inversely related to nitrogen status contradicting the positive correlation with nitrogen status as modelled by Mairet et al. (2011). During this stage glycolysis becomes activated (J. Li et al., 2014) suggesting that starch may be broken down to produce TAGs explaining why the concentration decreases across many species during nitrogen depletion (Takeshita et al., 2014). This behaviour has not been simulated by any models reviewed in this study and should be the subject of future composition modelling work.

2.4.3 Model Implementation

Now that the reader is familiarised with how models are developed in the literature the next step is implementation of the model, which involves minimisation of an objective function and tuning parameters. The tuned parameters would ideally have a biological basis thus, would follow imposed theoretical constraints as well as having agreement with previously published literature parameter values, all of which will be discussed in this section.

2.4.3.1 Error Minimisation

To reduce the deviation of model predicted values from experimental data the objective function defining the sum error is minimised. In the algal modelling composition literature this typically involves using the sum squared error method (Adesanya et al., 2014; Packer et al., 2011) with others modifying it to include a weighted sum error to account different error calculated for each measured data point (De la Hoz Siegler et al., 2011; J. Yang et al., 2011; Yoo et al., 2014).

$$WSSE = \sum_{i=1}^{n} \sum_{j=1}^{m} W_{ij} \left(y_{ij} - \hat{y}_{ij}\right)^2 \tag{2.1}$$

where $WSSE$ is the weighted sum error, n is the number of experimental data points for each state variable, m is the number of measured state variables, y_{ij} is the experimental measurement of a state variable j for a sample number or time i, $\hat{y}_{ij}$ is the corresponding predicted value and W_{ij} is the corresponding error weight of the data point. The error weight provides greater priority on minimising the model error for measured data points that have low variability relative to other measured data points and is normally expressed in the following manner (J. Yang et al., 2011; Yoo et al., 2014).

$$W_{ij} = \frac{1}{\sigma_j \lambda_j} \tag{2.2}$$

where σ_{ij} is the standard deviation of the experimental state variables and λ_j is a scaling factor to normalise the measured values against one of the measured states (Yoo et al., 2014).

$$\lambda_j = \frac{\sum_{i=1}^{n} \left| y_{ij} - \bar{y}_{ij} \right|}{\sum_{i=1}^{n} \left| y_{ij_r} - \bar{y}_{ij_r} \right|} \tag{2.3}$$

where y_{ij_r} is the measurement of the reference variable and $\bar{y}_{ij}$ and $\bar{y}_{ij_r}$ are the average value of the state variable and reference variable in their data sets.

One problem with using the sum of squared error as the objective function is that it puts a bias on minimising the state variables, which have the largest magnitude since they have the greatest contribution towards increasing the sum of squared difference between the model and the measured states. This would not be a problem if the state variables in question were of a similar magnitude. However, many composition papers (Adesanya et al., 2014; De la Hoz Siegler et al., 2011; J. Yang et al., 2011) minimise model error where variables such as chlorophyll content, nitrogen quota and nitrogen concentration are 2-3 orders of magnitude less than composition fractions such as proteins, carbohydrates and lipids.

Therefore using a relative sum error as the objective function would be more appropriate as it would remove the bias on large magnitude variables (Shammas, 2012).

$$RSSE = \sum_{i=1}^{n} \sum_{j=1}^{m} \left(\frac{\hat{y}_{ij}}{y_{ij}} \right)^2 \tag{2.4}$$

where $RSSE$ is the relative sum squared error. The error weight can also be applied to this objective function in a similar manner to (2.1). To gauge the goodness of fit the R^2 value may be calculated in the following manner (Shammas, 2012).

$$R^2_{RSSE} = \frac{\sum_{i=1}^{n}\sum_{j=1}^{m}\left(\left(\hat{y}_{ij} - \bar{y}_{ij}\right)/y_{ij}\right)^2}{\sum_{i=1}^{n}\sum_{j=1}^{m}\left(\left(y_{ij} - \bar{y}_{ij}\right)/y_{ij}\right)^2} \tag{2.5}$$

where R^2_{RSSE} is the coefficient of determination using the relative sum squared error as the objective function. An alternative function which simultaneously acts as an objective function and an indication of goodness of fit could be the average percentage error. This term converts the sum of squared error into an average absolute percentage difference between the model and the measured data. The derivation of this term is shown below by transforming the relative sum squared error (2.4).

$$RSSE = \sum_{i=1}^{n}\sum_{j=1}^{m}\left(\frac{\hat{y}_{ij}}{y_{ij}}\right)^2$$

The difference between the model and measured variable was introduced in the numerator to limit the range between $0 < RSSE < 1$. The square root was introduced to convert the relative sum error to an absolute value.

$$= \sum_{i=1}^{n}\sum_{j=1}^{m}\sqrt{\left(\frac{y_{ij}-\hat{y}_{ij}}{y_{ij}}\right)^2}$$

$$= \sum_{i=1}^{n}\sum_{j=1}^{m}\left|\frac{y_{ij}-\hat{y}_{ij}}{y_{ij}}\right|$$

Multiplying by 100 converts the decimal relative sum difference to a percentage sum difference.

$$= 100 \sum_{i=1}^{n} \sum_{j=1}^{m} \left| \frac{y_{ij} - \hat{y}_{ij}}{y_{ij}} \right|$$

The product of the number of measured state variables and sample size gives the total number of data points. Dividing by this value will give the average absolute percentage model error for each data point.

$$= \frac{100}{n \times m} \sum_{i=1}^{n} \sum_{j=1}^{m} \left| \frac{y_{ij} - \hat{y}_{ij}}{y_{ij}} \right| \tag{2.6}$$

This expression of the percentage divergence between experimental and simulated data makes it easier to interpret the quality of the fit, which is not as intuitive using a sum squared error method or R^2 value.

2.4.3.2 Biological Parameter Constraints

Minimising the model error to within the error margin of experimental measurement does not ensure model validity. Once a set of parameters has been obtained it is important to ensure that they are realistic in magnitude. Parameter validation is commonly done by comparing fitted results with literature values. However, this does not necessarily validate the link between the parameter and biological processes, which are instead determined by a set of constraints. In the emerging field of algal composition, modelling constraints may also be pertinent as literature values for comparison may be scarce or completely lacking. Constraints on parameters may be imposed because of theoretical biological limits or due to changing environmental conditions related to nitrogen, light and growth status. Parameter constraints as a function of environmental conditions are more likely to be difficult to satisfy than the theoretically limited ones. This is

because the parameters themselves are in fact dynamic quantities dependant on environmental conditions, which will vary over time thus, the fitted value is an average value, which may not show expected trends or satisfy constraints. However, even if parameters are dynamic, they still cannot violate the theoretical biological limits therefore exceeding the limits will mean there is a problem with the model or the assumptions used to develop the constraint.

Table 2.6 below summarises a proposed set of constraints for the more common parameter values used in composition modelling. The reader is referred to more extensive nutrient kinetic studies for a more comprehensive description of parameters values used in algal nutrient-kinetic modelling (Arhonditsis & Brett, 2005; Hamilton & Schladow, 1997; Zhao, Ramin, Cheng, & Arhonditsis, 2008). Some carbon specific parameters are reported as being specific to functional biomass using the notation of recent composition modelling papers (Adesanya et al., 2014; Packer et al., 2011) rather than being specific to total cell carbon used in traditional nutrient kinetics papers (M.R. Droop, 1975; R. J. Geider et al., 1998).

Table 2.6 Reported literature values of common model parameters with proposed constraints

Parameter	Symbol	Units	Constraints
Minimum nitrogen cell quota	$Q_{n,min}$	g N/g F	$Q_{n,min} < Q_{n,max}$
Maximum nitrogen cell quota	$Q_{n,max}$	g N/g F	$Q_{n,max} > Q_n$, $Q_{n,max} < 0.17$
Quantum yield	φ	g C/mol photons	φ <1.344
Maximum specific photosynthesis rate	P_o	g C/g Chl.d	150 <E_k<500 µmol/m^2.s
Carbon to starch yield	$Y_{S/C}$	g S/g C	$Y_{S/C}$ <2.25
Carbon to lipid yield	$Y_{L/C}$	g L/g C	$Y_{L/C}$ <1.3
Carbon to functional biomass yield	$Y_{F/C}$	g F/g C	$Y_{F/C}$ <1.98

The specific absorption coefficient is a photosynthetic parameter that can be interpreted as the slope of light limited photosynthesis. As the incident light intensity approaches the saturating flux the photosynthetic yield from light decreases approaching an asymptotic value, which represents the maximum photosynthetic rate (Subramanian et al., 2013). If the light flux continues to increase eventually, photoinhibition will be initiated reducing the photosynthetic yield. This behaviour of the curve varies depending on the units used to describe the specific absorptivity (Behrenfeld, Prasil, Babin, & Bruyant, 2004). Table 2.7 below summarises absorption coefficients from the literature. It shows that empirical measurements and model fitted values agree well.

Table 2.7 Literature values of the chlorophyll specific absorptivity. All values are model fitted unless stated otherwise in the operating details

Reference	Operating Details	Light absorption coefficient (m^2/g Chl)
Anning et al., 2000	*S. costatum,* Photosynthetic, 50 µmol/m^2.s, empirical measurement	16
	S. costatum, Photosynthetic, 1200 µmol/m^2.s, empirical measurement	24
Adesanya et al., 2014	*C. Vulgaris,* Photosynthetic and mixotrophic, initial nitrogen concentration of 25 g N/m^3 and 125 g N/m^3, light flux of 85 µmol/m^2.s.	25.5
Packer et al., 2011	*Pseudochlorococum* sp., photosynthetic, 60 g N/m^3. Model predicted	4.8
Blache, Jakob, Su, & Wilhelm, 2011	*C. Vulgaris*, 8 g N/m^3, 40 µmols/m^2.s, empirical measurement, initial lag phase measurement	14
	Exponential phase measurement	19
	Late exponential/ reduced growth phase	24
	N. Salina, 40 g N/m^3, 40 µmols/m^2.s, empirical measurement, initial lag phase	34
	Exponential phase measurement	35
	Late exponential/ reduced growth phase	36
Klok et al., 2013	*N. oleoabundans*, photosynthetic, 460 µmols/ m^2.s, 25 g N/m^3.d, empirically measured	0.05 m^2/g F
	N. oleoabundans, photosynthetic, 460 µmols/ m^2.s, 75 g N/m^3.d, empirically measured	0.075 m^2/g F

When defined in terms of cell mass or volume the absorptivity varies as a function of the specific light active pigment content of the cells. Therefore some theoretical expressions express the absorption coefficient as a dynamic value being the sum of the light absorption by a specific

component (Morel & Bricaud, 1981) or more recently in composition models as a fraction of the absorbed photons channelled to biomass synthesis (Klok et al., 2013). Factors that could create transient behaviour of absorptivity include non-photochemical quenching, fraction of active light harvesting complexes, photoinhibition and light intensity (Behrenfeld et al., 2004) and the proportion of light absorbed by other minor light harvesting complexes such as chlorophyll b and carotenoids.

Most of these factors are influenced by light which may indicate that it is related to photo-acclimation (R.J. Geider, MacIntyre, & Kana, 1997). Experiments for multiple algal species confirm that greater light flux increased the chlorophyll specific absorptivity (Anning et al., 2000; MacIntyre, Kana, Anning, & Geider, 2002), providing a light specific constraint for the light absorption coefficient. Variation of absorptivity under influence of nitrogen is unclear due to different measuring metrics with some authors showing model fitted values had little sensitivity to initial nitrogen and growth mode under batch conditions staying constant at 25.5 m^2/g Chl (Adesanya et al., 2014). Others showed a positive linear relationship between absorptivity and nitrogen under a continuous culture (Klok et al., 2013), ranging from 0.05-0.075 m^2/ g F although the different units, for chlorophyll specific activity, make these findings difficult to compare.

Experimentally determined chlorophyll specific absorption for *C. Vulgaris* indicated that the absorption coefficient increased with decreasing initial nitrogen concentration. As the culture cell density increased from 15-55$\times10^6$ cell/ml the chlorophyll content decreased, 0.91-0.25 pg Chl/cell, but the absorptivity increased to compensate for the reduced pigment content from 14-24 m^2/ g Chl. This provides further evidence of the ability of the chlorophyll specific absorption coefficient to adapt to changing environmental conditions. However, once the

cells reached the stationary phase, indicated by no further cell division, the absorption coefficient decreased from 24-18 m^2/g Chl, (Blache et al., 2011) suggesting a significant change in the metabolic functions of the cells. The result of a lower specific absorption would be to reduce photosynthetic activity and biomass growth since less light is being absorbed per cell, which is supported by downstream enzymes in the Calvin cycle being down regulated to reducing CO_2 fixation (Jing Li et al., 2014). The Calvin cycle is the enzymatic process responsible for fixing CO_2. In summary, the chlorophyll specific absorptivity has a high degree of variability as a fitted parameter since it has been demonstrated to be a function of nutrient, light and growth status. This variability is a result of absorptivity changing to maintain the cellular energy balance between photon energy entering the cells and downstream energy utilisation for carbon fixation and biomass synthesis.

The next parameter for analysis is nitrogen quota. In contrast to bacterial culture algal kinetics is more strongly coupled to intracellular concentrations of nitrogen rather than extracellular concentration (Bernard, Sciandra, & Sallet, 2001). The nitrogen quota is the quantity of nitrogen stored within the cells during luxury uptake. The maximum nitrogen quota has been suggested to be linked to biosynthesis cost of nutrient uptake whilst the minimum cell quota has been linked to the minimum subsistence level to maintain cellular processes (Pahlow & Oschlies, 2013). The obvious constraint is that maximum nitrogen quota must be greater than the minimum nitrogen quota. However, the possible range of maximum and minimum quota values can vary substantially. This means that comparison of quota values may yield maximum quotas within the minimum quota range and vice versa when comparing between different studies. Further complications arise from different units used to describe cell quota with composition models

depicting functional biomass specific nitrogen content and nutrient kinetics papers defining values specific to total biomass carbon as shown in Table 2.8 below.

Table 2.8 Model fitted maximum and minimum nitrogen quota values used in composition and nutrient-kinetics models

Reference	Operating Details	Maximum Nitrogen quota	Minimum Nitrogen quota	Units
Adesanya et al., 2014	*C. Vulgaris,* photosynthetic, 25 g N/m^3	0.088	0.07	g N/g F
	photosynthetic, 125 g N/m^3	0.095	0.03	g N/g F
	C. Vulgaris, mixotrophic, 25 g N/m^3	0.098	0.07	g N/g F
	mixotrophic, 125 g N/m^3	0.065	0.03	g N/g F
Packer et al., 2011	*Pseudochlorococum* sp., photosynthetic	0.094	0.028	g N/g F
R. J. Geider et al., 1998	*Pavlova lutheri,* *S. costatum,* *Thalassiosira pseudonana,* *I. Galbana* photosynthetic	0.20	0.04	g N/g C
Yoo et al., 2014	*C. protothecoides*, mixotrophic	0.53	0.008	g N/ g F
Arhonditsis & Brett, 2005	Phytoplankton, photosynthetic	0.18	0.08	g N/g C

Protein stoichiometry data of *Nannochloropsis* sp. (Zhang et al., 2014) indicates that the functional biomass specific nitrogen quota could have a maximum theoretical value of 0.17 g N/g F. Most values do not approach the theoretical limit indicating that there may be other factors, which limit the maximum cell nitrogen quota. The maximum nitrogen quota value in one study (Yoo et al., 2014) was three times greater than the theoretical limit proposed earlier (Zhang et al., 2014). Although it is for a different species of algae it appears unrealistic that the discrepancy would be so great considering that all other maximum values specific to functional biomass were below the theoretical limit regardless of species. The reason for the discrepancy is possibly due to the expression of nitrogen kinetics.

The uptake of nitrogen is dependent on the nitrogen source with ammonia being the preferred source followed by nitrate and then urea. This is a result of the higher metabolic costs of reducing alternative nitrogen source to ammonium before assimilation. The uptake of nitrogen can be the result of a high affinity transport system which is regulated by cellular nitrogen status and a low affinity system, which increases as a result of increasing external nitrogen concentration (Perez-Garcia et al., 2011). As such, commonly employed nitrogen kinetic expressions have two factors dictating uptake being external nitrogen concentration and internal nitrogen quota (Lehman et al., 1975). Table 2.9 shows that there can be relatively large species dependant divergence in the maximum nitrogen uptake rate for some studies (R. J. Geider et al., 1998) whilst other show little divergence (Adesanya et al., 2014). The maximum nitrogen uptake rate of (Ketheesan & Nirmalakhandan, 2013) at 0.004 g N/g biomass.d may be unrealistic, when considering the similarity of operating conditions to other studies shown in Table 2.9. In fact, the maximum nitrogen uptake rate of Ketheesan and Nirmalakhandan (2013) is orders of magnitude below values reported by other studies.

Table 2.9 Model fitted values of the maximum specific nitrogen uptake rate.

Reference	Operating Details	Maximum Specific Nitrogen uptake	Units
Adesanya et al., 2014	*C. Vulgaris*, photosynthetic & mixotrophic for initial 25 g N/m^3 and 125 g N/m^3 concentration, 85 µmol/m^2.s	0.68	g N/g F
R. J. Geider et al., 1998	*P. lutheri, S. costatum,* photosynthetic	0.6	g N/g C
	I. Galbana	0.5	g N/g C
	T. pseudonana	1	g N/g C
Kunikane & Kaneko, 1984	*S. dimorphus*, photosynthetic	0.6	g N/g biomass.d
Ketheesan & Nirmalakhandan, 2013	*N. salina*, photosynthetic, 40 g N/m^3, 85 µmol/m^2.s	0.004	g N/g biomass.d
Packer et al., 2011	*Pseudochlorococum* sp., photosynthetic, 60 g N/m^3, 600 and 85 µmol/m^2.s	0.596	g N/g F

The half saturation coefficient of nitrogen uptake is the concentration at which nitrogen uptake is half the maximum uptake rate. It is commonly employed in nutrient-kinetic and composition models using a Monod function to show limiting concentration effects on uptake kinetics (Adesanya et al., 2014; Ketheesan & Nirmalakhandan, 2013). The half saturation coefficient was reported to be a function of the external nitrogen concentration, increasing from 0.00252 g N-NO_3^-/m^3 for an external nitrogen concentration greater than 0.014 g N-NO_3^-/m^3 and 0.0014 g N-NO_3^-/m^3 when the bulk nitrogen concentration was less than 0.014 g N-NO_3^-/m^3 (Kristiansen & Farbrot, 1991).

However, as shown in Table 2.10 below, the initial nitrogen concentration reported is orders of magnitude higher than the half saturation constant, which may indicate that the system is insensitive to this parameter. A reason for such as large discrepancy between the culture concentration and the half saturation is that algae has adapted to efficiently absorb nitrogen at much lower concentrations in the natural environment where concentration can be less than 1 g N/ m^3 (Kristiansen & Farbrot, 1991). Therefore, employing a nitrogen related constraint might not be practical as it is likely the parameter may violate it due to model insensitivity. This may indicate that other factors such as nitrogen quota are more important in dictating nitrogen uptake kinetics and cell division for experimental cultures on synthetic media (M.R. Droop, 1975).

Table 2.10 Estimates of the half saturation coefficients. Values are fitted unless stated otherwise

Reference	Operating Details	Half saturation coefficient (g N/m^3)
Adesanya et al., 2014	*C. Vulgaris*, photosynthetic & mixotrophic for initial 25 g N/m^3 & 125 g N/m^3 concentration	0.0602
R. J. Geider et al., 1998	*P. lutheri, S. costatum,* *T. pseudonana,* photosynthetic	1.4×10^{-3}
	I. Galbana, photosynthetic	4.2×10^{-3}
Kunikane & Kaneko, 1984	*S. dimorphus*, photosynthetic, 0.1 g N/m^3	0.018
Ketheesan & Nirmalakhandan, 2013	*N. salina*, photosynthetic, 40 g N/m^3	0.02
Packer et al., 2011	*Pseudochlorococum* sp., photosynthetic, 60 g N/m^3	1.03×10^{-5}
Nielsen, 1978	*Selenastrum capricornutum,* photosynthetic, experimental measurement	5×10^{-5}
Kristiansen & Farbrot, 1991	Marine phytoplankton, in-situ measurement at the Barents Sea, > 0.014 g N-NO_3^-/m^3	0.0182 g N-NH_4^+/m^3 0.0252 g N-NO_3^-/m^3 0.0028 g N-urea/m^3
	< 0.014 g N-NO_3^-/m^3	0.0014-0.0028 g N/ m^3 for NH_4^+, NO_3^- and urea

No experimentally determined theoretical maximum values for the chlorophyll to nitrogen ratio could be found to validate the fitted results tabulated below. However, dynamic chlorophyll to nitrogen ratio measurements in batch cultures indicate for the same algal species the ratio decreases from 0.38-0.15 g Chl /g N from culture nitrogen ranging from 2.68-0.18 g N-NO_3^-/m^3 (Yentsch & Vaccaro, 1958) over 2 days. When higher initial nitrogen of 17.6 g N-NO_3^-/m^3 was

used for a culture of axenic *Scenedesmus* sp. the chlorophyll content in biomass increased from 5-10 mg Chl/g X during the exponential growth phase in the first 30 hours, but then decreased once nitrogen was exhausted to less than 1 mg Chl/g X. The model fitted chlorophyll content for *Chlorella* sp. was also higher from 0.28-1.06 mg Chl/g X for both mixotrophic and photosynthetic cultures when initial nitrogen was adjusted from 25-125 g N-NO_3-/m^3 (Adesanya et al., 2014; Halfhide, Åkerstrøm, Lekang, Gislerød, & Ergas, 2014) shown in Table 2.11. This indicates that increasing bulk nitrogen concentration increases nitrogen flux towards synthesising chlorophyll.

Table 2.11 Fitted values of the maximum chlorophyll to nitrogen ratio

Reference	Operating Details	Maximum chlorophyll to nitrogen ratio (g Chl/ g N)
Adesanya et al., 2014	*C. Vulgaris*, 25 mg N/l, photosynthetic and mixotrophic	0.28
	C. Vulgaris, 125 mg N/l, photosynthetic	0.81
	C. Vulgaris, 125 mg N/l, mixotrophic	1.06
Packer et al., 2011	*Pseudochlorococum* sp., photosynthetic	0.28
R. J. Geider et al., 1998	*P. lutheri, S. costatum, I. Galbana,* photosynthetic	0.3
	T. pseudonana, photosynthetic	0.4

The quantum yield is a ratio that describes the efficiency at which light energy is harnessed to fix carbon per mol of photons. The inverse of the quantum yield is the quantum requirement, which describes how many photons are fixed per gram or mol of carbon. It is also common to express

these values in terms of oxygen rather than carbon, (Silkman, 2008) however carbon specific yields will be the subject of this paper. Table 2.12 below summarise the average quantum yield of selected photosynthetic and mixotrophic cultures.

Table 2.12 Model fitted values of the average quantum yield

Reference	Operating Details	Quantum yield (g C/ mol photons)
Packer et al., 2011	*Pseudochlorococum* sp., photosynthetic, 600 PAR µmols/m^2.s, 60 mg N/l	1.18
Adesanya et al., 2014	*C. Vulgaris*, photosynthetic & mixotrophic, 25 mg N/l	1.19
	C. Vulgaris, photosynthetic & mixotrophic, 125 mg N/l	0.44
Quinn et al., 2011	*N. oculata*, photosynthetic, 165 mg N/l	0.65

The theoretical quantum requirement to fix one mol of CO_2 was initially proposed to be 8 photons (Emerson, 1958). Some authors have argued on whether a theoretical quantum requirement of 8 is possible due to additional processes such as cyclic photophosphorylation increasing the requirement to 9 photons or yield of 0.112 mol CO_2/mol photons (Singsaas, Ort, & DeLucia, 2001; Subramanian et al., 2013). This value was used as the basis for the calculation of a more conservative theoretical maximum specific carbon yield of 1.344 g C/mol photons.

Numerous factors increase the apparent quantum requirement such as nutrient stress (Subramanian et al., 2013), photorespiration (Singsaas et al., 2001) and light saturation (Lluz & Dubinsky, 2013). Nutrient stress such as depletion was observed to increase the quantum requirement to 20 mol of photons per mol of CO_2 fixed (Babin et al., 1996; Subramanian et al.,

2013). Therefore, a higher average quantum yield is expected to be found for cultures, which have a higher nitrogen concentration forming a nutrient related constrain. Photorespiration is not expected to be an important factor influencing quantum yield since many experiments operate at CO_2 flow volume concentrations of 5-10 % reducing competitive inhibition from O_2 which would otherwise reduce carbon fixation (Singsaas et al., 2001). Light saturation will result in a reduction in quantum yield due to the rate of light capture exceeding the rate of utilisation. The excess energy within activated chlorophyll molecules is released via heat, fluorescence or transferred to form reactive oxygen species that can damage the photosynthetic apparatus (Subramanian et al., 2013). These environmental factors all act to reduce the quantum yield of carbon to less than the theoretical limit. Since many composition models describe dynamic systems, the effect of these factors on quantum yield will be transient; therefore, the fitted yield is the average of the quantum yield over a specific time period.

The light saturation intensity is the rate at which photosynthetic electron transport reaches a maximum (Gorbunov, Falkowski, & Kolber, 1999). This marks the transitions from being light limited to light saturated in kinetics (Sutherland, Turnbull, Broady, & Craggs, 2014). Light fluxes exceeding the maximum value will damage light harvesting antennae requiring continuous repair. As shown below in Eq. 2.7 the light saturation intensity can be expressed as a function of photosynthetic parameters (Quinn et al., 2011).

$$E_k = \frac{P_{max}}{\alpha\varphi} \tag{2.7}$$

where E_k is the saturation light intensity (μmols/m^2.s) and the other symbols are described in Table 2.6. The saturation light intensity appears to vary significantly between different species and varying culture light intensity and nutrient load suggesting cellular biology and acclimation

result in a range of possible light saturation intensities. This has led some authors to describe the ratio as the adaptation index (Gorai, Katayama, Obata, Murata, & Taguchi, 2014; Sakshaug et al., 1997) as it adjusts according to environmental stress to balance the energy of photon capture and carbon dioxide fixation. At light intensities above this level cellular processes change from being optimised towards energy to biomass conversion to reductant formation (Sakshaug et al., 1997). Some composition models of starch, TAGs and functional biomass have incorporated this effect (Klok et al., 2013). Table 2.13 below shows measured saturation light flux intensities.

Table 2.13 Literature values of the saturation light intensity of photosynthetic algal cultures

Reference	Operating details	Light Saturation Intensity (µmols/m^2.s PAR)
Moore, Suggett, Hickman, Kim, & Tweddle, 2006	Primarily *Synechococcus* phytoplankton culture, Measured at depth > 2m ocean water at a wavelength of 478 nm	74-128
Sukenik & Wahnon, 1991	*I. galbana*	300
Sutherland et al., 2014	*90% Mucidosphaerium pulchellum* mixed culture, Medium nutrient load	387
	High Nutrient load condition	314
Gorai et al., 2014	*I. galbana*	400
	D. salina	200
	Centruroides gracilis	400
	Heterocapsa circularisquama	400
Atta, Idris, Bukhari, & Wahidin, 2013	*C. Vulgaris,* Maximum volumetric biomass productivity used to indicate saturation light intensity	100-200
Bhola et al., 2011	*C. Vulgaris,* Electron transport rate was used to determine the saturation rate	300
Dauta, Devaux, Piquemal, & Boumnich, 1990	*C. Vulgaris,* Interpolated from experimental data	150
Imaizumi, Nagao, Yusoff, Taguchi, & Toda, 2014	*C. zofingiensis,* Determined from specific growth rat	1000
Quinn et al., 2011	*N. Oculata*, Photosynthetic, alternating 12:12 light-dark cycle	200

Light above the saturation limits can deactivate photosystem II centres with empirical observations indicating that an incident photon flux of 1000 μmols/m^2.s could continuously deactivate 30 % of photosystem II reaction centres (Baker & Bowyer, 1994). This would result in conversion of excess energy to reduced compounds such as TAGs (Kurpan Nogueira, Silva, Araújo, & Chaloub, 2015; Takeshita et al., 2014).

Given the wide range of saturation light intensities and the variability as a function of nutrient status, incident light flux and algal species the proposed range of saturated light intensities in Table 2.13 may have to be adjusted on a case-by-case basis depending on algal species to ensure constraints are appropriate. The nitrogen concentration can also contribute to saturation variability as depletion reduces the synthesis rate of chlorophyll decreasing the saturation light flux (K. J. Flynn, Davidson, & Leftley, 1993). This would form the basis of a nitrogen dependant constraint for mathematical models.

The maximum yield coefficients for the conversion of carbon to different algal composition fractions was determined from the following set of empirical stoichiometric equations on *Nannochloropsis* sp. for fractions of starch, TAGs and proteins (assumed to represent the metabolically active functional biomass fraction) (Zhang et al., 2014).

$$CO_2 + 0.665H_2O + 0.292H^+ + 0.292NO_3^- \rightarrow CH_{1.622}O_{0.338}N_{0.292} + 1.601O_2 \qquad (2.8)$$

$$CO_2 + 0.903H_2O \rightarrow CH_{1.805}O_{0.136} + 1.383O_2 \qquad (2.9)$$

$$CO_2 + H_2O \rightarrow CH_{1.667}O_{0.833} + O_2 \quad (2.10)$$

The theoretical maximum conversion can now easily be calculated from the molar mass using the following expression.

$$Y_{i/C} = \frac{M_i}{M_C} \quad (2.11)$$

where M_i is the molar mass of the specific component, being either proteins, starch or TAGs (g i/mol), M_C is the molar mass of carbon (g C/mol) and $Y_{i/C}$ is the theoretical yield of the specific biomass fraction form carbon (g X/g C). The starch to TAGs yield could be calculated by using the quotient of the TAGs molar mass (M_X) and starch molar mass in the place of M_C, assuming that the stoichiometry is 1:1 like previous. The theoretical yields were determined to be 1.98 g F/g C for functional biomass, 2.25 g S/g C for starch and 1.3 g L/g C for TAGs.

Energy is required to synthesis new cellular components therefore some fixed carbon is utilised to produce ATP. This represents the synthesis cost or growth respiration related to the accumulation of biomass in a system. Mathematically this would mean the observed fractional biomass yield is less than the theoretical yield. The dynamic yields from the literature satisfy this constraint being 1.44-1.64 g F/g C (Adesanya et al., 2014; Packer et al., 2011) and 0.478 g L/g C (Yoo et al., 2014). No literature value for carbon to starch or carbon to carbohydrates conversion could be found due to a scarcity of composition models simulating carbohydrates behaviour.

2.5 Conclusion and Recommendations

A review on the composition kinetics modelling of algae was performed in this chapter. It was found that the fractions modelled by the literature varied as well as the mechanism used to simulate algal composition kinetics. Models could be divided into ones, which simulated algae as lipids and functional biomass, storage molecule and functional biomass or starch, TAGs and functional biomass. The former two models were the most common approaches for dynamic batch studies, whilst steady state models were able to simulate the algae as a function of the three major components. However, no dynamic models have been developed yet for photosynthetic algae that can simultaneously model starch, TAGs and functional biomass.

When implementing models, the parameters are optimised buy minimising an objective function. This objective function is most commonly the sum of squared error. However, weighted sum squared, error can be utilised or relative error can be used. The advantage of using a weighted error is that there is no bias towards minimising large magnitude variables such as starch, TAGs and functional biomass, over smaller magnitude variables such as chlorophyll content and nitrogen concentration. Expressing this objective function as a percentage error of the model is an intuitive way to express the objective function. Another factor when implementing parameters is the choice of initial parameter estimates. This can be obtained from the literature. Parameter constraints can also be implemented to ensure values are realistic and compared with literature results to ensure they are valid.

3 Model Development

3.1 Introduction

Numerous experiments have been performed on algal composition (Fernandes et al., 2013; Takeshita et al., 2014) with the objective to elucidate the influence of light and nitrogen on algae kinetics. However, scaling up laboratory experiments requires significant investment and optimisation. Modelling represents a cost effective method to supplement experimental research, which can also be used for optimisation of different fractions of algae as a function of growth limiting factors such as nitrogen and light intensity.

Composition models are composed of two parts: the carbon assimilation model, which is a function of nitrogen and light and the composition kinetic model, which is responsible for conversion of fixed carbon into the algal constituents (Adesanya et al., 2014; Packer et al., 2011; Yoo et al., 2014). Different approaches have been taken to divide the algae into its constituent components as described in Chapter 2 (De la Hoz Siegler et al., 2011; Klok et al., 2013).

Most dynamic models simulate algae either as a function of lipids and functional biomass (Packer et al., 2011) or as storage molecules and functional biomass (Adesanya et al., 2014) due to the interest in conversion of lipids into biofuels. However, neglecting starch may result in model inaccuracies. To date, there have been no batch mode photosynthetic studies that have separately simulated starch or any possible interdependence between starch and TAGs. In contrast, there are steady state continuous process models that have simulated starch, TAGs and functional biomass. These continuous models are limited for two reasons. The first reason is that they model only steady state conditions and they oversimplify biological processes, which may be occurring on a cellular level under dynamic conditions when nitrogen is depleted or light

becomes limited. The second reason is that some models relied on empirically measuring the photosynthetic quotient, the ratio of oxygen released to CO_2 absorbed, to calculate composition kinetics, meaning they are not linking nitrogen and light with composition kinetics (Zhang et al., 2014).

One hypothesised process that three component steady state models have not considered is starch glycolysis (Kumar et al., 2010). This term links starch kinetics to TAGs kinetics. The starch glycolysis process involves the breakdown of starch into glucose, which is then converted into TAGs via the fatty acid synthesis pathways. This mechanism has been proposed as starch has been shown for some species to accumulate relatively quickly under short term nitrogen depletion and then degrade under longer term depletion once it has reached a maximum (Adesanya et al., 2014; Takeshita et al., 2014). This degradation corresponds with an accumulation of TAGs.

This chapter proposes the general modelling approach based on literature equations and when appropriate, modified expressions. In addition, the model independently considers the three main fractions found in the algae, i.e., starch, TAGs and functional biomass. This chapter models starch-TAGs kinetics and then validates the proposed mechanism as a function of nitrogen and light intensity in Chapters 4 and 5.

3.2 State Variable Equations

This section outlines the model developed to simulate algal kinetics in Chapters 4 and 5. The model is composed of six state variables being starch, TAGs, functional biomass, chlorophyll, nitrogen quota and extracellular nitrogen. The variation with time of these six state variables are given by six ordinary coupled differential equations. However, the algae is assumed to be composed of only three primary fractions being starch, TAGs and functional biomass. Therefore, at any time within the system, the total biomass is equal to the sum of these three fractions:

$$X = F + T + S \tag{3.1}$$

where X is the total biomass concentration, F is the functional biomass concentration, T is the TAG concentration, S is the starch concentration.

Nitrogen quota was simulated since when extracellular nitrogen exceeds the rate at which it is assimilated for functional biomass production, nitrogen was stored in the algae cell. In addition, to account for the entire biomass polar lipids, cell wall mass i.e. cellulose and ash will be lumped with the functional biomass component. These fractions represent a minor component of total algae and are relatively constant regardless of nutrient status when compared to the kinetics of non-polar storage molecules such as starch and TAGs (Biller & Ross, 2014; Fernandes et al., 2013).

The six ordinary differential equations that model algae metabolism for extracellular nitrogen, N, chlorophyll content, B, functional biomass, F, starch, S, TAGs, T, and nitrogen quota, Q_n, are:

$$\frac{dN}{dt} = -\rho_n F \tag{3.2}$$

$$\frac{dB}{dt} = \theta_{max} \frac{\mu_A}{p_n Y_{F/C}} \rho_n - B\mu \tag{3.3}$$

$$\frac{dF}{dt} = \mu_A F \tag{3.4}$$

$$\frac{dS}{dt} = \frac{dS_p}{dt} - \frac{dS_g}{dt} \tag{3.5}$$

$$\frac{dT}{dt} = Y_{T/C} \frac{dT_p}{dt} + Y_{T/S} \frac{dS_g}{dt} \tag{3.6}$$

$$\frac{dQ_n}{dt} = \frac{\rho_n F - Q_n \frac{dF}{dt}}{F} \tag{3.7}$$

where μ is the specific growth rate of algae via photosynthesis, $Y_{T/C}$ is the carbon to TAGs yield, $Y_{T/S}$ is the carbohydrate to TAGs yield, T_p is the concentration of TAGs directly formed from photosynthesis, S_g is the concentration of starch that has been degraded to form TAGs, S_p is the concentration of starch synthesised from photosynthesis, θ_{max} is the maximum chlorophyll to nitrogen ratio, p_n is the net rate of photosynthesis, $Y_{F/C}$ is the carbon to functional biomass yield and ρ_n is the rate of extracellular inorganic nitrogen-nitrates uptake.

3.3 Equations for Secondary Variables

Nitrogen uptake rate, ρ_n, influences the uptake of extracellular nitrogen as well as storage of nitrogen into nitrogen quota. The nitrogen uptake rate is given as (Adesanya et al., 2014):

$$\rho_n = V_{n,max} \frac{N}{N + K_n} \frac{Q_{n,max} - Q_n}{Q_{n,max} - Q_{n,min}} \tag{3.8}$$

where $Q_{n,max}$ is the maximum nitrogen cell quota, $Q_{n,min}$ is the minimum nitrogen cell quota, $V_{n,max}$ is the maximum extracellular uptake of nitrogen and K_n is the half saturation constant of extracellular nitrogen uptake. The maximum nitrogen quota is the total amount of nitrogen that can be stored whilst the minimum quota is the minimum nitrogen requirement for subsistence.

Extracellular Monod kinetics, ($\frac{N}{N+K_n}$), and intracellular nitrogen quota feedback, ($\frac{q_{n,max}-Q_n}{q_{n,max}-q_{n,min}}$), processes have been used to define the uptake of extracellular nitrogen from the bulk culture. Together the two functions describe the effect of bulk nutrient limitation and internal storage limitation on fixation of nitrogen within biomass (Lehman et al., 1975).

The cell division of algae is accounted for in the specific growth rate which is dependent on the two primary limiting factors of the system being light and nitrogen (Adesanya et al., 2014).

$$\mu = Y_{F/C} p_n \left(1 - \frac{Q_{n,min}}{Q_n}\right) \tag{3.9}$$

Cell division in Eq. 3.9 depicts a positive, linear relationship with nitrogen quota indicating that greater nitrogen supply enhances cell division as it facilitates the synthesis of proteins for new cells. Increased carbon flux would clearly facilitate further cell division as specific growth is

proportional to photosynthetic fixation. The net photosynthetic rate is modelled in the following manner:

$$p_n = p - b \tag{3.10}$$

where p is the gross photosynthetic carbon uptake rate and b is the respiration constant. The respiration rate, a lumped term, accounts for loss of fixed carbon from photosynthesis due to maintenance and cell death.

The gross photosynthetic rate, shown below in Eqs 3.11 and 3.12 is a function of chlorophyll content, B, light intensity, I, and nitrogen quota mediated photosynthetic rate, p_0. Two expressions have been depicted for carbon fixation, as the dependency of algae on light is species dependent. The first expression was utilised by Macintyre et al. (2002) while the second was simplified version developed as part of this thesis:

$$p = Bp_0\left(1 - exp\left(-\frac{\alpha I\varphi}{p_o}\right)\right) \tag{3.11}$$

$$p = Bp_0 exp\left(-\frac{\alpha I\varphi}{p_o}\right) \tag{3.12}$$

where α is the specific absorption coefficient of chlorophyll related to the absorption cross section, φ is the quantum efficiency, the ratio of fixed carbon per mol of photons, I is the average light intensity and p_{max} is the nitrogen quota mediated maximum photosynthetic rate. Eq. 3.11 was used for *C. vulgaris* in Chapter 4 whilst Eq. 3.12 was used for *S. obliquus* in Chapter 5. The argument of the exponential is essentially the ratio of the apparent photosynthetic rate ($\alpha I\varphi$) and the maximum photosynthetic rate. It is dependent on the absorption characteristics of the algae, the average culture light intensity and the yield of fixed CO_2 for each mol of

photons absorbed. It is important to note that Eq. 3.12 will provide a nonzero photosynthetic rate for a zero light intensity and therefore, its applicability to low intensity cases may be limited.

Due to the small light path of experimental reactors (< 10 cm) and the high mixing rate (>100 rpm), the average culture light intensity is used to determine the average light intensity experienced by the biomass for Eq. 3.13 (Adesanya et al., 2014; Ketheesan & Nirmalakhandan, 2013).

$$I = \frac{I_o}{\alpha BFh}(1 - \exp(-\alpha BFh)) \tag{3.13}$$

$$I = I_o \exp(-\alpha BFh) \tag{3.14}$$

where I_o is the incident light intensity and h is the length of the light path. As different species of algae may follow alternate light kinetics, an exponential decay function has also been considered (Eq. 3.14). Eqs 3.11 and 3.13 is used for *C. vulgaris* in Chapter 4 whilst Eqs 3.12 and 3.14 is used for *S. obliquus* in Chapter 5.

When Eq. 3.14 is coupled with Eq. 3.12, lower values of light intensity give greater photosynthetic carbon fixation than high light intensity. Higher light intensities give a lower photosynthetic carbon uptake due to a more dilute culture absorbing less light and having a lower biomass concentration. Nevertheless, the expressions given by Eqs. 3.12 to 3.14 are not applicable for very high light intensities where photoinhibition occurs.

The nitrogen quota mediated photosynthetic rate is defined in the following manner (Quinn et al., 2011). The dependency of algal growth on nitrogen is expressed in this equation with lower nitrogen quota inhibiting algal photosynthesis, by deactivating and reducing the efficiency of

photosystem II as well as inducing photoinhibition (J.A. Berges, Charlebois, Mauzerall, & Falkowski, 1996).

$$p_o = p_{max} \frac{(FQ_n)^2}{(FQ_n)^2 + {Q_{n,min}}^2 (F + T + S)^2} \tag{3.15}$$

where $p_{max}$is the maximum photosynthetic rate and $Q_{n,o}$ is the initial nitrogen quota. The absorption of light is due to pigments composed of nitrogen thus, nitrogen deficiency would deactivate photosystem II reducing the maximum possible rate of photosynthesis (J.A. Berges et al., 1996).

The rate at which starch is synthesised from photosynthetically fixed carbon is shown below as a mass balance of the difference between total net photosynthesis and the rate of carbon fixed into functional biomass and lipids:

$$\frac{dS_p}{dt} = Y_{S/C} \left(p_n F - \frac{dT_p}{dt} - \frac{1}{Y_{F/C}} \frac{dF}{dt} \right) \tag{3.16}$$

The rate of starch consumption depicted by starch glycolysis is shown below in Eq. 3.17. This was used in Chapters 4 and 5. This starch glycolysis term, Eq. 3.17, was also compared to other expressions known as limiting conditions in Chapter 4.

$$\frac{dS_g}{dt} = V_{S,max} \left(1 - \frac{Q_n}{q_{max}} \right) F \tag{3.17}$$

where $V_{S,max}$ is the maximum starch glycolysis rate. In this term, the starch is catabolised and used as substrate for fatty acid synthesis, producing TAGs.

It is proposed that the two anabolic processes governing TAGs synthesis are direct conversion of photosynthetically fixed carbon into TAGs and starch glycolysis shown in Eq. 3.17. The rate at which photosynthetically fixed carbon is transformed into TAGs is given below in Eq. 3.18. It was used in Chapters 4 and 5. Note in Chapter 4 Eq. 3.18 was also compared to other limiting conditions to simulate algal kinetics to determine the best fit limiting condition.

$$\frac{dT_p}{dt} = p_n F \frac{K_g}{p + K_g} \tag{3.18}$$

Where K_g is the half saturation rate of photosynthetic activity.

3.4 Model Implementation & Validation

The parameters were tuned using a combination of manual refinement of parameters and the utilisation of a Matlab objective function minimisation code using the command *fminsearchbnd*.

The objective function minimised was the average percentage error between model and experiment. A relative error such as the one described was used rather than a sum squared method as it does not put a bias on minimising large magnitude variables such as starch, TAGs and functional biomass over small magnitude variables such as chlorophyll.

$$E(\hat{y}) = \sum_{i=1}^{N_d} \sum_{j=1}^{N_s} 100 \left| \frac{y_{ij} - \hat{y}_{ij}}{y_{ij}} \right| \tag{3.19}$$

where $E(\hat{y})$ is the absolute relative error, $\hat{y}_{ij}$ represents the experimentally measured value of the state variable and y_{ij} is the calculated value, which is obtained by solving Eqs 3.1 - 3.18 simultaneously, N_s is the maximum number of state variables to be compared with the

experimental data, which is 6, and N_d is the number of experimental measurements for each variable, which is 17.

The average absolute error for each data point could be calculated by dividing by the product of the number of data points and measured states.

$$A_E = \frac{E(\hat{y})}{N_d N_s} \tag{3.20}$$

where A_E is the average absolute error per data point. The average percentage error was calculated by finding the minimum final error of this objective function from a number of different initial parameter estimations.

A Matlab algorithm was developed to calculate the minimum final error in the following manner:

1. The initial guess was read from an excel file with values from literature
2. Each of the variables is multiplied by a factor. The factor is the same for all variables. The parameter multiplier for the first iteration was equal to one.
3. *Fminsearchbnd* was used to optimise the parameter values to minimise the objective function, which was the sum of the relative error between the simulated state variables and their corresponding experimental data points. The parameter set and final error was saved.
4. The code selects a new multiplier based on the equations below for even iterations:

   $$k_{multiplier} = 1 + iMS - MS \tag{3.21}$$

   For odd iterations, the following formula was used to find the multiplier:

   $$k_{multiplier} = 1 - iMS + MS \tag{3.22}$$

where $k_{multiplier}$ is the multiplier, i is the iteration number and MS is the multiplier step or difference.

5. The process given by steps two to four is repeated 10 more times with a multiplier difference of 0.15. These settings allow the magnitude of the initial guess parameters to vary by ± 0.75 units of the first parameter values read from the excel file. The setting is arbitrary and the user may increase the number of iterations and reduce the multiplier differential to find a lower final error at the cost of increased computation time.
6. Once the 11 iterations have been finished, the set of parameters is used for a second set of seven iterations. Therefore, steps one to five are repeated seven times using a multiplier step of 0.05.

Figure 3.1 below shows that the final relative error as a function of the initial parameter guess. It is illustrated that an initial guess of 0.75 units lower than the base scenario resulted in a significant final error of 90 % compared with a minimum final error of 31.6 % for an initial parameter set value 70 % of the original parameter guess. By using this method, the final error could be reduced from 35.1 % under the base parameter guess to 31.6 % when the initial parameter guess magnitude was 70 % of the base case. This error was further reduced by repeated the sequence again.

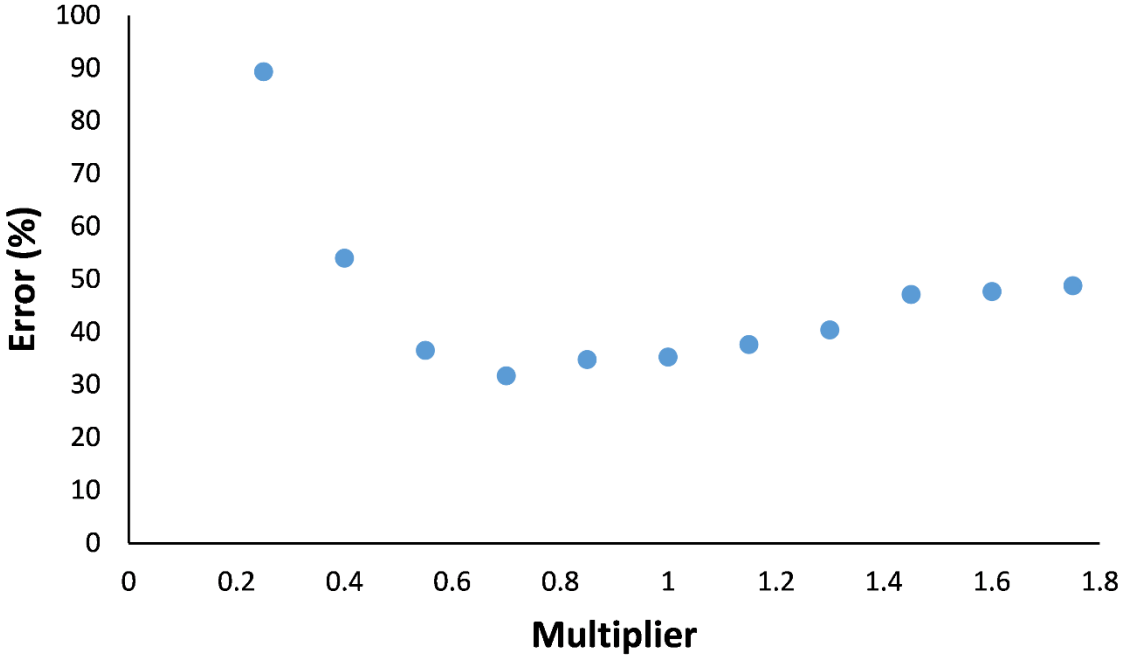

Figure 3.1 Plot of the final relative error between the experimental and simulated state variables as a function of the magnitude of the parameter multiplier.

Table 3.1 below shows an example of the initial parameter guess, its corresponding optimised parameter set and the minimum error parameter set after 11 iterations with a multiplier of 0.15. This process was repeated again to reduce final error further or to find a different parameter set, which will satisfy the parameter constraints better.

Table 3.1 Parameter sets and relative error for the simulation for the initial un-optimised parameter guess, the optimised parameter set for the initial guess and the parameter set of the minimum final error from 11 different initial guesses.

Parameter		Initial Guess	Optimised parameter set after 1st set of 11 iterations	Optimised parameter set after2nd set of 7 iterations
Error	%	70.87	35.1	31.6
a	m^2/g Chl	25.48	26.57	23.29
Q_n	g N/g F	0.070	0.072	0.073
Q_{nm}	g N/g F	0.088	0.095	0.092
V_{mn}	g N/g F.d	0.680	0.799	0.454
K_n	g N/m^3	0.060	0.069	0.033
$M_{b/n}$	g Chl/g N	0.277	0.278	0.208
qy	g C/mol photons	1.190	0.627	0.610
p_o	g C/g Chl.d	90.00	73.10	58.90
Q_{no}	g N/g F	0.080	0.107	0.051
$Y_{L/S}$	g L/g S	1.300	1.405	0.772
$Y_{L/C}$	g L/g C	0.590	0.296	0.207
$Y_{F/C}$	g F/g C	1.980	2.288	1.258
$Y_{S/C}$	g S/g C	0.821	0.726	0.503
V_{sm}	g S/g F.d	1.000	1.309	0.660
K_s	g S/m^3	0.050	0.059	0.041

3.5 Conclusion

A model has been developed to simulate the composition kinetics of algae. It is composed of six state variables being nitrogen concentration, nitrogen quota, chlorophyll content, starch, TAGs and functional biomass. These state variables were solved as a series of coupled differential

equations being functions of secondary equations such as specific growth rate, rate of nitrogen uptake, average culture light intensity, photosynthetic carbon fixation rate, photosynthetically fixed carbon to starch, photosynthetically fixed carbon to TAGs and starch glycolysis. Two different sets of equations for average culture light intensity and photosynthetic carbon fixation were used depending on the species of algae.

At least 14 parameters were optimised by minimising the objective function of a Matlab algorithm. This objective function of was minimised by using the *fminsearchbnd* command, utilising the simplex algorithm of parameter estimation for objective function minimisation. The process of parameter estimation involved reading an initial parameter estimate from an excel file followed by multiplication by a factor, which for the first iteration was one. For subsequent iterations, the multiplier was determined from the iteration number and multiplier step. The adjusted parameter values served as the input parameters for objective function minimisation. The tuned parameters were stored in an array and the optimisation completed 11 times. After completion, the parameter set that led to the minimum objective function (average percentage error) value was used as the input to the next set of iterations. The next set of iterations was completed for a multiplier step of 0.05 and carried out for seven iterations. Overall, this method allowed a lower average percentage error to be calculated using a particular set of parameters.

ACKNOWLEDGMENT OF AUTHORSHIP

I hereby certify that the work embodied in this thesis contains published paper/s/scholarly work of which I am a joint author. I have included as part of the thesis a written declaration endorsed in writing by my supervisor, attesting to my contribution to the joint publication/s/scholarly work.

By signing below I confirm that Fahim Shamsuddin contributed as the first author in writing, model development, implementation and data analysis of the paper/ publication entitled "Modeling and Validation of Starch, TAGs and Functional Biomass Kinetics of Green Microalgae as a Function of Nitrogen Concentration"

8 July, 2019

Signature of Supervisor Date

Geoffrey Evans

4 Modelling Starch, TAGs and Functional Biomass Kinetics as a Function of Nitrogen Concentration

4.1 Introduction

This chapter focuses on analysing the effect of extracellular nitrogen on the kinetics of starch, TAGs and functional biomass of the algae *C. vulgaris*. Nitrogen is one of the most commonly studied variables in the literature (Adesanya et al., 2014; Packer et al., 2011; Takeshita et al., 2014). Nitrogen is studied because of its important role in regulating total biomass growth and algal composition kinetics. In the review of Chapter 2, it was shown that there was a scarcity of models simulating starch, TAGs and functional biomass simultaneously, as a function of nitrogen load. In addition, there are no photosynthetic composition models of batch studies. Thus, the aim of this chapter is to model the starch, TAGs and functional biomass for batch photosynthetic studies as a function of nitrogen load.

The data for model calibration was obtained from Adesanya et al. (2014). Six state variables were modelled being, starch, TAGs, functional biomass, extracellular nitrogen concentration, nitrogen quota and chlorophyll. The total biomass was simply the sum of the starch, TAGs and functional biomass.

In order to model the starch glycolysis and TAGs synthesis from photosynthesis, four sets of limiting conditions were tested. Depending on these limiting conditions, 15 to 17 secondary parameters controlling the whole algal kinetics were identified and tuned in order to model the six state variables. The model predictions for each set of limiting conditions were compared with experimental data and the error of the fitting was quantified. The four limiting conditions were

also compared with one another by calculating the error for each limiting condition as well as the Akaike Information Criterion (AIC). The best limiting condition for predicting kinetics was compared with TAGs literature (Breuer et al., 2015) data for *S. obliquus* to determine whether the model was applicable to other species. The best limiting condition was also tested for limitations by extending the simulation time frame to 150 days.

4.2 Model Development

4.2.1 Proposed Mechanism and Model Assumptions

The development of the model that incorporates a starch-to-TAGs photosynthetic conversion path is based on the microalgae conversion pathways shown in Fig. 4.1. Fig. 4.1 shows that carbon may be fixed into three primary components: Functional biomass (pathway 1), TAGs (pathway 2) and starch (pathway 3). Starch can be converted into TAGs via glycolysis (pathway 4). Nitrogen quota is a minor component of biomass (< 5 %) and it quantifies the stored excess nitrogen. It is important to note that photosynthetically fixed carbon is allocated first towards maintenance respiration with the excess being channelled towards starch, TAGs and functional biomass synthesis (Adesanya et al., 2014).

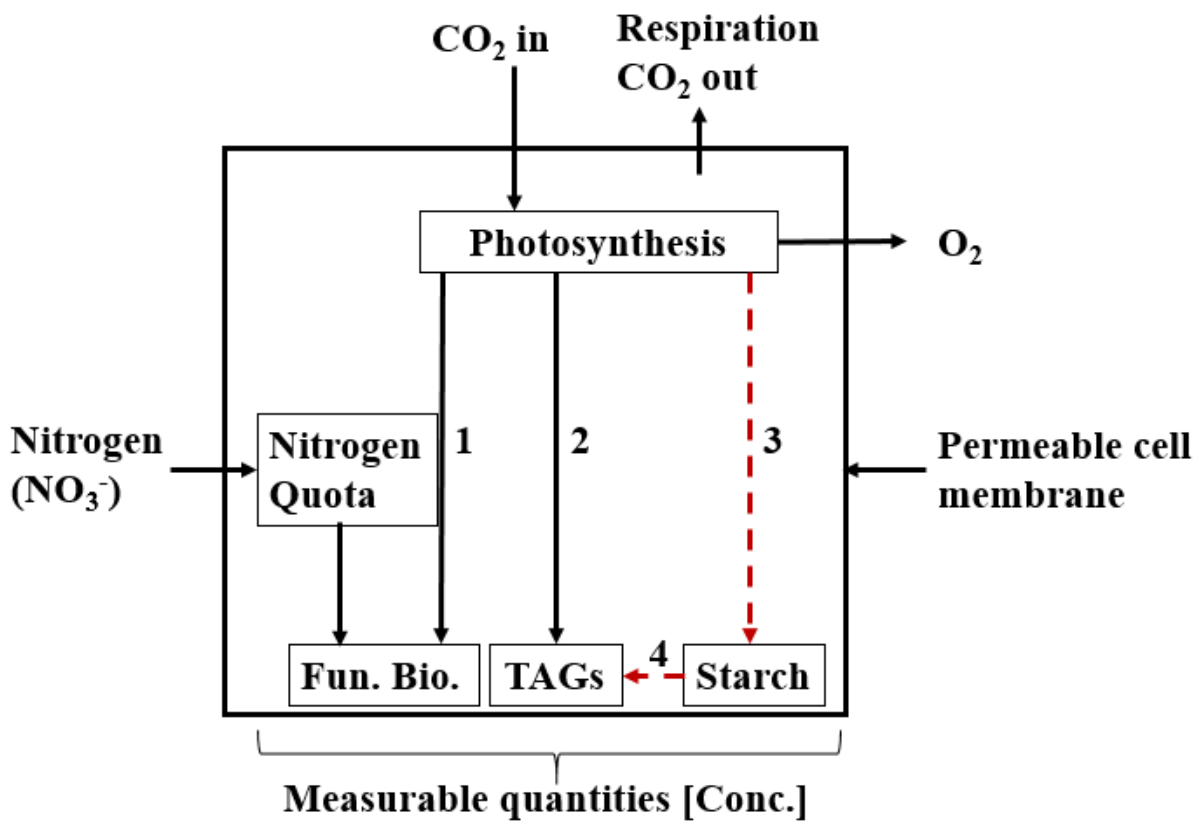

Figure 4.1 Proposed biological mechanism for composition kinetics within an algal cell. Modelled processes based on literature equations are represented by solid black arrows and the contribution of this study by dashed arrows.

The derivation of the composition kinetic mechanism depicted in Fig. 4.1 is based on the following assumptions, which are currently used in the literature:

1. Physicochemical related variables (CO_2 concentration and pH) and trace elements such as magnesium, iron, sulphur and phosphorous are in excess or remain constant, and thus have no effect on kinetics (Siaut et al., 2011).

2. Each pathway, 1-4 (Fig. 4.1), is a series of rapid chemical reactions where intermediary substrate concentrations are negligible (< 4 %) compared to starch, TAGs and functional

biomass accumulation (F. García-Camacho, A. Sánchez-Mirón, E. Molina-Grima, F. Camacho-Rubio, & J. Merchuck, 2012).

3. Small molecule excretion from the cell to the bulk culture and its consequent inhibition of cell growth are considered negligible due to assumed low substrate and biomass concentrations (Fernandes et al., 2013).

4. Starch, TAGs and functional biomass are not metabolized for respiration (De la Hoz Siegler, 2012).

In addition to the above assumptions, one of the main contributions to the present work is the consideration that TAG synthesis can also be produced due to starch glycolysis (Fig. 4.1, pathway 4). In order to explain the decrease in starch concentration experimentally observed under extended nitrogen depletion conditions, starch may be broken down into functional biomass or TAGs via glycolysis (Adesanya et al., 2014; R. J. Geider et al., 1998). However, there is no evidence of starch glycolysis to functional biomass conversion in known batch studies (Adesanya et al., 2014; Takeshita et al., 2014). Therefore, starch conversion to functional biomass is neglected in this study. Although, pathways exist that can link starch to protein synthesis this does not mean that the specific pathway is utilized by the microalgae (Perez-Garcia et al., 2011).

All these assumptions greatly simplify the kinetics of the algae, by reducing the number of state variables needed to be computed to six, making the simplified mechanism plausible (Fig. 4.1).

4.2.2 Modelling the Limiting Factors Affecting TAGs Production from Photosynthesis and Starch Glycolysis

The four sets of limiting conditions utilized to model production of TAGs from photosynthesis and starch glycolysis are presented in Table 4.1 below.

Table 4.1 Sets of equations for synthesis of TAGs from photosynthetic fixed carbon and starch glycolysis.

Limiting Condition	Equation	Number
LCs 1	$\frac{dT_p}{dt} = \left(1 - \frac{FQ_n}{X}\right)\left(1 - \frac{T}{X}\right)\left(\frac{S}{X}\right)F$	(4.1a)
	$\frac{dT_g}{dt} = Y_{T/C}V_{S,max}\frac{S}{S+K_S}\left(1 - \frac{FQ_n}{X}\right)\left(1 - \frac{T}{X}\right)\left(\frac{S}{X}\right)F$	(4.2a)
LCs 2	$\frac{dT_p}{dt} = p_nF\frac{p/\left(\frac{Q_n}{F}\frac{dF}{dt}\right)}{p/\left(\frac{Q_n}{F}\frac{dF}{dt}\right)+K_{pCN}}\left(1 - \frac{Q_n}{Q_{n,max}}\right)$	(4.1b)
	$\frac{dT_g}{dt} = Y_{T/C}V_{S,max}\frac{S}{S+K_S}\frac{p/\left(\frac{Q_n}{F}\frac{dF}{dt}\right)}{p/\left(\frac{Q_n}{F}\frac{dF}{dt}\right)+K_{gCN}}\left(1 - \frac{Q_n}{Q_{n,max}}\right)F$	(4.2b)
LCs 3	$\frac{dT_p}{dt} = p_nF\frac{K_g}{p+K_g}$	(4.1c)
	$\frac{dT_g}{dt} = Y_{T/C}V_{S,max}\frac{S}{S+K_S}\frac{p/\left(Q_n\frac{dF}{dt}\right)}{p/\left(Q_n\frac{dF}{dt}\right)+K_{gCN}}\left(1 - \frac{Q_n}{Q_{n,max}}\right)F$	(4.2c)
LCs 4	$\frac{dT_p}{dt} = p_nF\frac{K_g}{p+K_g}$	(4.1d)
	$\frac{dT_g}{dt} = Y_{T/C}V_{S,max}\left(1 - \frac{Q_n}{Q_{n,max}}\right)F$	(4.2d)

where $V_{S,m}$ is the maximum glycolytic rate, K_S is the half-saturation coefficient of starch conversion, K_{pCN} and K_{gCN} are the half-saturation constants for the carbon-to-nitrogen uptake ratio for carbon fixed into TAGs from photosynthesis and carbon fixed into TAGs from starch glycolysis, respectively, K_s is the half-saturation constant for starch accumulation and K_g is the half-saturation constant of photosynthetic activity.

LCs 1: This first set of limiting conditions considers starch concentration,$\left(\frac{S}{S+K_S}\right)$ and saturation kinetics of starch, $\left(\frac{S}{X}\right)$, TAGs, $\left(1-\frac{T}{X}\right)$, and nitrogen quota, $\left(1-\frac{FQ_n}{X}\right)$, as limiting factors. For LCs 1 it was proposed that linear kinetics dictated starch glycolysis and TAGs synthesis. As TAGs content increased, there was a negative feedback towards photosynthetic TAGs uptake, which put a limit on how much TAGs could be incorporated into the microalgae biomass. As starch content increased the carbon fixation rate towards TAGs increased, suggesting that high starch content could trigger TAGs accumulation. Nitrogen content had a negative feedback on TAGs accumulation from photosynthesis since higher nitrogen content favoured functional biomass accumulation. Please note that the expression for the starch concentration represents an enzyme substrate reaction.
LCs 2: The second set of limiting conditions uses carbon-to-nitrogen uptake ratio and nitrogen quota for TAGs fixation from photosynthesis, and starch concentration, carbon-to-nitrogen uptake ratio and nitrogen quota as limiting factors for starch-to-TAGs glycolysis.

It is known that carbon can accumulate due to nitrogen depletion, and thus increasing the carbon- to-nitrogen ratio. This excess carbon is then channelled towards TAGs production as proposed in earlier studies (Adesanya et al., 2014). Therefore, we hypothesize that the ratio between the carbon uptake rate, p, and the intracellular

nitrogen fixation rate $\left(\frac{Q_n}{F}\frac{dF}{dt}\right)$, acts as a regulator for TAGs production. The carbon-to-nitrogen uptake ratio was expressed in terms of Monod kinetics with the hypothesis that this was a process that affected enzyme substrate reactions for TAGs synthesis from both photosynthesis and starch glycolysis. The nitrogen quota dependency was expressed as a linear function that limited TAGs synthesis from both sources when at higher contents, much like the nitrogen quota saturation term in LCs 1. In addition, we proposed that the maximum nitrogen quota, $Q_{n,max}$, may affect TAGs synthesis.

LCs 3 considers photosynthetic fixation rate, carbon-to-nitrogen uptake ratio, starch concentration and nitrogen quota as limiting factors. It is also possible in the fixation of carbon to indirectly include whether light has an impact on dictating carbon partitioning between starch and TAGs through the use of photosynthetic uptake, p_n, as a regulator.

The same kinetic expression for TAGs synthesis from starch has been used in Eq. 4.2b and Eq. 4.2c. LCs 3 is similar to LCs 2 as it contains the same kinetic expression for TAGs production from starch glycolysis. However, TAGs synthesis from photosynthesis is a more simplified version of LCs 2.

LCs 4 employs the photosynthetic uptake ratio and nitrogen quota as the only limiting factors. Therefore, a simplification of the expression of TAGs from glycolysis as given in Eq. 4.2c is considered in Eq. 4.2d. This simplification has been used as the carbon-to-nitrogen uptake ratio may be strongly correlated to internal nitrogen quota. Therefore, TAGs kinetics may be able to be described simply by using the nitrogen quota without compromising accuracy.

4.2.3 Elemental Mass Balance Validation

The model was validated using an elemental carbon and nitrogen balance to ensure consistency between generation and consumption (Siaut et al., 2011) for a batch culture:

$$\frac{dn_i}{dt} = G_i - C_i \tag{4.3}$$

where n_i is the concentration of elemental species i, G_i is the generation rate of the species and C_i is the consumption rate of the species. The equations used to model elemental mass balances are outlined in the Supporting Information.

4.2.4 Model Selection

The error was minimised according to Eq. 3.19. The Akaike Information Criterion (AIC) is generally used to assess how well the specific set of equations estimates the true mechanism governing a physical process (De la Hoz Siegler et al., 2011). The lower the AIC the closer the model is to describing the true mechanism. The real mechanism would not be discernible if only the minimum error was used to compare between multiple candidates with a different number of parameters. The reason for this is that the minimum error does not factor in over-parameterization as a reason for inaccuracy (Tredici et al., 2015). A model may be accurate due to a large number of fitting parameters. However, this does not ensure a biological basis. Over parameterization is factored into the AIC calculations, representing a compromise between accuracy and number of parameters. The AIC criterion selects the best-fit model by optimizing the error and the penalty from over-parameterization (Burnham & Anderson, 2002). The second order Akaike expression (Burnham & Anderson, 2002;

Wagenmakers & Farrell, 2004) modified for the average absolute relative error was used:

$$AIC = 2N_p + \frac{2N_p(N_p + 1)}{N_d - N_p - 1} + N_d ln(N_s A_E) \tag{4.4}$$

where N_p is the number of parameters. The first two terms represent the penalty from over-parameterization, whilst the third term is the penalty from a higher error between the predicted values and the experimental data. The relative strength of each set of equations can be compared using the Akaike difference (Wagenmakers & Farrell, 2004),

$$\Delta_i = AIC_i - AIC_{min} \tag{4.5}$$

where Δ_i is the AIC difference relative to the best candidate model, AIC_i is the AIC of each set of limiting conditions or options and AIC_{min} the minimum AIC of the four options tested in this study.

The relative AIC weight can be obtained using Eq. 4.6 (Wagenmakers & Farrell, 2004)

$$w_i = \frac{e^{-\Delta_i/2}}{\sum_{k=1}^{N} e^{-\Delta_k/2}} \tag{4.6}$$

where w_i is the AIC weight. If each of the four sets of equations (LCs 1-4) has an equal probability of being the best candidate for predicting kinetics, each set would have an AIC weight of 25 %.

4.2.5 Input Parameters

The initial values for the state variables used to solve the equations are shown below in Table 4.2. They were collected from literature (Adesanya et al., 2014; De la Hoz

Siegler et al., 2011; Packer et al., 2011; Quinn et al., 2011; J. Yang et al., 2011; Yoo et al., 2014) with the functional biomass being calculated from a mass balance according to Eq. 3.1. The initial value of the nitrogen quota was estimated as no experimental value for it could be obtained from the literature.

Two constants were used in the study, namely: length of light path and incident light intensity with values of 0.02 m and 150 µmols/m^2.s, respectively.

Table 4.2 Reported state variables and their initial values. The initial value of the nitrogen quota was determined by estimation, because no measured data were found.

Variable	Symbol	Initial Value Data set 25 g/m^3 of N	Initial Value Data set 125 g/m^3 of N	Units
Nitrogen concentration	N	25	125	g/m^3
Chlorophyll content	B	0.04	0.04	g Chl/g F
Functional biomass concentration	F	150	180	g F/m^3
Starch concentration	S	10	10	g S/m^3
TAGs concentration	T	200	200	g T/m^3
Nitrogen Quota concentration	Q_n	0.086	0.06	g N/g F

Error! Reference source not found.4.3 below shows the initial parameter estimations for predicting algal kinetics.

Table 4.3 The initial parameter estimates to be optimized by the MATLAB code.

Parameter	Symbol	Value
Specific absorption coefficient of chlorophyll	α	22.150
Minimum nitrogen quota	$Q_{n,min}$	0.026
Maximum nitrogen quota	$Q_{n,max}$	0.112

Maximum nitrogen uptake rate	$V_{n,max}$	0.780
Nitrogen half-saturation constant	K_n	0.029
Maximum chlorophyll to nitrogen ratio	θ_{max}	0.625
Quantum yield	φ	0.174
Maximum photosynthetic rate	p_{max}	61.148
Starch and TAGs yield coefficient	$Y_{T/S}$	0.151
Carbon-to-TAGs yield coefficient	$Y_{T/C}$	0.517
Carbon-to-functional biomass yield coefficient	$Y_{F/C}$	0.757
Maximum starch glycolysis rate	$V_{S,max}$	1.072
Half-saturation of starch conversion	$K_{S/X}$	0.075
Half-saturation ratio of C/N uptake ratio for carbon fixed into TAGs from photosynthesis	K_{pCN}	0.1
Half-saturation constant for carbon fixed into TAGs from starch glycolysis	K_{gCN}	0.2
Half-saturation photosynthetic activity	K_g	0.7
Respiration rate	b	0.01

4.3 Results and Discussion

The values of the six state variables as well as the total biomass are shown below in Figs 4.2 and 4.3 for the four different sets of limiting conditions (LCs 1-4) as given by Eqs 4.1 and 4.2, for two different nitrogen concentrations of 25 g N/m^3 and 125 g N/m^3, respectively. The experimental data that was used to minimize the error has been added to Figs 4.2 and 4.3, with the exception of the nitrogen quota for which experimental data was not available. The computational time of the program was half an hour after multiple iterations were carried out to arrive at the final parameter estimate.

The values of the parameters that minimized the errors are given in Table 4.4 for the two different nitrogen concentrations. Table 4.4 also reports the typical values of the same parameters as reported in the literature. Generally, there is good agreement

between model predictions and reported literature values except for the maximum photosynthetic rate. In Table 4.4 new parameters are listed, which have not been used in the literature before. These parameters are the carbon-to-starch coefficient, $Y_{S/C}$, starch-to-TAGs yield coefficient, $Y_{T/S}$, maximum starch glycolysis rate, $V_{S,max}$, half-saturation constant of starch glycolysis, $K_{S/X}$, half-saturation constant of carbon-to-nitrogen uptake ratio for photosynthetic carbon to TAGs, K_{pCN}, half-saturation coefficient of carbon-to-nitrogen uptake ratio for starch glycolysis, K_{gCN}, and half-saturation coefficient of photosynthetic regulation, K_g.

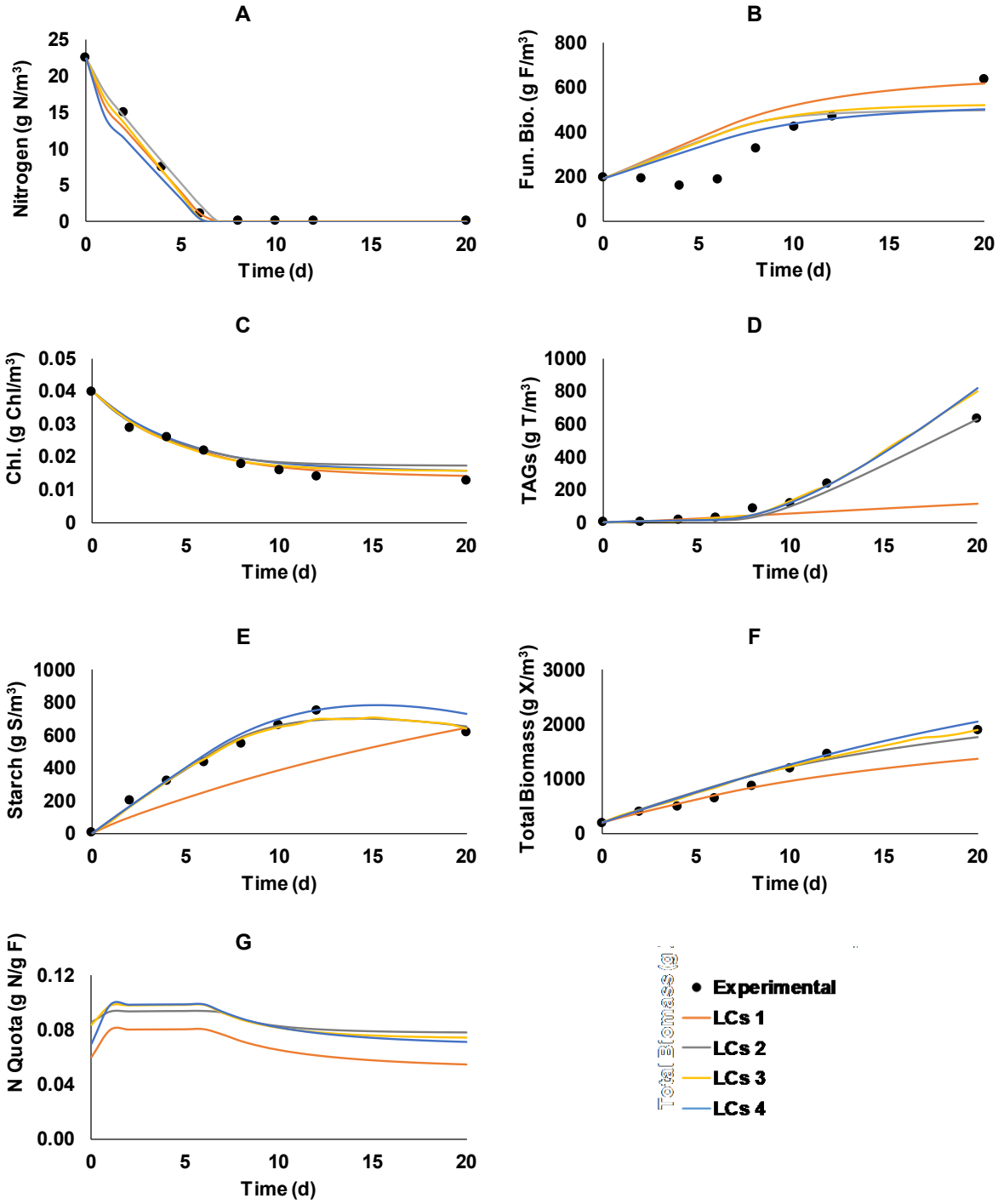

Figure 4.2 A comparison of the prediction of extracellular nitrogen uptake (A), functional biomass concentration (B), chlorophyll content (C), TAGs concentration (D), starch concentration (E), total biomass concentration (F) and nitrogen quota (G) for LCs 1-4 under an initial nitrogen (as nitrates) concentration of 25 g N/m^3 based on literature experimental data (Adesanya et al., 2014).

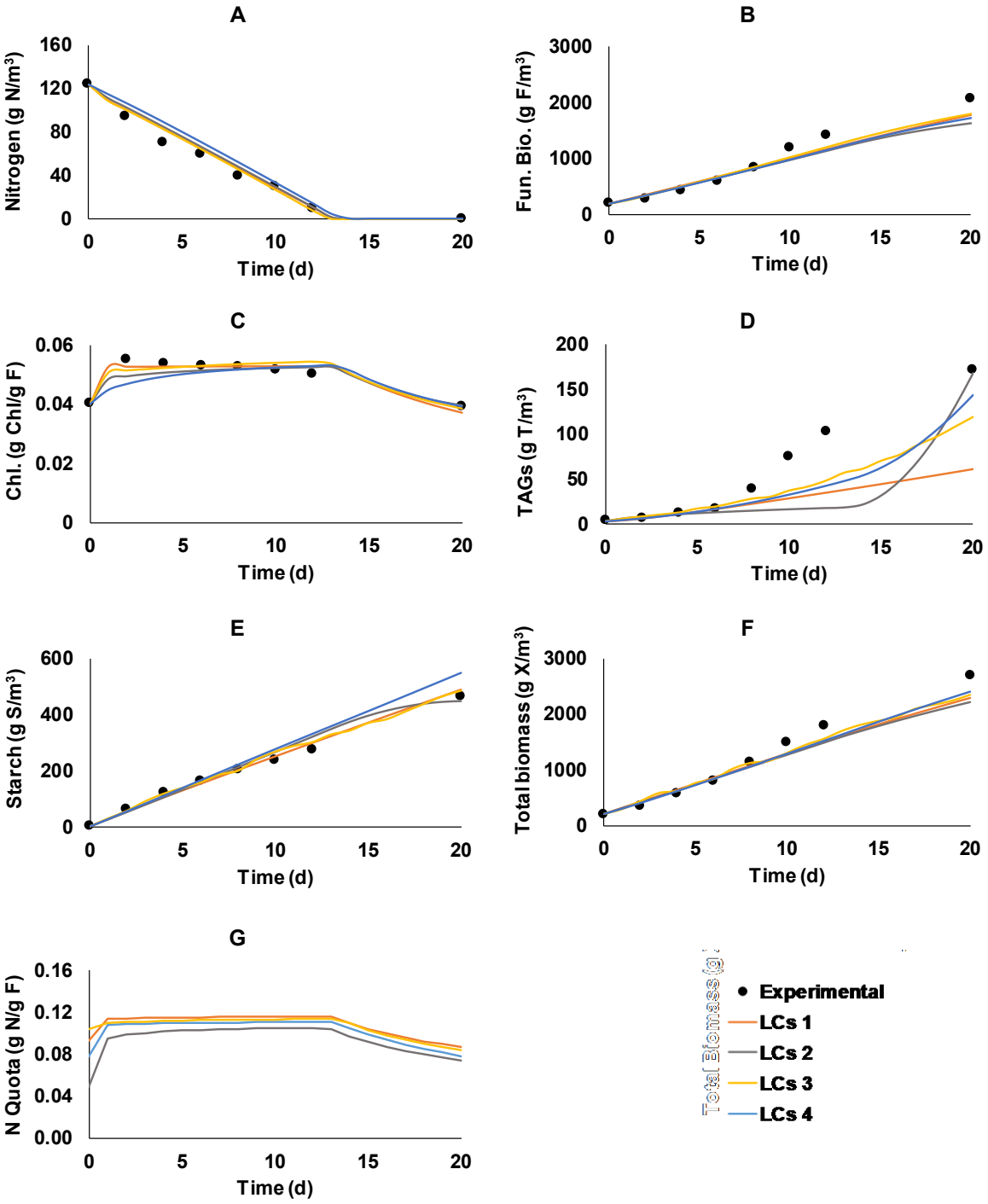

Figure 4.3 Comparison of the prediction of extracellular nitrogen uptake (A), functional biomass concentration (B), chlorophyll content (C), TAGs concentration (D), starch concentration (E), total biomass concentration (F) and nitrogen quota (G) for LCs 1-4 under an initial nitrogen concentration (as nitrates) of 125 g N/m^3 based on **literature experimental data (Adesanya et al., 2014).**

Table 4.4 Best-fit parameter sets for 25 g N/m^3 and 125 g N/m^3 for all Starch-TAGs kinetic sets of equations. Parameter values as reported in the literature are also shown.

		125 g N/m^3				25 g N/m^3			
Param.	Lit. Value	LCs 1	LCs 2	LCs 3	LCs 4	LCs 1	LCs 2	LCs 3	LCs 4
Av. Error		37.2	24.4	26.2	24.7	13.9	15.0	11.2	10.5
α	3-40[8-14]	20.73	33.25	19.27	19.42	26.32	19.58	24.49	11.95
$Q_{n,min}$	0.008-0.08[8-14]	0.030	0.070	0.59	0.050	0.050	0.078	0.073	0.068
$Q_{n,max}$	0.0875-0.2[8-14]	0.11	0.12	0.050	0.11	0.080	0.095	0.099	0.099
$V_{n,max}$	0.004-1[8-14]	0.80	0.56	0.11	0.35	0.40	0.25	0.22	0.42
K_n	0.014-0.3[8-14]	0.03	0.06	0.17	0.06	0.06	0.041	0.056	0.035
θ_m	0.17-1.06[8-14]	0.63	1.2	0.060	0.93	0.15	0.27	0.088	0.054
ϕ	0.43-1.19[8-14]	0.17	0.52	0.96	0.47	0.41	0.85	0.45	0.55
p_{max}	90-93[14]	62.79	114.1	89.88	55.80	38.62	109.6	168.3	153.0
$Y_{T/C}$	0.478[12]	0.48	0.88	0.21	0.36	0.29	0.99	0.44	0.27
$Y_{F/C}$	1.44-1.64[10, 12]	0.78	1.9	0.51	1.7	0.80	1.6	1.5	0.99
b ($\times 10^{-4}$)	0.001[10]	0.104	0.100	0.0761	0.0103	1.00	1.12	1.35	0.0883
$Q_{n,o}$	-	0.080	0.090	0.67	0.10	0.060	0.086	0.084	0.070
$Y_{S/C}$	-	0.32	0.54	20.49	0.70	0.62	0.84	1.55	1.29
$Y_{T/S}$	-	0.14	0.42	0.70	1.7	0.31	0.73	1.2	0.94
$V_{S,max}$	-	1.1	0.19	1.2	0.019	0.073	0.73	0.48	0.61
$K_{S/X}$	-	0.080	0.070	0.050	-	0.083	0.090	38	-

K_{pCN}	-	-	1.94	-	-	-	3.15	-	-
K_{gCN}	-	-	20.42	0.01	-	-	2.74	5.19	-
K_g	-	-	-	0.040	0.014	-	-	0.016	0.015

4.3.1 Nitrogen Concentration, Nitrogen Quota, Chlorophyll Content, and Functional Biomass Concentration Results

Figs 4.2 and 4.3 show close correlations between experimental results and modelling predictions, with 15 % deviation when simulating nitrogen concentration, *N*, nitrogen quota, Q_N, chlorophyll content, *B*, and functional biomass concentration *F*. The only exception is the discrepancy between 0 to 10 days of the functional biomass concentration under initial nitrogen conditions of 25 g N/m^3, (Fig. 4.2B). This agreement is expected as the equations governing these four variables are well established (Y. Chen & Vaidyanathan, 2103).

The discrepancy between the functional biomass and the experimental data appears as a lag phase in the 25 g N/m^3, which was not observed for the 125 g N/m^3 case, indicating that acclimation was dependent on initial nitrogen concentration. The proportionality between functional biomass growth rate and nitrate uptake whilst there is nitrogen in the bulk culture has been reported previously (Morris et al., 1974; Valenzuela-Espinozaa et al., 2002; L. Wang et al., 2013). However, there is no clear explanation of the existence of this lag phase in the literature. It may be possible that this phase is induced by nitrogen limited stress conditions, which resulted in protein degradation and excretion (Yentsch & Vaccaro, 1958) This is hypothetical as dissolved organic nitrogen in the culture was not measured. A future study on simulating the interaction between nitrates,

extracellular proteins and functional biomass may be developed to simulate the initial lag phase as a function of initial nitrogen concentration.

4.3.2 Prediction of Starch-TAGs Kinetics Based on the AIC Criterion

The quality of the fit has been quantified using the AIC criterion that measures the degree to which a model can accurately depict the true mechanism by taking into account the model error and the number of parameters. To select the best sets of equations and limiting factors affecting starch-TAG kinetics, the AIC was calculated for all sets under both initial nitrogen conditions of 25 g N/m^3 and 125 g N/m^3. The results are shown below in **Error! Reference source not found.**4.5. The differences in the errors between the predictions and the experimental data were smaller than 15% when the initial nitrogen concentration was 125 g N/m^3, but larger than 25 % when the initial nitrogen concentration was
25 g N/m^3. This was primarily due to the lag phase, as discussed earlier, not being accounted for by the equations.

Table 4.5 Comparison of four different kinetic sets of equations for Starch-TAG composition under two initial nitrogen concentrations (25 g N/m^3 and 125 g N/m^3).

Initial [N] g N/m^3	Option	Error (%)	No. of Parameters	AIC Likelihood (%)
25	LCs 1	31.8	15	15.4
	LCs 2	26.7	17	10.0
	LCs 3	22.4	17	20.2
	LCs 4	23.2	15	54.4
125	LCs 1	13.8	15	32.9
	LCs 2	15.1	17	7.4
	LCs 3	12.1	17	18.0
	LCs 4	13.0	15	41.8

LCs 1 had a relatively low AIC likelihood at only 15.4 % for an initial nitrogen concentration of nitrogen 25 g N/m^3 but had the second best chance of being the most likely equations for predicting kinetics when concentration was increased to 125 g N/m^3 at 31.8 % AIC likelihood. This wide discrepancy (Table 4.5) in predictability may suggest that this first set of equations is not robust and the quality of the fit for the 125 g N/m^3 case may be due to mathematical correlation rather than due to any biological mechanism being predicted by the model. In addition, LCs 1 did not accurately predict TAGs and starch as shown in Fig. 4.2D and 4.2E and Fig. 4.3D. This suggests that microalgae behaviour does not follow saturation kinetics as depicted in Eqs 4.1a and 4.2a. Eqs 4.1a and 4.2a are functions of the amount of TAGs already present in the system. This assumption may not hold true as most biological organisms

can accumulate lipids independently of the amount of the amount of lipids already present in them. In addition, when the nitrogen load was 25 g N/m^3, the experimental starch concentration peaked at 750 g/m^3 at day 12 before decreasing to 600 g/m^3 at day 20, but was still predicted as a linear function by LCs 1 (Fig. 4.3E). Furthermore, this first set of equations had the poorest prediction for TAGs accumulation (Fig. 4.2D and 4.3D). The low AIC likelihood value of this limiting condition suggests that saturation kinetics may not play a significant role in composition kinetics as proposed by other authors (Packer et al., 2011; Yoo et al., 2014). This may be because cells can deform and expand as storage molecules accumulate allowing more carbon to be stored.

In the second option (LCs 2), the carbon-to-nitrogen uptake ratio and the nitrogen quota regulated both the photosynthetic and starch glycolytic carbon fluxes towards TAGs and starch concentration. For both nitrogen conditions, this option had the lowest likelihood of fit at 10 and 7.4 % for 25 g N/m^3 and 125 g N/m^3, respectively. This would suggest that the C-N uptake ratio is not an important regulator for the fixation of TAGs from photosynthesis.

LCs 3 had photosynthetic activity regulating fixed carbon-to-TAGs, and nitrogen quota, starch concentration and carbon-to-nitrogen uptake ratio regulating glycolysis of starch. In view that the second set of equations seemed to highlight that carbon-to-nitrogen uptake ratio was not an important regulator, LCs 3 simplified the fixation of TAGs from photosynthesis by taking carbon photosynthetic fixation directly into account. In addition, the condition of a maximum nitrogen quota influencing the carbon fixation into TAGs was not considered in this option. These two simplifications yielded higher AIC values for both initial nitrogen concentrations.

LCs 4 was a simplification of LCs 3, as the carbon-to-nitrogen uptake ratio and starch concentration were not considered as regulators for starch glycolysis. For both data sets, the errors with respect to the experimental data were 23.2 and 13.0 %, respectively. This error was less than 1% greater than that of LCs 3 as shown in Table 4.5, despite the current set of equations having two fewer parameters. This suggests over-parameterization and redundancy in LCs 3. Furthermore, the AIC was the highest at 54.4 and 41.8 % AIC likelihood for 25 g N/m^3 and 125 g N/m^3, respectively, indicating that carbon-to-nitrogen uptake ratio and starch concentration are not important in dictating starch glycolysis to TAGs.

In summary, component saturation, starch concentration and carbon-to-nitrogen uptake ratio were not significant in predicting composition kinetics, whilst nitrogen quota and photosynthetic carbon uptake were important regulators.

4.3.3 Comparison with Literature

The most likely candidate for predicting algal kinetics, LCs 4, was tested against literature (Breuer, Martens, Draaisma, Wijffels, & Lamers, 2015) data for *S. obliquus* to determine whether it could predict TAGs evolution under different experimental conditions. Fig. 4.4 shows the model predictions according to the fourth set of limiting conditions (LCs 4) and the experimental data of TAGs concentration as a function of time according to Breuer et al. (2015). The same light path length of two centimetres (Section 2.5) was assumed as none was given in the study and initial values for nitrogen, TAGs, starch and functional biomass of 0 g N/m^3, 107.7 g T/m^3, 211.6 g S/m^3 and 738.5 g F/m^3 were used, respectively. The value of initial starch concentration was assumed to be 20 % of the total biomass as no data on starch were given and the initial functional biomass concentration was calculated from a mass balance of the difference

between the total biomass concentration and the sum of the TAGs and starch. The initial chlorophyll content and nitrogen quota of 0.04 g Chl/g F and 0.08 g N/g F were taken from our study (Table 4.2) when predicting the TAGs concentration of Breuer et al. (2015) since no such data was available. Finally, the values of the auxiliary parameters correspond to the best-fit obtained for LCs 4 given in Table 4.4 column 10.

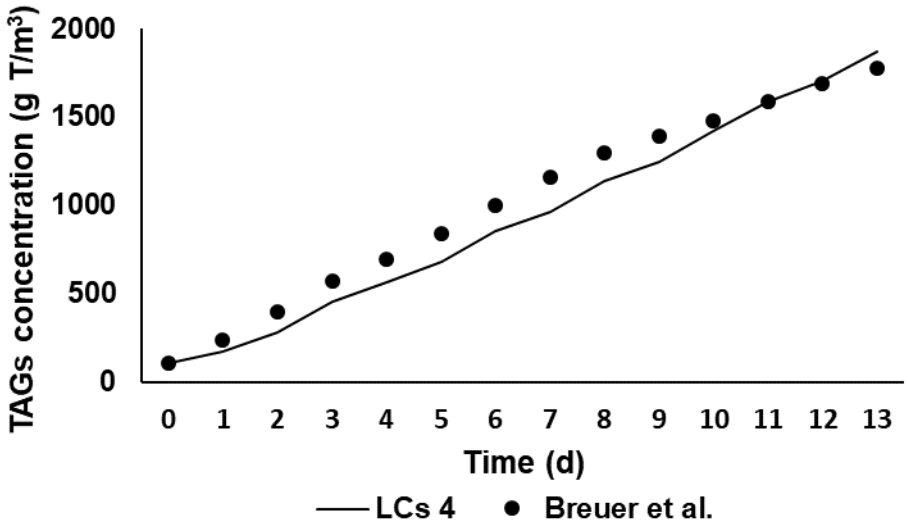

Figure 4.4 Comparison of experimental data of TAGs and model prediction based on fitting parameters of 25 g N/m^3 for microalgal growth (Breuer, Lamers, Martens, Draaisma, & Wijffels, 2012).

As illustrated in Fig. 4.4, there is close agreement between the predicted and experimentally measured values of TAGs. This agreement suggests that the proposed equations with their corresponding limiting factors have the ability to predict, rather than being a parameter fitting exercise, for low nitrogen loads in batch experiments. Future studies may test the ability of the model to predict or be fitted to data of different species of microalgae, nitrogen loads and light flux, as well as different fractions.

4.3.4 Testing Model Limitations

In order to determine the predictability for the late stationary phase beyond the experimental range, the time for simulation of LCs 4 was extended to 150 days for both nitrogen loads. The results are presented in Fig. 4.5. For both nitrogen concentrations (Fig. 4.5), the functional biomass reaches a maximum concentration value with time. This maximum depends on the initial nitrogen concentration. For both initial nitrogen conditions, starch concentration shows a peak at day 12 for 25 g N/m^3 and at 125 for 125 g N/m^3, before a decline, due to glycolysis to TAGs was observed. However, the starch concentration becomes negative reaching -500 g S/m^3 at day 40, whilst TAGs increases linearly without bound. Both scenarios are not realistic. This scenario forms because starch is continuously being broken down during glycolysis to produce more TAGs without considering a maximum TAGs content in biomass and a minimum starch concentration. Starch and TAGs saturation were incorporated to some degree in LCs 1 and 2 but they were not found to be important during algal growth from days 0-21 where experimental measurements were taken.

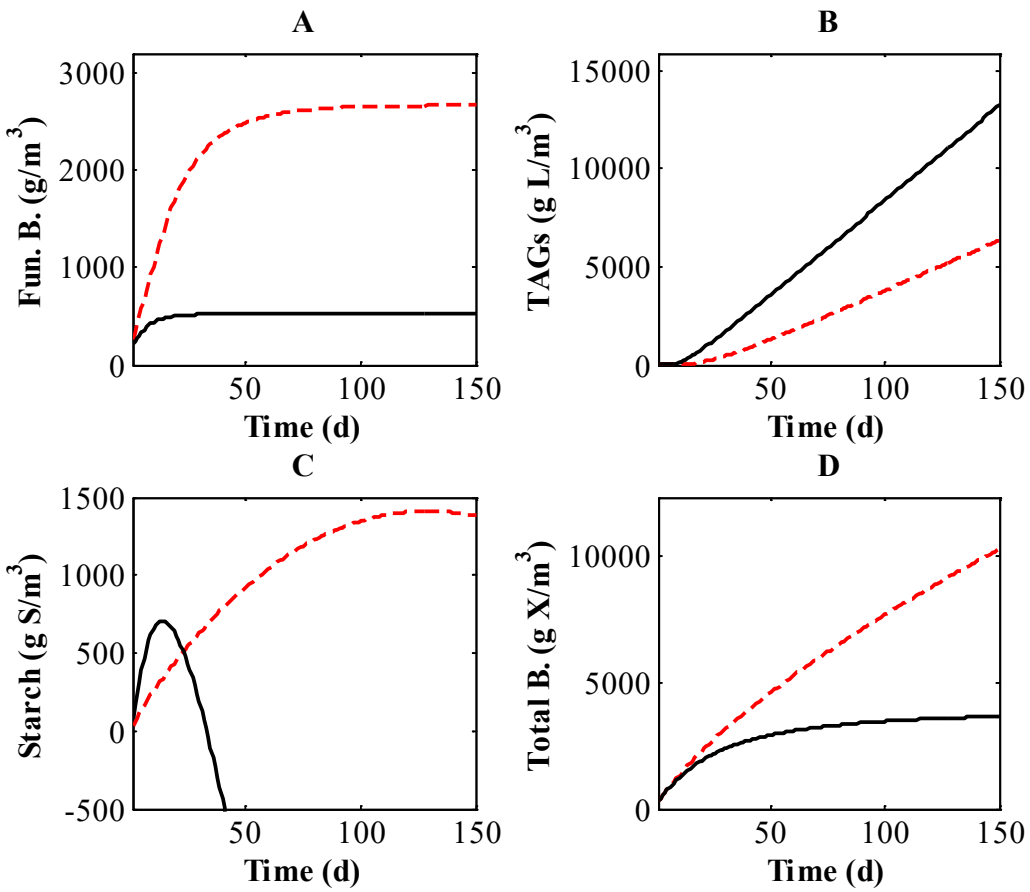

Figure 4.5 Simulated concentration of functional biomass (A), TAGs (B), starch (C) and total biomass (D) over 150 days for LCs 4, tested at initial nitrogen concentrations of 25 g N/m^3 (dashed lines) and 125 g N/m^3 (solid lines).

However, it appears that when testing beyond the measured experimental time frame, a maximum TAG content and minimum starch content may be important factors. To test this hypothesis, a minimum and maximum quota for starch and TAGs were included in the modelling equations for TAGs kinetics. A TAGs saturation expression modified from Yoo et al., (2014) was incorporated. This expression was asymptotic towards the maximum TAGs content of biomass rather than, as originally assumed, being asymptotic towards the total biomass concentration. The latter assumption contained in LCs 4 is unrealistic since some biomass needs to be reserved as functional biomass,

which is involved in metabolic reactions. In addition, it is necessary to have some reserved starch as an energy store. Starch limitation as a substrate for TAGs production is also shown by using the Monod function, which has been modified to incorporate a minimum fraction of starch that must be stored within the biomass.

$$\frac{dT_p}{dt} = p_n F \frac{K_g}{p + K_g}\left(1 - \frac{T/X}{f_{T,max}}\right) \tag{4.7}$$

$$\frac{dS_g}{dt} = V_{S,m} F \left(1 - \frac{Q_n}{Q_{n,max}}\right) \frac{S/X - f_{s,min}}{S/X - f_{s,min} + K_{S/X}} \left(1 - \frac{T/X}{f_{T,max}}\right) \tag{4.8}$$

where maximum $f_{T,max}$ is the maximum fraction of TAGs that can be stored in biomass (g TAG/g X), $f_{s,min}$ is the minimum starch content of the total biomass (g S/g X) and $K_{S/X}$ is the half-saturation constant for starch glycolysis (g S/g X). The maximum TAGs content, minimum starch content and half-saturation starch content were assumed to be 0.7 g L/g X, 0.05 g S/g X and 0.1 g S/g X, respectively. The data were taken from literature values (Adesanya et al., 2014; Packer et al., 2011).

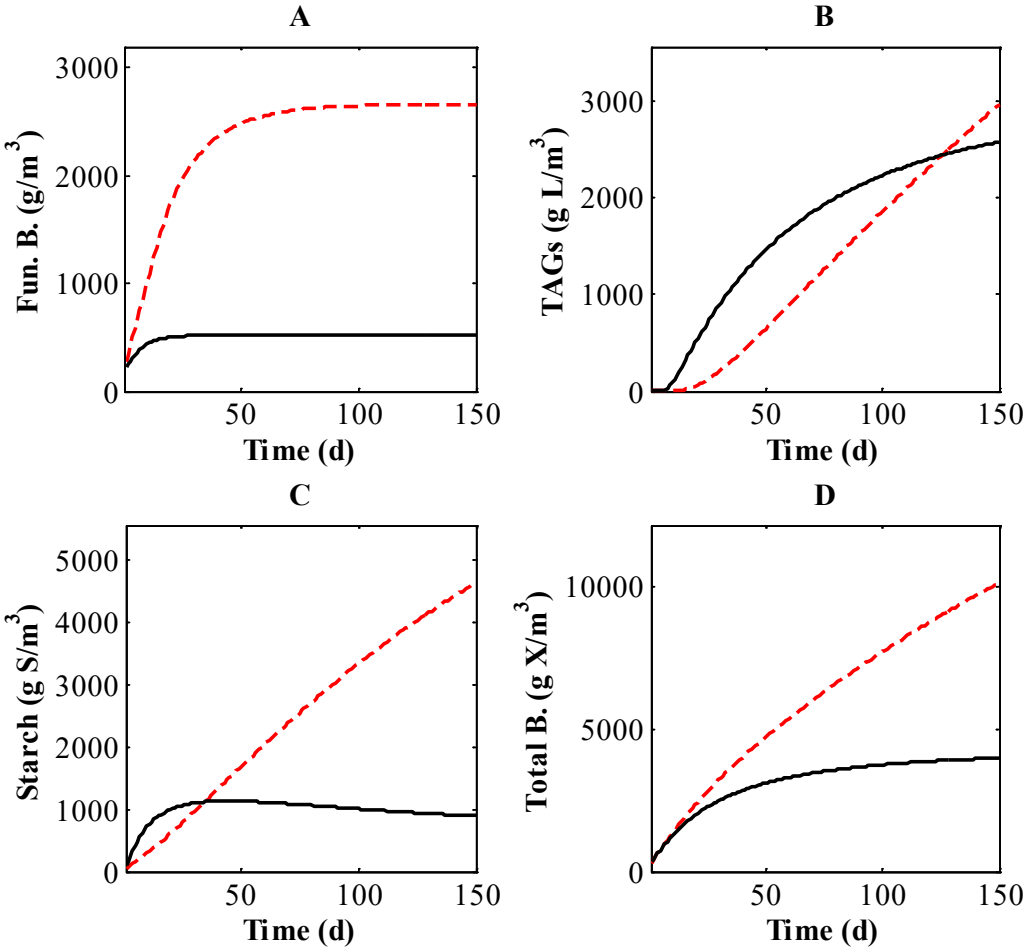

Figure 4.6 Effect of minimum and maximum starch and TAGs content on functional biomass (A), TAGs (B), starch (C) and total biomass (D) concentration up to 150 days for LCs 4, tested at initial nitrogen concentrations of 25 g N/m^3 (solid lines) and 125 g N/m^3 (dashed lines).

Fig. 4.6 shows the composition kinetics and total biomass kinetics as a function of time, extended to 150 days with modifications to LCs 4 according to Eqs 4.7 and 4.8 for initial nitrogen concentrations of 25 and 125 g N.m^3. For 25 g N/m^3, starch concentration (Fig. 4.6) reached a global maximum with time decreased slowly rather than becoming negative as in the case shown in Fig. 4.5. The total biomass approached a maximum value of 4000 g/m^3, but it did not appear to decrease due to aerobic respiration. For 125 g N/m^3 the starch and TAGs continued to increase without bound

but it is possible that if the simulation time frame was increased, they would also approach a constant value as shown for starch and TAGs for 25 g N/m^3. However, such a long time frame may be argued to be unrealistic for the kinetics to be limited by a maximum TAGs content and a minimum starch content. This is because other processes such as catabolism of TAGs and starch for respiration has been observed to occur within a week of inoculation under mixotrophic conditions (T. Li et al., 2015). Thus, future models may be applied to data sets, which have late stationary phase composition kinetics, to validate whether a maximum and a minimum fraction concentration or catabolism is playing an important role.

Another model limitation is that it was not applied to higher light intensities above saturation. Some authors have observed that above saturation, light intensity may induce higher TAGs accumulation at the price of reducing productivity (Klok et al., 2013). This could be due to excessive light intensity producing more reducing power (Erb & Zarzycki, 2016) than can be utilized by carbon fixation via photosynthetic activity as it transitions from being a light-limited to carbon-fixation-limited system. Future studies may test whether the photosynthetic activity regulator for a light intensity above saturation favours carbon flux towards TAGs formation, whilst starch may be preferred at intensities below saturation.

4.4 Conclusion and Future Recommendations

This work presents the study of the kinetics of carbon fixation by considering three independent components: functional biomass, starch and TAGs. In order to explore the most suitable kinetics to reproduce experimental data, an error minimization technique was carried out with the help of an in-house code written in MATLAB. Four different

sets of limiting conditions (LCs) were considered and their evaluation was carried out by using the AIC criterion.

The AIC weight suggests that a system regulated by photosynthetic activity and nitrogen quota had a 40 and 55 % chance out of four candidates to be the most accurate model in predicting composition kinetics for two different nitrogen conditions. This most suitable set of limiting conditions used the photosynthetic uptake rate as well as the nitrogen quota as regulators for dictating starch and TAGs kinetics. In addition, it was shown that the use of a maximum nitrogen quota parameter was important to determine the starch glycolysis rate.

Furthermore, once the best kinetic modelling option was determined, the robustness of the method was tested by comparing the predictions of the TAGs concentration as a function of time with results published in the literature. A good agreement was found between modelling and experimental data.

In future, optimization studies of starch and TAGs may be carried out to determine which nitrogen loads favour either starch or TAGs production in algal cultures. Future studies may also investigate the effect of differing light intensities on starch and TAGs kinetics. Other variables that may be investigated in future are dissolved organic nitrogen to determine if during the lag phase intracellular nitrogen is being excreted by the microalgae, reducing functional biomass concentration as observed for the condition of 25 g N/ m^3.

5 Modelling the Effect of Light Intensity on the Composition Kinetics of *Scenedesmus Obliquus*

5.1 Introduction

This chapter focuses on modelling and validating the composition kinetics of the algae *S. obliquus* as a function of light intensity. In this chapter, experimental data from the literature for two different light intensities (200 µmols.m^2.s and 1000 µmols.m^2.s) at an initial nitrogen concentration of 0 g N/m^3 was employed to obtain the values of the main parameters that control algae metabolism. Simulation of light intensity is an important factor as this variable provides the energy required to split water into protons and oxygen, the former of which is responsible for CO_2 reduction into sugars (Griffin & Seemann, 1996). Photosynthesis in algae and can be either limiting, saturated or inhibitory depending on the light intensity. Light limited conditions denote a situation where kinetics is linearly dependent on the light intensity. The saturated region describes light intensities where photosynthetic fixation is constant as a function of light intensity and inhibitory intensities relate to light fluxes where photoinhibition occurs due to the production of damaging free radicals of oxygen and damage to the photosynthetic apparatus (Juneja, Ceballos, & Murthy, 2013). This chapter will study light intensities in the light limited (200 µmols.m^2.s) and saturated regions (1000 µmols.m^2.s).

The model developed solved six coupled ordinary differential equations for the state variables of nitrogen concentration, nitrogen quota, chlorophyll content, functional biomass concentration, starch concentration and TAGs concentrations. The total biomass was also calculated and plotted as the sum of starch, TAGs and functional

biomass. The results of the model for the six variables plus total biomass are plotted and compared between model prediction and experimental measurement. The results and discussion section first analyses the chlorophyll and nitrogen kinetics discussing the similarities in trends for the nitrogen quota and chlorophyll content. This is followed by a discussion about the functional biomass and then the starch and TAGs. The starch and TAGs are further compared with one another by comparing starch content to storage molecule content as a function of light intensity and time. Carbon fluxes of photosynthetic fixation, starch glycolysis, TAGs synthesis from photosynthetically fixed carbon, starch synthesis from photosynthetically fixed carbon and functional biomass production were calculated and plotted to determine what was happening to *S. obliquus* on an intracellular level. Finally, the model compared the composition kinetics of 40, 200 and 1000 μmols.m^2.s to determine the effect of light intensity on starch, TAGs and functional biomass kinetics.

5.2 Model Implementation

In order to analyse the influence of light intensity on the parameters that characterise algae metabolism, the experimental data of Breuer et al. (2015) on nitrogen, chlorophyll, functional biomass, starch, TAGS and nitrogen quota were utilised. The dynamics of these six variables are given by Eqs. 3.2 to 3.7. The initial conditions of the state variables are shown in Table 5.1. The experiments carried out by Breuer et al. (2015) correspond to light intensities of 200 and 1000 μmol.m^2s and to an initial nitrogen concentration of 0 g N/m^3.

Table 5.1 The initial conditions of state variables for the modelling of algae cultivation

Variable	Units	Breuer et al., (2015), 200 µmols.m^{2}s *	Breuer et al., (2015), 1000 µmols.m^{2}s
Nitrogen	g N/m^3	0.0000	0.0000
Chlorophyll	g Chl/g F	0.04000	0.04000
Functional Biomass	g F/m^3	1329	1278
Starch	g S/m^3	88.45	230.3
TAGs	g T/m^3	147.9	106.3
Nitrogen Quota	g N/g F	0.12	0.1190

* These conditions were also used to simulate the 40 µmol.m^{2}s case.

In order to solve the dynamics of the six state variables it is also necessary to solve 9 secondary equations that express, rate of extracellular nitrogen uptake, specific growth rate, net photosynthetic rate, gross photosynthetic rate, maximum nitrogen quota dependent photosynthetic rate, culture light intensity, starch synthesis rate from photosynthesis, starch glycolysis and TAGs synthesis from photosynthesis. Eq. 3.12 was used to model the photosynthetic rate as a function of light intensity.

In order to optimise the 15 parameters that appear in the set of six coupled ordinary differential equations to be solved, initial estimated values were needed. The same input parameters were used for both light conditions, depicted in Table 5.2 below. They were obtained from the optimised parameter output of LCs 4 in Chapter 4 for 25 g N/m^3.

Table 5.2 The input parameters tuned by the minimisation of the objective function and manual input. These parameters were the input for both experimental light intensities of 200 and 1000 µmol.m^{2}s.

Parameter	LCs 4
Av. Error	10.5
α	11.95
$Q_{n,min}$	0.068
$Q_{n,max}$	0.099
$V_{n,max}$	0.42
K_n	0.035
θ_m	0.054
φ	0.55
p_{max}	153.0
$Y_{T/C}$	0.27
$Y_{F/C}$	0.99
b ($\times 10^{-4}$)	0.0883
$Y_{S/C}$	1.29
$Y_{T/S}$	0.94
$V_{S,max}$	0.61
K_g	0.015

In addition, once the parameter estimates for both light conditions (200 and 1000 µmol.m^{2}s) were obtained, the modelling of algae kinetics was also carried out for a light intensity of 40 µmol.m^{2}s. The values of the 15 parameters (excluding the six state variables) were obtained from the fitting of the 200 and 1000 µmol.m^{2}s cases. Out of the 15 parameters, 11 of them did not show any sensitivity to the light intensity and, thus, the same values were used to simulate the 40 µmols/m^{2}s

case. The only differences between the 200 and 1000 μmols/m^{2}s cases were found in the maximum photosynthetic rate, carbon-to-starch yield, maximum starch glycolysis rate and starch-to-TAGs yield coefficient. The values of these first three parameters, i.e., photosynthetic rate, carbon to starch yield and maximum starch glycolysis rate, employed to simulate the 40 μmols/m^{2}s case were obtained by linear extrapolation. The fourth parameter that showed light sensitivity was the starch-to-TAGs yield coefficient. Linear extrapolation using the 200 and 1000 μmols/m^{2}s cases predicted an unreasonably high value compared to literature prediction (Zhang et al., 2014). Therefore, the value of the starch-to-TAGs yield coefficient employed corresponded to the 200 μmols/m^{2}s case

5.3 Results and Discussion

Table 5.3 shows the optimised parameter estimates given by the model to predict the experimental data of Breuer et al. (2015) for the 200 and 1000 μmols/m^{2}s of *S. obliquus*. In addition, the parameters utilised to model the kinetics of the 40 μmols/m^{2}s case and the values corresponding to the low nitrogen case of Chapter 4 (25 g N/m^3) for *C. vulgaris* at a light flux of 150 μmols/m^{2}s were added for comparison.

The only differences between the 200 μmols/m^{2}s and 1000 μmols/m^{2}s cases were found in the maximum photosynthetic rate, carbon to starch yield, starch to TAGs yield and maximum starch glycolysis rate (Table 5.3). In most cases, the tuned parameters for *C. Vulgaris* obtained in Chapter 4 were within the same order of magnitude as the parameters reported in Table 5.3. The only exceptions were the maximum nitrogen uptake rate, half saturation constant of nitrogen uptake, respiration rate, chlorophyll to nitrogen ratio and maximum starch glycolysis rate. Since there was no extracellular nitrogen in the cases of *S. obliquus*, the parameters that depend on nitrogen

concentration may not have been fitted adequately. Furthermore, the respiration rate for *C. vulgaris* was also orders of magnitude smaller than the respiration rate for *S. obliquus*. However, in both cases, the respiration rate was much smaller than the gross photosynthetic rate. Therefore, the respiration rate magnitude will have little effect on kinetics. Divergence between maximum chlorophyll to nitrogen ratio and starch glycolysis are likely to be species dependent. The average errors of the model as calculated using Eq 3.19 were 10.60 % for 200 µmols/m^{2}s and 17.20 % for 1000 µmols/m^{2}s.

Table 5.3 Parameter estimates from the fitting the model to the two experimental data sets for light intensities of 200 and 1000 µmol.m^{2}s. The parameters estimate for analysing the prediction of the 40 µmol.m^{2}s case

Parameter	Chapter 4 25 g N/m^3, 150 µmols/m^{2}s	40 µmols/m^{2}s	200 µmols/m^{2}s	1000 µmols/m^{2}s	Units
α	11.95	10	10	10	m^2/g Chl
$Q_{n,min}$	0.068	0.030	0.030	0.030	g N/g F
$Q_{n,max}$	0.099	0.15	0.15	0.15	g N/g F
$V_{n,max}$	0.42	0.020	0.020	0.20	g N/g F.d
K_n	0.035	0.0010	0.0010	0.0010	g N/m^3
θ_m	0.054	0.70	0.70	0.70	g Chl/g N
ϕ	0.55	1.2	1.2	1.2	g C/mol photons
p_{max}	153.0	175	350	400	g C/g F.d
$Y_{T/C}$	0.27	1.5	1.5	1.5	g T/g C
$Y_{F/C}$	0.99	1.3	1.3	1.3	g F/g C
b	0.0000883	0.0010	0.0010	0.0010	g C/g F.d

$Y_{S/C}$	1.29	0.42	0.65	1.0	g S/g C
$Y_{T/S}$	0.94	0.60	0.60	0.10	g T/g S
$V_{S,max}$	0.61	0.0050	0.010	0.025	g S/m^3.d
K_g	0.015	0.075	0.075	0.075	g S/m^3

The model predictions of the experimental data are shown below in Figs 5.1 and 5.2. The model was coded in Matlab whilst the experimental data was read from an excel file. The plots of experimental and simulated results were produced in Matlab. Figs 5.1 and 5.2 depict the composition kinetics of *S. obliquus* as a function of light intensity grown under nitrogen-depleted conditions. The detailed analysis of Figs 5.1 and 5.2 is provided in the following subsections.

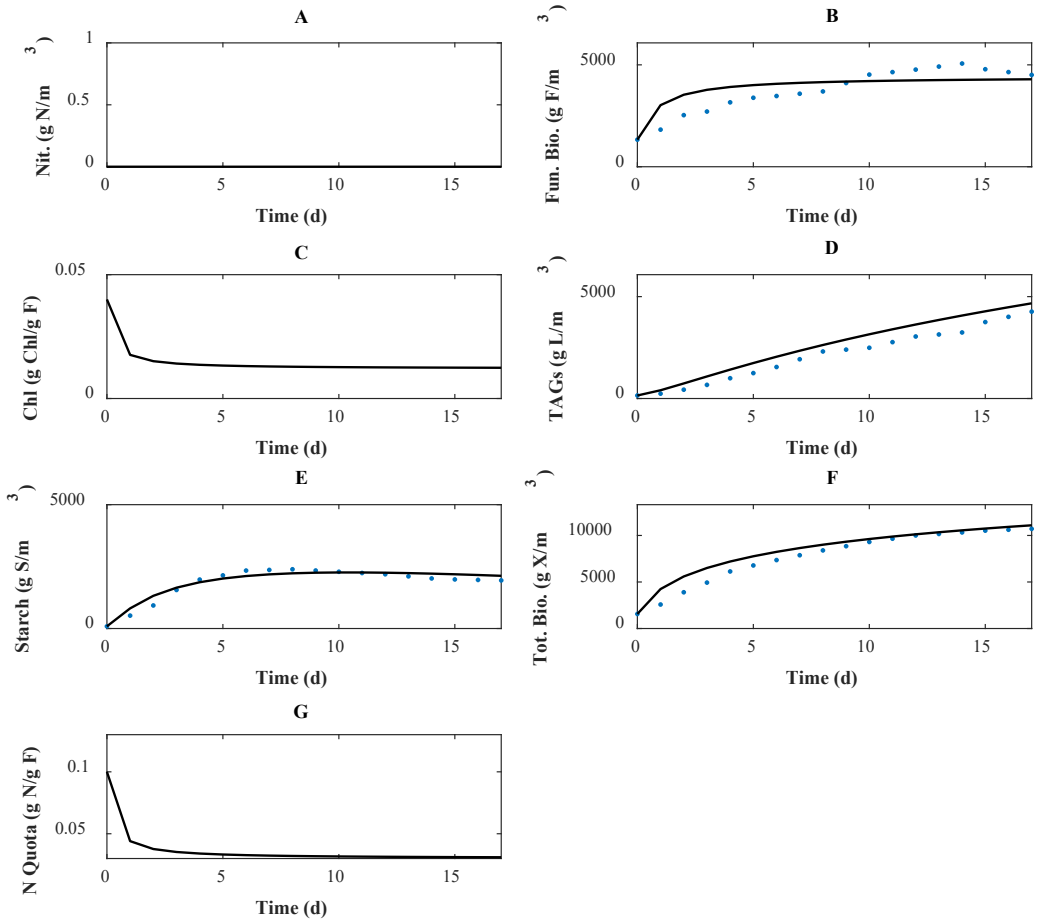

Figure 5.1 Plots of model and experimental data at an initial nitrogen concentration of 0 g N/m^3 and incident light flux of 200 µmols/m^2.s for *S. Obliquus*. The data was collected from Breuer et al., (2015).

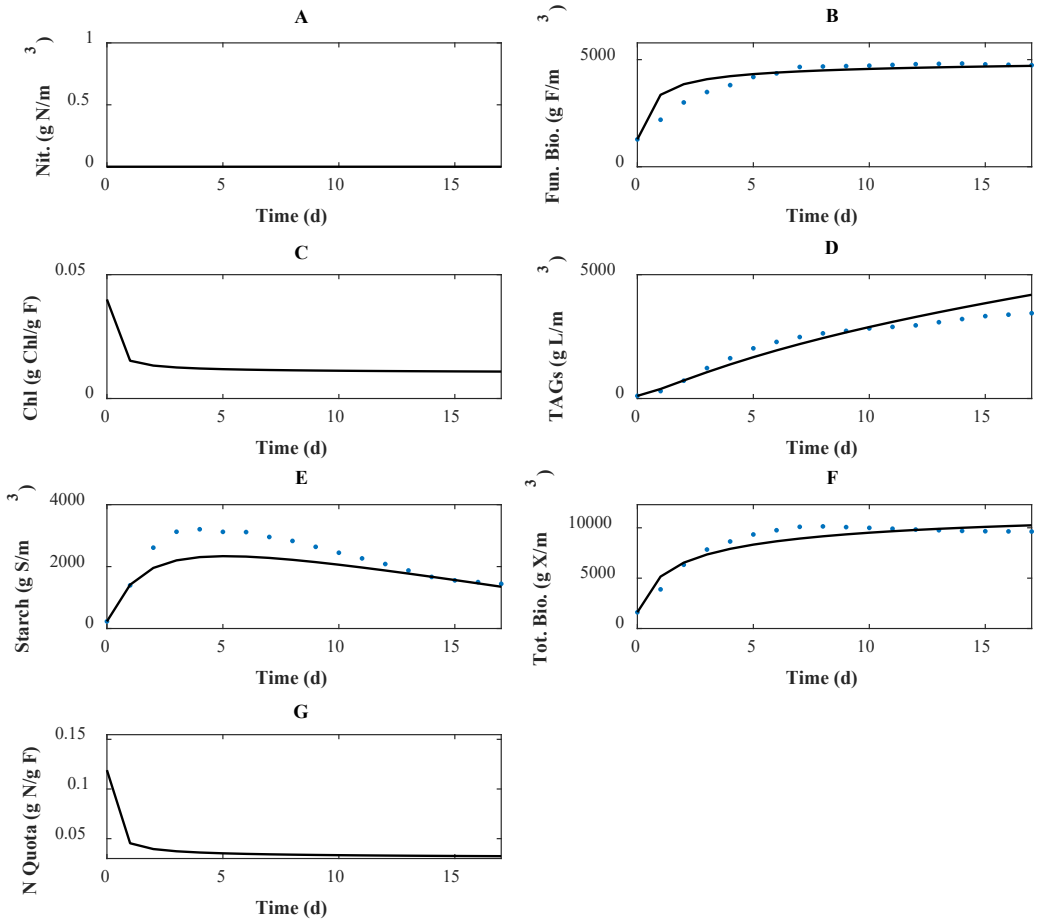

Figure 5.2 Plots of model and experimental data at an initial nitrogen concentration of 0 g N/m^3 and incident light flux of 1000 µmols/m^2.s for *S. Obliquus*. The data was collected from Breuer et al., (2015).

5.3.1 Nitrogen and Chlorophyll kinetics

The model's output for nitrogen is still shown in Fig. 5.1A and Fig. 5.2A to demonstrate that the model can accurately depict microalgae growth under nitrogen-depleted conditions and to verify that there is no error in the code. As there is no extracellular nitrogen, it is expected that during the time of the experiment, the internal nitrogen reserves were being consumed to meet growth requirements. Consequently, the simulated nitrogen quota was always below the maximum cell quota of 0.15 g N/g F and it showed a non-linear decline with time as cellular reserves of nitrogen were

consumed. In addition, also due to the lack of extracellular nitrogen, the chlorophyll content was predicted to decline rapidly from the very first day from 0.04-0.01 g Chl/g F.

Figs 5.1C and 5.2C show that chlorophyll kinetics closely correlated with nitrogen quota kinetics for all data sets. This is an interesting finding, as the rate equations for chlorophyll synthesis Eq. 3.3 and nitrogen quota synthesis Eq. 3.7 are not apparently proportionally related. However, they are dependent on auxiliary variables such as specific growth rate and photosynthetic carbon fixation, therefore may simplify to proportional expressions. This hypothesis was tested by expanding and simplifying the rate equations for chlorophyll synthesis and nitrogen quota to yield the following:

$$\frac{dB}{dt} = \frac{\theta_m \rho_N (p-b)(Q_n - Q_{n,min})}{Q_n} - \frac{BpY_{F/C}(p-b)(Q_n - Q_{n,min})}{Q_n} \tag{5.1}$$

Let ε and κ be:

$$\varepsilon = \frac{\theta_m (Q_n - Q_{n,min})(p-b)}{Q_n} \quad \kappa = \frac{Bp}{Q_n}$$

Therefore, the expression for the chlorophyll rate can be written as:

$$\frac{dB}{dt} = \varepsilon \rho_N - \kappa Y_{F/C}(p-b)(Q_n - Q_{n,min}) \tag{5.2}$$

And recalling the equation for the nitrogen quota

$$\frac{dQ_n}{dt} = \rho_N - Y_{F/C}(p-b)(Q_n - Q_{n,min}) \tag{5.3}$$

From Eqs 5.1 and 5.3 it can be seen that even when the expressions for chlorophyll synthesis and nitrogen quota are expanded and simplified algebraically, both expressions are proportional to the difference between predicted nitrogen quota and the

minimum nitrogen quota. Furthermore, Eq. 5.2 shows how chlorophyll synthesis rate may be shown to look similar to nitrogen quota rate if parameters ε and κ are used to simplify the expression. Since chlorophyll kinetics and nitrogen quota contents are within a similar range (0.03 – 0.12 g /g F) ε and κ must be close to one for Eq. 5.2 to simplify to Eq. 5.3 and show the same kinetic behaviour between chlorophyll and nitrogen quota.

5.3.2 Functional Biomass Kinetics

Functional biomass, the metabolically active fraction of the algae, was simulated as a function of the specific growth rate itself dependant on the net photosynthetic rate of carbon fixation and nitrogen quota. Functional biomass, for the low light intensity case (200 μmol/m^{2}s), showed some discrepancy between the model and experimental data in Fig. 5.1B, with the model overpredicting the experimental measurements by 20 % within the first 10 days and underpredicting it by 10 % in the last seven days. The model predicted a rapid rate of increase in functional biomass growth, reaching 5000 g F/m^3 in three days to plateau at this level. However, the experimental data, for 200 μmol/m^{2}s, showed a more linear increase in the functional biomass growth until the biomass reached 5000 g F/m^3 at day 14 and later the functional biomass value plateaued (Fig. 5.1B). The reason for this discrepancy between data and model is due to the model predicting a greater than apparent rate of nitrogen quota consumption to biomass synthesis. What has actually been observed, in the case when there is no initial nitrogen in the system, is an inhibition in the rate at which nitrogen quota was used to supply nutrient for functional biomass growth.

When the light flux was increased to 1000 μmols/m^2.s, while keeping the same all the other process conditions, the model showed an almost perfect prediction of

experimental data within 10 % of measured values. The functional biomass increased rapidly as the nitrogen quota was being depleted, reaching 5000 g F/m^3 within seven days. In this case, the increased light can be seen as upregulating the rate at which nitrogen quota is broken down to produce functional biomass.

5.3.3 Starch and TAGs Kinetics

Starch and TAGs are two groups of molecules that are carbon sinks (Sharma, Saharia, Srivstava, Kumar, & Sahoo, 2018). The relative rate at which carbon is fixed into these two substrates depends on process conditions such as nitrogen and light. For a light flux of 200-1000 µmols/m^2.s TAGs increased almost linearly from 150-4000 g L/m^3 over 17 days (Fig. 5.1D). It was predicted well by the model, correlating within 15 % of the experimental data.

For a light intensity of 200 µmol/m^{2}s, starch increased rapidly in the first eight days, from an initial concentration of 90 g S/m^3, until reaching a maximum concentration of 2400 g S/m^3 on the eighth day. The starch then decreased slowly reaching a concentration of 1950 g S/m^3 by day 17. This type of behaviour is rather typical of starch kinetics as evidenced by the literature (Adesanya et al., 2014; Takeshita et al., 2014). The accumulation of starch was likely to be initiated by nitrogen depletion as reported in the literature (Takeshita et al., 2014). In addition, long-term depletion of nitrogen favours TAGs production, which in the previous chapter was proposed to result in the degradation of starch. Nevertheless, the model showed good correlation between the data and prediction, within 10 %, suggesting that the mechanism of starch kinetics dictated by photosynthetic fixation and glycolysis to TAGs is an accurate representation of transient behaviour. Therefore, photosynthetic fixation is regarded as being responsible for the rapid accumulation of starch in the first eight days (Fig. 5.1B), whilst

glycolysis, which is activated by a decreasing nitrogen quota, dominates after day eight (Fig. 5.1B). The regulation of glycolysis by nitrogen quota could be an example of cell signalling processes dictating enzyme kinetics. Cell signalling in biological organisms is a common evolutionary feature that allows organisms to adapt to environmental stresses. For instance, diatoms when exposed to decadienal at sublethal levels were able to immunise themselves against lethal doses. In the study, it was proposed that the algae had used the decadienal as a signalling molecule to prevent calcium in the cells from being utilised to generate nitrogen oxide at toxic levels (Vardi, 2008). Similarly, nitrogen quota may act as a signalling molecule for starch glycolysis. This regulation represents an extension of the Droop model of nitrogen quota regulation, which states that the internal nitrogen storage dictates extracellular nitrogen uptake and cell division (M. R. Droop, 1983). It would appear that internal nitrogen reserves have a much broader role in cellular kinetics than just nutrient kinetics.

When the light flux to *S. Obliquus* was increased from 200 to 1000 μmols/m^2.s, TAGs concentration depicted a non-linear increase as shown in Fig. 5.2D. TAGs increased more rapidly in the first seven days from 100 to 2500 g T/m^3, representing a 25-fold increase. In contrast, after day seven, the rate at which the concentration of TAGs increased was slower, increasing by 36 % from 2500-3400 g T/m^3. The model predicted TAGs within 15 % of experimental data.

Starch, for the light intensity case of 1000 μmols/m^2.s (Fig. 5.2E), showed a faster increase in concentration compared to that of 200 μmols/m^2.s. For 1000 μmols/m^2.s, the experimental value of starch peaked at 3200 g S/m^3 by day four, compared with 2400 g S/m^3 by day eight, for 200 μmols/m^2.s representing a 33 % greater starch yield at 1000 μmols/m^2.s. After this peak was reached, the starch concentration declined at a

rate of 130 g S/m^3.d, reaching 1400 g S/m^3 by day 17. The model, however, could not accurately predict starch kinetic behaviour, increasing more slowly to peak at 2000 g S/m^3.d by day four before declining and converging towards the experimental data due to glycolysis.

It is clear that the increased light flux had favoured greater starch accumulation in the algal culture, which was accounted for by tuning the parameters such as maximum photosynthetic rate, p_{max}.. The nitrogen quota regulates the quantity of starch broken down to form TAGs (Eq. 3.17) and quantity of photosynthetic fixed carbon channelled towards functional biomass (3.4 and 3.9). The photosynthetic activity, as explained earlier, regulates the quantity of photosynthetically fixed carbon channelled towards TAGs (3.18). The photosynthetic activity or gross photosynthetic fixation rate is itself a function of light flux and nitrogen quota. At a greater light flux, the photosynthetic activity increases, which increases the portion of carbon channelled towards starch. Therefore, the model should predict greater starch concentration during the beginning of the experiment. However, it shows an underestimation of the experimental measurement for the first 10 days in Fig. 5.2E. This may be due to parameters such as the maximum photosynthetic rate being too low.

Increasing the maximum photosynthetic rate parameter (not shown) allowed the model to reach the peak starch concentration, but resulted in the overprediction of starch after day 7. Increasing the glycolysis rate to compensate for this, improved the fit for starch, but at the expense of poorer TAGs prediction. Therefore, there is a trade-off between accurately predicting either starch or TAGs kinetics. Prediction of a lower than expected starch concentration may suggest problems with the photosynthetic carbon uptake model, whilst greater than predicted TAGs may suggest that the TAGs may be

catabolised for energy under the nitrogen-depleted conditions. The latter may be more likely since the light model (Eqs. 3.12 and 3.14) was already changed in order to better simulate algal kinetics in this chapter. Metabolite catabolism of TAGs may have been reached at 1000 µmols/m^2.s rather than 200 µmols/m^2.s due to the greater light flux increasing kinetics hence potential catabolic reactions within the algal cells. Therefore, future studies may aim to investigate the effect of storage molecule degradation for respiration under nutrient depleted conditions.

In order to better understand the relationship between starch and TAGs kinetics, Fig. 5.3 shows the ratio of starch to the sum of starch and TAGs concentrations using the experimental data of Breuer et al. (2015). For *S. obliquus* in Fig. 5.3 the starch content rose for the first three days before decreasing again from day four onwards, indicating a preference for TAGs in the later stages of growth. Thus, algae have a preference for TAGs during extended nitrogen depletion as nitrogen quota monotonically decreased from day 1. Light played a role in upregulating the synthesis of starch when increased from 200-1000 µmols/m^2.s. Starch content in storage molecule peaked at 0.3 in day two for 1000 µmols/m^2.s whilst it peaked at a lower level later at 0.25 on day three for 200 µmols/m^2.s. However, the starch to storage molecule fraction converged to a similar value for the two light fluxes quickly after showing divergent behaviour in the first few days.

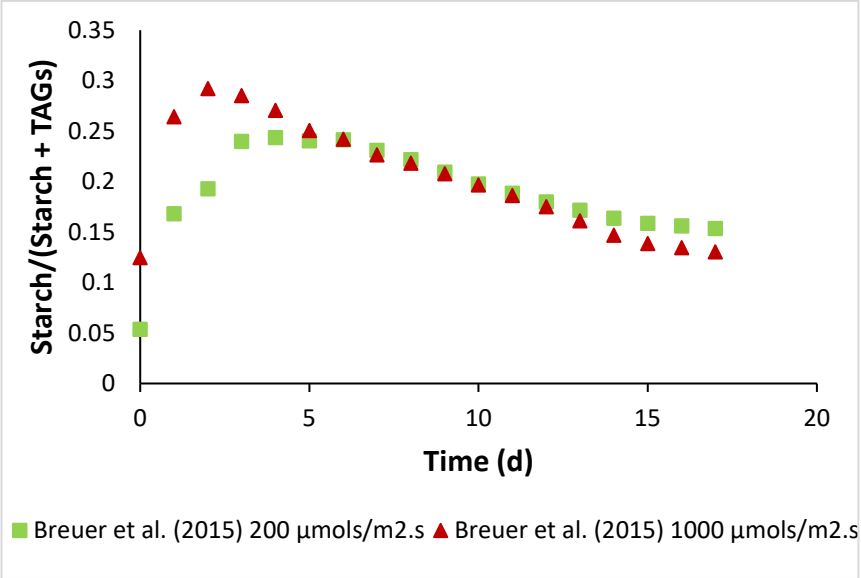

Figure 5.3 Plot of the starch to TAGs fraction against time for *S. Obliquus* at an initial nitrogen concentration of 0 g N/m^3 and light fluxes of 200 and 1000 µmols/m^2.s respectively (Data from Breuer et al., 2015)

This illustrates that the effect of light flux is most prominent during more nitrogen replete conditions when cell quotas are still relatively high. However, as nitrogen quota decreases, nitrogen quota becomes a stronger regulating factor than light regardless of intensity. Another reason for nitrogen becoming dominant in the later stages of biomass growth is that as the biomass concentration increases the average culture light intensity decreases, inhibiting the regulatory effect of light. From a modelling perspective nitrogen quota depletion results in activation of TAGs synthesis from glycolysis (Eq. 3.17). Biologically, nitrogen quota depletion may be upregulating the pathways, which are responsible for TAGs production through a type of cell signalling process.

5.3.4 Intracellular Carbon Flux Analysis

Fig. 5.4 compares the carbon fluxes in the algae as a function of light for

200 µmols/m^2.s and 1000 µmols/m^2.s, respectively. The carbon fluxes were obtained from calculating and plotting the gross photosynthetic rate (Eq. 3.11), starch glycolysis (Eq. 3.17), TAGs production from photosynthesis (Eq. 3.18), starch production from photosynthesis (Eq. 3.16) and functional biomass production rate (Eq. 3.4). They were all plotted in carbon equivalents.

The rates of photosynthetic carbon fixation (Fig. 5.4A) for 1000 µmols/m^2.s showed a higher initial photosynthetic carbon fixation rate than the 200 µmols/m^2.s case, but later declined rapidly to the same magnitude as time progressed. No other differences between both light cases were observed. This suggests that light is not a limiting factor in either case.

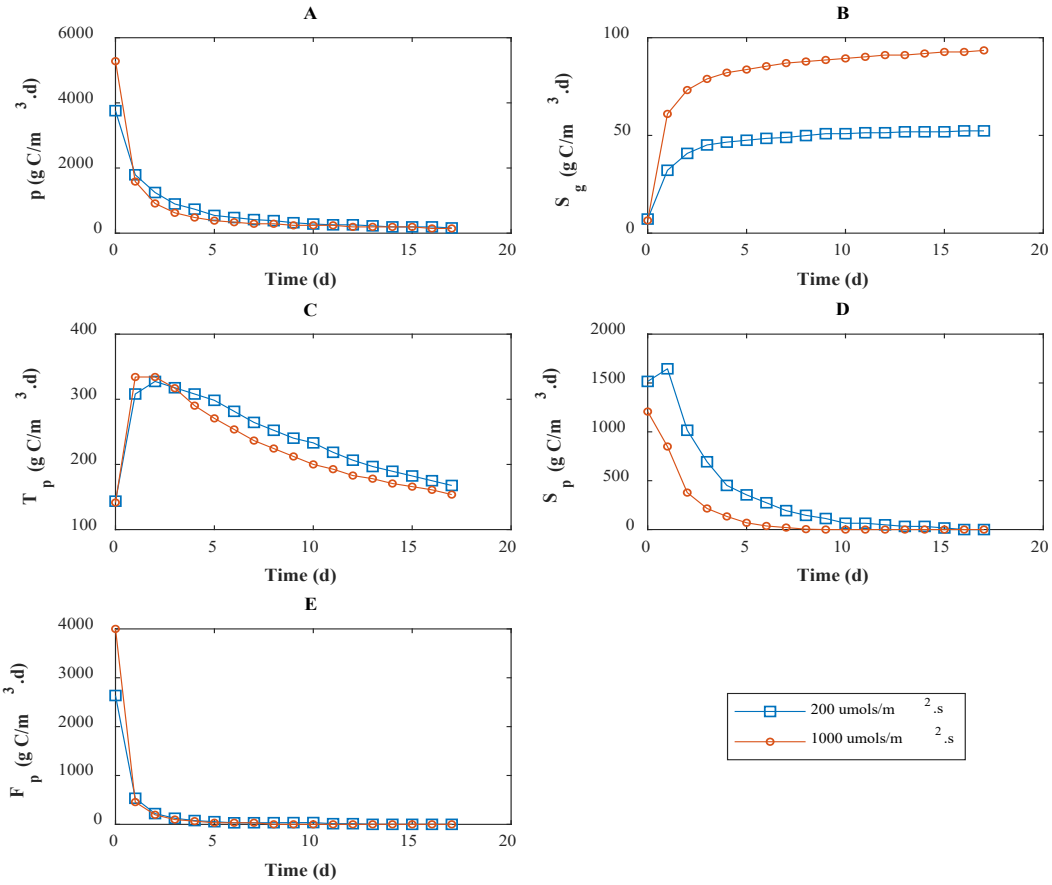

Figure 5.4 Model predicted carbon fluxes of *S. Obliquus* at 200 µmols/m^2.s and 1000 µmols/m^2.s where *p* is the photosynthetic rate (g C/m^3.d), S_g is the starch glycolysis rate (g C/m^3.d), T_P is the TAGs synthesis rate from photosynthetic fixed carbon (g C/m^3.d), S_P is the starch synthesis rate from photosynthesis (g C/m^3.d) and F_P is the rate of functional biomass synthesis (g C/m^3.d)

Starch glycolysis rate in Figure 5.4B showed the most discrepancy between the two different light fluxes. As time progressed from days zero to five, the carbon flux increased from 0-50 g C/m^3.d for 200 µmols/m^2.s, and reached 90 % of its maximum value by day five at 75 g C/m^3.d for 1000 µmols/m^2.s. TAGs from photosynthesis in Figure 5.4C showed little variation between the two light intensities. The small variation observed between the two data sets is a result of the different parameter value for maximum starch glycolysis rate, which was 0.01 g S/g F.d for 200 µmols/m^2.s and

0.025 g S/g F.d for 1000 µmols/m^2.s. Although TAGs synthesis from photosynthesis is slightly higher under 200 µmols/m^2.s this is more than compensated by the greater carbon flux towards TAGs from starch glycolysis. Therefore, the model predicts that starch glycolysis is responsible for the increase in TAGs concentration in algae as light flux increases. Metabolically, what may be happening, is that carbon being fixed via photosynthesis is first being converted to starch via gluconeogenesis and then, being broken down rapidly to form TAGs via glycolysis for *S. obliquus*.

The model predicted that carbon fluxes from fixed photosynthetic carbon towards starch have similar trends but they have different values (Figure 5.4D). For 200 µmols/m^2.s, the carbon flux reached a maximum in day one at a value of 1600 g C/m^3.d and then, decreased exponentially from 1600-0 g C/m^3.d by day 15. In contrast, within the same period the carbon flux of photosynthetically fixed starch for 1000 µmols/m^2.s decreased from 1200-0 g C/m^3.d from days 0-7. The low initial rate of starch formation from the culture receiving a light flux of 1000 µmols/m^2.s underpredicted starch synthesis in Figure 5.2E. If the model were to accurately predict starch production rate, the starch synthesis rate would be higher than the 200 µmols/m^2.s case explaining the higher starch to TAGs ratio in *S. obliquus* in Figure 5.3.

For the functional biomass synthesis rate (Fig. 5.4.E), overall there appeared to be close correlation between productivity as a function of light intensity. The only exception was the greater initial functional biomass carbon flux for 1000 µmols/m^2.s at 4000 g C/m^3.d compared with 2800 g C/m^3.d for 200 µmols/m^2.s. This shows that functional biomass synthesis was not dependent on light intensity after the first 2 days. This was because the functional biomass synthesis rate was only dependant on nitrogen quota in the algae and nitrogen uptake kinetics, which dictated cell nitrogen quota in turn. Since nitrogen

uptake was also light independent all nitrogen uptake related processes were mathematically and physically light independent.

For the carbon flux towards TAGs from photosynthesis, there was little difference between the two different light intensities (Fig. 5.4C). Both showed an initial increase in carbon flux maximising at 320 g C/m^3.d by day one and then, decreased gradually to 170 g C/m^3.d.

5.3.5 Comparing the Effect of Light Intensity on Composition Kinetics

To better determine the effect of light intensity on composition kinetics the measured results of 200 µmols/m^2.s and 1000 µmols/m^2.s were plotted and compared with a simulated result for 40 µmols/m^2.s in Fig. 5.5. The simulated results were plotted for a maximum photosynthetic rate of 175 g C/g F.d and maximum starch glycolysis rate of 0.005 g S/g F.d. The maximum photosynthetic rate and glycolysis rate for the other light intensities are presented in Table 5.3.

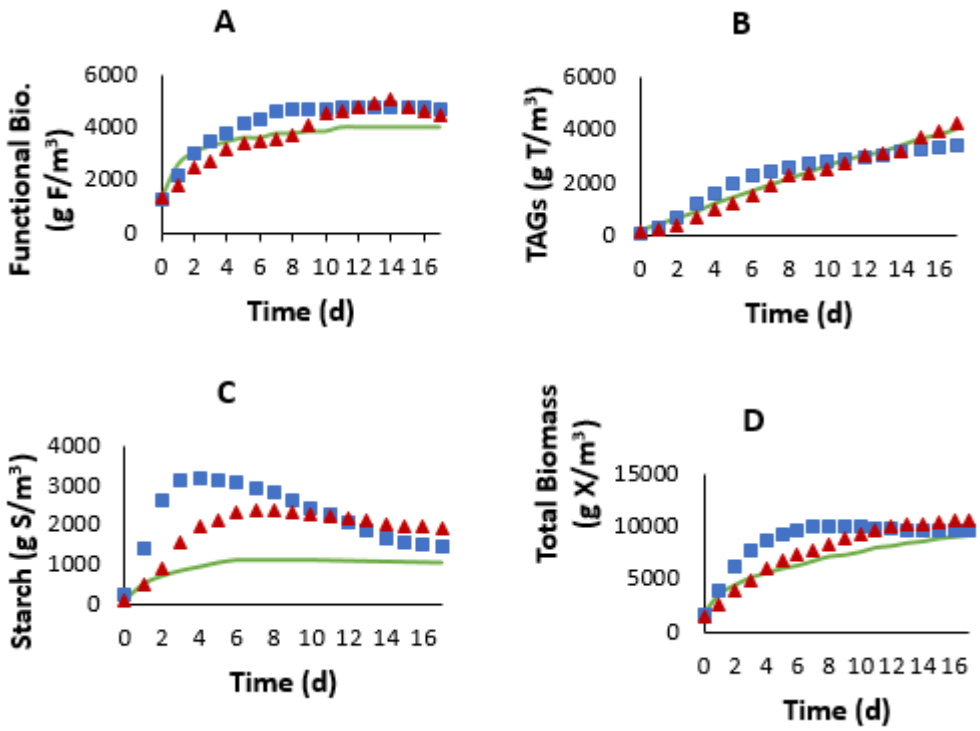

Figure 5.5 Plots of the composition and total biomass of *S. obliquus* as a function of time and light intensity. Light intensities plotted were 40 µmols/m^2.s (solid line), 200 µmols/m^2.s (triangles) and 1000 µmols/m^2.s (squares). The light data for light fluxes of 1000 µmols/m^2.s and 200 µmols/m^2.s were measured data whilst 40 µmols/m^2.s is a model prediction.

Fig. 5.5A shows that the functional biomass yield is lower for 40 µmols/m^2.s than 1000 µmols/m^2.s. The intermediate light flux of 200 µmols/m^2.s shows a different trend in kinetics from the other two light intensities. Under a light flux of 1000 µmols/m^2.s the concentration of functional biomass peaked at day seven and stayed essentially constant once it had reached the maximum. For 40 µmols/m^2.s, the functional biomass increased more slowly peaking at 4000 g F/m^3 by day 11. The slower kinetics can be explained by lower light intensity reducing the energy flux into cells. The lower maximum concentration however is more complex.

Theoretically, since the intracellular nitrogen pool and the carbon to functional biomass yield are the same in the three cases, it would be expected that the yield of functional biomass would be the same. However, different carbon to functional biomass yields are apparent from Fig. 5.5A. This suggests that light intensity may have an effect on the protein composition of algae, which may have lower C-N ratios for lower light intensities. This may be deemed plausible as algal fatty acid composition is known to be a function of light intensity (Seyfabadi, 2012). It is also possible that a lag phase may be observed for the low intensity cases 40 µmols/m^2.s and 200 µmols/m^2.s. Therefore, it would be interesting for future experiments to measure the functional biomass content of algae as a function of a wider set of light intensities to determine whether there are compositional changes or lags phase induced under different light intensities.

TAG kinetics in Fig. 5.5B depicted similar kinetics regardless of light intensity. Although the measured value of TAGs for 1000 µmols/m^2.s showed a higher productivity earlier on in the experiment from days 2-10, the yield of TAGs was lower for this light intensity at 3250 g T/m^3 compared with 3750 g T/m^3 for 40 and 200 µmols/m^2.s. TAGs concentration is shown to plateau after day 10 for the maximum light intensity. This may be because once a maximum quantity of TAGs has been reached a greater quantity of carbon is channelled towards respiration and maintenance. This may be more evident at a higher light intensity due to the possibility of greater concentrations of oxygen free radicals produced, which damage the cellular machinery, enzymes, which then need to be repaired.

Starch showed the greatest variation as a function of light. The variation of starch concentration can be explained by how the most sensitive parameters change as a function of light. Maximum photosynthetic rate varied from 175-400 g C/g F.d for

40-1000 μmols/m^2.s. Maximum photosynthetic rate increased as a light intensity increased, which increased the maximum starch concentration. The quantity of starch produced, however, especially in the later portion of the experiment, was limited by the maximum glycolysis rate, which was activated by light intensity. Thus, a more pronounced decrease in starch concentration was evidenced in Fig. 5.5C for 1000 μmols/m^2.s than for the lower light intensity. Glycolysis was not clearly evident for starch for a light flux of 40 μmols/m^2.s since the maximum starch glycolysis rate was much smaller at 0.005 g S/g F.d compared with 0.025 g S/g F.d. Since total biomass in Fig. 5.5 D was a function of starch, it showed some variation in productivity, increasing with light intensity, although the yield was essentially the same by day 17.

5.4 Conclusion and Recommendations

A mathematical model was tested against two experimental data sets for *S. obliquus* under two different light conditions, of 200 μmols/m^2.s and 1000 μmols/m^2.s. Agreement between the model and experimental data for TAGs, starch and total biomass for *S. obliquus* at a light flux of 200 μmols/m^2.s was found. However, some discrepancies were identified in the functional biomass prediction. The differences could be due to the functional biomass having an alternate kinetic relationship with nitrogen quota mediated specific growth rate than the one stipulated in Eq. 3.9.This point needs further study. Nevertheless, the overall error of the fitting was less than 15%.

For a light flux of 1000 μmols/m^2.s, the model predicted functional biomass and TAGs kinetics accurately. However, it underpredicted starch concentration in the first 12 days of analysis. This may have been due to the activation of the catabolism of TAGs in the

latter half of the experiment due to an increased starch, functional biomass (initially) and total biomass production rate from a higher light intensity. If this were the case, increasing the parameters for maximum photosynthesis and glycolysis would allow for an accurate fit of the starch data at the expense of TAGs. TAGs prediction could be improved by having a TAGs catabolism term. Thus, it is recommended that further investigation be carried out on determining the effect of light in the late stationary phase to determine whether catabolism of TAGs is occurring.

Carbon flux analysis of starch, TAGs and functional biomass showed that the increase in light intensity upregulated the starch glycolysis rate, initial photosynthetic rate and initial functional biomass synthesis rate. Carbon flux towards TAGs from photosynthesis did not show appreciable sensitivity to light.

Finally, the model was extended to a light flux of 40 μmols/m^2.s and compared against the two other light intensities for composition kinetics and total biomass. Functional biomass concentration was predicted to be lower for a light intensity of 40 μmols/m^2.s when compared with 200 and 1000 μmols/m^2.s, whilst no significant differences were found for TAGs. In contrast, starch showed some dependency on light, decreasing its maximum concentration with decreasing light intensity. Starch glycolysis was also less effective at lower light intensities. Future studies may investigate storage molecule degradation for energy under long-term nitrogen depletion and study the effect of light intensity on functional biomass yields at lower light intensities to determine if lower light intensities reduce functional biomass yield.

6 Trial Experiments on Photosynthetic and Mixotrophic Algae

6.1 Introduction

In the literature review of Chapter 2, it was found that mixotrophy could significantly improve the growth rate of microalgae. This was due to organic carbon adding an additional carbon and energy source to otherwise photosynthetic algae. Another benefit of mixotrophy was optimisation of CO_2 and O_2 production and consumption due to a cycling effect within the cells between phototrophic and heterotrophic compartments. This is important since commercial scale photobioreactors suffer from CO_2 limitation and oxygen inhibition (Grima et al., 1999). The consumption of oxygen for heterotrophic growth reduces oxygen concentrations hence inhibition, whilst simultaneously producing CO_2 replenishing this compound for photosynthetic uptake overcoming CO_2 limitation. Photoinhibition of outdoor cultures is another problem that mixotrophy mitigates. It was shown in the review of Chapter 2 that chlorophyll content was lower in mixotrophic cultures due to glucose uptake, which inhibited chlorophyll synthesis resulting in 20-90 % less chlorophyll. Lower chlorophyll content reduced the cellular light absorption, hence photoinhibition. The consumption of glucose also reduce the cellular oxygen concentration, therefore the population of damaging free radical oxygen atoms was also reduced (Chojnaka & Marquez, 2004).

However, one factor that has not been discussed at length is the effect of bacterial contamination and growth on glucose in mixotrophic cultures. It is well known that contamination by algal grazers reduce photosynthetic algae yields in open raceway ponds (White, Pagarette, Rooks, & Ali, 2013). However, the impact of competitive

uptake of glucose by bacteria has not been well studied. Trial experiments by researchers at the Wageningen University and Research Centre found that bacteria contaminated mixotrophic algal cultures, severely reducing yield. Therefore, before proper experiments are carried out a series of trial experiments will be performed to determine whether the green algae at the PSFI culture collection can be grown mixotrophically without bacterial contamination. In addition, it will also be determined whether physicochemical variables such as pH and CO_2 concentration can be optimised so that these variables can be blocked in the experiment.

This section presents the experimental culturing procedure for trial experiments, the proposed analytical procedure for measurements of algal total biomass, chlorophyll, glucose, TAGs, proteins and starch for proper experiments and the results of the trial experiment. The green algae to be grown mixotrophically and compared with photosynthetic controls were *N. oculata* and *T. chuii* with additional experiments on other species left in the Appendix. The algal samples that were analysed for composition were *S. obliquus*.

6.2 Materials and Methods for Experimental Design

6.2.1 Materials

The algal cultures used for cultivation were obtained from the stock cultures of PSFI. The species grown were *N. oculata*, *T. chuii*, *Chaetoceros muelleri*, *Pavlova lutheri* and *Isochrysis* sp. Results for *N. oculata* and *T. chuii* are reported in this section with the results of the remaining algae in the Appendix.

The culture media was composed of estuarine water mixed with Guillard's f/2 1000 times concentrate. f/2 medium components had the following concentration, shown in Table 6.1, when 1 part f/2/ media was diluted 1000 times into estuarine water.

Table 6.1 Concentration of the different compounds in 1 L of culture media composed of estuarine water and f/2 nutrient media.

Compound	Concentration in Final Medium (M)
$NaNO_3$	8.82×10^{-4}
$NaH_2PO_4H_2O$	3.62×10^{-5}
Na_2CO_3	1.06×10^{-4}
$FeCl_3\cdot6H_2O$	1.17×10^{-5}
$Na_2(EDTA)_2\cdot H_2O$	1.17×10^{-5}
$CuSO_4\cdot5H2O$	3.93×10^{-8}
$Na_2MoO_4\cdot2H_2O$	2.60×10^{-8}
$ZnSO_4\cdot7H_2O$	7.65×10^{-8}
$CoCl_2\cdot6H_2O$	4.20×10^{-8}
$MnCl_2\cdot4H_2O$	9.10×10^{-7}
Vitamin B1	2.96×10^{-7}
Vitamin H	2.05×10^{-9}
Vitamin B12	3.69×10^{-10}

Other materials required were: 5 % HCl, NaOH pellets, 96 % ethanol, RO water, sodium azide, 1 M ammonium formate, 3-(N-morpholino)propanesulfonic acid (MOPS), $CaCl\cdot2H_2O$, sodium acetate, a Megazyme starch analysis kit, a Megazyme D-Glucose assay kit, DC Protein assay kit, amyloglucosidase, methanol, Tris(hydroxymethyl)aminomethane, Sodium dodecyl sulfate (SDS), Bovine serum

albumin (BSA), n-Hexane, chloroform, sodium chloride, sulfuric acid, diethylether, acetone, internal standard – Glyceryl trinonadecanoate (C19:0 TAG) and Dipentadecanoyl-sn-Glycero-3[Phospho-rac-(1-glycerol)} (Sodium Salt) C15:0 PG, N_2 gas and CO_2 gas.

Equipment used for trial experiments were UV-Vis spectrophotometers, Eppendorf pipettes (1-10µL, 10-100µL, 20200µL, 100µL-1mL and 0.5-5mL), glass pipettes, analytical balance, oven, vortex, desiccator, fume hood, aluminium trays, tweezers, freezer, water batch, ice bath, an ultrasound bath, microtiterplates 96-wells., plate reader Biotek EL800, block heater, centrifuge, eppendorf tubes, 15mL tubes, beating tubes, bead-beater, positive displacement pipette, Sep-Pak VacSilica cartridge 6cc/1000mg (125 Å, 55-105 µm, Waters, 186004617), test-tube rotator, spider, glass heat resistance tubes with caps containing a Teflon layer, sonicator bath, vials and caps and a gas chromatograph.

6.2.1.1 Stock Solutions for Starch Analysis

Before starch analysis could be carried out, a number of solutions were required to be made. An 80 % Ethanol solution was made by combining 417 ml 96 % ethanol with 83 ml of RO water. 20 ml of ethanol is required for every experimental sample. A 1 M NaOH solution was made by addition of 4g NaOH to every 100 ml of RO water. 1 M HCl was made through the addition of 82 ml of 37.5 % HCl (w/w) to 918 ml of RO water.

The MOPS Buffer (50 mM, pH 7) was to be made by addition of 11.55 g of MOPS to 900 ml of water and pH was adjusted to seven by adding 1 M NaOH (~ 60 ml). 0.74 g of $CaCl{\cdot}2H_2O$ was added to the mixture and 0.2 g of sodium azide was also added in a fume

hood. The volume was adjusted to 1 L by adding water and stored the buffer in a fridge at 4°C where it is stable for 6 months.

The sodium acetate buffer (200 mM, pH 4.5) was made by addition of 16.4 g of sodium acetate to 900 mL of RO water. The pH was adjusted to 4.5 by addition of 1M HCl (~ 17mL). In a fume hood, 0.2 g of sodium azide was dissolved in the solution. The volume was adjusted to 1 L using RO water and stored in a fridge at 4°C where it is stable for 6 months. 8 ml of sodium acetate buffer was required for each experimental sample.

The thermostable α-amylase (bottle 1 of Megazyme kit) plus MOPS buffer was next prepared. 1 mL of α-amylase was added for every 30mL MOPS buffer. Approximately 6 ml of α-amylase + MOPS buffer is required per experimental sample.

The GOPOD reagent buffer (bottle 3 Megazyme kit) was prepared in a fume hood with the entire contents of the reagent buffer diluted by 1L of water. To 20 ml of this solution (solution 1), all of the GOPOD reagent enzymes (bottle 4 of Megazyme kit) was added. The solution produced was then mixed with the rest of the reagent buffer producing the GOPOD plus reagent enzymes solution. This was stored at -20 °C in 40 ml aliquots and kept in the dark. 6 ml of GOPOD + reagent enzymes was required per experimental sample.

6.2.1.2 Cell Lysis Buffer Solution for Protein Analysis

A tris(hydroxymethyl)aminomethane stock solution was made by dissolving 6.06 g of the substance in 95 ml of RO water. HCl was added until the pH was 9. The remaining volume was made up to 100 ml. An SDS stock solution was made by dissolving 10 g of SDS in 100 ml of RO water. To make the cell lysis buffer 2.4 ml of

tris(hydroxymethyl)aminomethane solution at pH 9 was added to 4 ml of SDS and made up to 20 ml using RO water.

6.2.1.3 Stock Solutions for TAGs Measurement

A 180 ml stock solution of chloroform and methanol mixture was prepared by mixing 80 ml of chloroform with 100 ml of methanol. 8.1 mg of internal standard Glyceryl trinonadecanoate (C19:0 TAG) and 11.25 mg of internal standard Dipentadecanoyl-sn-Glycero-3[Phospho-rac-(1-glycerol)} (Sodium Salt) C15:0 PG was added to the mixture.

In 120 ml of RO water 0.725 g of Tris (hydroxymethyl)aminomethane and 7 g of NaCl was dissolved. The pH was adjusted to 7.5 by adding HCl. The stock solution containing Tris (hydroxymethyl)aminomethane and NaCl was stable for one month at room temperature. To 114 ml of methanol, 6 ml of 5 % H_2SO_4 was added making up the total volume of the stock solution to 120 ml. This solution was stable for 1 month.

To 472.5 ml of hexane, 67.5 ml of diethylether was added making up the total volume to 540 ml. To 180 ml of methanol, 180 ml of acetone was added as well as 90 ml of hexane. Stock solutions of pure chloroform (90 ml), hexane (550 ml) and RO water (250 ml) were also kept.

6.2.2 Experimental Setup

A photo of the bioreactor setup is shown below for trial experiments at PSFI in Fig. 6.1. It is composed of 1 L vessels with a 500 ml working volume. Each vessel had a sample port on the side. A rubber stopper sealed the top of each of the flasks and two holes were drilled into the stoppers. One of the holes allowed CO_2 enriched air (2 % v/v) to flow into the reactor at 0.4 Litres per Minute (LPM) and the other hole allowed for the

off-gas composed of oxygen-enriched air to flow out of the reactors without risk of contamination of cultures. The CO_2 came from a pressurised tank and was mixed with air from outside before being filtered by sterile filters and pumped into the reactors.

Figure 6.1 Bioreactor setup for culturing algae during the trial experiments at PSFI

A flow metre was used to measure the flow rate of CO_2 enriched air into the reactors. Fluorescent lights supplied light with a measured photon flux using a detector to be approximately ~300 µmols/m^2.s. For *N. oculata,* the light flux was operated under a day-night cycle and for *T. chuii,* it was operated continuously without light timers as an unknown source was found to be interfering with the timers. The temperature was kept

constant by an air conditioner and was measured to be approximately 21 ºC at the time of cultivation.

6.2.3 Culturing Procedure

6.2.3.1 Sterilisation of the Reactor Vessel

6×500 ml reactors were rinsed with water and 5 % HCl. The outlets of the flasks were covered in aluminium foil. The fittings allowing CO_2 enriched gas to flow into the vessels were wrapped in heatproof polyethylene bags. The reactors, fittings and 10 L tank of fresh estuarine water were placed in an autoclave at 120 °C for 20 minutes. Once completed the apparatus were cooled until room temperature and taken to a laminar flow cabinet for aseptic addition of algal cultures.

6.2.3.2 Inoculation of Experimental Reactors

Before the makeup of the experimental cultures, the laminar flow cabinet was wiped with ethanol. Every day the laminar flow cabinet was put under UV light for sterilisation for at least half an hour. From a 5 L tank of algal stock culture already prepared, 10-20 ml of culture was poured into a 50 ml beaker in laminar flow cabinet. The algal stock cultures are shown below in Fig. 6.2.

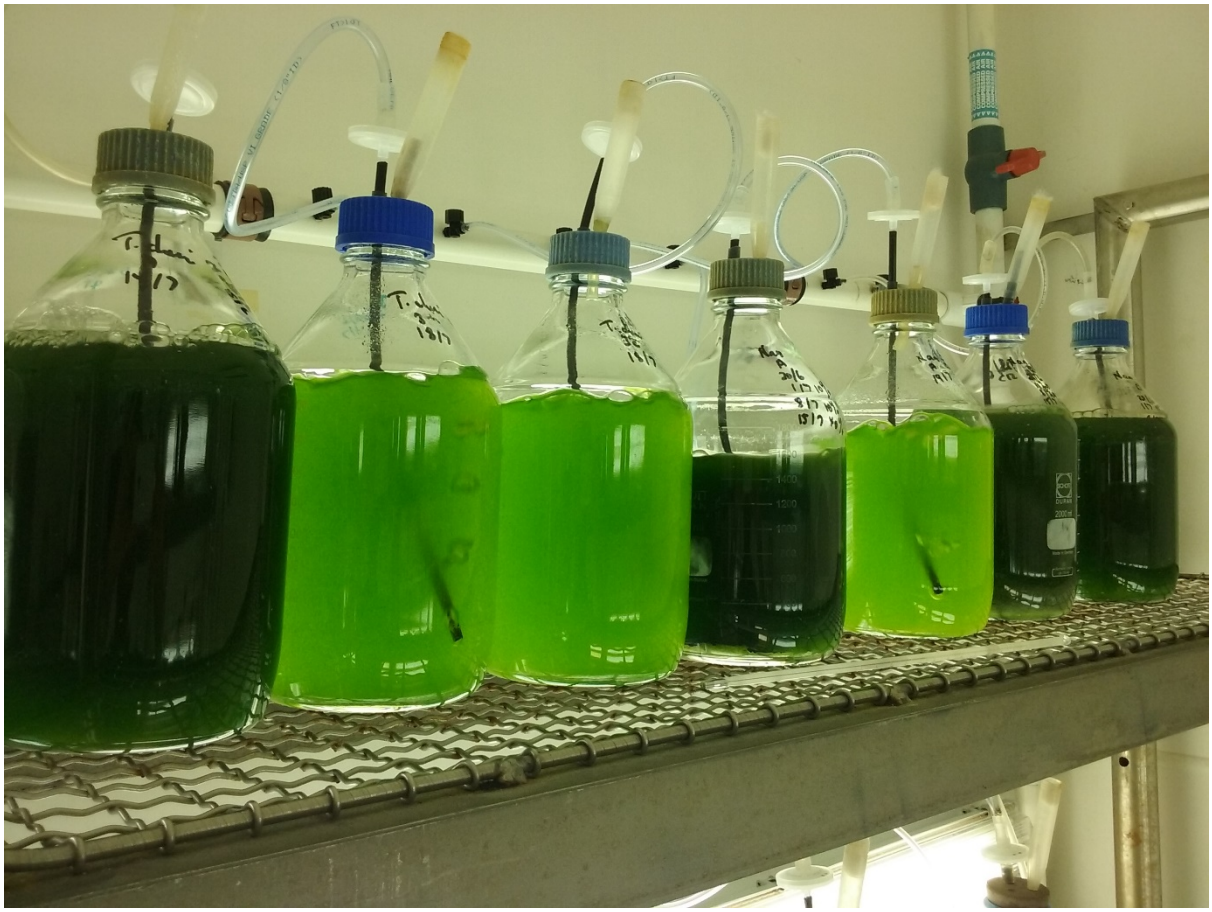

Figure 6.2 Algal stock cultures shown for *N. oculata*

A cell sample of approximately 2 ml was taken and transferred onto a haemocytometer for cell counting under a microscope. Once counted, approximately 50 ml (depending on algal cell counts it could be more or less) of inoculation culture was transferred to a 500 ml experimental vessel by pipette. This was made up to 500 ml by addition of 450 ml of autoclaved estuarine water and 0.5 ml of Guillard's f/2 medium concentrate.

6.2.3.3 Experimental Reactor Operation: CO_2 and Light

The experimental reactors were connected to gas lines with CO_2 enriched air at approximately 1 % (v/v) CO_2 concentration. The gas entered at a flow rate of 0.4 LPM and was measured using a flow metre capable of measuring between 0.1-1 LPM. The

gas was added to ensure that there was adequate mixing, pH was constant and CO_2 was not limiting. pH was measured during one set of trial experiments using a pH metre, and CO_2 concentration was adequate for growth. In the experiment, CO_2 was the buffering gas. Sterile filters were used to pump CO_2 into the cultures ensure there was no bacterial contamination. The harvested pellet was to be vacuum filtered, dried and weighed giving dry weight biomass, which could later be used for biochemical analysis.

6.2.3.4 Cell Counting

In the preliminary experiments, the cells were counted using a haemocytometer under a microscope with magnification of 40x. The cells of *N. oculata* and *Tetraselmis Chuii* were counted using cell counting within the squares. For each sample, five squares were counted and the average cell number was calculated and converted into cell density of the culture. One sample was taken for counting from each reactor. Each experimental condition was performed in triplicate, therefore 30 squares were counted each day. Each cell number count was multiplied by 40 000 to convert to cells/ml.

6.2.4 Biochemical and Nutrient Measurement Experimental Design

6.2.4.1 Total Biomass Analysis

The filters for collecting the biomass were placed in an aluminium tray, which was also placed on top of another tray. The trays and filter were dried at 95 °C for 24 hr. During cooling, the trays were placed in a desiccator for at least 2 hours. The mass of the filter inside any given tray was recorded on an analytical balance.

25 ml of culture sample was taken (minimum 25 mg of biomass) via pipette. The culture was diluted 5 times to 125 ml by combining with 100 ml of 0.5 M ammonium formate into a 250 ml beaker. The filter was pre-washed in a vacuum pump using an additional 5

ml of ammonium formate. The diluted sample was filtered and washed, including the glassware, with 250 ml of ammonium formate twice. The filter containing the biomass was dried in an oven at 95º C for 24 h and placed in a desiccator for 2 hours. The mass was recorded, again placing the filter plus biomass in an aluminium tray using tweezers, and converted into a concentration using the following formula.

$$DW = \frac{w_f - w_i}{x \times 10^{-6}} \tag{6.1}$$

where DW is the dry weight concentration (g/l), w_f and w_i are the final and initial masses of the filter plus tray, before and after algae was filtered (g) and x is the sample volume (ml). The factor 10^{-6} converts the concentration to g/m^3.

6.2.4.2 Glucose

A Megazyme D-Glucose assay kit was used to measure the glucose concentration in the experimental culture. The blank sample and experimental samples were prepared by adding 100 µL of buffer (solution 1 of kit) and 100 µL of $NADP^+$/ATP (solution 2 of kit) to each sample. To the blank 2.1 ml of RO water was added whilst for samples 2 ml of RO water and 100 µL of sample were added to the tubes. The samples and blank were capped and shaken gently and after 3 minutes, the absorbance (A_1) at 340 nm was read. This was to check for any excreted cellular glucose-6-phosphate.

To each blank and sample 20 µL of Hexokinase (solution 3) was added, which phosphorylated the glucose to glucose-6-phosphate. The reaction takes at least 5 minutes after which the absorbance was read at 340 nm (A_2). The absorbance of glucose was determined in the following manner:

$$\Delta_{sample} = A_{2,s} - A_{1,s} \tag{6.2}$$

$$\Delta_{blank} = A_{2,b} - A_{1,b} \tag{6.3}$$

$$\Delta_{glucose} = \Delta_{sample} - \Delta_{blank} \tag{6.4}$$

$$C_g = \frac{VM_g}{\varepsilon bv}\Delta_{glucose} \tag{6.5}$$

where $A_{2,s}$ is the absorbance at 340 nm of the sample containing glucose-6-phosphate, $A_{1,s}$ is the absorbance of the solution before addition of hexokinase at 340 nm, $A_{2,b}$ is the absorbance of the blank at 340 nm with hexokinase added, $A_{1,b}$ is the absorbance of the blank at 340 nm at before addition of hexokinase, Δ_{sample} is the absorbance difference of the sample, Δ_{blank} is the absorbance difference of the blank, $\Delta_{glucose}$ is the absorbance difference of the between sample and blank, C_g is the glucose concentration, V the final volume of the diluted sample after addition of RO water, buffer, $NADP^+$/ATP and hexokinase (2.32 ml), M_g is the glucose molar weight (180.16 g/mol) ε is the extinction coefficient (6300 1/mol.cm), b is the light path (1 cm) and v is the sample volume (0.1 ml) The ratio of V/v gives the dilution factor of the sample. Thus, using the values of the above parameters, the above expression (6.5) can be simplified through substitution, yielding the following:

$$c = \frac{2.32 \times 180.16}{6300 \times 0.01 \times 0.1}\Delta_{glucose}$$
$$= 0.663 \times \Delta_{glucose} \tag{6.6}$$

6.2.4.3 Nitrates Analysis

A nitrate kit was used to determine the nitrate concentration. This can be measured from the culture supernatant after it has been filtered. The Fluka Analytical Aquanal plus nitrate (NO_3) kit was used. A calibration curve was provided in the kit and the absorbance was measured at 515 nm and compared with the standard curve to determine the concentration.

6.2.4.4 Total Chlorophyll

For each experimental state 2×2 mg samples of biomass were taken and 5 ml of methanol was added to each sample. For a triplicate experiment, this would mean that six samples of chlorophyll were measured. The mixture was placed in an ultrasound bath for 5 minutes to disrupt the cell wall and extract chlorophyll into the methanol phase. The suspension was incubated in a water bath at 60 °C for 50 minutes and then incubated in an ice bath for 20 minutes. The suspension was centrifuged at 4400 rpm for 8 minutes to separate the extracted chlorophyll from the remaining biomass. If the biomass pellet at the bottom layer was not white then more methanol was added and the extraction procedure was repeated. The absorption for 652 and 665 nm was measured and the values inserted in the following equation to determine the chlorophyll content in biomass.

$$Chl_{tot} = Chl_a + Chl_b \tag{6.7}$$

$$Chl_a = (16.72 \times A_{665.2} - 9.16 \times A_{652.4}) \times D_F \tag{6.8}$$

$$Chl_b = (34.09 \times A_{652.42} - 15.28 \times A_{665.2}) \times D_F \tag{6.9}$$

where Chl_a is the chlorophyll concentration, Chl_b is the chlorophyll b concentration, $A_{665.2}$ and $A_{652.4}$ are the absorption of chlorophyll at 665.2 and 652.4 nm respectively and D_F was the dilution factor.

6.2.4.5 Protein Analysis

A sample of dry biomass was weighed and placed into a bead-beater tube. To the sample 1 ml of cell lysis buffer was added. The bead-beater was set to 3 cycles of 60 seconds 6500 rpm with 120 seconds break between cycles. The beat-beater tubes were taken and incubated for 30 minutes in a heating block at 100 ºC. The tube was then centrifuged in an Eppendorf centrifuge for 10 minutes at 3500 rpm. 400-500 µL of the supernatant was transferred to a fresh Eppendorf tube. The supernatant was diluted two times by addition of an equal volume of cell lysis buffer.

A bovine serum albumin standard curve was made in glass tubes according to the concentrations in Table 6.2 below.

Table 6.2 Volumes of BSA and lysis buffer required to make the standard curves for protein analysis

Tube number	2 mg/l BSA (µL)	Lysis buffer (µL)	Final BSA Concentration (mg/ml)
1	0	100	0
2	2.5	97.5	0.05
3	5	95	0.1
4	10	90	0.2
5	20	80	0.4
6	30	70	0.6
7	40	60	0.8
8	50	50	1.0
9	60	40	1.2
10	70	30	1.4

10 µL of BSA or sample was pipetted into a 96-wells Greiner microplate. The samples and BSA standard were vortex mixed for five seconds. From the Bio-Rad Dc protein assay kit, 20µL of reagent S was added to every ml of reagent A forming reagent A'. 25 µL of reagent A' was added to each well of the plate containing sample or standard. From the Bio-Rad Dc protein assay kit 200 µL of reagent B was added to each well. The plate was then covered with aluminium foil and incubated at room temperature for 15 minutes. The absorbance was measured at 750 nm using a Tecan M200 plate reader. By comparing the absorbance of the standard and the samples the concentration of protein could be determined.

6.2.4.6 Starch Analysis

The dry weight biomass samples for starch measurement were obtained from *S. obliquus* grown under the following nitrogen and light conditions shown below in Table 6.3. These reactors were not operated by the author. They had a light flux of approximately 500 µmols/m^2.s under white LED lights and were operated under continuous conditions. See section 6.22 for reactor operating procedure and equipment.

Table 6.3 Experimental operating conditions for biomass samples used for starch measurement.

Run number	Nitrogen load (g N/l.d)	Light Mode
1	0.173	Continuous Light
2	0.173	Continuous Light
3	0.173	Continuous Light
4	0.173	Continuous Light
5	0.173	Day-night cycle
6	0.173	Day-night cycle
7	0.0519	Day-night cycle
8	0.0519	Day-night cycle
9	0.0519	Day-night cycle
10	0.0519	Day-night cycle

2×0.5 g samples of starch were weighed. For each experiment 2×2 g samples of biomass were weighed. The starch, experimental and blank (duplicate) samples were dissolved in 5ml of 80 % (v/v) ethanol and put in a sonicator for 10 minutes for cell disruption and extraction of starch into the ethanol phase. The samples were vortex mixed and incubated at 80-85 °C for 5 minutes for further extraction. Another 5 ml of 80% (v/v) ethanol was added and the sample vortexed and centrifuged for 5 minutes at 2500 rpm. The supernatant was discarded using a glass pipette. If needed the samples were stored overnight at -20 °C.

3 ml of α-amylase + MOPS buffer was added to starch and experimental samples whilst 3 ml of RO water was added instead to the sample blanks and vortexed. All samples were incubated in water at 80-85 °C for 2 minutes and then incubated at 50 °C for

5 minutes. 4 ml of sodium acetate buffer was added to all samples. To starch and experimental samples, 0.1 ml of amyloglucosidase was added whilst to blanks 0.1 ml of RO water was added and vortexed. All samples were incubated at 50 °C for 30 minutes and centrifuged for 10 minutes at 2500 rpm.

A glucose standard range was prepared in the following manner according to Table 6.4.

Table 6.4 Volumes of standard and RO water required to obtain the required glucose concentration.

Glucose concentration (mg/l)	Volume of Standard (µl)	Volume of RO water (µl)
1	100	0
0.8	80	20
0.6	60	40
0.4	40	60
0.2	20	80
0.1	20	180
0.075	30	370
0.05	20	380
0.025	20	780

Glucose concentrations from 0.2-1 mg/l were made directly in 12 ml glass tubes whilst lower concentrations from 0.025-0.1 mg/l were made in Eppendorf tubes first and then 100 µL was transferred to glass tubes. If needed the samples were stored overnight at -20 °C.

0.1 ml of starch, experimental and blank samples were transferred to glass test tubes and 3 ml of GOPOD reagent was added to all samples and the 0.1 ml glucose standards, previously prepared, and vortexed. The solutions were incubated between 20-60 minutes at 50 °C and after cooling to room temperature the absorbance was measured at

510 nm. This step involved measuring the glucose standard and all samples against a reagent blank made from 0.1 ml of RO water and 3 ml of GOPOD reagent. The colour of the solution was stable for a number of hours.

6.2.4.7 TAGs Analysis

The dry weight biomass samples used for TAGs measurement were cultivated under the following nitrogen conditions shown below in Table 6.5.

Table 6.5 Relative nitrogen loads used for cultivation of continuous mode *S. obliquus* for TAGs analysis.

Sample number	Nitrogen load (g N/l.d)
1	0.1384
2	0.1384
3	0.1384
4	0.1038
5	0.1038
6	0.1038
7	0.0519
8	0.0519
9	0.0519

5-10 mg of biomass sample dry weight was weighed in each bead-beater tube in an analytical balance in duplicate. 1 ml of chloroform/methanol/IS mix was added to the sample in the beating tube by using a positive displacement pipette. The bead-beater tubes were placed in the bead-beater for a cycle involving three 60-second cycles at 2500 rpm interspersed with 120-second pauses. This process was carried out twice and

then followed by two 60-second cycles at 2500 rpm interspersed with 120-second pauses.

The solution and the beads were transferred to a fresh 10 ml glass tube. To the bead-beater tubes were added 3 × 1 ml of the chloroform/methanol/C15:0 TAG solution. The mixed liquid was transferred to the glass tubes. The glass tubes with sample were vortexed for five seconds and placed in a sonicator for 10 minutes. 2.5 ml of the Tris NaCl stock solution was added to the samples in the glass tubes. The samples were vortexed for another five seconds and sonicated for 10 minutes. The samples were centrifuged for five minutes at 2500 rpm.

The chloroform phase that was the bottom phase was extracted by using a glass pipette into a new glass tube. 1 ml of chloroform was added to the old glass tube. The tube was vortexed for five seconds, placed in a sonicator bath for 10 minutes and centrifuged for five minutes at 2500 rpm. The chloroform layer at the bottom was collected again with a glass pipette and transferred into the new glass tube. A new pipette was used for each sample.

The Sep-Pak Vac Silica cartridges were placed on the spider (a type of rack for holding tubes), which was a type of rack for tubes, was set up in the fume hood. One column of the spider was used for each sample. Each of the columns was equilibrated with 10 ml of hexane. To the samples, 0.5 ml of hexane-diethylether mixture was added. An empty glass tube was placed beneath the column before the sample with 0.5 mls of hexane-diethylether mixture was added. The glass tube that used to contain the lipid sample was washed with 1 ml of hexane-diethylether and added to the column. Once the entire sample had been loaded, the column was eluted by addition of 10 ml of hexane-diethylether. The liquid containing the TAGs, which dripped from the column,

was collected by glass tubes below. Once all the liquid had been collected a second glass tube was placed beneath the column and the column was eluted with 10 ml of methanol-acetone-hexane solution. The solvents containing the polar lipids and non-polar lipids (TAGs) were evaporated by passing nitrogen gas.

To each of the samples in the glass tubes 3 ml of methanol containing 5 % H_2SO_4 was added. The sample was mixed using a vortex for five seconds and incubated in a block heater or a water bath for three hours at 70 ºC. The samples were cooled to room temperature and 3 ml of water and 3 ml of hexane were added. The samples were then mixed using a vortex for five seconds and placed in a sonicator for 15 minutes. The sampled were centrifuged for five minutes at 2500 rpm.

2 ml of the top phase (hexane) was collected and transferred to a glass tube. To the new tube, 2 ml of water was added to wash the hexane. The sample was again mixed using a vortex for five seconds and centrifuged for five minutes at 2500 rpm. From the hexane phase (top phase) 1 ml of sample was added to a GC vial. The caps of GC vials were capped before the vials were put into the GC and the TAGs and polar lipids profile read.

6.3 Preliminary Experiment Results and Discussion

Before experiments can be conducted, it is necessary to optimise the physico-chemistry of the reactors in terms of CO_2 mass transfer and pH. Other considerations taken into account in the trials were growth in terms of cell number of phototrophic and mixotrophic algae and biochemical measurement. It is important that mass transfer be optimised, pH be stable, algae grow without contamination and biochemical measurement be carried out with precision and accuracy so that the experimental results are valid.

6.3.1 Biochemical Analysis

Biochemical analysis of the continuous cultures of the algae *S. obliquus* was performed at the Wageningen University and Research Centre. Dry weight samples of the algae from trials experiments were used for analysis in a number of trials to determine whether the composition and pigment content could be determined accurately following experimental procedure described earlier.

The results for chlorophyll content as a percentage of total biomass is shown below in Fig. 6.3. The error margin of the measurements is within 5 % of the averaged experimental measurement. This suggests that the proper protocol was able to be followed to measure chlorophyll content. The measured total chlorophyll content is similar to literature measurements of chlorophyll a content, which is reported to vary between 0.7-1.6 % of the total biomass. In our measurements chlorophyll a accounted for at least 90 % of total chlorophyll when compared with chlorophyll b using Eqs 6.8 and 6.9. Therefore, a reasonable agreement between literature and experimental measurement has been obtained. The literature study reported chlorophyll a for a range of phosphorous concentrations from 1-10 mg P/l (M. Chen, Li, Dai, Sun, & Chen, 2011). Chlorophyll a content increased as the initial phosphorus concentration increased. Therefore, the experimentally measured content averaging about 1.62 % would suggest that the algae was cultivated at relatively high phosphorus concentrations, which was the case since phosphorus was not a limiting nutrient.

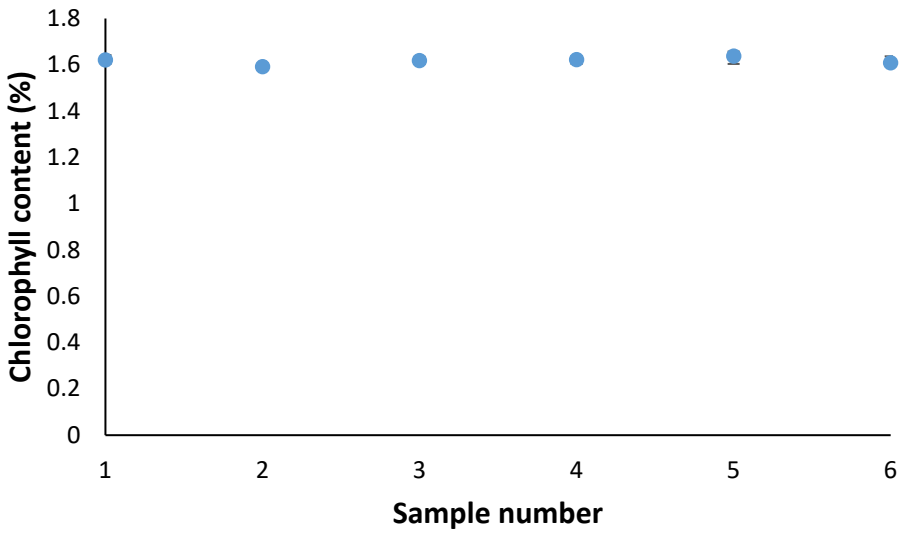

Figure 6.3 Plot of the chlorophyll content as a percentage of total biomass for a number of samples of *S. Obliquus*. The results show a tight fit for chlorophyll measurements for all samples.

The protein content of the algae was measured by comparing with a protein standard curve made from bovine serum. Figure 6.4 shows the protein content for 5 different samples cultivated under the same conditions. Each data point was the average of three measurements. In some cases, the measurements were very precise and the error bars are not visible. The results in Fig. 6.4 show that the protein content for each sample did not vary more than ± 7.5 % suggesting that the experimental procedure was able to be followed and repeated adequately with precision. The protein content of the algae varied from 33-48 % of total biomass. This range is in agreement with literature protein values for *S. obliquus*, which has reported values between 34-55 % (A Toyub, Miah, Habib, & Rahman, 2012; Becker, 2007; González López et al., 2010). The wide variation of protein content in the measured samples is most likely a result of different nitrogen loads fed to the continuous reactor as there was no process control to minimise fluctuations in the nitrate concentration. Lower protein content values suggest a lower

nitrogen load and more carbon fixed into starch and TAGs whilst a higher protein content is reflective of a greater nitrogen load.

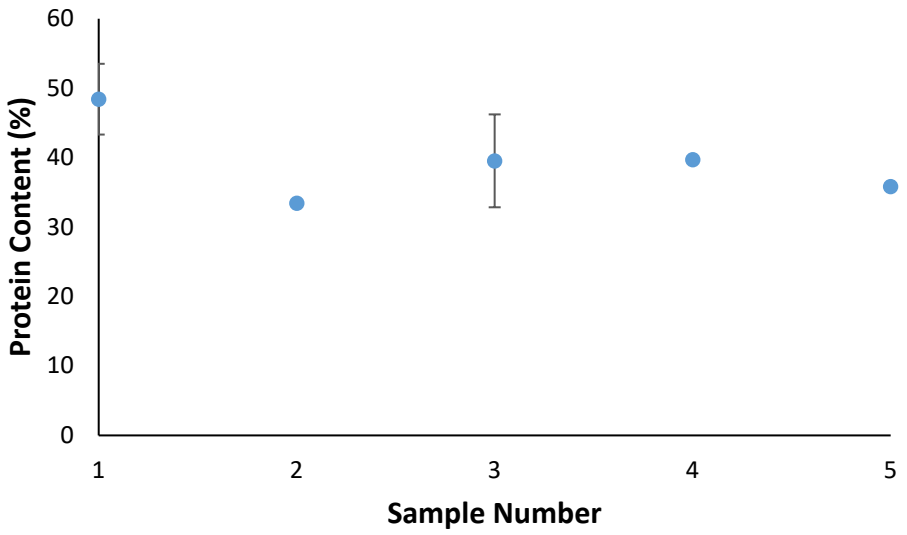

Figure 6.4 Protein content of biomass for a number of samples. The varying protein content amongst sample number is most likely due to different nitrogen loads on the continuous cultures of *S. obliquus*.

Starch content as a percentage of total biomass was measured by extracting starch using ethanol, converting starch to glucose by reaction with amyloglucosidase and then comparing absorption to a glucose standard curve. The starch content in Fig. 6.5 varied from 5-40 % of total biomass. Literature studies report total carbohydrates, of which starch is a major component, between 10-50 % of total biomass (Ho et al., 2017; Khatoon, Rahman, Suleiman, Banerjee, & Bolong Abol-Munafi, 2017) indicating agreement between measured results and literature.

The wide range of starch content in biomass was a result of different operating conditions for the culture, reported in Table 6.3. Samples 1-4 show relatively similar

starch content between 11-14 %, whilst samples 5 and 6 show much lower starch content at 5-6 %. This discrepancy is evident although the nitrogen load was the same at the 0.173 g N/l.d condition. The reason for the divergence was due to the first four samples being cultivated under continuous light and samples 5 and 6 being cultivated under a 12:12 day-night cycle. Interestingly the introduction of a day night cycle reduced the starch content. This may be due to consumption of starch during the dark period as starch can be consumed as an energy source.

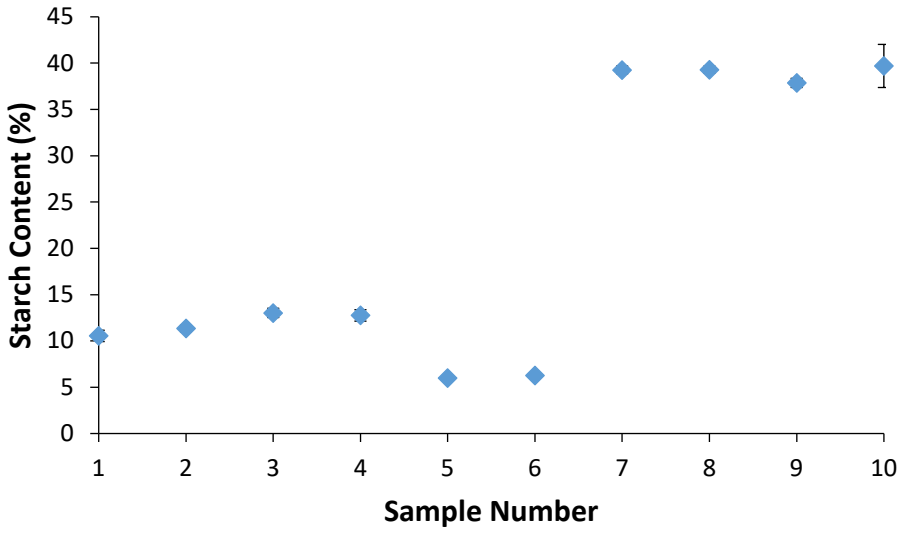

Figure 6.5 Plot of the starch content as a percentage of total biomass for a number of different samples of experimental runs of *S. obliquus*.

Samples 7-10 depict a relatively high starch content at 40-42 %. This is due primarily because of a low nitrogen load, which was 0.0519 g N/l.d, used in samples 1-6. Starch normally has an inverse relationship with nitrogen concentration for many species of algae (Takeshita et al., 2014). Therefore, the greater starch content at lower nitrogen is in agreement with literature.

The final component that was measured was the lipids in terms of TAGs and polar lipids shown below in Fig. 6.6. Both types of lipids were measured with an error margin of at most ± 7.5 %. This confirms that we were able to reliably measure TAGs and polar lipids of *S. obliquus*. Three different nitrogen loads were used for the continuous cultures. They were: 0.1384 g N/l.d for samples 1-3, 0.1038 g N/l.d for samples 4-6 and 0.0519 g N/l.d for samples 7-9. The polar lipids formed a part of the functional biomass modelled in Chapters 4 and 5 and was assumed constant. From Fig. 6.6 the polar lipids content of *S. obliquus* remained constant regardless of nitrogen load suggesting the underlying assumption of the model is sound. However, the TAGs showed variability of content as a function of nitrogen load. For samples collected from the same nitrogen load there was much less variation ranging from as a little as ± 2 % for 0.1384 g N/l.d and 0.1038 g N/l.d nitrogen load runs up to ± 10 % for the 0.0519 g N/l.d runs.

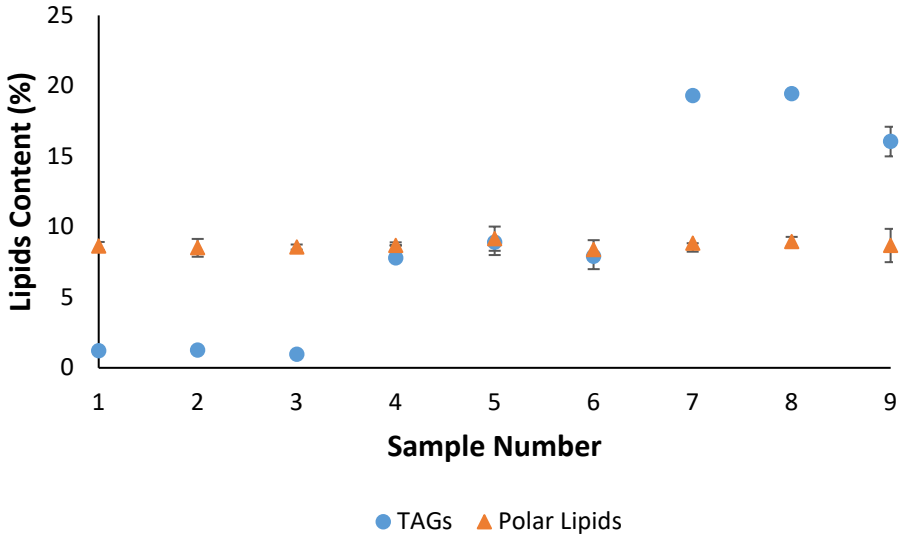

Figure 6.6 Plot of the TAGs and polar lipids of *S. obliquus*. Run number 1-3 was for 0.1384 g N/l.d nitrogen load, runs 4-6 for 0.1038 g N/l.d nitrogen load and runs 7-9 for 0.0519 g N/l.d nitrogen load.

TAGs content was 2 % for a nitrogen load 0.1384 g N/l.d, 8-9 % for a nitrogen load of 0.1038 g N/l.d and 16-20 % for the 0.0519 g N/l.d load runs. The accumulation of TAGs during lower nitrogen loads is well documented across a range of studies (Adesanya et al., 2014; Takeshita et al., 2014) so the inverse relationship between TAGs and nitrogen load is expected. This further supports the observation that the experimental measurements were carried out appropriately.

6.3.2 Batch Model Predictions for 500 µmols/m^2.s and 0 g N/m^3

The samples that were measured for biochemical analysis were grown under 500 µmols/m^2.s of light at various nitrogen loads for continuous reactors. Batch model predictions were simulated and shown below in Fig. 6.7 using the model of Chapter 5.

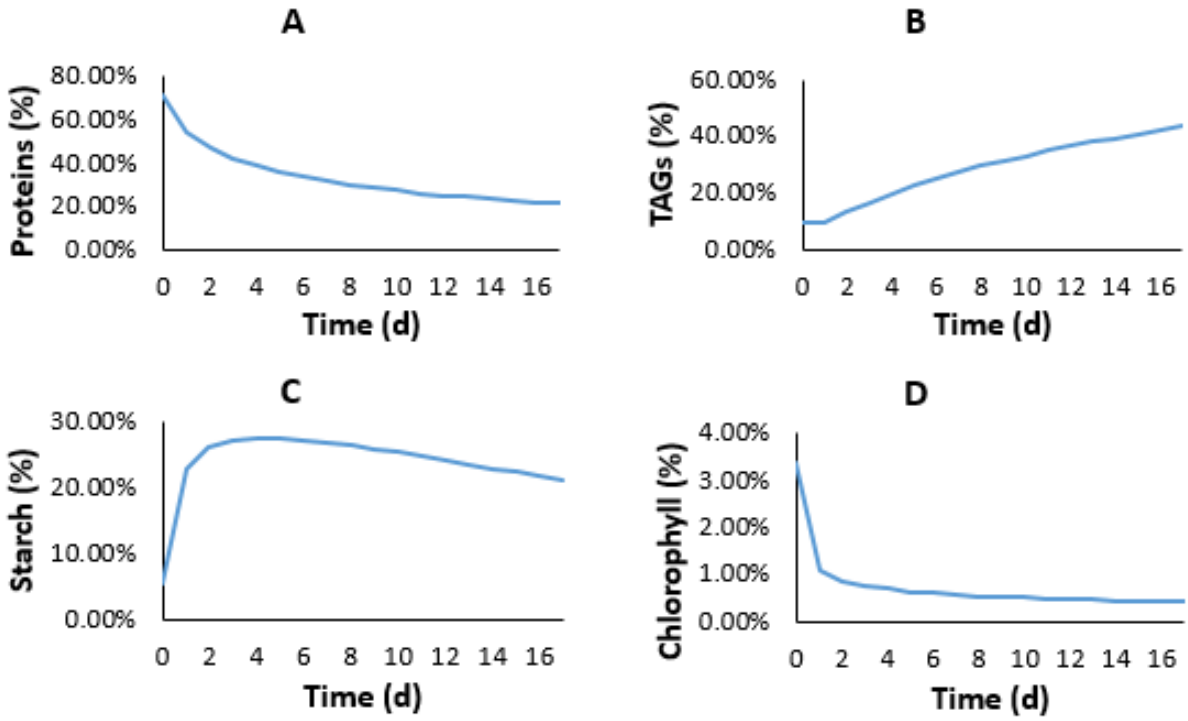

Figure 6.7 starch, TAGs, proteins and chlorophyll content as a percentage of total biomass for a light flux of 500 µmols/m^2.s and initial nitrogen concentration of 0 g N/m^3. The results correspond to *S. Obliquus*.

Although different reactor configurations have been used in sections 6.3.1 and 6.3.2 some comparisons can be made since the values of starch, TAGs, proteins and chlorophyll in Figs 6.3-6.7 are within the same range of values. This agreement between continuous reactors and batch reactors may be due to cellular nitrogen status governing composition and pigment kinetics independent of reactor configuration. As cellular nitrogen status, or nitrogen quota, is depleted in the batch cultures its value transitions from values found under high nitrogen load continuous cultures to low nitrogen load continuous cultures.

The protein content prediction under batch conditions was estimated by subtracting polar lipids content (8.5 %) and cell wall mass (5 %) from functional biomass percentage. Protein content for the continuous cultures varied from 33-48 % in Fig. 6.4. This protein value coincides with protein content on days 2 (~50 % protein) and day 6 (~33 % protein) in the batch cultures. Starch content varied from 10-12 % of total biomass under continuous cultures for samples 1-4, which coincided with starch content within the first day of the batch culture prediction. Samples 7-10 depicted starch content of 40 %, which was more than the maximum starch content of 28 % reached for the batch cultures. The deviation suggests that the some starch production may be reactor configuration dependent.

TAGs content varied from 2 % for samples 1-3, 8-9 % for samples 4-6 to 17-20 % for samples 7-10. The results of samples 1-3 were lower than the lowest recorded TAGs content in the batch cultures by 4 % on day 0. The values for samples 4-6 in the continuous reactors coincided with TAGs values from days 0-1 in the batch cultures. The values of samples 7-10 in the continuous cultures coincided with TAGs values on days 4-6 of the batch cultures. In general, the values of TAGs between continuous

reactors and batch cultures agreed well. However, the model predicted that higher TAGs content could be attained, meaning that lower nitrogen loads in continuous cultures could theoretically be used to obtain a higher TAGs content.

The chlorophyll content measured for the continuous cultures correlated with a batch chlorophyll content found in day 1. This suggests that the cells were relatively replete in nitrogen in the continuous culture samples. Chlorophyll content could be reduced much further depending on cellular nitrogen status, which coincided with increasing starch and TAGs content. Overall, the batch studies suggest that TAGs content could be increased in the continuous culture reactors by reducing nitrogen load further. Whether or not this will increase overall TAGs productivity, is a matter for further research. For instance, a study (Benvenuti et al., 2016) on TAGs productivity (g T/m^2 d) in batch and semi-continuous reactors found that the batch reactor outperformed the semi-continuous reactor by producing 0.97–2.46 g T/m^2.d, compared with only 0.35-0.85 g T/m^2.d. The higher TAGs productivity in the batch reactors was due in part due to the higher TAGs content (15-25 %) compared with only 10-13 % for the semi continuous reactors. The lower TAGs content of the continuous reactors was because of the relatively high nitrogen load of the semi continuous reactors and, thus, the inhibition TAGs synthesis. Therefore, future work may investigate TAGs productivity of continuous or semi continuous reactors at lower nitrogen loads.

6.3.3 Bioreactor Mass Transfer Optimisation

The algal cell density was measured as a function of gas flow rate with 2 % (v/v) CO_2. Two CO_2 flow rates were tested, 0.4 and 0.6 LPM. The results are illustrated below in Fig. 6.8 in triplicate showing little difference in cell density between the two flow rates.

This suggests that the mass flow of CO_2 had been optimised and was not limiting the growth of the algae.

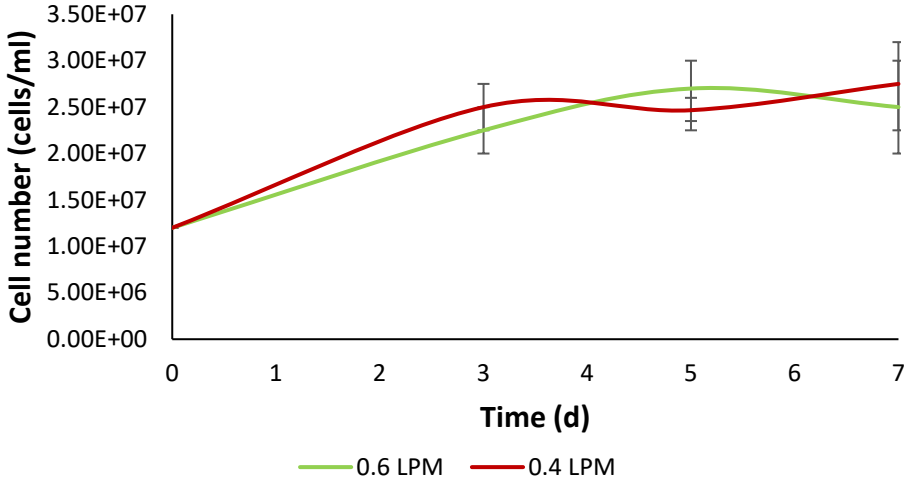

Figure 6.8 Comparison of the effect of gas flow rate on algal growth *N. oculata*. Approximately 2 % CO_2 (v/v) enriched air was passed through the cultures. The total flow rate was 0.6 LPM for reactors 1-3 and 0.4 LPM for reactors 4-6.

6.3.4 pH Measurement of the Cultures

The pH of the cultures was measured by a pH metre for every sample obtained depicted in Fig. 6.9. Two different flow rates of CO_2 were tested at 0.4 and 0.6 LPM. There was no difference in pH between the two flow rates and the pH was stable, within the timescale of the measurements. This pH is typical of estuarine water which ranges from 7.5-10 (Howland, Tappin, Uncles, Plummer, & Bloomer, 2000).

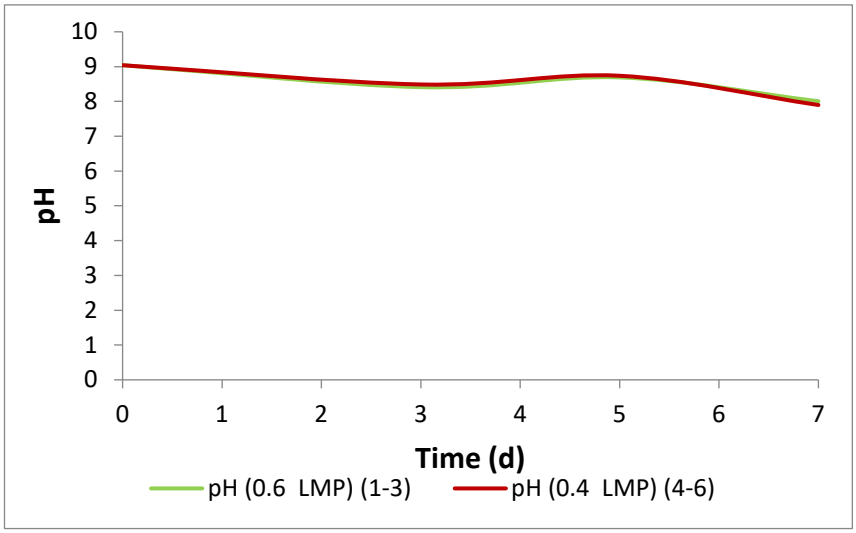

Figure 6.9 The pH of the photosynthetic cultures of *N. oculata* operating at 0.4 and 0.6 LMP did not change significantly.

6.3.5 Phototrophic and Mixotrophic Culture Trials

To determine whether microalgae could be grown under mixotrophic conditions at higher yields a series of trial experiments were conducted. The primary objective was to grow mixotrophic algae without bacterial contamination illustrated for mixotrophic *N. oculata* against a photosynthetic control shown below in Fig. 6.10.

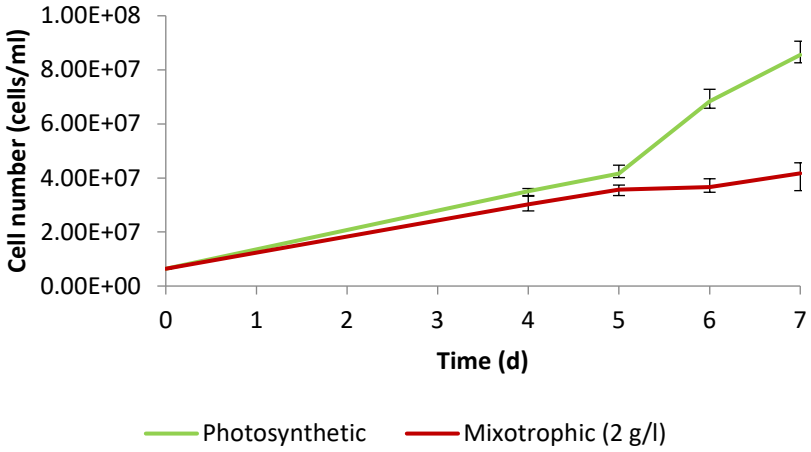

Figure 6.10 Growth of *N. Oculata* on 2 g/l glucose added from day 0 for three of the reactors. The culture where glucose was added had half the cell number yield after 7 days.

In the preliminary trials mixotrophic *N. oculata* had half the cell density of the phototrophic control after 7 days. The stationary phase in the mixotrophic culture was reached at day 5 whilst the control continued growing in the exponential phase for the duration of the experiment. Bacterial contamination of rod like bacteria was observed in mixotrophic cultures from day 4 whilst the phototrophic control was free of contamination. These results contrast with the literature, which demonstrated that *N. oculata* grew faster when glucose at 0.1 g/l was added in comparison to photosynthetic controls without contamination (Pagnanelli, Altimari, Trabucco, & Toro, 2014). Cell number for the literature study was 4.9×10^6 cells/ml for mixotrophic cultures after six days when 170 g N/m^3 was added. In comparison photosynthetic cultures were 25 % lower at 4×10^6 cells/ml after six days. It could not be determined what species of bacteria had contaminated the culture to yield our results.

Due to bacterial contamination, another trial on *T. chuii* was performed in triplicate with results depicted below in Fig. 6.11. The light was now provided 24 hours a day without the use of timers.

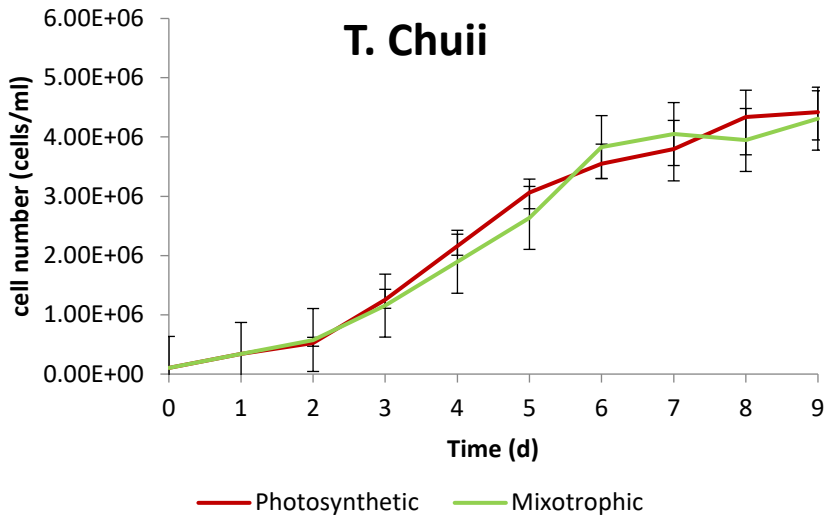

Figure 6.11 Comparison of photosynthetic and mixotrophic *T. Chuii* under the effect of 0 and 3 g/l of glucose in triplicate. There was no significant difference in algal growth as a function of glucose load.

Phototrophic and mixotrophic modes were within error of one another indicating that the addition of glucose did not have any net benefit on yield. Contamination was also present in mixotrophic cultures, which suggests that bacteria consumed the glucose in the place of algae. Contamination of mixotrophic cultures was found in other trials for *Chaetoceros muelleri* and *Pavlova* sp., which is shown in the Appendix. A literature study of *T. chuii* found that photosynthetic cultures had a much lower optical density, hence biomass yield, than mixotrophic cultures depending on carbon to nitrogen ratio for a glucose feed. For instance a mixotrophic culture with a carbon to nitrogen ratio of 4 had an optical density of 0.9 after 30 days whilst the optical density for a photosynthetic culture was only 0.3 (Lu, Wang, Yang, Zhu, & Pan, 2017).

Experimental studies (J. Han et al., 2016) on the co-culturing of bacteria and algae found that bacterial concentrations actually decreased with time when grown under mixotrophic conditions for two species of algae: *T. chuii* and *Nannochloropsis gaditana*. The bacterial species cultured were two strains of *Muricauda* sp. It was found that the bacterial concentration of the strain Mur1 decreased from 155-20 $\times 10^6$ CFU/ml

by the end of the 33-day experiment although this minimum was reached after 9 days when co-cultured with *T. chuii*. Similarly, for *N. gaditana* the cell concentration of Mur1 decreased from 155-40 $\times 10^6$ CFU/ml by the end of day nine and stayed constant thereafter. Algal densities meanwhile increased from 300-1000 $\times 10^6$ cells/ml in 33 days for *T. chuii*. This was twice as a high as the control where *T. chuii* was cultivated mixotrophically without co-culturing with bacteria. However, for the case of *N. gaditana* the algal cell density decreased from 2000-0 $\times 10^6$ cells/ml in 9 days. In contrast the control showed cell count increasing to 2200 $\times 10^6$ cells/ml in 9 days. Thus, for the case of *N. gaditana* there was inhibition of algal growth when bacteria was present, whilst *T. chuii* exhibited synergistic growth (J. Han et al., 2016).

In our work *T. chuii* grew at the same rates under mixotrophic and photosynthetic conditions whilst *N. oculata* was inhibited like the case of *N. gaditana*. It would seem unlikely that the mixotrophic cultures of *T. chuii* and *N. oculata* were not taking up the glucose because there is literature evidence of both species being capable of mixotrophic growth (Lu et al., 2017; Pagnanelli et al., 2014). Furthermore, for photosynthetic cultures we did not observe bacterial proliferation indicating that the glucose was the key variable, which promoted their growth. For the case of *N. oculata* the bacteria may have been excreting metabolites, which inhibited algal growth similar to the case of *N. gaditana* whilst *T. chuii* was unaffected by bacterial metabolite excretion. We ensured that strict protocol was followed when culturing algae to limit contamination, but found that our efforts could not yield aseptic culturing of mixotrophic algae. This problem was also evidenced by researchers at the Wageningen University and Research Centre when they cultured mixotrophic algae. Thus, even with proper facility, bacterial contamination has been a major issue on more than one occasion.

The scope of the experiments after the trials was to model aseptic mixotrophic growth of algae. However, since bacteria had contaminated the mixotrophic cultures this was not possible. Therefore, this data was not further analysed for nitrates, starch, glucose, chlorophyll, or total dry weight biomass. Thus, due to widespread bacterial contamination of mixotrophic cultures of trials the experiments were halted and no further work on this chapter was performed. Future studies may attempt to grow algae using acetate rather than glucose, which is known to inhibit bacterial growth under elevated concentrations (Pinhal, Ropers, Geiselmann, & de Jong, 2019).

6.3.6 Comparison between Experimental and Model Prediction for Biomass Yield

The yields of *N. oculata* and *T. chuii* were compared with *C. vulgaris* at 25 g N/m^3 and 150 µmols/m^2.s, shown below in Fig. 6.12. The cell number of *N. oculata* and *T. chuii* were converted to biomass weight by multiplying by their respective cell masses (Hu, 2014).

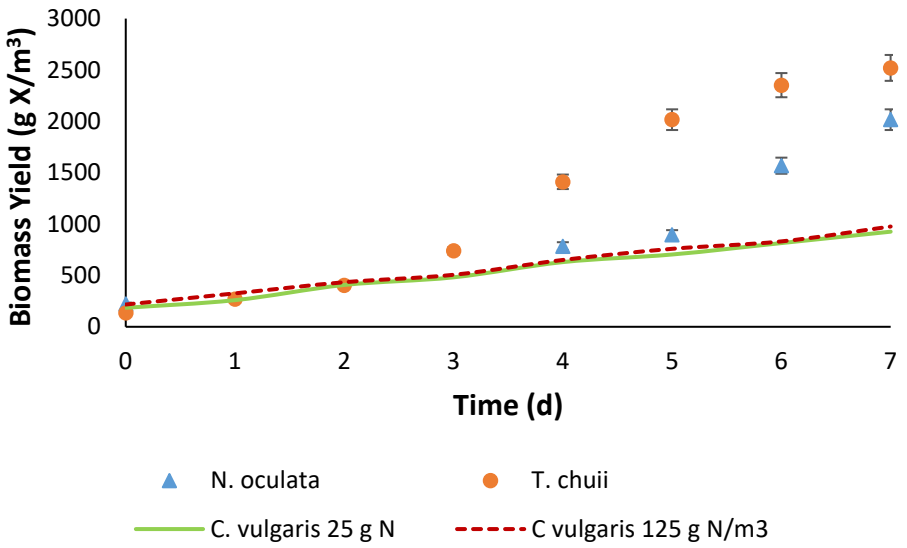

Figure 6.12 Comparison of the photosynthetic yield of *N. oculata* (triangles), *T. chuii* (circles) experiments with modelling for *C. vulgaris* at 25 g N/m^3 (solid line) and *C. vulgaris* at 125 g N/m^3 (dotted line).

The experimental measurements of the *N. oculata* and the *T. chuii* in Fig. 6.12 are shown for a nitrogen load of 50 g N/m^3.d, whilst the two *C. vulgaris* cultures are simulated model plots at 25 g N/m^3 and 125 g N/m^3. The *N. oculata* and the *T. chuii* were grown under a light intensity of approximately 300 µmols/m^2.s whilst the *C. vulgaris* was grown under a light intensity of 150 µmols/m^2.s. Thus, the greater yields after day three for *N. oculata* and the *T. chuii* can be explained by an increased light flux relative to *C. vulgaris* and nitrogen load. Interestingly, whilst a clear exponential phase is evident for both *N. oculata* and the *T. chuii* the *C. vulgaris* does not show such a phase. Instead, it increased almost linearly. There was also little difference in yield between 25 g N/m^3 and 125 g N/m^3 indicating that nitrogen quota depletion had not affected biomass kinetics yet. In contrast, *T. chuii* appears to be approaching the stationary phase by day 7 suggesting that nitrogen quota had been almost completely depleted.

6.4 Conclusion and Recommendations

Biochemical measurement trials of *S. obliquus* for chlorophyll, starch, TAGs and protein demonstrated that experimental procedure could be followed and measurements could be taken with a high degree of precision. The measurements were also deemed accurate, because of agreement with the literature values found for *S. obliquus*. It was also found that the polar lipids fractions was relatively constant, which was assumed in the model developed in Chapter 2 and implemented in Chapters 4 and 5. Comparison between the measurements made for continuous reactors and batch predictions indicated that TAGs content could be increased further. Future work could investigate whether reducing nitrogen load in continuous reactors could increase TAGs productivity.

Trial experiments on *N. oculata* and *T. chuii* were conducted, where algae were grown under photosynthetic and mixotrophic conditions with glucose as the organic carbon source. Bacterial inhibition was observed in both cases during cell counting by rod like bacteria. The bacteria severely inhibited *N. oculata* growth whilst the effect on *T. chuii* was less noticeable. Bacterial contamination was not observed for the photosynthetic cultures. Literature experiments indicated that both species could be grown mixotrophically using glucose as a substrate without bacterial contamination. It was also found that bacteria could have an either synergistic or inhibitory effect on algal growth depending on bacterial species. Future studies could use acetate as a potential source of organic carbon for algae since it is known to inhibit the growth of bacteria.

7 Conclusion and Recommendations

In this thesis, a composition model able to independently simulate starch, TAGs and functional biomass was developed. The model was based on the simulation of six state variables and 16-18 biological parameters. In addition, a starch glycolysis path was considered as part of the kinetics model.

As a first step, a literature review on algal composition models was performed and reported in Chapter 2. In general, it was found that composition models were made of two parts: A nutrient kinetic process and carbon partitioning process between component fractions. Carbon uptake in phototrophic algae was modelled as a function of light and based on either a Monod kinetic model or a Poisson's model. However, heterotrophic algal, carbon uptake was defined using Monod kinetics or variants of this kinetic expression. Nitrogen was also included in composition models as a rate limiting micronutrient modelled using Monod kinetics or the Droop cell quota kinetic model. The Droop cell quota model built on extracellular nitrogen limitation by including internal storage of nitrogen as a balance between extracellular uptake and consumption.

The review of the composition models also show that algae composition can be simulated in terms of two fractions being TAGs and functional biomass. There was a scarcity of literature that simulated algal kinetics based on the three primary fractions as a whole being starch, TAGs and functional biomass, especially for batch photosynthetic studies. Furthermore, there has been little work on the interrelation of composition kinetics between TAGs and starch. This point was used as the premise of Chapter 4 and Chapter 5.

When fitting parameters to simulate algal composition kinetics, the most common method is to minimise an objective function and use sum squared regression analysis.

Weighting factors can be incorporated as a product of each sum squared difference to show the effect of experimental measurement error on regression. Alternatively, the objective function may be defined as a relative sum error converted into a percentage. This shows the average percentage difference between measured and simulated values of state variables. The advantage of this approach is that it eliminates any bias for minimising large magnitude variables in preference for small magnitude variables. Next, parameter constraints may be imposed based on theoretically determined yield coefficients from carbon into TAGs, starch or functional biomass. Other theoretical parameter constraints determined in the review were for maximum nitrogen quota, maximum photosynthetic rate and photosynthetic quantum yield. Initial guesses for biological parameter values could be determined from literature parameter values. Literature parameter values of other models act as a further validation check to ensure that tuned parameter values are realistic.

The theoretical development of the model was described in Chapter 3. The model was comprised of six state variables being nitrogen concentration, nitrogen quota, chlorophyll content, starch, TAGs and functional biomass. The total biomass was also modelled as the sum of the intracellular components. The state variables were solved as a series of coupled ordinary differential equations. The state variables themselves were a function of a number of secondary equations such as cell division rate, rate of extracellular nitrogen uptake, photosynthetic fixation rate, average culture light intensity, starch glycolysis rate, TAGs synthesis from photosynthetic carbon fixation and starch synthesis from photosynthetic carbon fixation. The model was a function of at least 14 parameters, which were solved by minimising an objective function. The objective function was the average percentage error between model prediction and experimental measurement. Finding the parameter set that gave the minimum error

involved using literature values as initial parameter estimates. A multiplier factor that allowed the variation of the initial estimates was considered. The multiplier factor was varied using a multiplier step of 0.15. The minimisation of the error was repeated 11 times. The set of parameters that produced the minimum error in the 11 runs was used for a second group of iterations using a smaller multiplier step of 0.05. This process effectively reduced the final error of the model.

In Chapter 4 the starch, TAGs and functional biomass kinetics was simulated as a function of an incident light flux of 150 µmols/m^2.s and initial nitrogen concentration of 25 g N/m^3 and 125 g N/m^3 from literature experimental data (Adesanya et al., 2014). The hypothesis of two distinct sources of carbon for TAGs production, from starch glycolysis and direct photosynthetic carbon conversion, regulated by photosynthetic activity and nitrogen quota is valid for this particular growth mode, light intensity and range of initial nitrogen concentration. The AIC weight suggests that a system regulated by photosynthetic activity and nitrogen quota had a 40-55 % chance out of four candidate cases to be the most accurate model in predicting composition kinetics for both nitrogen conditions.

Saturation kinetics and C-N uptake did not have a significant impact on kinetics between days 0-21. Starch concentration and bulk nitrogen concentration were two substrate specific regulators also found to be unimportant in dictating algal kinetics. In this study, it was found that nitrogen quota is dominant in regulating composition during nitrogen depletion with photosynthetic activity being important during periods of higher light intensity and nutrient replete conditions.

Composition kinetics was found to follow two distinct phases for 25 g N/m^3 and

125 g N/m^3, before and after nitrogen depletion. Since intracellular nitrogen quota was constant before nitrogen depletion composition kinetics was primarily regulated by photosynthetic activity, which favoured carbon towards starch and functional biomass. After depletion, carbon partitioning favoured TAGs formation over starch and functional biomass. This was because nitrogen quota was now decreasing in content suggesting nitrogen quota dominated composition kinetics.

When testing model limitations, by extending simulation time to 150 days, the minimum and maximum content of starch and TAGs, and starch content became important regulatory factors. However, it was also likely that catabolism of starch and TAGs was also occurring in the late stationary phase or substrate content limitation.

In Chapter 5, a model for photosynthetic algal growth was applied to *S. obliquus* for a nitrogen load of 0 g/m^3 as a function of two different light intensities: 200 µmols/m^2.s and 1000 µmols/m^2.s. The model fitted the experimental data well for most variables except for starch in the case of 1000 µmols/m^2.s. Starch synthesis was modelled as lower than expected due to the model not accounting for catabolism of TAGs under the higher light flux. This factor was perceived as affecting the high light intensity case since algal kinetics progressed faster, or the culture aged quicker under higher light intensities resulting in a the cells reaching the necessary conditions for component catabolism for energy.

The starch and storage molecule ratio comparison between the two light fluxes showed that higher light intensities upregulated the production of starch initially, but that the ratio of starch to storage molecule between the two experiments converged as time progressed. Therefore, in the nitrogen depleted phase there was no difference in preference for starch. When carbon fluxes were compared between the two experiments

it was found that starch glycolysis was light dependant and was activated during extended periods of nitrogen deprivation. The glycolytic flux peaked at 95 g C/m^3.d for 1000 µmols/m^2.s, which was greater than the 50 g/m^3.d peak at 200 µmols/m^2.s. Functional biomass was found to be initially dependent on light flux with higher light intensities favouring functional biomass synthesis, but carbon fluxes towards functional biomass synthesis converged between the two experiments as time progressed. The model also showed that photosynthetic carbon-to-starch yielded light dependent results. According to the model predictions, higher light intensities reduced the carbon flux from photosynthesis to starch. However, it was also shown that starch was underpredicted by the model for this light intensity. Thus, the carbon flux should have been higher for 1000 µmols/m^2.s. Since starch concentration as a fraction of total storage molecule was higher at 1000 µmols/m^2.s it would be expected that the carbon flux towards starch from photosynthesis would be greater than for 200 µmols/m^2.s. Light did not have a significant impact on the photosynthetic carbon flux to TAGs.

In Chapter 6, trial experiments were conducted at PSFI for green algae *N. oculata*. and *T. chuii*. Mixotrophic *N. oculata* were half the cell number at the end of the 7-day trial experiment in comparison to the photosynthetic control. This was due to bacterial contamination of the culture. When a trial run of *T. Chuii* was conducted, the same issue of contamination was found. These results were in contrast to literature studies, which demonstrated that these algae could grow mixotrophically at increased growth rates. However, according to the literature when co-cultured with bacteria it was shown that the bacteria could have either synergistic or negative effects on algal concentration depending on species. In our case, bacteria had a negative effect for *N. oculata* and little effect on *T. chuii*. Furthermore, as bacteria-algae interactions were beyond the scope of this study the experiments were not continued. Although we were not successful in

cultivating algae, it was demonstrated that the biochemical composition of algae could be measured for chlorophyll, TAGs, starch and proteins (the major component of functional biomass). These are all outputs of the model developed in Chapter 3 and required to be measured for validation.

Future studies should determine whether it is substrate catabolism or maximum TAGs and starch content dictating composition kinetics in the late stationary phase. Other model limitations that may be the subject of future studies are nitrogen excretion from biomass and the effect it has on acclimation and impact of different light intensities in the photo-inhibitory region on composition kinetics. Future studies may also attempt to validate this model for species other than green algae or for different growth modes such as heterotrophy or mixotrophy. It is recommended that further efforts be taken on finding a suitable organic carbon substrate that algae incorporates in preference to bacteria if validating the model for heterotrophic and mixotrophic cultures. Acetate may be one such organic carbon source that may be used as it is a known substance for algal growth and bacterial inhibition at elevated concentrations.

Now that a composition kinetic model for starch, TAGs and functional biomass has been developed, it may be integrated with a physicochemical model of CO_2, O_2 and pH. The focus of integration with physicochemical variables would be on optimising mass transfer and minimisation of oxygen inhibition in tubular photobioreactors. In such reactors, the CO_2 concentration becomes limited as the tube length increases limiting growth whilst the oxygen concentration increase inhibiting growth. The purpose of such integration between composition kinetic and physicochemical models would be to validate pilot scale studies.

The model may even be applied to techno-economic analysis. Since a model for the composition of algae in terms of its major metabolites has been developed, the model may be optimised for a particular fraction or maximised for greatest profit. Most techno-economic models assume constant values for algae metabolites, but it is clear from our research that composition is dynamic and varies with fluctuations in light and nitrogen. Although nitrogen can be controlled, somewhat light flux is variable and is known to change the accumulation of starch and TAGs, respectively.

Since internal metabolites, such as starch and TAGs accumulate at nitrogen depletion a two stage culturing approach may be implemented composed of a growth phase and metabolite accumulation phase, which may be optimised for either starch or TAGs accumulation. Although there have been studies, which investigate this type of culturing they have not been validated by modelling, which could potentially optimise the system. Finally, the composition model could be applied to different temperatures as temperature fluctuates greatly due to seasonal variability and may affect yield of different components.

8 References

Aaronson, S. (1973). Effect of Incubation Temperature on the Macromolecular and Lipid Content of the Phytoflagellate *Ochromonas Danica*. *Journal of Phycology, 9*, 111-113.

Adams, C., Godfrey, V., Wahlen, B., Seefeldt, L., & Bugbee, B. (2013). Understanding precision nitrogen stress to optimize the growth and lipid content tradeoff in oleaginous green microalgae. *Bioresource Technology, 131*, 188-194.

Adesanya, V. O., Davey, M. P., Scott, S. A., & Smith, A. G. (2014). Kinetic modelling of growth and storage molecule production in microalgae under mixotrophic and autotrophic conditions. *Bioresource Technology, 157*, 293-304.

Ajayan, K., Selvaraju, M., & Thirugnanamoorthy, K. (2012). Enrichment of chlorophyll and phycobiliproteins in Spirulina platensis by the use of reflector light and nitrogen sources: An in-vitro study. *Biomass and Bioenergy, 47*, 436-441.

Anning, T., MacIntyre, H. L., Pratt, S. M., Sammes, P. J., Gibb, S., & Geider, R. (2000). Photoacclimation in the marine diatom Skeletonema costatum. *Limnol. Oceanographer*, *45*.

Arhonditsis, G. B., & Brett, M. T. (2005). Eutrophication model for Lake Washington (USA): Part I. Model description and sensitivity analysis. *Ecological Modelling, 187*, 140-178.Atkinson, D., Ciotti, B. J., & Montagnes, D. J. S. (2003). Protists decrease in size linearly with temperature. *Proceedings of the Royal Society of London. Series B: Biological Sciences, 270*, 2605-2611.

Atta, M., Idris, A., Bukhari, A., & Wahidin, S. (2013). Intensity of blue LED light: A potential stimulus for biomass and lipid content in fresh water microalgae Chlorella vulgaris. *Bioresource Technology, 148*, 373-378.

Babin, M., Morel, A., H., C., Bricaud, A., Kolber, Z., & Falkowski, P. G. (1996). Nitrogen- and irradiancedependent variations of the maximum quantum yield of carbon fixation in

eutrophic, mesotrophic and oligotrophic marine systems *Deep Sea Research I, 43*, 1241-1272.

Baker, N. R., & Bowyer, J. R. (1994). *Photoinhibition of photosynthesis from molecular mechanisms to the field*. In N. R. B. a. J. R.Bowyer (Ed.), *BIOS Scientific Publishers*.

Baroukh, C., Muñoz-Tamayo, R., Steyer, J.-P., & Bernard, O. (2014). DRUM: A New Framework for Metabolic Modeling under Non-Balanced Growth. Application to the Carbon Metabolism of Unicellular Microalgae. *PloS one, 9*,

Baroukh, C., Turon, V., & Bernard, O. (2017). Dynamic metabolic modeling of heterotrophic and mixotrophic microalgal growth on fermentative wastes. *PLoS computational biology, 13*.

Becker, E. W. (2007). Micro-algae as a source of protein. *Biotechnology Advances, 25*, 207-210.

Behrenfeld, M., Prasil, O., Babin, M., & Bruyant, F. (2004). In search of a physiological basis for covariation in light-limited and light saturated photosynthesis. *Journal of Phycology, 40*, 4-25.

Benvenuti, G., Bosma, R., Ji, F., Lamers, P., Barbosa, M. J., & Wijffels, R. H. (2016). Batch and semi-continuous microalgal TAG production in lab-scale and outdoor photobioreactors. *Journal of Applied Phycology, 28*, 3167-3177.

Berges, J. A., Charlebois, D. O., Mauzerall, D. C., & Falkowski, P. G. (1996). Differential Effects of Nitrogen Limitation on Photosynthetic Efficiency of Photosystems I and II in Microalgae. *Plant Physiology, 110*, 689-696.

Berges, John & R. Mulholland, M. (2008). Enzymes and nitrogen cycling.

Bernacchi, C., Singsaas, E., Pimentel, C., Portis Jr, A., & Long, S. (2001). Improved temperature response functions for models of Rubisco-limited photosynthesis. *Plant, Cell & Environment, 24*, 253-259.

Bernard, O., Sciandra, A., & Sallet, G. (2001). A non-linear software sensor to monitor the internal nitrogen quota of phytoplanktonic cells. *Oceanologica Acta, 24*, 435-442.

Bhatnagar, A., Chinnasamy, S., Singh, M., & Das, K. C. (2011). Renewable biomass production by mixotrophic algae in the presence of various carbon sources and wastewaters. *Applied Energy, 88*, 3425-3431. doi:http://dx.doi.org/10.1016/j.apenergy.2010.12.064

Bhola, V., Desikan, R., Santosh, S. K., Subburamu, K., Sanniyasi, E., & Bux, F. (2011). Effects of parameters affecting biomass yield and thermal behaviour of Chlorella vulgaris. *Journal of Bioscience and Bioengineering, 111*, 377-382.

Biller, P., & Ross, A. B. (2014). Pyrolysis GC–MS as a novel analysis technique to determine the biochemical composition of microalgae. *Algal Research, 6*, 91-97.

Blache, U., Jakob, T., Su, W., & Wilhelm, C. (2011). The impact of cell-specific absorption properties on the correlation of electron transport rates measured by chlorophyll fluorescence and photosynthetic oxygen production in planktonic algae. *Plant Physiology and Biochemistry, 49*, 801-808.

Boussiba, S., Vonshak, A., Cohen, Z., Avissar, Y., & Richmond, A. (1987). Lipid and biomass production by the halotolerant microalga Nannochloropsis salina. *Biomass, 12*, 37-47.

Bozell, J. J., & Petersen, G. R. (2010). Technology development for the production of biobased products from biorefinery carbohydrates—the US Department of Energy's "top 10" revisited. *Green Chemistry, 12*, 539-554.

Breuer, G., Lamers, P. P., Martens, D. E., Draaisma, R. B., & Wijffels, R. H. (2012). The impact of nitrogen starvation on the dynamics of triacylglycerol accumulation in nine microalgae strains. *Bioresource Technology, 124*, 217-226.

Breuer, G., Lamers, P. P., Martens, D. E., Draaisma, R. B., & Wijffels, R. H. (2013). Effect of light intensity, pH, and temperature on triacylglycerol (TAG) accumulation induced by nitrogen starvation in Scenedesmus obliquus. *Bioresource Technology, 143*, 1-9.

Breuer, G., Martens, D. E., Draaisma, R. B., Wijffels, R. H., & Lamers, P. P. (2015). Photosynthetic efficiency and carbon partitioning in nitrogen-starved Scenedesmus obliquus. *Algal Research, 9*, 254-262.

Burnham, K. P., & Anderson, D. R. (2002). *Model Selection and Multimodel Inference: a practical information-theoretic approach* (2nd ed.). New York: Springer-Verlag.

Cao, J., Yuan, H., Li, B., & Yang, J. (2014). Significance evaluation of the effects of environmental factors on the lipid accumulation of Chlorella minutissima UTEX 2341 under low-nutrition heterotrophic condition. *Bioresource Technology, 152*, 177-184.

Celia Y. Chen, & Durbin, E. G. (1994). Effects of pH on the growth and carbon uptake of marine phytoplankton *Mar. Ecol. Prog. Ser., 109*, 83-94.

Cheirsilp, B., & Torpee, S. (2012). Enhanced growth and lipid production of microalgae under mixotrophic culture condition: Effect of light intensity, glucose concentration and fed-batch cultivation. *Bioresource Technology, 110*, 510-516.

Chen, C. Y., & Durbin, E. G. (1994). Effects of pH on the growth and carbon uptake of marine phytoplankton. *Marine Ecology-Progress Series, 109*, 83-83.

Chen, M., Li, J., Dai, X., Sun, Y., & Chen, F. (2011). Effect of phosphorus and temperature on chlorophyll a contents and cell sizes of Scenedesmus obliquus and Microcystis aeruginosa. *Limnology, 12*(2), 187-192.

Chen, T., Liu, J., Guo, B., Ma, X., Sun, P., Liu, B., & Chen, F. (2015). Light attenuates lipid accumulation while enhancing cell proliferation and starch synthesis in the glucose-fed oleaginous microalga Chlorella zofingiensis. *Scientific Reports, 5*, 14936.

Chen, Y., & Vaidyanathan, S. (2103). Simultaneous assay of pigments, carbohydrates, proteins and lipids in microalgae. *Analytica Chimica Acta, 776*, 31–40.

Chia, M. A., Lombardi, A. T., da Graça Gama Melão, M., & Parrish, C. C. (2015). Combined nitrogen limitation and cadmium stress stimulate total carbohydrates, lipids, protein and amino acid accumulation in Chlorella vulgaris (Trebouxiophyceae). *Aquatic Toxicology, 160*, 87-95.

Chinnasamy, S., Ramakrishnan, B., Bhatnagar, A., & Das, K. (2009). Biomass production potential of a wastewater alga Chlorella vulgaris ARC 1 under elevated levels of CO2 and temperature. *International Journal of Molecular Sciences, 10*, 518-532.

Choi, Y.-K., Kumaran, R. S., Jeon, H. J., Song, H.-J., Yang, Y.-H., Lee, S. H., . . . Kim, H. J. (2015). LED light stress induced biomass and fatty acid production in microalgal biosystem, Acutodesmus obliquus. *Spectrochimica Acta Part A: Molecular and Biomolecular Spectroscopy, 145*, 245-253.

Chojnacka, K., & Noworyta, A. (2004). Evaluation of Spirulina sp. growth in photoautotrophic, heterotrophic and mixotrophic cultures. *Enzyme and Microbial Technology, 34*, 461-465.

Chojnaka, K., & Marquez, F. J. (2004). Kinetic and Stoichiometric Considerations of the Energy and Carbon Metabolism in the Culture of Microalgae *Biotechnology, 3*, 21-34.

Chrismadha, T., & Borowitzka, M. (1994). Effect of cell density and irradiance on growth, proximate composition and eicosapentaenoic acid production ofPhaeodactylum tricornutum grown in a tubular photobioreactor. *Journal of Applied Phycology, 6*, 67-74.

Coleman, J. R., & Colman, B. (1980). Effect of Oxygen and Temperature on the Efficiency of Photosynthetic Carbon Assimilation in Two Microscopic Algae. *Plant Physiology, 65*, 980-983.

Converti, A., Casazza, A. A., Ortiz, E. Y., Perego, P., & Del Borghi, M. (2009). Effect of temperature and nitrogen concentration on the growth and lipid content of Nannochloropsis oculata and Chlorella vulgaris for biodiesel production. *Chemical Engineering and Processing: Process Intensification, 48*, 1146-1151.

Craggs, R., Sutherland, D., & Campbell, H. (2012). Hectare-scale demonstration of high rate algal ponds for enhanced wastewater treatment and biofuel production. *Journal of Applied Phycology, 24*, 329-337.

Dauta, A., Devaux, J., Piquemal, F., & Boumnich, L. (1990). Growth rate of four freshwater algae in relation to light and temperature. *Hydrobiologia, 207*, 221-226.

De la Hoz Siegler, H. (2012). Optimization of microalgal productivity using an adaptive, non-linear model based strategy. *Bioresource Technology, 104*, 537-546.

De la Hoz Siegler, H., Ben-Zvi, A., Burrell, R. E., & McCaffrey, W. C. (2011). The dynamics of heterotrophic algal cultures. *Bioresource Technology.*102, 5764–5774.

De la Hoz Siegler Jr, H. (2011). *Optimization of biomass and lipid production in heterotrophic microalgal cultures.* (Thesis), University of Alberta,

Dragone, G., Fernandes, B. D., Abreu, A. P., Vicente, A. A., & Teixeira, J. A. (2011). Nutrient limitation as a strategy for increasing starch accumulation in microalgae. *Applied Energy, 88*, 3331-3335. d

Droop, M. (1974). The nutrient status of algal cells in continuous culture. *Journal of the Marine Biological Association of the United Kingdom, 54*, 825-855.

Droop, M. R. (1975). The nutrient status of algal cells in batch culture. *Journal of the Marine Biological Association of the United Kingdom, 55*, 541-555.

Droop, M. R. (1983). 25 Years of Algal Growth Kinetics A Personal View. In *Botanica Marina, 26*, 99-105

Emerson, R. (1958). The quantum yield of photosynthesis. *Annu Rev Plant Physiol, 9*, 1-24.

Erb, T. J., & Zarzycki, J. (2016). Biochemical and synthetic biology approaches to improve photosynthetic CO2-fixation. *Current Opinion in Chemical Biology, 34*, 72-79.

Espen Granum, Ståle Kirkvold, & Myklestad, S. M. (2002). Cellular and extracellular production of carbohydrates and amino acids by the marine diatom *Skeletonema costatum*: diel variations and effects of N depletion. *Marine Ecology Progress Series, 242*, 83-94.

Evens, T. J., Niedz, R. P., & Kirkpatrick, G. J. (2008). Temperature and irradiance impacts on the growth, pigmentation and photosystem II quantum yields of *Haematococcus pluvialis* (Chlorophyceae). *Journal of Applied Phycology, 20*, 411-422.

Fakhry, M. G., Massoud, A., & Ahmed, S.). *Selective harmonic elimination for quasi seven-level operation of cascaded-type multilevel converters with unequal DC sources.* FirstWorkshop on Smart Grid and Renewable Energy (SGRE); 2015, March 22-23; Doha Qatar.

Fernandes, B., Teixeira, J., Dragone, G., Vicente, A. V., Kawano, S., Bišová, K., . . . Vítová, M. (2013). Relationship between starch and lipid accumulation induced by nutrient depletion and replenishment in the microalga *Parachlorella kessleri*. *Bioresource Technology, 144*, 268–274.

Flynn, K. J., Davidson, K., & Leftley, J. W. (1993). Carbon-nitrogen relations during batch growth ofNannochloropsis oculata (Eustigmatophyceae) under alternating light and dark. *Journal of Applied Phycology, 5*, 465-475.

Flynn, K. J., & Mitra, A. (2009). Building the “perfect beast”: modelling mixotrophic plankton. *Journal of Plankton Research, 31*, 965-992.

Foley, P. M., Beach, E. S., & Zimmerman, J. B. (2011). Algae as a source of renewable chemicals: opportunities and challenges. *Green Chem., 13*, 1399-1405.

García-Camacho, F., Sánchez-Mirón, A., Molina-Grima, E., Camacho-Rubio, F., & Merchuck, J. (2012). A mechanistic model of photosynthesis in microalgae including photoacclimation dynamics. *Journal of Theoretical Biology, 304*, 1-15.

García-Camacho, F., Sánchez-Mirón, A., Molina-Grima, E., Camacho-Rubio, F., & Merchuck, J. C. (2012). A mechanistic model of photosynthesis in microalgae including photoacclimation dynamics. *Journal of Theoretical Biology, 304*, 1-15.

García, F., Freile-Pelegrín, Y., & Robledo, D. (2007). Physiological characterization of Dunaliella sp. (Chlorophyta, Volvocales) from Yucatan, Mexico. *Bioresource Technology, 98*, 1359-1365.

Geider, R. J., MacIntyre, H. L., & Kana, T. M. (1997). Dynamic model of phytoplankton growth and acclimation: responses of the balanced growth rate and the chlorophyll a:carbon ratio to light, nutrient-limitation and temperature. *Marine Ecology Progress Series, 148*, 187-200.

Geider, R. J., MacIntyre, H. L., & Kana, T. M. (1998). A Dynamic Regulatory Model of Phytoplankton Acclimation to Light, Nutrients and Temperature. *Limnol. Oceanographer, 43*, 679-694.

González López, C. V., García, M. d. C. C., Fernández, F. G. A., Bustos, C. S., Chisti, Y., & Sevilla, J. M. F. (2010). Protein measurements of microalgal and cyanobacterial biomass. *Bioresource Technology, 101*, 7587-7591.

Gorai, T., Katayama, T., Obata, M., Murata, A., & Taguchi, S. (2014). Low blue light enhances growth rate, light absorption, and photosynthetic characteristics of four marine phytoplankton species. *Journal of Experimental Marine Biology and Ecology, 459*, 87-95. d

Gorbunov, M. Y., Falkowski, P. G., & Kolber, Z. S. (1999). Measurement of photosynthetic parameters in benthic organisms in situ using aSCUBA-based fast repetition rate fluorometer. *Limnol. Oceanographer, 45*, 242–245.

Gordillo, F. J., Goutx, M., Figueroa, F. L., & Niell, F. X. (1998). Effects of light intensity, CO2 and nitrogen supply on lipid class composition of Dunaliella viridis. *Journal of Applied Phycology, 10*, 135-144.

Griffin, K. L., & Seemann, J. R. (1996). Plants, CO2 and photosynthesis in the 21st century. *Chemistry & Biology, 3*, 245-254.

Grima, E. M., Camacho, F. G., Pérez, J., Sevilla, J., Fernandez, F., & Gomez, A. C. (1994). A mathematical model of microalgal growth in light-limited chemostat culture. *Journal of chemical technology and biotechnology, 61*, 167-173.

Grima, E. M., Fernández, F. A., Camacho, F. G., & Chisti, Y. (1999). Photobioreactors: light regime, mass transfer, and scaleup. *Journal of biotechnology, 70*, 231-247.

Grobbelaar, J. (2004). Chapter 6 Algal Nutrition-Mineral Nutrition. *Handbook of Microalgal Culture: Biotechnology and Applied Phycology, Éditions Amos Richmond, Blackwell Publishing*.

Grobbelaar, J. U. (2008). Factors governing algal growth in photobioreactors: the “open” versus “closed” debate. *Journal of Applied Phycology, 21*, 489.

Grobbelaar, J. U., Nedbal, L., & Tichý, V. (1996). Influence of high frequency light/dark fluctuations on photosynthetic characteristics of microalgae photoacclimated to different light intensities and implications for mass algal cultivation. *Journal of Applied Phycology, 8*, 335-343.

Halfhide, T., Åkerstrøm, A., Lekang, O. I., Gislerød, H. R., & Ergas, S. J. (2014). Production of algal biomass, chlorophyll, starch and lipids using aquaculture wastewater under axenic and non-axenic conditions. *Algal Research, 6,*, 152-159.

Hamilton, D. P., & Schladow, S. G. (1997). Prediction of water quality in lakes and reservoirs. Part I — Model description. *Ecological Modelling, 96*, 91-110.

Han, F., Wang, W., Li, Y., Shen, G., Wan, M., & Wang, J. (2013). Changes of biomass, lipid content and fatty acids composition under a light–dark cyclic culture of Chlorella pyrenoidosa in response to different temperature. *Bioresource Technology, 132*, 182-189.

Han, J., Zhang, L., Wang, S., Yang, G., Zhao, L., & Pan, K. (2016). Co-culturing bacteria and microalgae in organic carbon containing medium. *Journal of Biological Research-Thessaloniki, 23*, 8.

Ho, S.-H., Chen, C.-Y., & Chang, J.-S. (2012). Effect of light intensity and nitrogen starvation on CO2 fixation and lipid/carbohydrate production of an indigenous microalga Scenedesmus obliquus CNW-N. *Bioresource Technology, 113*, 244-252.

Ho, S.-H., Chen, Y.-D., Chang, C.-Y., Lai, Y.-Y., Chen, C.-Y., Kondo, A., . . . Chang, J.-S. (2017). Feasibility of CO2 mitigation and carbohydrate production by microalga Scenedesmus obliquus CNW-N used for bioethanol fermentation under outdoor conditions: effects of seasonal changes. *Biotechnology for Biofuels, 10*, 27.

Howland, R. J. M., Tappin, A. D., Uncles, R. J., Plummer, D. H., & Bloomer, N. J. (2000). Distributions and seasonal variability of pH and alkalinity in the Tweed Estuary, UK. *Science of The Total Environment, 251-252*, 125-138.

Hu, W. (2014). *Dry Weight and Cell Density of Individual Algal and Cyanobacterial Cells for Algae Research and Development.* (Master of Science), Missouri-Columbia, Missouri.

Illman, A. M., Scragg, A. H., & Shales, S. W. (2000). Increase in Chlorella strains calorific values when grown in low nitrogen medium. *Enzyme and Microbial Technology, 27*, 631-635.

Imaizumi, Y., Nagao, N., Yusoff, F. M., Taguchi, S., & Toda, T. (2014). Estimation of optimum specific light intensity per cell on a high-cell-density continuous culture of Chlorella zofingiensis not limited by nutrients or CO2. *Bioresource Technology, 162*, 53-59.

James, S. C., & Boriah, V. (2010). Modeling algae growth in an open-channel raceway. *Journal of Computational Biology, 17*, 895-906.

Jiménez, C., Cossı, amp, x, o, B. R., & Niell, F. X. (2003). Relationship between physicochemical variables and productivity in open ponds for the production of Spirulina: a predictive model of algal yield. *Aquaculture, 221*, 331-345.

Jonker, J. G. G., & Faaij, A. P. C. (2013). Techno-economic assessment of micro-algae as feedstock for renewable bio-energy production. *Applied Energy, 102*, 461-475.

Juneja, A., Ceballos, R., & Murthy, G. (2013). Effects of Environmental Factors and Nutrient Availability on the Biochemical Composition of Algae for Biofuels Production: A Review. *Energies, 6*, 4607.

Kaewkannetra, P., Enmak, P., & Chiu, T. (2012). The effect of CO 2 and salinity on the cultivation of Scenedesmus obliquus for biodiesel production. *Biotechnology and bioprocess engineering, 17*, 591-597.

Kakinuma, M., Coury, D. A., Kuno, Y., Itoh, S., Kozawa, Y., Inagaki, E., . . . Amano, H. (2006). Physiological and biochemical responses to thermal and salinity stresses in a sterile mutant of Ulva pertusa (Ulvales, Chlorophyta). *Marine Biology, 149*, 97-106.

Kalacheva, G. S., Zhila, N. O., Volova, T. G., & Gladyshev, M. I. (2002). The Effect of Temperature on the Lipid Composition of the Green Alga Botryococcus. *Microbiology, 71*, 286-293.

Katarzyna, C., & Facundo-Joaquin, M.-R. (2004). Kinetic and stoichiometric relationships of the energy and carbon metabolism in the culture of microalgae. *Biotechnology, 6,* 293-300.

Ketheesan, B., & Nirmalakhandan, N. (2013). Modeling microalgal growth in an airlift-driven raceway reactor. *Bioresource Technology, 136*, 689-696.

Khatoon, H., Rahman, N., Suleiman, S., Banerjee, S., & Bolong Abol-Munafi, A. (2017). Growth and Proximate Composition of Scenedesmus obliquus and Selenastrum bibraianum Cultured in Different Media and Condition*, Proceedings of the National Academy of Sciences, India Section B: Biological Sciences, 89*, 251–257).

Kilham, S., Kreeger, D., Goulden, C., & Lynn, S. (1997). Effects of nutrient limitation on biochemical constituents of Ankistrodesmus falcatus. *Freshwater Biology, 38*, 591-596.

Klok, A. J., Verbaanderd, J. A., Lamers, P. P., Martens, D. E., Rinzema, A., & Wijffels, R. H. (2013). A model for customising biomass composition in continuous microalgae production. *Bioresource Technology, 146*, 89-100. doi:http://dx.doi.org/10.1016/j.biortech.2013.07.039

Kobayashi, M., Kakizono, T., Yamaguchi, K., Nishio, N., & Nagai, S. (1992). Growth and astaxanthin formation of Haematococcus pluvialis in heterotrophic and mixotrophic conditions. *Journal of Fermentation and Bioengineering, 74*, 17-20.

Kok, B. (1953). Experiments on photosynthesis by Chlorella in flashing light. *Algal culture: from laboratory to pilot plant, 600*, 63-75.

Kristiansen, S., & Farbrot, T. (1991). Nitrogen uptake rates in phytoplankton and ice algae in the Barents Sea *Polar Research, 10*, 187-192.

Kró, M., Maxwell, D. P., & Huner, N. P. A. (1997). Exposure of Dunaliella salina to Low Temperature Mimics the High Light-Induced Accumulation of Carotenoids and the Carotenoid Binding Protein (Cbr). *Plant and Cell Physiology, 38*, 213-216.

Krzemińska, I., Pawlik-Skowrońska, B., Trzcińska, M., & Tys, J. (2014). Influence of photoperiods on the growth rate and biomass productivity of green microalgae. *Bioprocess and Biosystems Engineering, 37*, 735-741.

Kucharoenphaibul, S., Limtong, S., & Yongmanitchai, W. (2014). Enhancement of growth and lipid accumulation by Chlorella sorokiniana 1019 under mixotrophic culture conditions. *Kasetsart Journal, Natural Science, 48*, 433-441.

Kumar, V., Sahu, N. P., Pal, A. K., Kumar, S., Sinha, A. K., Ranjan, J., & Baruah, K. (2010). Modulation of key enzymes of glycolysis, gluconeogenesis, amino acid catabolism, and TCA cycle of the tropical freshwater fish Labeo rohita fed gelatinized and non-gelatinized starch diet. *Fish Physiology and Biochemistry, 36*, 491-499.

Kunikane, S., & Kaneko, M. (1984). Growth and nutrient uptake of green alga, Scenedesmus dimorphus, under a wide range of nitrogen/phosphorus ratio—II. Kinetic model. *Water Research, 18*(, 1313-1326.

Kurpan Nogueira, D. P., Silva, A. F., Araújo, O. Q. F., & Chaloub, R. M. (2015). Impact of temperature and light intensity on triacylglycerol accumulation in marine microalgae. *Biomass and Bioenergy, 72*, 280-287.

Lalibertè, G., & de la Noüie, J. (1993). Auto-, Hetero-, and Mixotrophic Growth of *Chlamydamonas Humicola* (Cmloroimiyckak) on Acetate. *Journal of Phycology, 29*, 612-620.

Langley, N., Harrison, S., & Van Hille, R. (2012). A critical evaluation of CO2 supplementation to algal systems by direct injection. *Biochemical Engineering Journal, 68*, 70-75.

Laws, E. A. (1991). Photosynthetic quotients, new production and net community production in the open ocean. *Deep Sea Research Part A. Oceanographic Research Papers, 38*, 143-167.

Laws, E. A., Taguchi, S., Hirata, J., & Pang, L. (1988). Optimization of microalgal production in a shallow outdoor flume. *Biotechnology and bioengineering, 32*, 140-147.

Lee, S. H., Jo, B. H., Shin, S. Y., & Lee, S. H. (2014). Higher Biomass Productivity of Microalgae in an Attached Growth System, Using Wastewater. *Journal of microbiology and biotechnology, 24*, 1566-1573.

Lehman, J. T., Botkin, D. B., & Likens, G. E. (1975). The assumptions and rationales of a computer model of phytoplankton population dynamics. *Limnol. Oceanogr. ,20*, 343-364.

Lemesle, V., & Mailleret, Æ. L. (2007). A Mechanistic Investigation of the Algae Growth ‘‘Droop’’ Model. *Acta Biotheor*, *56*, 87-102.

Leverenz, J. W. (1987). Chlorophyll content and the light response curve of shade-adapted conifer needles. *Physiologia Plantarum, 71*, 20-29.

Li, J., Han, D., Wang, D., Ning, K., Jia, J., Wei, L., . . . Xu, J. (2014). Choreography of Transcriptomes and Lipidomes of Nannochloropsis Reveals the Mechanisms of Oil Synthesis in Microalgae. *The Plant Cell Online*.

Li, J., Han, D., Wang, D., Ning, K., Jia, J., Wei, L., . . . Xu, J. (2014). Choreography of Transciptomes and Lipidomes of *Nannochloropsis* Reveals the Mechanisms of Oil Synthesis in Microalgae. *Plant Cell, 26*, 1645-1665.

Li, T., Gargouri, M., Feng, J., Park, J.-J., Gao, D., Miao, C., . . . Chen, S. (2015). Regulation of starch and lipid accumulation in a microalga Chlorella sorokiniana. *Bioresource Technology, 180*, 250-257.

Li, T., Zheng, Y., Yu, L., & Chen, S. (2014). Mixotrophic cultivation of a Chlorella sorokiniana strain for enhanced biomass and lipid production. *Biomass and Bioenergy, 66*, 204-213.

Li, X., Přibyl, P., Bišová, K., Kawano, S., Cepák, V., Zachleder, V., . . . Vítová, M. (2013). The microalga Parachlorella kessleri—A novel highly efficient lipid producer. *Biotechnology and bioengineering, 110*, 97-107.

Liang, K., Zhang, Q., Gu, M., & Cong, W. (2013). Effect of phosphorus on lipid accumulation in freshwater microalga Chlorella sp. *Journal of Applied Phycology, 25*, 311-318.

David Iluz and Zvy Dubinsky (June 12th 2013). Quantum Yields in Aquatic Photosynthesis, Photosynthesis, Zvy Dubinsky, IntechOpen. Available from: https://www.intechopen.com/books/photosynthesis/quantum-yields-in-aquatic-photosynthesis

Lu, L., Wang, J., Yang, G., Zhu, B., & Pan, K. (2017). Biomass and nutrient productivities of Tetraselmis chuii under mixotrophic culture conditions with various C:N ratios. *Chinese Journal of Oceanology and Limnology, 35*, 303-312. Luque, R. (2010). Algal biofuels: the eternal promise? *Energy & Environmental Science, 3*, 254-257.

MacIntyre, H. L., Kana, T. M., Anning, T., & Geider, R. J. (2002). Photoacclimation of Photosynthesis Irradiance Response Curves and Photosynthetic Pigments in Microalgae and Cyanobacteria. *Journal of Phycology, 38*, 17-38.

Mairet, F., Bernard, O., Masci, P., Lacour, T., & Sciandra, A. (2011). Modelling neutral lipid production by the microalga *Isochrysis galbana* under nitrogen limitation. *Bioresource Technology, 102*, 142-149.

Maity, S. K. (2015). Opportunities, recent trends and challenges of integrated biorefinery: Part II. *Renewable and Sustainable Energy Reviews, 43*, 1446-1466.

Marquez, F. J., Sasaki, K., Kakizono, T., Nishio, N., & Nagai, S. (1993). Growth characteristics of Spirulina platensis in mixotrophic and heterotrophic conditions. *Journal of Fermentation and Bioengineering, 76*, 408-410.

Martínez, F., & Orús, M. I. (1991). Interactions between Glucose and Inorganic Carbon Metabolism in Chlorella vulgaris Strain UAM 101. *Plant Physiology, 95*, 1150-1155.

Maxwell, D. P., Falk, S., Trick, C. G., & Huner, N. (1994). Growth at Low Temperature Mimics High-Light Acclimation in Chlorella vulgaris. *Plant Physiology, 105*, 535-543.

Maxwell, D. P., Falk, S., Trick, C. G., & Huner, N. P. (1994). Growth at low temperature mimics high-light acclimation in Chlorella vulgaris. *Plant Physiology, 105*, 535-543.

Maxwell, K., & Johnson, G. N. (2000). Chlorophyll fluorescence—a practical guide. *Journal of Experimental Botany, 51*, 659-668.

McGinnis, K., Dempster, T., & Sommerfeld, M. (1997). Characterization of the growth and lipid content of the diatom Chaetoceros muelleri. *Journal of Applied Phycology, 9*, 19-24.

Mitra, D., van Leeuwen, J. H., & Lamsal, B. (2012). Heterotrophic/mixotrophic cultivation of oleaginous Chlorella vulgaris on industrial co-products. *Algal Research, 1*, 40-48.

Mizuno, Y., Sato, A., Watanabe, K., Hirata, A., Takeshita, T., Ota, S., . . . Kawano, S. (2013). Sequential accumulation of starch and lipid induced by sulfur deficiency in Chlorella and Parachlorella species. *Bioresource Technology, 129*, 150-155.

Moore, M. C., Suggett, D. J., Hickman, A. E., Kim, Y.-N., & Tweddle, J. F. (2006). Phytoplankton photoacclimation and photoadaptation in response to environmental gradients in a shelf sea. *Limnol. Oceanographer, 51*, 936–949.

Morel, A., & Bricaud, A. (1981). Theoretical results concerning light absorption in a discrete medium and application to specific absorption of phytoplankton. *Deep Sea Research, 28A*, 1375-1393.

Morris, I., Glover, H. E., & Yentsch, C. S. (1974). Products of photosynthesis by marine phytoplankton: the effect of environmental factors on the relative rates of protein synthesis. *Marine Biology, 27*, 1-9.

Müller, P., Li, X.-P., & Niyogi, K. K. (2001). Non-Photochemical Quenching. A Response to Excess Light Energy. *Plant Physiology, 125*, 1558-1566.

Nakamura, Y., & Miyachi, S. (1982a). Change in starch photosynthesized at different temperatures in Chlorella. *Plant Science Letters, 27*, 1-6.

Nakamura, Y., & Miyachi, S. (1982b). Effect of Temperature on Starch Degradation in Chlorella vulgaris 11h Cells. *Plant and Cell Physiology, 23*, 333-341.

Neidhardt, J., Benemann, J. R., Zhang, L., & Melis, A. (1998). Photosystem-II repair and chloroplast recovery from irradiance stress: relationship between chronic photoinhibition, light-harvesting chlorophyll antenna size and photosynthetic productivity in Dunaliella salina (green algae). *Photosynthesis Research, 56*, 175-184.

Nielsen, E. S. (1978). Growth of plankton algae as a function of N-concentration, measured by means of batch technique. *Marine Biology, 46*, 185-189.

Ogawa, T., & Aiba, S. (1981). Bioenergetic analysis of mixotrophic growth in Chlorella vulgaris and Scenedesmus acutus. *Biotechnology and bioengineering, 23*, 1121-1132.

Ördög, V., Stirk, W. A., Bálint, P., van Staden, J., & Lovász, C. (2012). Changes in lipid, protein and pigment concentrations in nitrogen-stressed Chlorella minutissima cultures. *Journal of Applied Phycology, 24*, 907-914.

Ozkan, A., Kinney, K., Katz, L., & Berberoglu, H. (2012). Reduction of water and energy requirement of algae cultivation using an algae biofilm photobioreactor. *Bioresource Technology, 114*, 542-548.

Packer, A., Li, Y., Anderson, T., Hu, Q., Kuang, Y., & Sommerfeld, M. (2011). Growth and neutral lipid synthesis in green microalgae: A mathematical model. *Bioresource Technology, 102*, 111-117.

Pagnanelli, F., Altimari, P., Trabucco, F., & Toro, L. (2014). Mixotrophic growth of Chlorella vulgaris and Nannochloropsis oculata: interaction between glucose and nitrate. *Journal of Chemical Technology & Biotechnology, 89*, 652-661.

Pahlow, M., & Oschlies, A. (2013). Optimal allocation backs Droop's cell-quota model. *Marine Ecology Progress Series, 473*, 1-5.

Park, B. K. (2013). *Enhancing harvestable algal biomass production in wastewater treatment high rate algal ponds by recycling.* Massey University, Palmerston North, New Zealand.

Park, J., Craggs, R., & Shilton, A. (2011). Wastewater treatment high rate algal ponds for biofuel production. *Bioresource Technology, 102*, 35-42.

Patterson, G. W. (1970). Effect of culture temperature on fatty acid composition ofChlorella sorokiniana. *Lipids, 5*, 597-600.

Perez-Garcia, O., Escalante, F. M. E., de-Basahn, L. E., & Bashan, Y. (2011). Heterotrophic cultures of microalgae: Metabolism and potential products. *Water Research, 45*, 11-36.

Pinhal, S., Ropers, D., Geiselmann, J., & de Jong, H. (2019). Acetate metabolism and the inhibition of bacterial growth by acetate. *Journal of Bacteriology*, 201.

Quaas, T., Berteotti, S., Ballottari, M., Flieger, K., Bassi, R., Wilhelm, C., & Goss, R. (2015). Non-photochemical quenching and xanthophyll cycle activities in six green algal species suggest mechanistic differences in the process of excess energy dissipation. *Journal of Plant Physiology, 172*, 92-103.

Quinn, J., de Winter, L., & Bradely, T. (2011). Microalgae bulk growth model with application to industrial scale systems. *Bioresource Technology, 102*, 5083-5092.

Recuenco-Muñoz, L., Offre, P., Valledor, L., Lyon, D., Weckwerth, W., & Wienkoop, S. (2015). Targeted quantitative analysis of a diurnal RuBisCO subunit expression and

translation profile in Chlamydomonas reinhardtii introducing a novel Mass Western approach. *Journal of proteomics, 113*, 143-153.

Renaud, S. M., Thinh, L.-V., Lambrinidis, G., & Parry, D. L. (2002). Effect of temperature on growth, chemical composition and fatty acid composition of tropical Australian microalgae grown in batch cultures. *Aquaculture, 211*, 195-214.

Rhee, G.-Y., & Gotham, I. J. (1981). The effect of environmental factors on phytoplankton growth: Temperature and the interactions of temperature with nutrient limitation1. *Limnology and Oceanography, 26*, 635-648.

Richardson, B., Orcutt, D. M., Schwertner, H. A., Martinez, C. L., & Wickline, H. E. (1969). Effects of Nitrogen Limitation on the Growth and Composition of Unicellular Algae in Continuous Culture. *Applied Microbiology, 18*, 245-250.

Riemann, B., Simonsen, P., & Stensgaard, L. (1989). The carbon and chlorophyll content of phytoplankton from various nutrient regimes. *Journal of Plankton Research, 11*, 1037-1045.

Rodjaroen, S., Juntawong, N., Mahakhant, A., & Miyamoto, K. (2007). High biomass production and starch accumulation in native green algal strains and cyanobacterial strains of Thailand. *Kasetsart Journal - Natural Science, 41*, 570-575.

Ruangsomboon, S. (2012). Effect of light, nutrient, cultivation time and salinity on lipid production of newly isolated strain of the green microalga, Botryococcus braunii KMITL 2. *Bioresource Technology, 109*, 261-265.

Saha, S., & Murray, P. (2018). Exploitation of Microalgae Species for Nutraceutical Purposes: Cultivation Aspects, *Fermentation*, *4, 46*

Sajjadi, B., Chen, W.-Y., Raman, A. A. A., & Ibrahim, S. (2018). Microalgae lipid and biomass for biofuel production: A comprehensive review on lipid enhancement

strategies and their effects on fatty acid composition. *Renewable and Sustainable Energy Reviews, 97*, 200-232.

Sakshaug, E., Bricaud, A., Dandonneau, Y., Falkowski, P. G., JKiefer, D. A., Legendre, L., . . . Takashi, M. (1997). Parameters of photosynthesis: definitions, theory and interpretations of results. *Journal of Plankton Research, 19*, 1637-1670.

Salih, F. M. (2011). Microalgae tolerance to high concentrations of carbon dioxide: a review. *Journal of Environmental Protection, 2*, 648.

Schubert, H., Schiewer, U., & Tschirner, E. (1989). Fluorescence characteristics of cyanobacteria (blue-green algae). *Journal of Plankton Research, 11*, 353-359.

Seyfabadi, J. (2012). Effect of light intensity and photoperiod on biomass and fatty acid composition of the microalgae, *Chlorella vulgaris*, *Aquaculture International, 20*, 41-49.

Sforza, E., Cipriani, R., Morosinotto, T., Bertucco, A., & Giacometti, G. M. (2012). Excess CO2 supply inhibits mixotrophic growth of Chlorella protothecoides and Nannochloropsis salina. *Bioresource Technology, 104*, 523-529.

Sforza, E., Simionato, D., Giacometti, G. M., Bertucco, A., & Morosinotto, T. (2012). Adjusted light and dark cycles can optimize photosynthetic efficiency in algae growing in photobioreactors. *PloS one, 7*, Shammas, N. (2012). *HP 39gII Regression: Part IV Least-Squares Relative Error Regression*. Retrieved from http://www.namirshammas.com/HP39gII/HP39gII_part4.pdf

Sharma, P. K., Saharia, M., Srivstava, R., Kumar, S., & Sahoo, L. (2018). Tailoring Microalgae for Efficient Biofuel Production. *Frontiers in Marine Science, 5*.

Siaut, M., Cuiné, S., Cagnon, C., Fessler, B., Nguyen, M., Carrier, P., . . . Peltier, G. (2011). Oil accumulation in the model green alga Chlamydomonas reinhardtii: characterization,

variability between common laboratory strains and relationship with starch reserves. *BMC Biotechnology, 11*, 1-15.

Silkman, J. B. (2008). Quantum yield variation across the three pathways of photosynthesis: not yet out of the dark. *Journal Experimental Botany, 59*, 1647-1661.

Singh, P., Guldhe, A., Kumari, S., Rawat, I., & Bux, F. (2015). Investigation of combined effect of nitrogen, phosphorus and iron on lipid productivity of microalgae Ankistrodesmus falcatus KJ671624 using response surface methodology. *Biochemical Engineering Journal, 94*, 22-29.

Singh, R., Balagurumurthy, B., & Bhaskar, T. (2015). Hydrothermal liquefaction of macro algae: Effect of feedstock composition. *Fuel, 146*, 69-74.

Singh, S. P., & Singh, P. (2014). Effect of CO2 concentration on algal growth: A review. *Renewable and Sustainable Energy Reviews, 38*, 172-179.

Singh, S. P., & Singh, P. (2015a). Effect of temperature and light on the growth of algae species: A review. *Renewable and Sustainable Energy Reviews, 50*, 431-444.

Singh, S. P., & Singh, P. (2015b). Effect of temperature and light on the growth of algae species: A review. *Renewable and Sustainable Energy Reviews, 50*, 431-444.

Singsaas, E. L., Ort, D. R., & DeLucia, E. H. (2001). Variation in measured values of photosynthetic quantum yield in ecophysiological studies. *Oecologia, 128*, 15-23.

Smetana, S., Sandmann, M., Rohn, S., Pleissner, D., & Heinz, V. (2017). Autotrophic and heterotrophic microalgae and cyanobacteria cultivation for food and feed: life cycle assessment. *Bioresource Technology, 245*, 162-170.

Smith, R. T., Bangert, K., Wilkinson, S. J., & Gilmour, D. J. (2015) Synergistic carbon metabolism in a fast growing mixotrophic freshwater microalgal species Micractinium inermum. *Biomass and Bioenergy, 82,* 73-86.

Spalding, M. H. (1989). Photosynthesis and photorespiration in freshwater green algae. *Aquatic Botany, 34*, 181-209.

Staehr, P. A., & Birkeland, M. J. (2006). Temperature acclimation of growth, photosynthesis and respiration in two mesophilic phytoplankton species. *Phycologia, 45*, 648-656.

Subramanian, S., Barry, A. N., Pieris, S., & Sayre, R. T. (2013). Comparative Eneregetics and kinetics of autotrophic lipid and starch metabolism in chlorophytic microalgae: implications for biomass and biofuel production. *Biotechnology for Biofuels, 150*, 1-12.

Suga, K., Honjoh, K.-i., Furuya, N., Shimizu, H., Nishi, K., Shinohara, F., . . . Iio, M. (2002). Two Low-temperature-inducible Chlorella Genes for Δ12 and ω-3 Fatty Acid Desaturase (FAD): Isolation of Δ12 and ω-3 fad cDNA Clones,…. *Bioscience, Biotechnology, and Biochemistry, 66*, 1314-1327.

Sukenik, A., & Wahnon, R. (1991). Biochemical quality of marine unicellular algae with special emphasis on lipid composition. I. Isochrysis galbana. *Aquaculture, 97*, 61-72.

Sun, X., Cao, Y., Xu, H., Liu, Y., Sun, J., Qiao, D., & Cao, Y. (2014). Effect of nitrogen-starvation, light intensity and iron on triacylglyceride/carbohydrate production and fatty acid profile of Neochloris oleoabundans HK-129 by a two-stage process. *Bioresource Technology, 155*, 204-212.

Sung, K. D., Lee, J., Shin, C., & Park, S. (1999). Isolation of a new highly CO2 tolerant fresh water microalga Chlorella sp. KR-1. *Renewable Energy, 16*, 1019-1022.

Surisetty, K., Hoz Siegler, H. D. l., McCaffrey, W. C., & Ben-Zvi, A. (2010). Model re-parameterization and output prediction for a bioreactor system. *Chemical Engineering Science, 65*, 4535-4547.

Sutherland, D. L., Turnbull, M. H., Broady, P. A., & Craggs, R. J. (2014). Effects of two different nutrient loads on microalgal production, nutrient removal and photosynthetic efficiency in pilot-scale wastewater high rate algal ponds. *Water Research, 66*, 53-62.

Szabó, I., Bergantino, E., & Giacometti, G. M. (2005). Light and oxygenic photosynthesis: energy dissipation as a protection mechanism against photo-oxidation. *EMBO Reports, 6*, 629-634.

Takagi, M., Watanabe, K., Yamaberi, K., & Yoshida, T. (2000). Limited feeding of potassium nitrate for intracellular lipid and triglyceride accumulation of Nannochloris sp. UTEX LB1999. *Applied microbiology and biotechnology, 54*, 112-117.

Takeshita, T., Ota, S., Yamaz, T., Hirata, A., Zachleder, V., & Kawano, S. (2014). Starch and lipid accumulation in eight strains of six Chlorella species under comparatively high light intensity and aeration culture conditions. *Bioresource Technology, 158*, 127-134.

Tevatia, R., Demirel, Y., & Blum, P. (2012). Kinetic modeling of photoautotropic growth and neutral lipid accumulation in terms of ammonium concentration in Chlamydomonas reinhardtii. *Bioresource Technology, 119*, 419-424.

Tredici, M. R., Bassi, N., Prussi, M., Biondi, N., Rodolfi, L., Chini Zittelli, G., & Sampietro, G. (2015). Energy balance of algal biomass production in a 1-ha "Green Wall Panel" plant: How to produce algal biomass in a closed reactor achieving a high Net Energy Ratio. *Applied Energy, 154*, 1103-1111.

Toyub, M., Miah, M., Habib, M. A., & Rahman, M. (2012). Growth Performance and Nutritional Value Of *Scenedesmus Obliquus* Cultured In Different Concentrations Of Sweetmeat Factory Waste Media, *Bangladesh Journal of Animal Science*, *37*, 86-93

Tsuzuki, M., Ohnuma, E., Sato, N., Takaku, T., & Kawaguchi, A. (1990). Effects of CO2 Concentration during Growth on Fatty Acid Composition in Microalgae. *Plant Physiology, 93*, 851-856.

Valenzuela-Espinozaa, E., Millán-Núñezb, R., & Núñez-Cebrero, F. (2002). Protein, carbohydrate, lipid and chlorophyll a content in Isochrysis aff. galbana (clone T-Iso)

cultured with a low cost alternative to the f/2 medium. *Aquacultural Engineering, 25*, 207–216.

Vanucci, S., Guerrini, F., Milandri, A., & Pistocchi, R. (2010). Effects of different levels of N- and P-deficiency on cell yield, okadaic acid, DTX-1, protein and carbohydrate dynamics in the benthic dinoflagellate Prorocentrum lima. *Harmful Algae, 9*, 590-599.

Vardi, A. (2008). Cell signaling in marine diatoms. *Communicative & integrative biology, 1*, 134-136.

Wagenmakers, E.-J., & Farrell, S. (2004). AIC model selection using Akaike weights. *Psychonomic bulletin & review, 11*, 192-196.

Wan, C., Bai, F.-W., & Zhao, X.-Q. (2013). Effects of nitrogen concentration and media replacement on cell growth and lipid production of oleaginous marine microalga Nannochloropsis oceanica DUT01. *Biochemical Engineering Journal, 78*, 32-38.

Wang, L., Lia, Y., Sommerfeld, M., & Hua , Q. (2013). A flexible culture process for production of the green microalga Scenedesmus dimorphus rich in protein, carbohydrate or lipid. *Bioresource Technology, 129*, 289–295.

Wang, Y., He, B., Sun, Z., & Chen, Y.-F. (2016). Chemically enhanced lipid production from microalgae under low sub-optimal temperature. *Algal Research, 16*, 20-27.

Wang, Y., Rischer, H., Eriksen, N. T., & Wiebe, M. G. (2013). Mixotrophic continuous flow cultivation of Chlorella protothecoides for lipids. *Bioresource Technology, 144*, 608-614.

Wen, X., Tao, H., Peng, X., Wang, Z., Ding, Y., Xu, Y., . . . Li, Y. (2019). Sequential phototrophic–mixotrophic cultivation of oleaginous microalga Graesiella sp. WBG-1 in a 1000 m2 open raceway pond. *Biotechnology for Biofuels, 12*, 27.

White, D., Pagarette, A., Rooks, P., & Ali, S. (2013). The effect of sodium bicarbonate supplementation on growth and biochemical composition of marine microalgae cultures. *Journal of Applied Phycology, 25*, 153-165.

Wilken, S., Huisman, J., Naus-Wiezer, S., & Donk, E. (2013). Mixotrophic organisms become more heterotrophic with rising temperature. *Ecology letters, 16*, 225-233.

Woodworth, B. D., Mead, R. L., Nichols, C. N., & Kolling, D. R. J. (2015). Photosynthetic light reactions increase total lipid accumulation in carbon-supplemented batch cultures of Chlorella vulgaris. *Bioresource Technology, 179*(0), 159-164.

Xia, A., Cheng, J., Lin, R., Lu, H., Zhou, J., & Cen, K. (2013). Comparison in dark hydrogen fermentation followed by photo hydrogen fermentation and methanogenesis between protein and carbohydrate compositions in Nannochloropsis oceanica biomass. *Bioresource Technology, 138*, 204-213.

Xin, L., Hong-ying, H., & Yu-ping, Z. (2011). Growth and lipid accumulation properties of a freshwater microalga Scenedesmus sp. under different cultivation temperature. *Bioresource Technology, 102*, 3098-3102. doi:https://doi.org/10.1016/j.biortech.2010.10.055

Xiong, W., Gao, C., Yan, D., Wu, C., & Wu, Q. (2010). Double CO2 fixation in photosynthesis–fermentation model enhances algal lipid synthesis for biodiesel production. *Bioresource Technology, 101*, 2287-2293.

Y. Nakano, K. M., H. Okuno, K. Hamazaki, S., & Takenaka, N. H., M. Kiyota, I. Aiga and J. Kondo. (1996). Growth of Photosynthetic Algae Euglena in High CO2 Conditions and Its Photosynthetic Characteristics. *Acta Horticulturae, 440*, 49-54.

Yang, C., Hua, Q., & Shimizu, K. (2000). Energetics and carbon metabolism during growth of microalgal cells under photoautotrophic, mixotrophic and cyclic light-autotrophic/dark-heterotrophic conditions. *Biochemical Engineering Journal, 6*, 87-102.

Yang, J., Rasa, E., Tantayotai, P., Scow, K. M., Yuan, H., & Hristova, K. R. (2011). Mathematical model of *Chlorella minutissima* UTEX2341 growth and lipid production under photoheterotrophic fermentation conditions. *Bioresource Technology, 102*, 3077-3082.

Yao, C., Ai, J., Cao, X., Xue, S., & Zhang, W. (2012). Enhancing starch production of a marine green microalga Tetraselmis subcordiformis through nutrient limitation. *Bioresource Technology, 118*, 438-444.

Yeh, K.-L., Chang, J.-S., & chen, W.-m. (2010). Effect of light supply and carbon source on cell growth and cellular composition of a newly isolated microalga Chlorella vulgaris ESP-31. *Engineering in Life Sciences, 10*, 201-208.

Yentsch, C. S., & Vaccaro, R. F. (1958). Phytoplankton Nitrogen in the Oceans]. *Association for the Sciences of Limnology and Oceanography, 3*, 443-448.

Yoo, S. J., Kim, J. H., & Lee, J. M. (2014). Dynamic modelling of mixotrophic microalgal photobioreactor systems with time-varying yield coefficient for the lipid consumption. *Bioresource Technology, 162*, 228-235.

Zhang, D., Yan, F., Sun, Z., Zhang, Q., Xue, S., & Cong, W. (2014). On-line modelling intracellular carbon and energy metabolism of *Nannochloropsis* sp. in nitrogen-repletion and nitrogen-limitation. *Bioresource Technology, 264*, 86-92.

Zhao, J., Ramin, M., Cheng, V., & Arhonditsis, G. B. (2008). Competition patterns among phytoplankton functional groups: How useful are the complex mathematical models? *Acta Oecologica, 33*, 324-344.

Zhu, C. J., Lee, Y. K., & Chao, T. M. (1997). Effects of temperature and growth phase on lipid and biochemical composition of Isochrysis galbana TK1. *Journal of Applied Phycology, 9*, 451-457.

Zhu, S., Huang, W., Xu, J., Wang, Z., Xu, J., & Yuan, Z. (2014). Metabolic changes of starch and lipid triggered by nitrogen starvation in the microalga Chlorella zofingiensis. *Bioresource Technology, 152*, 292-298.

9 Appendices

9.1 Elemental Mass balances

The mass balances below shows the derivation of the light limited carbon balance, nitrogen limited nitrogen balance and oxygen and hydrogen balances, which are coupled to carbon and nitrogen kinetics, as they were not involved in any rate limiting reactions.

9.1.1 Case Study on Literature Model

To demonstrate the important of mass balances a case study on a literature model will be performed. Fig. 9.1 below shows an overview of the proposed algal components and the carbon flow from the paper (Adesanya et al., 2014).

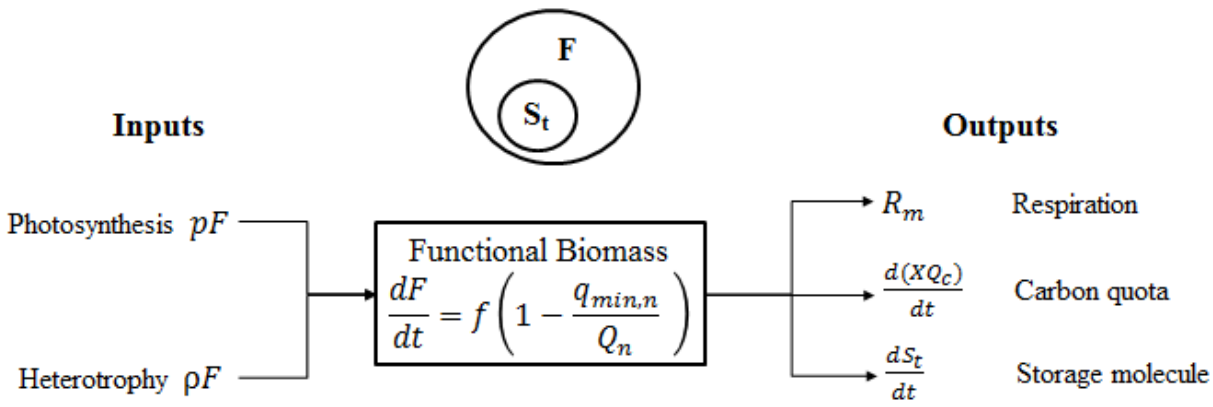

Figure 9.1 The composition of the algal biomass is divided into functional biomass (F) and storage molecules (S_t) for a literature system (Adesanya et al., 2014). The carbon flow diagram shows inputs as photosynthetic fixation and heterotrophic carbon uptake. Functional biomass accumulation is regulated by a linear nitrogen quota term whilst carbon loss from the system is from the sum of storage molecule, respiration and carbon quota (non-storage carbon) generation rate

Based on the schematic in Fig. 9.1, a mass balance over the functional biomass was performed to derive Eq. 9.1 in g F/m^3.d. This is compared with the functional biomass Eq. 9.2 from the study (Adesanya et al., 2014) regulated by nitrogen quota.

$$\frac{dF}{dt} = pF + \rho_{gf}F - \left(R_M + \frac{d(FQ_c)}{dt} + \frac{1}{Y_{St/C}}\frac{dS_t}{dt}\right) \tag{9.1}$$

$$\frac{dF}{dt} = \left(p + \rho_{gf}\right)\left(1 - \frac{Q_{n,min}}{Q_n}\right)F \tag{9.2}$$

where ρ_{gf} is the functional biomass specific uptake rate of glucose (g C/ g F.m^3.d), S_t is the storage molecule concentration (g S_t/m^3), R_M is the maintenance respiration rate (g C/m^3.d) defined in the study as 10 % of the photosynthetic rate, Q_c is the carbon quota (g C/ g F), $Y_{St/C}$ is carbon to storage molecule yield (g S_t/g C) and Q_n is the nitrogen quota (g N/g F).

Deriving functional biomass kinetics in Eq. 9.1 shows that carbon from photosynthesis and heterotrophy is also directed towards storage molecule production, respiration and carbon quota. The nitrogen quota in Eq. 9.2 operates as a regulator, which also dictates the proportion of the total incoming carbon flux, dedicated towards functional biomass synthesis, also used by others to simulate kinetics (Packer et al., 2011). Although Eqs 9.1 and 9.2 are different, they both account for carbon partitioning towards functional biomass. The deviation between the two is due to Eq. 9.2 using a limiting factor to model functional biomass rather than a mass balance approach.

The carbon quota term is not commonly used in composition kinetic modelling but from the mechanistic model of Fig. 9.1, it appears to be the concentration of free carbon not fixed into biomass. This may represent the fraction of carbon existing as metabolic intermediaries used in one such modelling study (Baroukh, Muñoz-Tamayo, Steyer, &

Bernard, 2014). The carbon quota in Eq. 9.3 was obtained by re-arranging Eq. 9.1. This was compared to Eq. 9.4, which was also obtained from a carbon mass balance by Adesanya et al., (2014).

$$\frac{d(FQ_c)}{dt} = pF + \rho_{gf}F - R_M - \frac{1}{Y_{St/C}}\frac{dS_t}{dt} - \frac{1}{Y_{F/C}}\frac{dF}{dt} \tag{9.3}$$

$$\frac{d(FQ_c)}{dt} = pF + \rho_{gf}F - R_M \tag{9.4}$$

Clearly these two expressions of the same variable differ with Eq. 9.4 based on the mechanistic model from Adesanya et al. (2014) differing from the carbon balance of the author. The balance of Eq. 9.4 depicts carbon quota as being the difference between total carbon uptake and respiration. Using a mass balance approach, it can be seen that there is a discrepancy between Eqs 9.3 and 9.4.

A similar problem can be seen for storage molecule kinetics when comparing Eq. 9.5, derived by rearranging Eq. 9.1, and what Adesanya et al. (2014) has claimed to be derived from a carbon mass balance in Eq. 9.6.

$$\frac{1}{Y_{St/C}}\frac{dS_t}{dt} = pF + \rho_{gf}F - \frac{1}{Y_{F/C}}\frac{dF}{dt} - R_M - \frac{d(FQ_c)}{dt} \tag{9.5}$$

$$\frac{dS_t}{dt} = pF + \rho_{gf}F - Q_{c,min}\frac{dF}{dt} \tag{9.6}$$

Eq. 9.6 does not include carbon loss from respiration and carbon quota. There may also be dimensional problems since the right hand side has units of g C/m^3.d and the left hand side has units of g S_t/m^3.d. Issues with carbon balance would make the validity of the resulting fit questionable, making it important to perform an elemental balance to validate biological mathematical models.

9.1.2 Carbon Balance

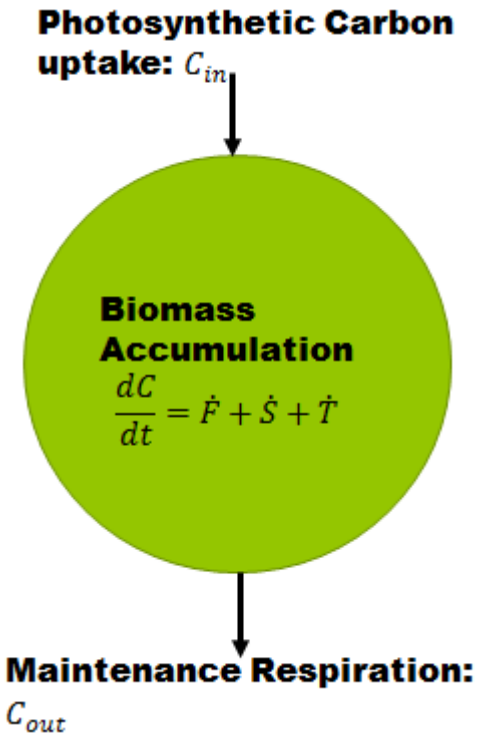

Figure 9.2 Diagram depicting the carbon flux and balance in algal cells.

The biomass accumulation rate ($\frac{dC}{dt}$) is balanced by the difference between gross photosynthetic uptake (C_{in}) and maintenance respiration (C_{out}). Units are in g C/m^3.d. It is assumed that generation of carbon through metabolite excretion and cell death is negligible.

$$\frac{dC}{dt} = C_{in} - C_{out} \tag{9.7}$$

The kinetic expressions governing gross photosynthetic uptake and respiration rate are given below respectively whose difference gives the net photosynthetic uptake.

$$\frac{dC}{dt} = p - b_m F \tag{9.8}$$

The accumulation of fixed biomass is the sum of the net functional biomass, starch and lipid accumulation rates in carbon equivalents (g C/m^3.d).

$$\frac{dC}{dt} = \dot{F} + \dot{S} + \dot{T} \tag{9.9}$$

$$\dot{F} = \frac{1}{Y_{F/C}} \frac{dF}{dt} \tag{9.10}$$

$$\dot{S} = S_p - \frac{1}{Y_{S/C}} S_g \tag{9.11}$$

$$\dot{T} = \frac{1}{Y_{L/C}} L_p + \frac{1}{Y_{S/C}} S_g \tag{9.12}$$

9.1.3 Nitrogen Balance

The nitrogen mass balance involved using the same system boundaries as the carbon balance. It is assumed that generation of nitrogen through metabolite excretion and cell death is negligible.

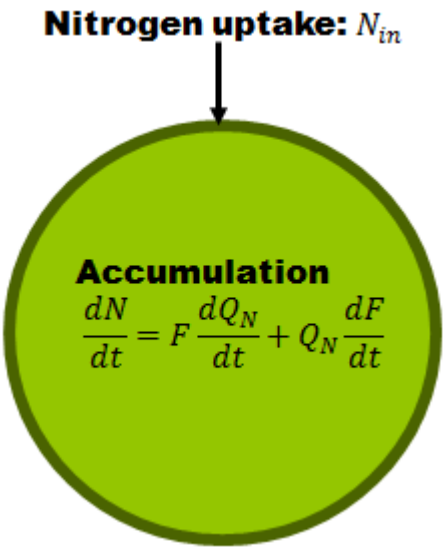

Figure 9.3 Mass balance of the nitrogen in the system.

$$\frac{dN}{dt} = N_{in} - N_{out} \tag{9.13}$$

All of the nitrogen is consumed in external environment and it is assumed that no fixed nitrogen is broken down and expelled from biomass.

$$\frac{dN}{dt} = N_{in} \tag{9.14}$$

The nitrogen accumulation rate in the cells is a function of the rate of nitrogen fixed into the biomass during luxury uptake and fixation into functional biomass (proteins).

$$\frac{dN}{dt} = F\frac{dQ_N}{dt} + Q_N\frac{dF}{dt} \tag{9.15}$$

The uptake rate of nitrogen is given by a kinetic expression, which is a function of external nitrogen concentration and internal nitrogen quota (Adesanya et al., 2014).

$$N_{in} = V_{n,m}\frac{N}{N + K_n}\frac{q_{n,max} - Q_n}{q_{n,max} - q_{n,min}}F \tag{9.16}$$

The removal of H^+ on a continuous basis from the system increase the pH but subsequent addition of CO_2 into the water will reduced the pH. Since the light is on 24 hours a day it is also assumed that the pH does not change rapidly due to changing metabolism.

9.1.4 Oxygen Balance

The inputs for oxygen into the system involve water absorption for splitting in the photosynthetic light reactions, elemental oxygen in CO_2 fixation in the dark reactions and in the form of elemental oxygen in nitrate uptake. Accumulation of oxygen occurs from the formation of biomass as starch, TAGs and Functional Biomass. Oxygen leaves the system via respiration from biomass synthesis and maintenance. The overall mass balance is described below in oxygen equivalents (g O.m^3.d).

$$\frac{dO}{dt} = input - output \tag{9.17}$$

$$= Y_{C02,O/C}p_{net} + Y_{H2O,O/C}p_{net} + Y_{O/N}\rho_N - Y_{O/N}R_G \tag{9.18}$$

The left hand side depicting biomass accumulation of elemental oxygen can be expressed in the following manner.

$$\frac{dO}{dt} = Y_{O/L}\frac{dL}{dt} + Y_{O/S}\frac{dS}{dt} + Y_{O/F}\frac{dF}{dt} \tag{9.19}$$

9.1.5 Hydrogen

Hydrogen enters the system via light driven water photolysis and stoichiometric uptake with nitrates to ensure charge neutrality. Hydrogen accumulation occurs due to CO_2 reduction to form biomass and reduction of nitrates to ammonium for protein synthesis. All the hydrogen taken up by the algae is assumed to be fixed into biomass thus there is no output from the system. The overall mass balance is described below in hydrogen equivalents (g H.m^3.d).

$$\frac{dH}{dt} = input - output \tag{9.20}$$

$$\frac{dH}{dt} = input \tag{9.21}$$

$$\frac{dH}{dt} = Y_{C02,H/C}p_{net} + Y_{H/N}\rho_N \tag{9.22}$$

The left hand side denoting the elemental hydrogen accumulation rate is expressed below.

$$\frac{dH}{dt} = Y_{H/L}\frac{dL}{dt} + Y_{H/S}\frac{dS}{dt} + Y_{H/F}\frac{dF}{dt} \tag{9.23}$$

The mass balance validation for carbon, nitrogen, oxygen and hydrogen is shown below in Figs 9.4 and 9.5.

.

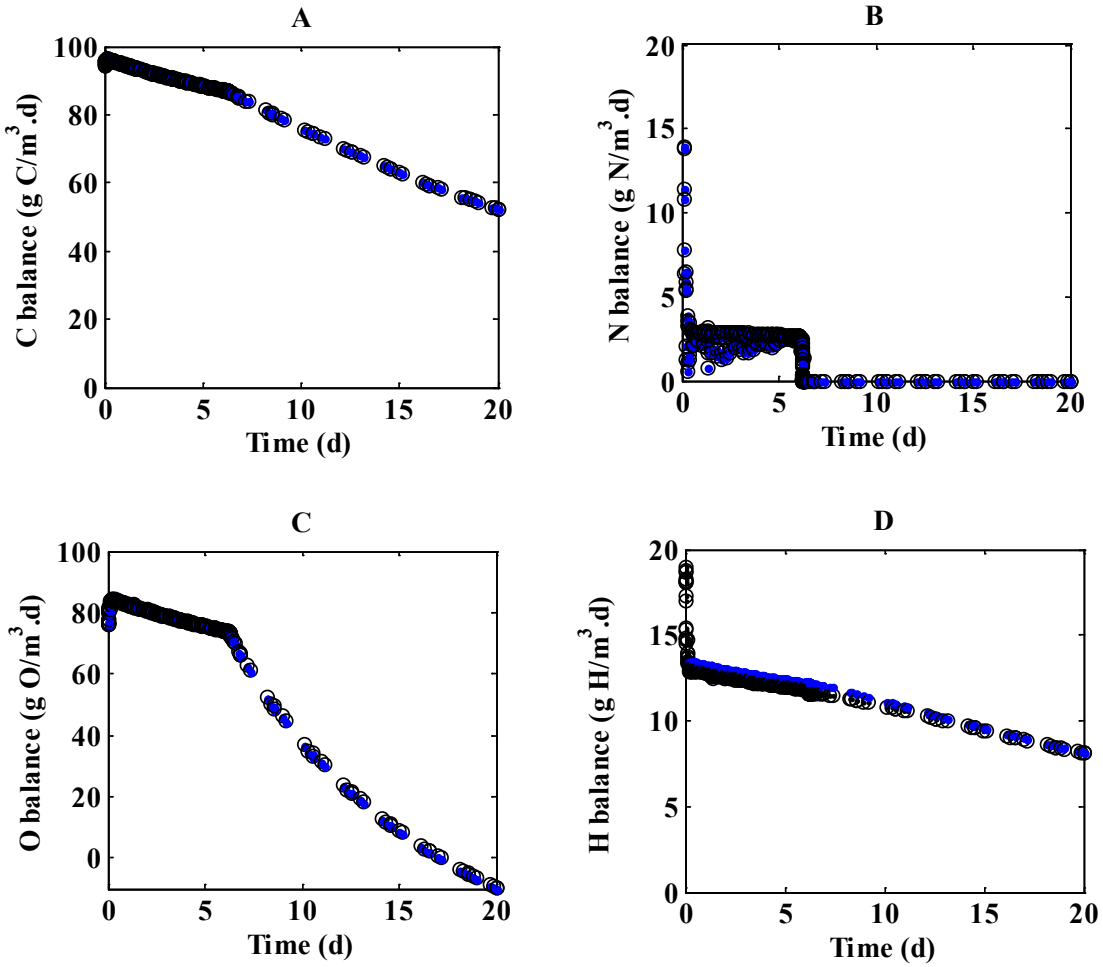

Figure 9.4 Example of elemental mass balance for 25 mg N-NO_3^-/l for batch culture for LCs 4. The closed circles show accumulation rate of the elemental species whilst the open circles show the difference between the generation and consumption rate of the species. For the model to be consistent in terms of conservation of mass, the accumulation rate must equal the difference between generation and consumption.

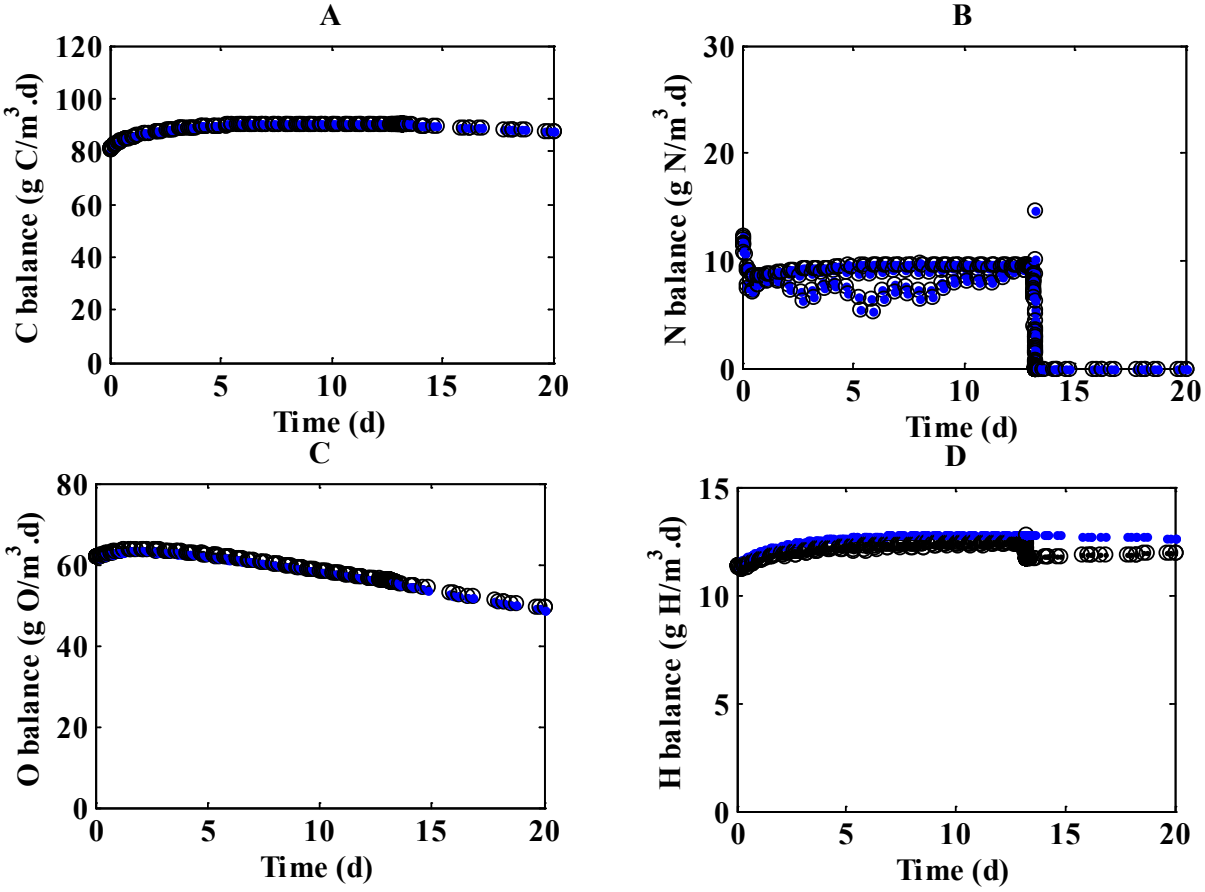

Figure 9.5 Example of elemental mass balance for 125 mg N-NO_3^-/l for batch culture for LCs 4. The closed circles show accumulation rate of the elemental species whilst the open circles show the difference between the generation and consumption rate of the species. For the model to be consistent in terms of conservation of mass, the accumulation rate must equal the difference between generation and consumption.

9.2 Additional Experimental work

Table 9.1Table 9.1 below depicts the measuring kits and prices for analysis. It also shows the variables which were to be measured.

Table 9.1 Variables affecting or controlled in trial experiments on microalgae

Variable	Type	Measurement process
Biomass	Dependant	Ammonium formate washing and oven drying
Total Chlorophyll	Dependant	Disruption by sonication, methanol extraction and spectroscopic absorption
Starch	Dependant	1×Megazyme kit $350 /100 assay. Disruption by sonication, ethanol extraction and spectroscopic absorption
F. Biomass/proteins	F. Biomass = Total biomass-Starch	Closes the mass balance. Metabolically active fraction as described by Adesanya et al.(2014) & Klok et al. (2013)
Glucose Load	Independent	Vary from 2-6 g/l 1×Megazyme kit €163 /60 assay
Nitrates concentration	Independent	~ 75 mg N/l. 1×Sigma Aldrich €361/100 assay
Incident Light	Independent	250 µmol/m^2.s.
pH	Constant	measure with pH meter
Temperature	Constant	25 °C

Additional cell counting data from different species of algae was collected and illustrated in Figs 9.7 to 9.13. In general, they show that mixotrophic cultures did not yield greater biomass when glucose was added. This was due to bacterial contamination.

9.2.1 Further Preliminary Results on Photosynthetic and Mixotrophic Cultivation

Further work was undertaken to determine if mixotrophic cultivation could yield higher biomass. From Figs 9.6 to 9.12 it is apparent that addition of glucose did not improve the yield of algae relative to photosynthetic cultures.

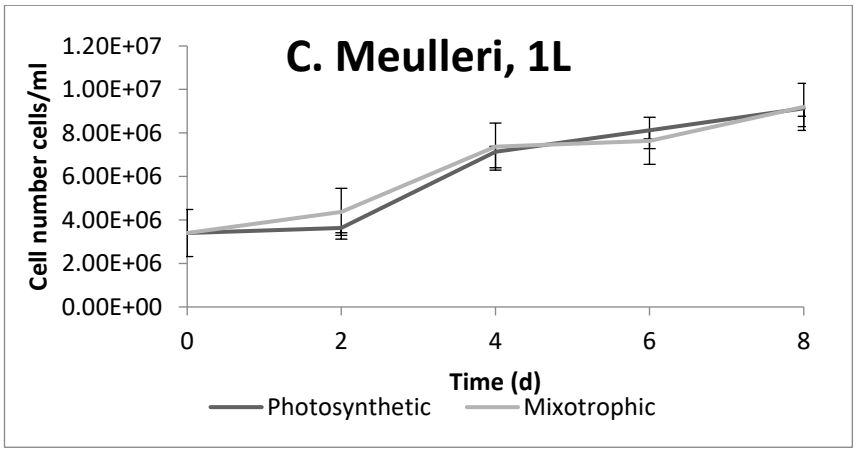

Figure 9.6 Cell number of *C. Muelleri* are within error regardless of whether it is under photosynthetic or mixotrophic growth. 0, 2 g/l of glucose was added to the cultures to determine whether addition of glucose had any effect.

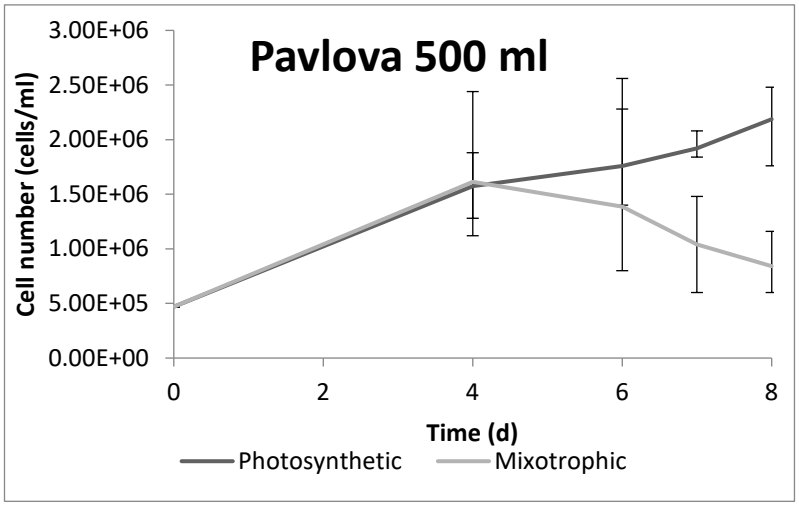

Figure 9.7 *P. lutheri* was grown in 500 ml reactors for 8 days under photosynthetic and mixotrophic (3 g/l glucose) conditions.

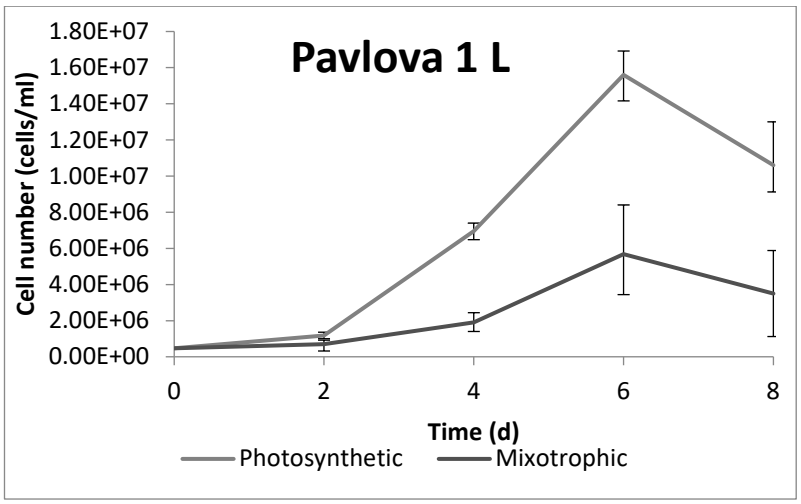

Figure 9.8 *P. lutheri* growth in 1 L reactors. Addition of 2 g/l of glucose did not improve yield compared with photosynthetic algae.

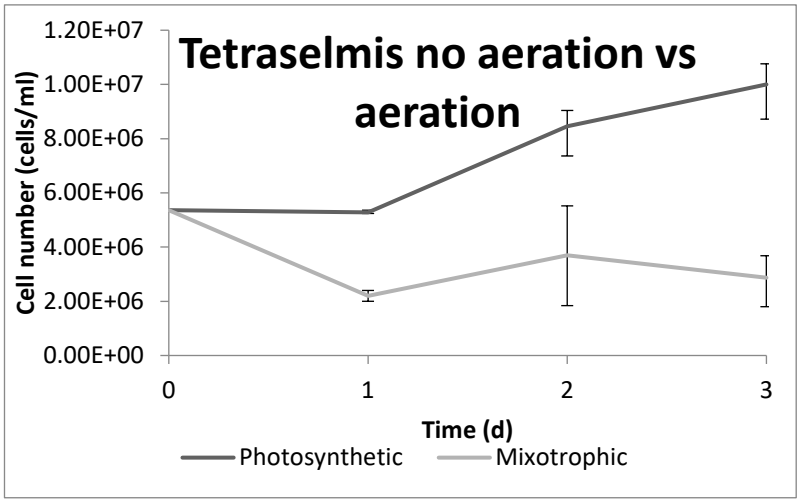

Figure 9.9 plot of aerated photosynthetic algae and non-aerated mixotrophic *T. Chuii*. Mixotrophic cultures did not grow as fast as photosynthetic algae.

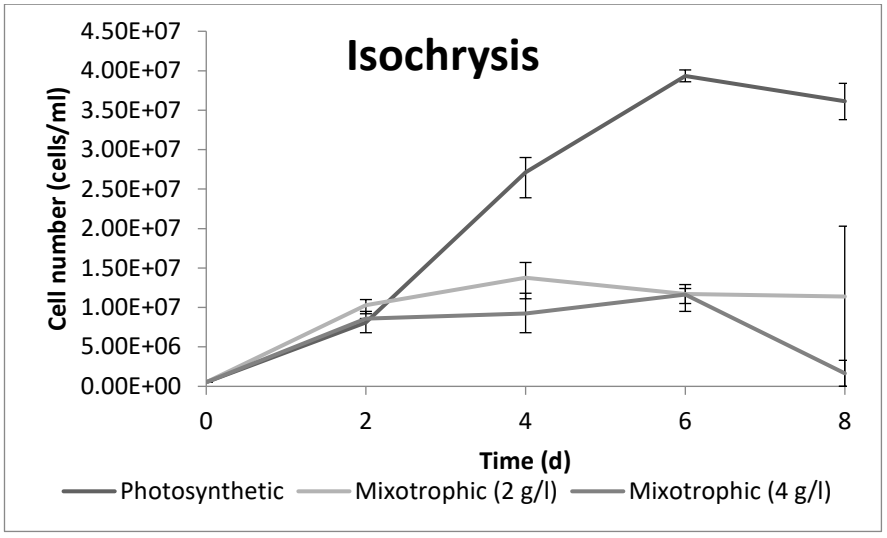

Figure 9.10 Comparison of *Isochrysis* sp. growth as a function of glucose load (0, 2, 4 g/l). Addition of glucose reduced algal growth possibly due to metabolite excretion or inhibition by bacterial proliferation.

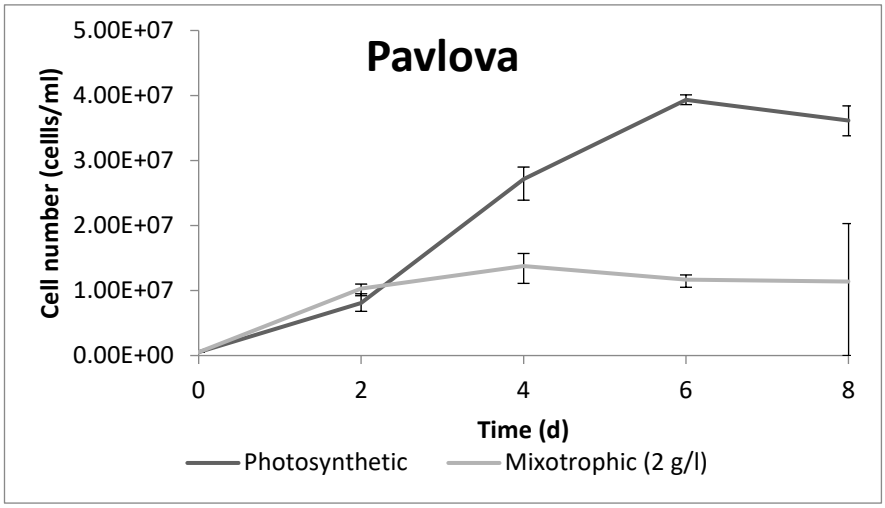

Figure 9.11 growth of *P. lutheri* as a function of glucose load (0, 2 g/l of glucose) in 1 L reactors with a 500 ml working volume.